NASA Contract Report 177959

P-334

Design Verification and Fabrication
of Active Control Systems
for the DAST ARW-2 High Aspect
Ratio Wing, Part 1

IN-08

117222

DATE

C. R. McGehee

The BOEING Co.
Wichita, KS 67277

Contract NAS1-16010
January 1986

Date for general release - January 1988

NASA
National Aeronautics and
Space Administration

Langley Research Center
Hampton, Virginia 23665

TABLE OF CONTENTS

TABLE OF CONTENTS (Continued)

TABLE OF CONTENTS (Continued)

TABLE OF CONTENTS (Continued)

*PART 2

APPENDICES

*Published under separate cover.

LIST OF FIGURES

6

FIGURE

10

12

LIST OF FIGURES

14

LIST OF FIGURES (CONCLUDED)

FIGURE

NOMENCLATURE

ACS	Active Control System
AFCS	Automatic Flight Control System
AR	Aspect Ratio
ARW-1	Aeroelastic Research Wing Number 1
ARW-2	Aeroelastic Research Wing Number 2
b	Wing Span, Inch
BCS	Backup Control System
BL	Buttock Line, Inch
BS	Body Station, Inch
$\bar{c}$	Mean Aerodynamic Chord Length, Feet
C_A	Actuator Coefficient, In^3
C_D, C_B, C_L	Force Coefficients-Drag, Sideslip and Lift, Respectively
C.G.	Center of Gravity
C_h	Control Surface Hinge Moment Coefficeint
C_{h0}, $C_{hS_\delta MAX}$	Control Surface Hinge Moment Coefficient at Zero and at Maximum Trailing Edge Down Deflection, Respectively
C_1, C_N, C_M	Moment Coefficient-Roll, Yaw and Pitch, Respectively
$C(E)$	Elastic (QSE) Coefficient
$C(R)$	Rigid Body Coefficient
$C_{M/4}$	Pitching Moment Coefficient at 1/4 Chord (25 Percent MAC)
$\bar{c}S$	Control Surface Mean Chord Length, Inch
$C_{(\square)(\diamond)}$	Force or Moment ($\square$) Coefficient Derivative with Respect to Motion Variable ($\diamond$)

NOMENCLATURE

DACE	Drone Active Control Electronics
DAST	Drones for Aerodynamic and Structural Testing
dB	Decibel
D.C.	Direct Current
D_{EQ}	Equivalent Viscous Damping of Hydraulic Fluid Trapped Between Servo Valve and Actuator (In-Lb)/(Rad/Sec)
DOF	Degree of Freedom
DT	Time Increment, Sec.
EOM	Equations of Motion
EMC	Electromagnetic Compatibility
FPS	Feet Per Second
FS	Flutter Suppression
FSS	Flutter Suppression System
g	Gravitational Constant, g = 32.17 Ft/Sec^2
GLA	Gust Load Alleviation
GW	Gross Weight, Lbs.
H	Altitude, Feet
$\dot{H}$	Altitude Rate, FPS
H M	Hinge Moment, In-Lb
Hz	Hertz (Cycles per Second)
i	Current, Amperes
I_{EQ}	Equivalent Rotary Mass Moment of Inertia of Hydraulic Fluid Trapped Between Servo Valve and Actuator, In-Lb-Sec^2

18

I_S	Rotary Mass Moment of Inertia of Control Surface Relative To Hinge Line, In-Lb-Sec^2
i_W	Wing Incidence
I_{XX}, I_Y, I_Z	Moment of Inertia About X, Y and Z Axis, Respectively, Slug-Ft^2
I_{XY}	Product of Inertia with Respect to X and Y Axis, Slug-Ft^2
j	Square Root of Minus One ($\sqrt{-1}$)
K_A	Servo Valve Drive Amplifier Gain, mA/Volt
KCAS	Knots Calibrated Airspeed
K_F	Servoactuator Position Feedback Gain, Volt/Deg
K_p	Servoactuator Pressure Feedback Gain, Volt/psi
$K_{S_{EQ}}$	Equivalent Rotary Spring Rate of the Actuator Shaft and One-Third Estimated Control Surface Spring Rate in Series, In-Lb/Rad
K_V	Servo Valve Flow Gain, In^3/Sec/mA
1	Rotary Actuator Vane Length, Inch
L	Random Gust Scale Length, foot
mA	Milliamperes
MAC	Mean Aerodynamic Chord, Inch
MARS	Mid Air Recovery System
M_C	Cruise Mach Number
MLA	Maneuver Load Alleviation
M_{MO}	Maximum Operating Mach Number
mV	Millivolt
M_X	Vertical Bending Moment (+ Tip Up), In-Lb

NOMENCLATURE

M_Y	Torsional Moment (+ Leading edge Up), In-Lb
N_Z	Normal Load Factor, g
ΔN_Z	Incremental Load Factor, Nz-1, g
P	Roll Rate About the Longitudinal Axis, (+Right Wing Down), Deg/Sec
P_a	Ambient Pressure, psi or psf
PCS	Primary Control system (Primary AFCS)
P_L	Actuator Load Pressure, psi
P_S	Hydraulic Supply Pressure, psi
psi	Pounds per Square Inch
psf	Pounds per Square Foot
PSD	Power Spectral Density
Q	Hydraulic Fluid Flow Rate, In^3/Sec
Q	Pitch Rate About the Drone Lateral Axis (+ Nose Up), Deg/Sec
q	Dynamic Pressure, psf
Q_0	Servo Valve No-Load Flow Rating, In^3/Sec
Q_c	Impact Pressure, psi or psf
QSE	Quasi-Static Elastic
R	Yaw Rate About the Drone Vertical Axis (+ Nose Right), Deg/Sec
r_D	Rotary Actuator Vane Radius, Inch
RMS	Root Mean Square
RPM	Revolutions per minute
RPRV	Remotely Piloted Research Vehicle

20

NOMENCLATURE

PRS	Radians per second
r_S	Rotary Actuator Shaft Radius, Inch
RSS	Relaxed Static Stability
S	Surface Area, Ft^2
S	Laplace Transform Variable, Rad/Sec
SL	Sea Level
S_S	Control Surface Area, In^2
T	Thrust, Lb
TE	Trailing Edge
TTL	Transistor-Transistor Logic
$T_{1/2}, T_2$	Time to Half and Double Amplitudes, Respectively, Second
U	True Airspeed, Ft/Sec
U_0	Reference Airspeed, Ft/Sec
V	Volume of Hydraulic Fluid Trapped on One Side Servovalve and Actuator, In^3
V	Volts
V_C	Cruise Speed, Ft/Sec
V_D	Dive Speed, Ft/Sec
VDC	Direct Current Voltage
V_f	Flutter Velocity, Ft/sec
$\bar{V}_H$	Horizontal Tail Volume Coefficient
V_{MO}	Maximum Operating Velocity, Ft/Sec
$\bar{V}_V$	Vertical Tail Volume Coefficient
V_Z	Vertical Shear (+ Up), Pounds

NOMENCLATURE

W	Velocity Along Drone Normal Reference Axis (+ Down), Ft/sec
WBL	Wing Buttock Line, Inch
WRVBM	Wing Root Vertical Bending Moment (M_X Wing Root), In-Lb
WS	Wing Station - Distance Outboard Along Rear Spar from Centerline of Body, Inch
Z	Drone Vertical Displacement from a Reference Altitude (+ Down), Feet
$\ddot{Z}$	Vertical Acceleration (+ Down), Ft/Sec2 or In/Sec2
α	Angle of Attack (+ Nose Up), Degree
β	Sideslip Angle (+ Right), Degree
β	Bulk Modulus, Lb/In^2
γ	Glide Angle (+ Down), Degree
δ_{IA}, δ_{OA}	Inboard and Outboard Aileron Deflection, Respectively, (+Trailing Edge Down), Degree
δ_{STAB}	Symmetric Stabilizer Deflection from Steady-State Trim Position (+ Trailing Edge Down), Degree
ϵ	Downwash Angle, Degree
ζ	Damping Ratio
ζ_d	Dutch Roll Mode Damping Ratio
ζ_p	Phugoid Mode Damping Ratio
ζ_{sp}	Short Period Mode Damping Ratio
ζ_v	Equivalent Second Order Damping Ratio of the Servovalve
η_p	Dynamic Pressure Effectiveness
η_w	Normal Wash Effectiveness

NOMENCLATURE

$\eta_{fb}, \eta_{wg}, \eta_{ht}$	Aerodynamic Effectiveness Scalers ($N_{(\ )} = N_{P(\ )} = N_{W(\ )}$) for the Forward Body, Wing and Horizontal Tail, Respectively
θ	Drone Pitch Angle (+ Nose Up), Degree
μ_v	Microvolt - 10^{-6} Volts
ρ	Mass Density of Air, Slug/Ft^3
σ	Real Part of Complex Numbers
σ	Root Mean Square (RMS)
τ_R	Roll Convergence Mode Time Constant
$\phi, \dot{\phi}$	Roll Attitude and Rate, Respectively (+ Right Wing Down), Degree
$\psi, \dot{\psi}$	Heading Attitude and Rate, Respectively (+ Nose Right), Degree
ω	Frequency, Rad/Sec
ω_N	Natural Frequency, Rad/Sec
ω_{nd}	Dutch Roll Mode Natural Frequency, Rad/Sec
ω_{np}	Phugoid Mode Natural Frequency, Rad/Sec
$\omega_{n_{sp}}$	Short Period Mode Natural Frequency, Rad/Sec
ω_{n_v}	Equivalent Second Order Undamped Natural Frequency of the Servo Valve

(This page intentionally left blank)

1. INTRODUCTION

A preceding study was performed under National Aeronautics And Space Administration (NASA) Contract NAS1-14665 (Reference 1) to establish an integrated design methodology and apply it to accomplish the integrated design of a high aspect ratio wing with active controls for flight test on a BQM-34E/F (Firebee II) drone. The wing will be used to study aeroelastic effects and to assess and validate the design and predicted performance of active control systems.

This study, a follow-on to the above, was performed under NASA Contract NAS1-16010 with the objective of accomplishing the final design and hardware fabrication for four active control systems compatible with and ready for installation in the NASA Aeroelastic Research Wing No. 2 (ARW-2) and Firebee II drone flight test vehicle.

The four active control systems enclosed in the Drone Active Control Electronics (DACE) unit are:

- Flutter Suppression (FS)
- Maneuver Load Alleviation (MLA)
- Gust Load Alleviation (GLA)
- Relaxed Static Stability (RSS)

This development effort also includes the definition of a ground based Primary Control System (PCS) and the final design and hardware fabrication of a Backup Control System (BCS) to be packaged and compatible with an existing NASA design electronics unit.

NASA is pursuing studies of aeroelastic effects on wing loads and integration of active control systems to reduce structural weight and improve efficiency of transport aircraft. Under the on-going Drones for Aerodynamic and Structural Testing (DAST) project, the ARW-2 is the second wing to be evaluated. The overall effort involves wing and hardware fabrication, analytical studies, and wind tunnel and flight test evaluation. The DAST ARW-2 configuration general arrangement is shown on Figure 1. Figure 2 shows the flight envelope.

The first wing to be designed for the Firebee II drone, ARW-1 was designed by Ryan Aeronautical under NASA Contract NAS1-13451 to exhibit flutter within the aircraft flight envelope. Preliminary and final design of the Flutter Suppression System (FSS) was accomplished by Boeing Military Airplane Company (BMAC) under Contracts NAS1-14028 (Reference 2) and NAS1-14675 (Reference 3). The ARW-1 configuration went into flutter and crashed during a flight test. The test mishap was attributed to nonlinear wing characteristics coupled with a gain implementation error in the flutter system.

WING

DESIGN C_L - - - - - - - - - - 0.53
GROSS AREA - - - - - - - - 35 SQ. FT.
ASPECT RATIO - - - - - - - 10.3
SPAN - - - - - - - - - - 227.84 IN.
TAPER RATIO (BASIC WING) - - - .4
SWEEP - 50% BASIC WING CHORD - 25°

	STREAMWISE TWIST	THICKNESS % CHORD
2y/b = 0.106	+2°	14.4
2y/b = 0.426	-.5°	12.0
2y/b = 1.00	-1.6°	10.6

STREAMWISE INCIDENCE ANGLE - - 0°
DIHEDRAL ANGLE - - - - - - - 0°

TAIL - HORIZONTAL

GROSS AREA - - - - - - - - 9.1 SQ. FT.
ASPECT RATIO - - - - - - - 3.5
INCIDENCE - - - - - - - - ALL MOVABLE
TAPER RATIO - - - - - - - - 0.40
DIHEDRAL - - - - - - - - - 0°

TAIL - VERTICAL

GROSS AREA - - - - - - - - 8.65 SQ. FT.
ASPECT RATIO (GEOMETRIC) - - - 1.2
TAPER RATIO - - - - - - - - 0.30
RUDDER HINGE AXIS- - - - - - 85% CHORD
RUDDER AREA- - - - - - - - 0.61 SQ. FT.

POWER PLANT

CONTINENTAL - - - - - - - - (YJ 69-T-406CAE MODEL 356.34)
RATED THRUST - - - - - - - 1810 LB SEA LEVEL STATIC
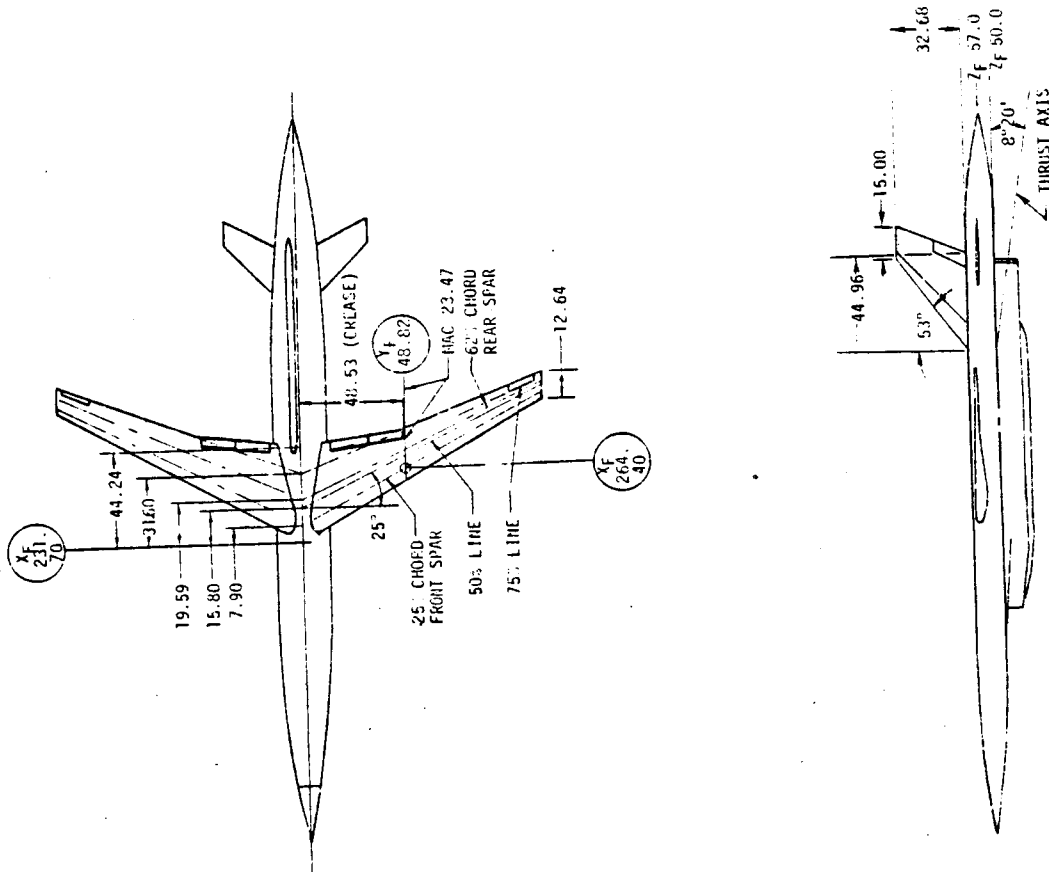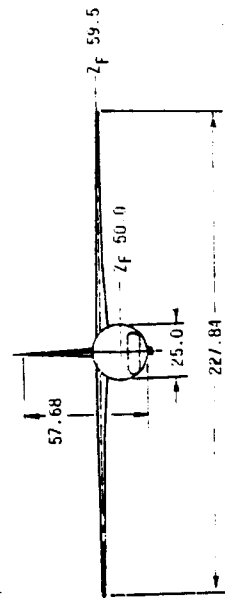
DAST ARW-2 GENERAL ARRANGEMENT
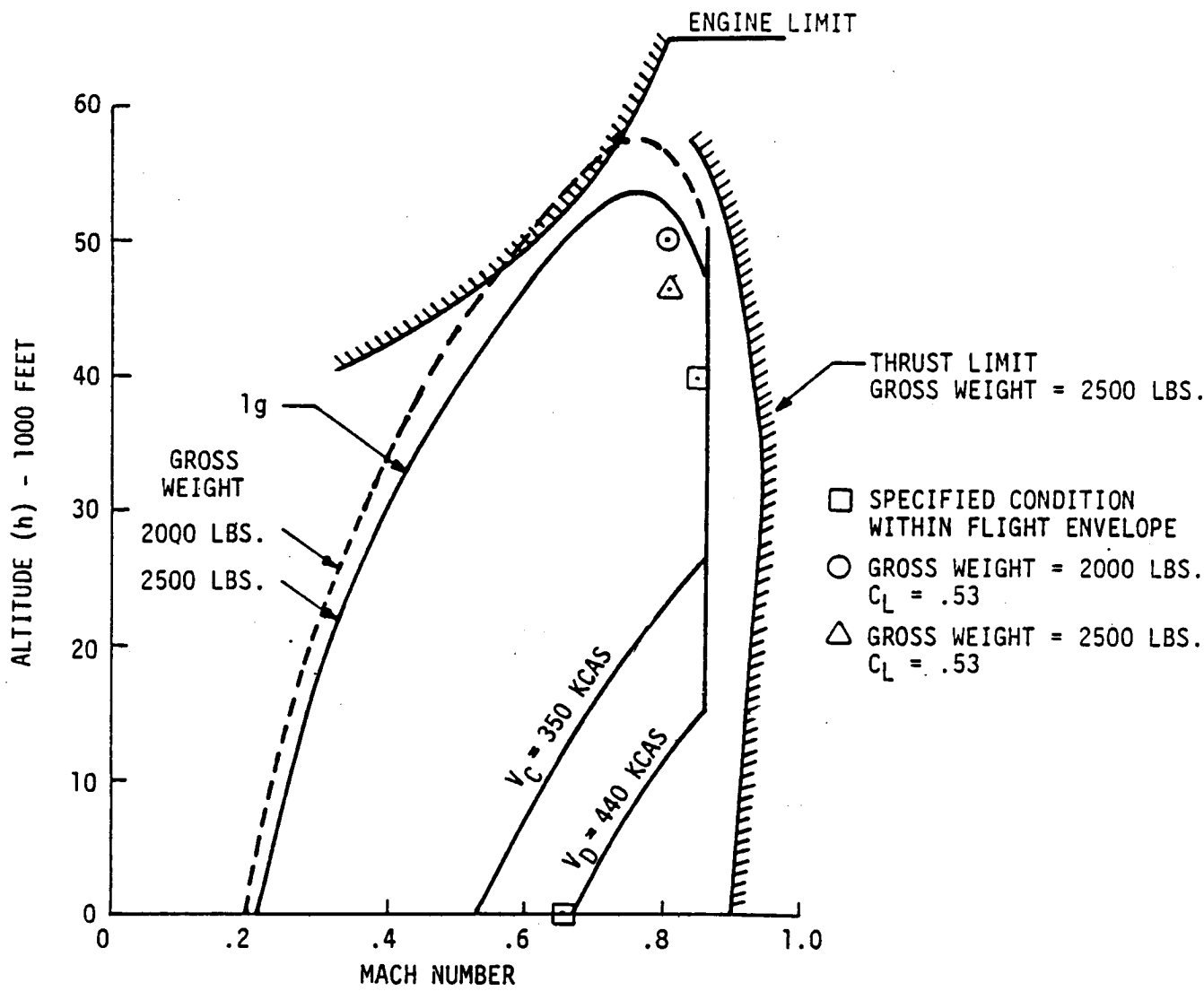
FIGURE 1

FIGURE 2

DAST ARW-2 OPERATIONAL FLIGHT ENVELOPE

The DAST ARW-2 test vehicle is air launched from a B-52B aircraft, controlled from a ground based cockpit and recovered by air snatching the recovery parachute with a helicopter. The vehicle will be flown as a Remotely Piloted Research Vehicle (RPRV) similar to the illustration shown on Figure 3 and described in Reference 1.

This report provides historical documentation and describes the completion of the third iteration of the Integrated Design Methodology initiated and discussed in Reference 1. Completion of the FSS, MLA, GLA and RSS systems synthesis, design of the electronic and mechanical components required to mechanize the systems on the drone, results of additional servoactuator actuator analysis, and the results of the flightworthiness tests conducted prior to delivery of the system components to NASA are contained herein.
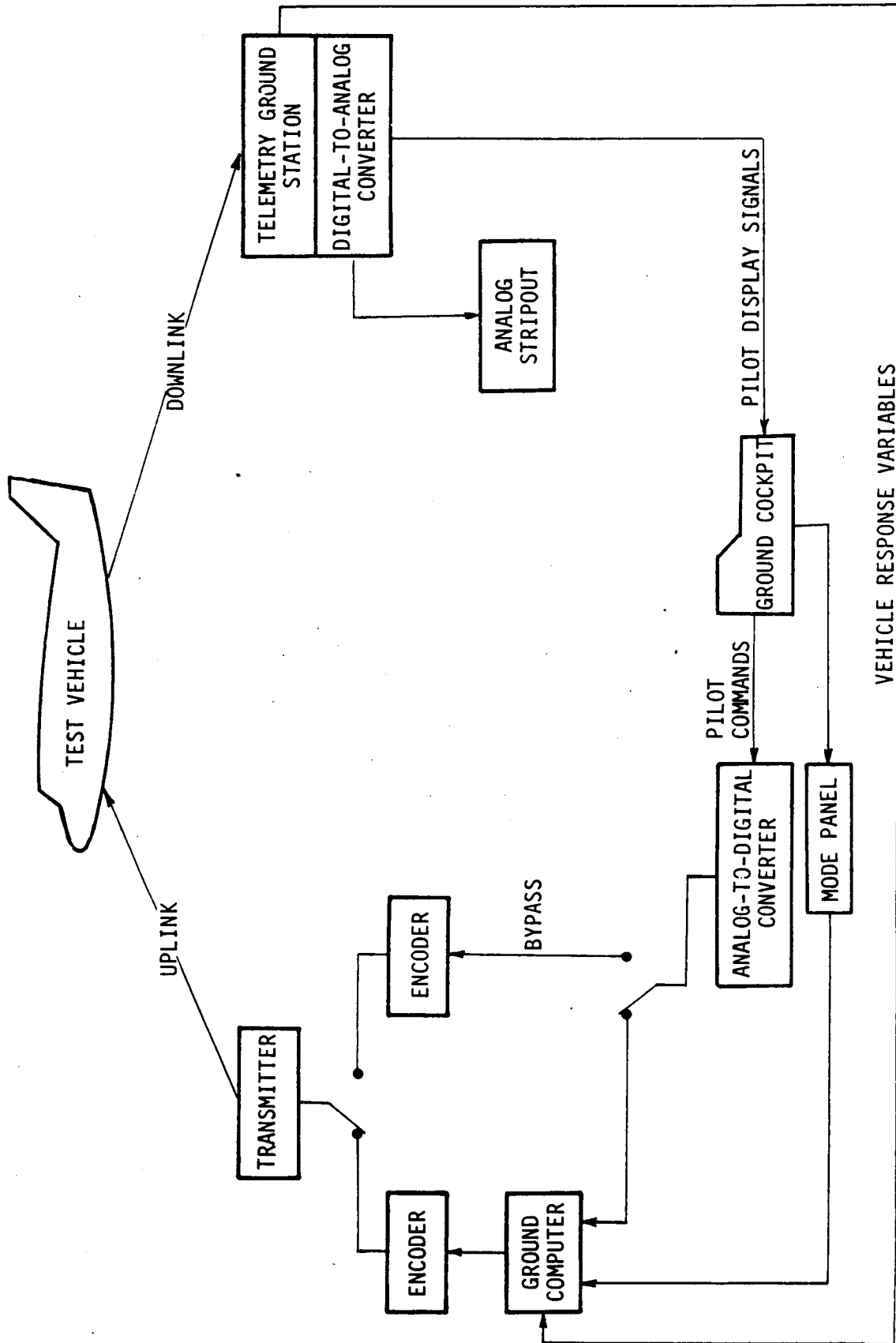
FIGURE 3   FUNCTIONAL BLOCK DIAGRAM OF THE REMOTELY PILOTED RESEARCH VEHICLE

(This page intentionally left blank)

2. SUMMARY

This is the final report on Contract NAS1-16010 for the integrated design of a high aspect ratio wing with active controls for flight tests on a BQM-34E/F drone.

The integrated design methodology shown on Figure 4 was used to develop a high aspect ratio wing design with integral critical control systems to derive substantial benefits in terms of reduced wing structure weight and stiffness. The active control systems are used for gust and maneuver load reduction and flutter control to allow reductions in structural strength and stiffness from conventional wing designs. The third and final cycle of the interactive design method of Figure 4 was completed during this study.

Performance goals and criteria were applied to individual systems and the systems collectively to assure that vehicle stability margins, flutter margins, flying qualities and load reductions were achieved. Figure 5 shows the Active Control System (ACS) and Automatic Flight Control System (AFCS) sensor and control surface locations and identifies their use for system applications. The control system equipment installation arrangement is shown on Figure 6.

Individual ACS system design and flight test conditions are shown on the flight envelope on Figure 7.

Quasi-Static Elastic (QSE) and scaled and unscaled elastic structure Equations of Motion (EOM) were used in the analysis and synthesis of the ACS and AFCS systems. The QSE EOM were the primary model for evaluation of airplane stability. The scaled elastic structure EOM matched basic airplane dynamics to QSE characteristics and were used to determine wing loads. The unscaled elastic structure EOM were used for flutter system analysis.

Load alleviation systems were defined which reduce structural loads over the critical inboard section of the wing. Load alleviation systems include both maneuver and gust reduction systems. Wing vertical bending moment reduction capability of the load alleviation system is shown on Figure 8. Eighteen percent reduction in critical wing root vertical bending was achieved with load alleviation control. The wing is gust load critical over the entire span.

The load reduction capability of the load alleviation system will be verified by flight tests. A system was implemented to generate random excitation of the inboard aileron with a power frequency content similar to wind turbulence in order to evaluate the gust load alleviation system. Comparisons of the power spectral density and root mean square characteristics of wing root vertical bending moment due to vertical turbulence and random inboard aileron excitation are shown on Figure 9.
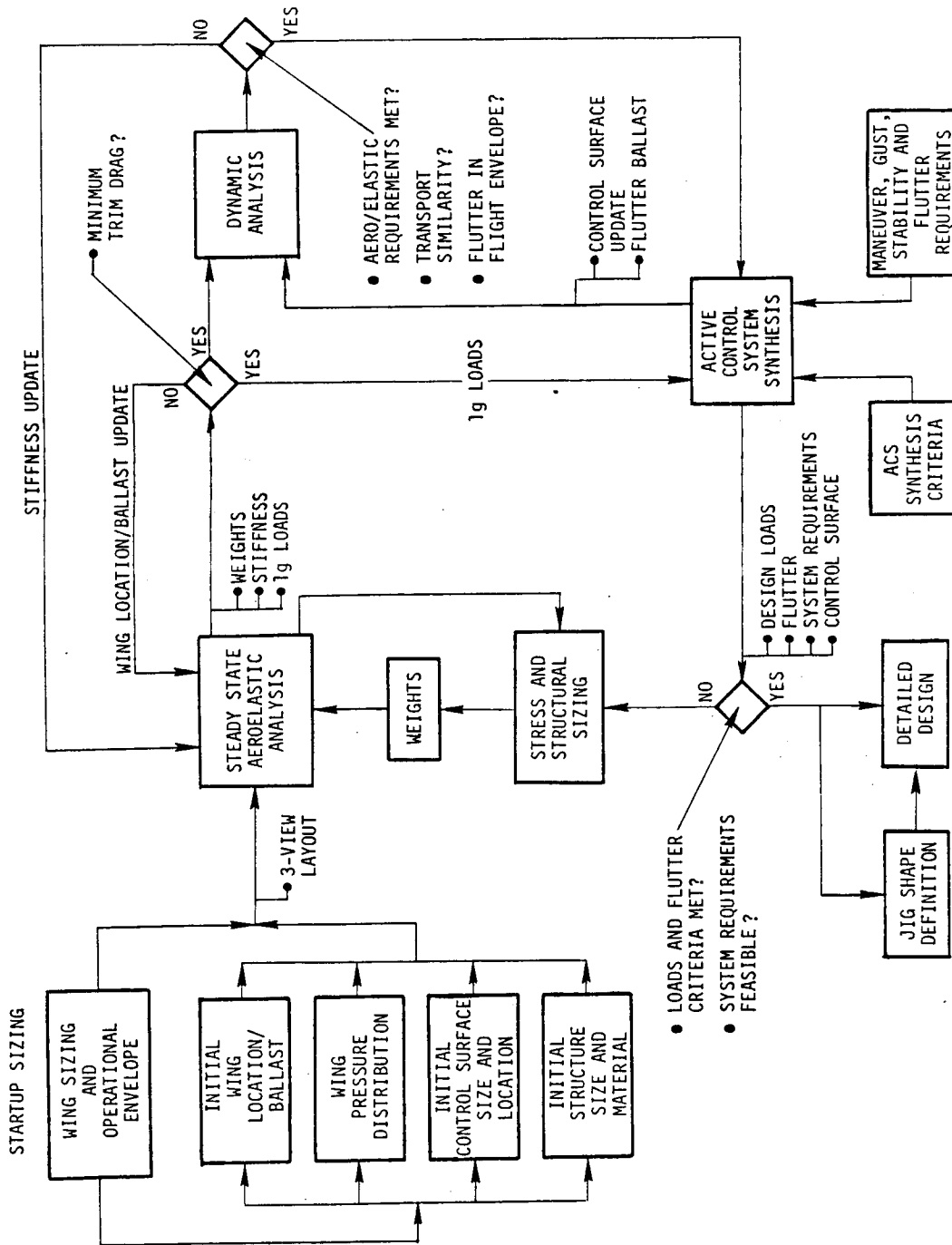
FIGURE 4

DAST ARW-2 INTEGRATED DESIGN METHODOLOGY

CONTROL SURFACES

OUTBOARD AILERON
(BL 89.7 - 107.7, 23% CHORD)
● FSS
● GLA
● MLA

STABILIZER
● RSS
● AFCS
● GLA
● MLA

RUDDER
● AFCS

INBOARD AILERON
(BL 13 -26.57 AND
BL 25.72 -45,
15% CHORD)
● MLA

SENSORS

VERTICAL ACCELEROMETERS
WBL 84 REAR SPAR
WBL 82 FRONT SPAR
WBL 92 REAR SPAR
WBL 92 FRONT SPAR
● FSS

VERTICAL ACCELEROMETER
BS 250
● GLA
● AFCS

ROLL, PITCH, YAW RATE
ANGLE-OF-ATTACK (NASA)
● RSS
● AFCS
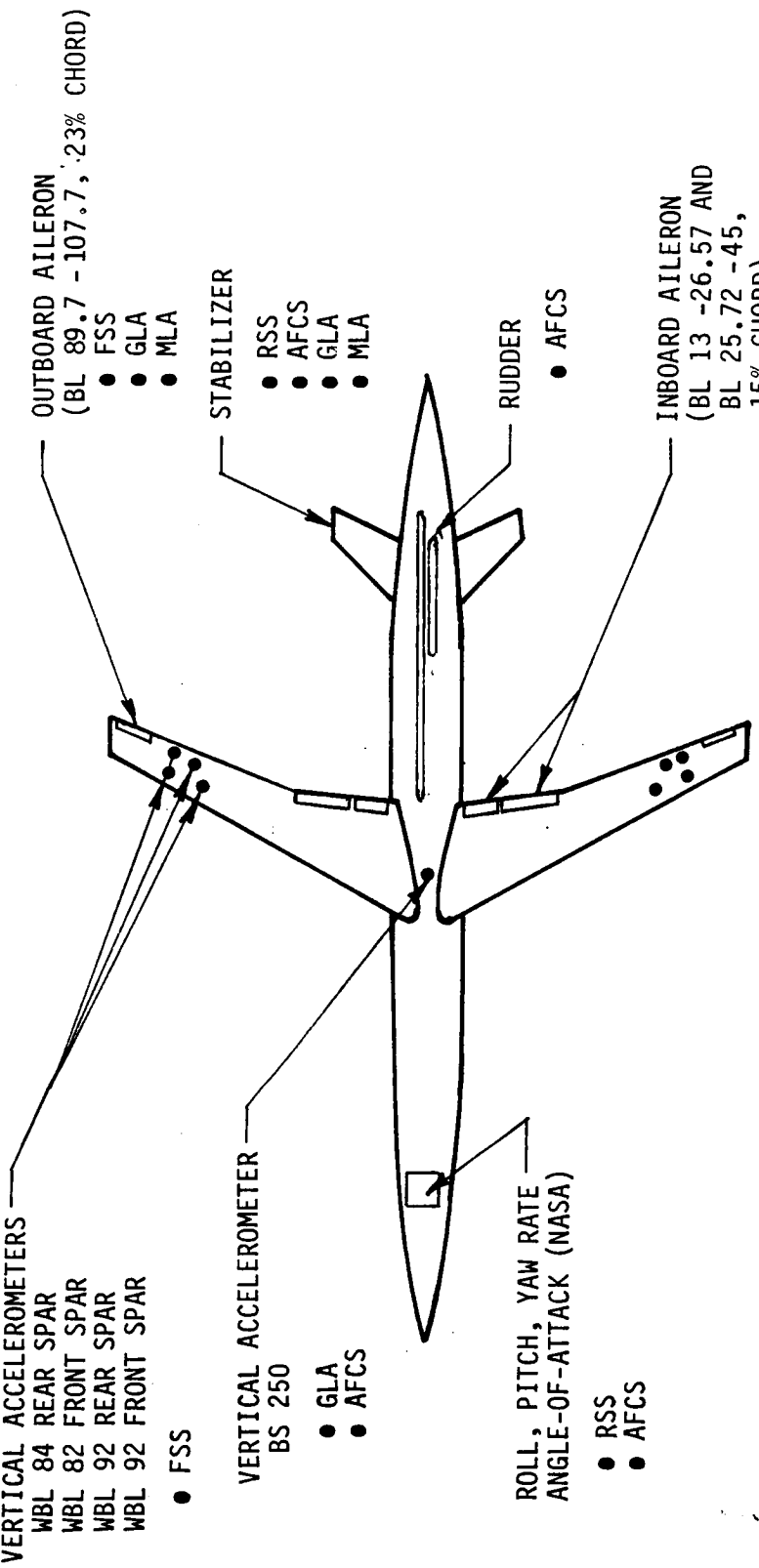
FIGURE 5

DAST ARW-2 ACS/AFCS SENSORS AND CONTROL SYSTEMS

33

FIGURE 6

EQUIPMENT INSTALLATION

HYDRAULIC PUMP

ACCUMULATOR

SERVOVALVE

ACCELEROMETER
(4 PER WING)

PRESSURE TRANSDUCER
(6 PER WING)

POTENTIOMETER
(R.H. & L.H.
OUTBOARD ACTUATOR)

ACTUATOR
(R.H. & L.H.
OUTBOARD)

POTENTIOMETER

SERVOVALVE

POTENTIOMETER

ACTUATOR

PRESSURE
TRANSDUCER
(6 PER WING)

SERVOVALVE
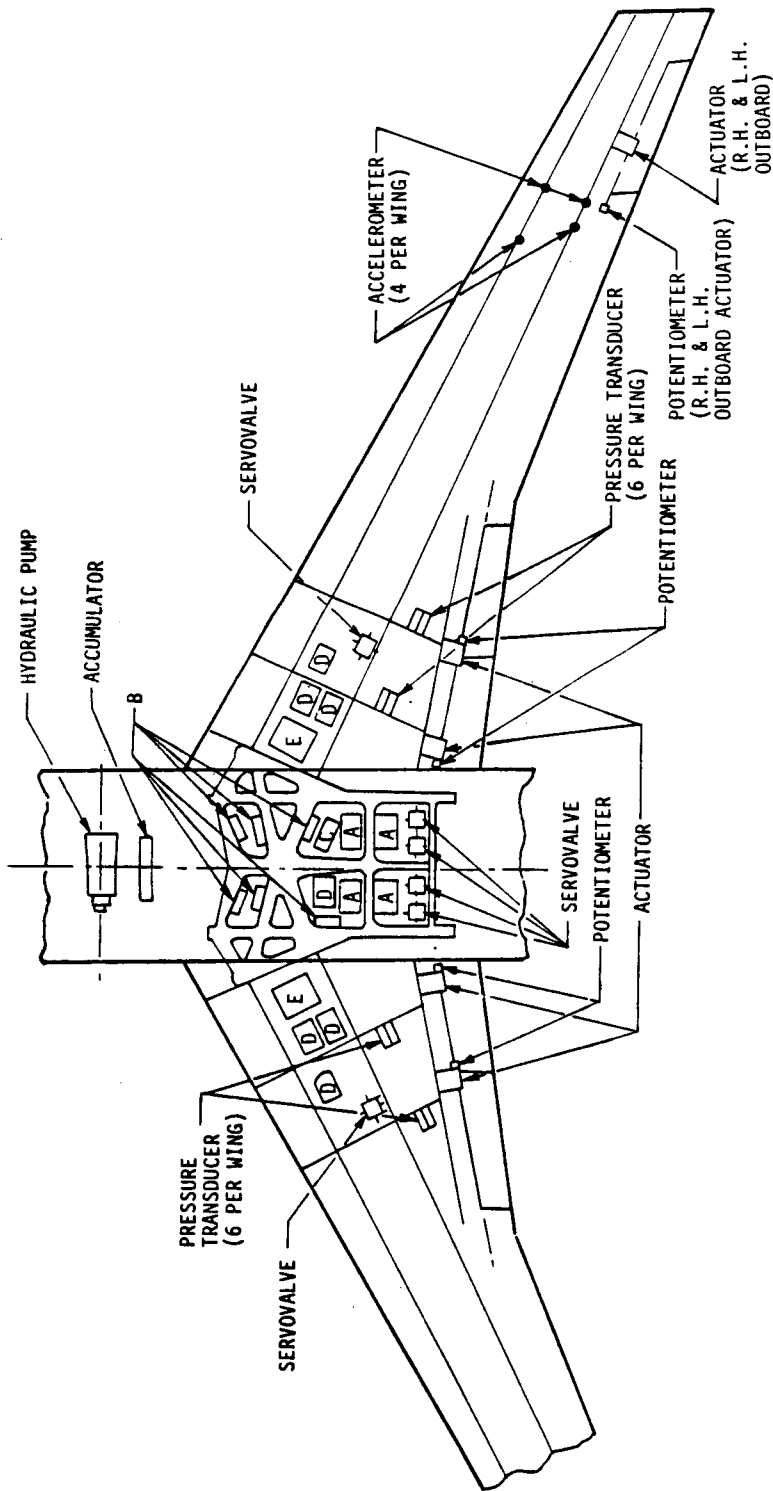
NASA EQUIPMENT

A - POWER MODULE (3.38 x 3.38 x 4.56)
B - POWER SUPPLY (3.50 x 2.50 x 1.38)
C - ENCODER (1.5 x 2.0 x 4.5)
D - SIGNAL CONDITIONING (4.3 x 2.8 x 3.5)
E - SIGNAL CONDITIONING (4.3 x 4.1 x 5.0)

FIGURE 7

DAST ARW-2 ACS DESIGN AND FLIGHT TEST CONDITIONS

35
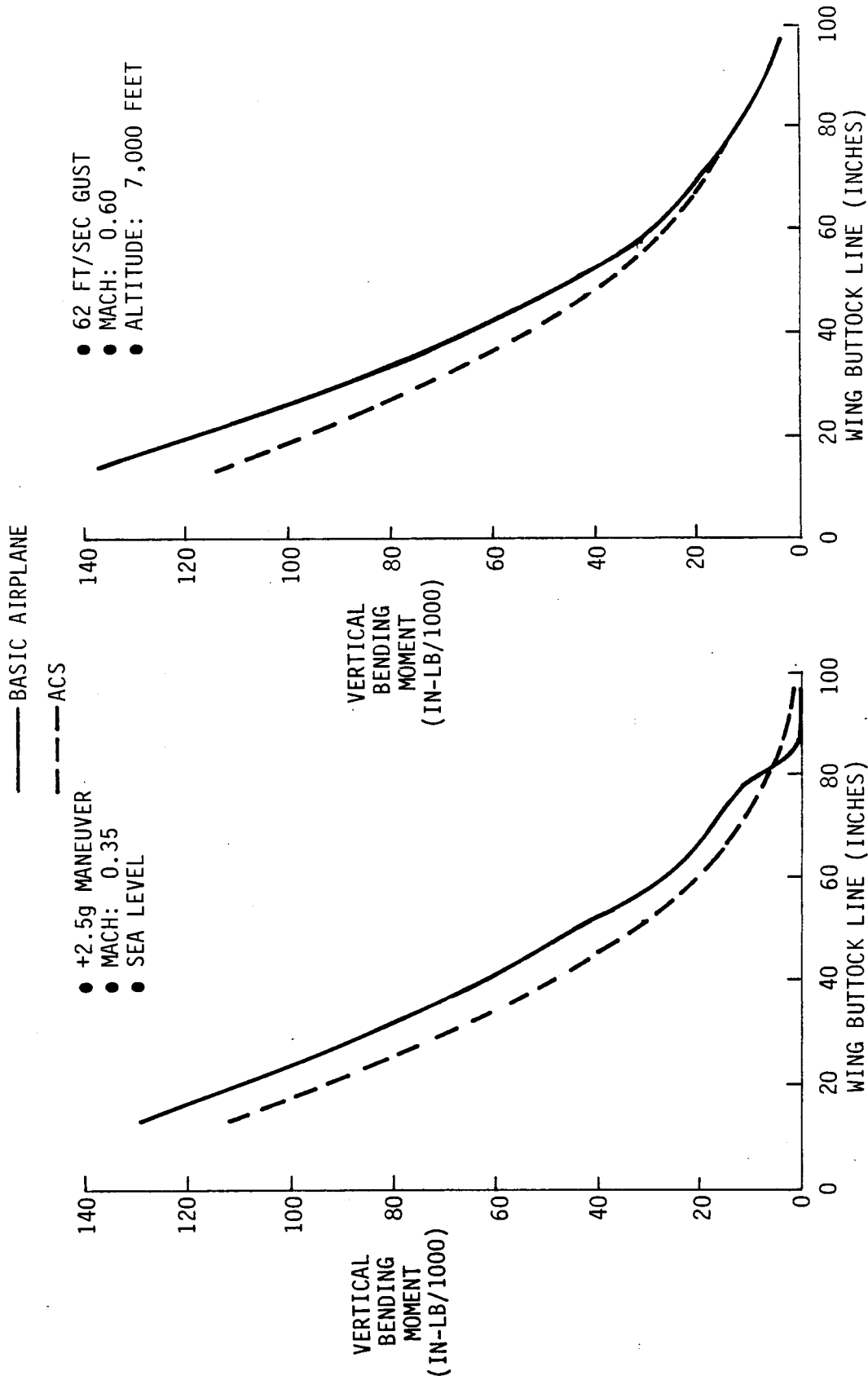
FIGURE 8

DAST ARW-2 WING VERTICAL BENDING MOMENT REDUCTION WITH ACS

VERTICAL TURBULENCE
INBOARD AILERON

• ACS SYSTEMS AND AFCS CLOSED
• MACH: 0.70
• ALTITUDE: 15,000 FEET
• GROSS WEIGHT: 2500 LBS.
• RMS NORMALIZED TO RMS AT 40 FPS
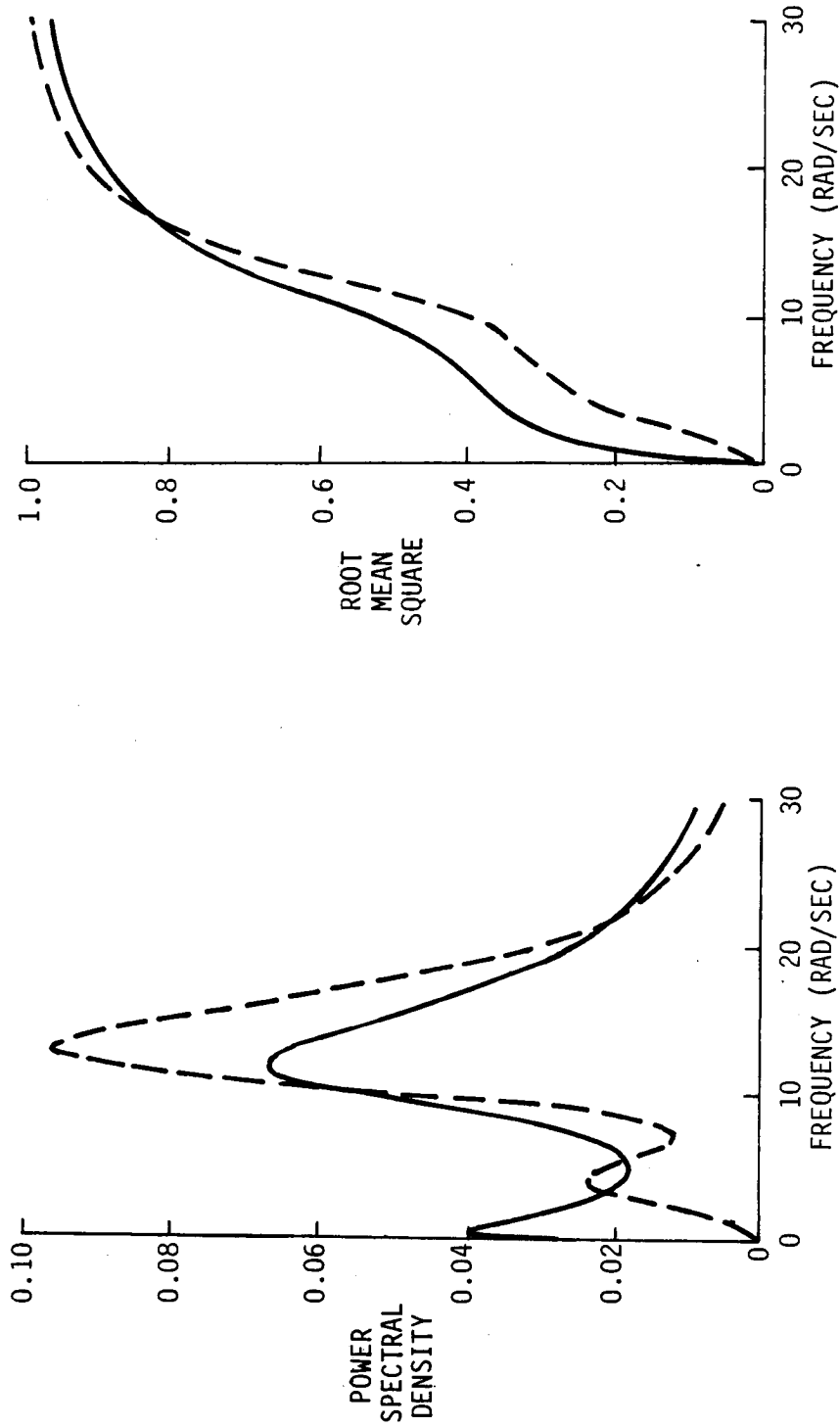
FIGURE 9

DAST ARW-2 COMPARISON OF WING ROOT VERTICAL BENDING MOMENT PSD AND RMS
FOR TURBULENCE AND RANDOM INBOARD AILERON EXCITATION

A Relaxed Static Stability system (RSS) was defined to provide flight at aft reduced trim drag, but unstable center of gravity positions. The RSS provides stability and handling characteristics with C.G. shifts aft to 33 percent mean aerodynamic chord (MAC) over the vehicle flight region. This provides stability 18 percent aft of the neutrally stable position at the critical flight condition.

A Flutter Suppression System (FSS) was synthesized to control symmetric and antisymmetric flutter modes occurring in the high dynamic pressure and Mach region within the vehicle flight envelope. Dual accelerometers mounted on the front spar at wing buttock lines 82 and 92 and dual accelerometers mounted on the rear spar at buttock lines 84 and 92 are combined and filter shaped to drive the outboard ailerons.

Longitudinal and lateral-directional primary automatic flight control systems were synthesized to provide adequate vehicle handling qualities for a ground based operator. Backup automatic flight control systems provide minimal control capability from a chase plane.

Maximum displacement and rate requirement for the control surfaces used for ACS and AFCS functions are summarized on Figure 10. The values on Figure 10 are within the design capability of the vehicle surface actuation systems at the critical design conditions.

CONTROL SURFACE	DISPLACEMENT (DEGREES)	RATE (DEG/SEC)
OUTBOARD AILERON	±15	640
INBOARD AILERON	20 T.E.D. 10 T.E.U.	50
SYMMETRIC STABILIZER (FROM TRIM)	4	17.2

FIGURE 10

CONTROL SURFACE MAXIMUM DISPLACEMENTS AND RATES

The major requirements accomplished under this contract are:

a. The design methodology to define the ARW-2 high aspect ratio wing and supporting active control systems, developed and partially completed under Contract NAS1-14665, was finalized. The finalized ACS systems include a flutter suppression system, a relaxed static stability system, and gust and maneuver load alleviation systems.

b. Primary and backup AFCS were finalized.

c. The ACS and AFCS hardware was procured and/or fabricated, assembled and tested.

38

In addition to this final report, the following items were delivered under this contract:

a. ACS component hardware, electronics, ground support equipment, and spare parts.

b. BCS printed circuit assemblies.

c. ACS assembly, installation, checkout, maintenance and operation procedure documentation.

d. Drawings and schematics of the ACS layout and assembly.

e. Flight assurance and EMC test procedures and test report.

(This page intentionally left blank)

3. INTEGRATED DESIGN METHODOLOGY

The integrated design methodology to define the DAST ARW-2 wing and the
ACS is illustrated on Figure 4. Under the previous contract study, two
major design iterations and the initiation of a third were conducted as
discussed in Section 3 of Reference 1. The previous contract study had
defined the ACS and a wing design. The last stress analysis results in
the previous contract study identified small modifications to the wing
design used in the last performance analysis. The changes were
incorporated in the final wing design but final performance analyses
were not conducted. With the possible exception of the FSS, the small
changes in the wing design were not expected to affect system
performance.

3.1 Final Integrated Design Cycle Completion. A final (third) system
performance analysis cycle conducted under the present contract is shown
on Figure 11. This final interactive cycle was initiated during the
previous study. The part of the final iteration conducted during the
previous study is indicated by the solid path of Figure 11. After the
final stress analysis of the previous study, the detailed structural
design and jig shape were defined because it was apparent that the
iterative design procedure had converged. The completion of the final
iterative cycle conducted during the present study is indicated by the
dashed paths shown on Figure 11.

The final performance analysis cycle included updated aerodynamic
modeling reflecting wind tunnel test data for the 0.237 scale ARW-2
model. The change in aerodynamics had a significant impact on final
wing loads as discussed in subsequent sections of this report.

In a task related to the efforts of this contract, the wing skin design
defined in the last contract study was revised by NASA to make the
torsional characteristics agree with that used in the mathematical
description of the wing design.

3.2 ARW-2 Performance and Synthesis Criteria. The ARW-2 design
criteria including design guidelines, performance objectives and active
control system synthesis criteria are presented in the following
paragraphs.

3.2.1 Active Control System Guidelines. The wing shall be designed to
use active control systems for control of gust and maneuver loads and
flutter to allow maximum reduction in structural strength and stiffness
from conventional wing design. This integrated design analysis effort
shall be performed in an iterative manner.

The active control system design techniques used should be applicable to
transport aircraft design.

FIGURE 11

DAST ARW-2 INTEGRATED DESIGN METHODOLOGY - THIRD ITERATION

42
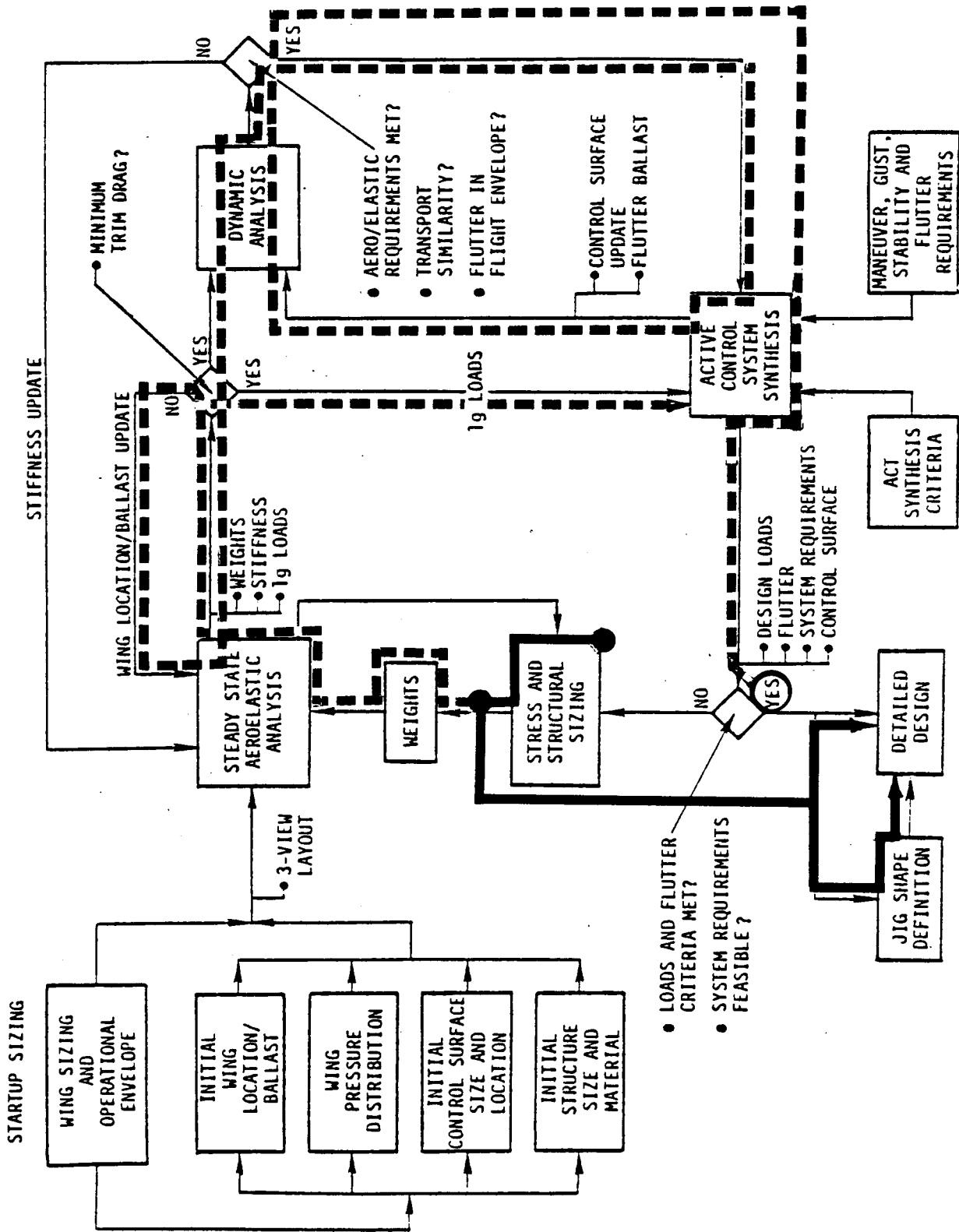
The wing structural design shall be such that it is necessary to have the active control systems functioning in the normal operating flight envelope. Minimization of trim drag through the use of relaxed static stability is a goal.

System reliability and redundancy should be considered as appropriate for unmanned, limited time operations.

3.2.2 ARW-2 Performance Objectives

3.2.2.1 Flutter Suppression System.
The wing shall be designed to be free of divergence and flutter at all speeds up to 120 percent of the design dive speed $(1.2V_D)$ with the FSS operating. At the design dive speed, V_D, at least one and one-half percent equivalent structural damping ratio ($\zeta = .015$) must exist for all flutter critical structural modes. The wing without the FSS shall exhibit flutter within the flight envelope.

3.2.2.2 Load Alleviation.
Wing design limit maneuver and gust loads shall be met with the MLA and GLA functions of the ACS operating. The ACS system shall be load critical and reduce wing bending moment approximately 20 percent. Design limit maneuver wing loads will be determined for maneuvering load factors of +2.5 and -1.0 per FAR Part 25.

The atmospheric turbulence model to be used for ACS synthesis will be Gaussian, stationary and isotropic random gust with the Von Karman spectral density as specified in MIL-A-008861A. Characteristic gust length of 2500 feet will be used for altitudes above 2500 feet.

The structure will be designed to meet limit gust velocity values from MIL-A-008861A as shown on Figure 12 for the cruise speed (V_C). The limit design response is obtained by multiplying the limit gust velocity by the response per unit gust as defined in MIL-A-008861A. Due to limited hydraulic flow capacity on the drone test vehicle, the design gust velocity at the flutter critical design dive condition will be 12 ft/sec.

Longitudinal maneuvers will be ramp style maneuvers as defined in MIL-A-008861A for a transport. This maneuver is illustrated on Figure 13. The structure shall be sized to meet requirements of gust and maneuver loads independently.

3.2.2.3 Relaxed Static Stability.
The goal of the RSS system is to provide longitudinal stability and flying qualities for the ARW-2 drone with an aft center of gravity for minimum trim drag. A requirement is for the drone to be stable at launch without the RSS system. If these two requirements are incompatible, emphasis shall be on vehicle stability at launch and the minimum trim requirement shall be relaxed. A droppable mass ballast shall not be used to achieve minimum trim drag.

- RANDOM TURBULENCE
  - VON KARMAN SPECTRUM
- MIL-A-008861A
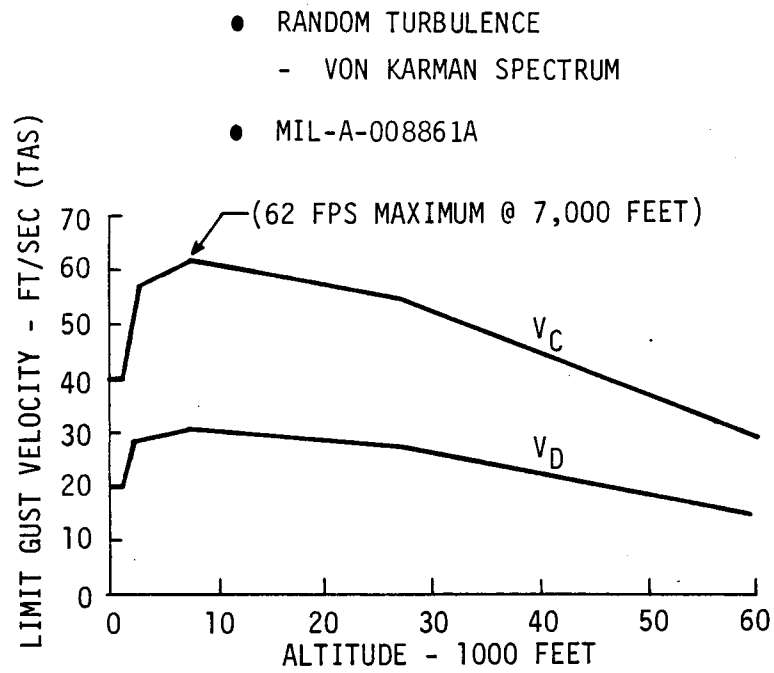
FIGURE 12

DAST ARW-2 LIMIT GUST VELOCITY FOR ACT SYSTEM DESIGN

- MANEUVER COMMANDS
  - ±2.5g MAXIMUM
- MIL-A-008861A
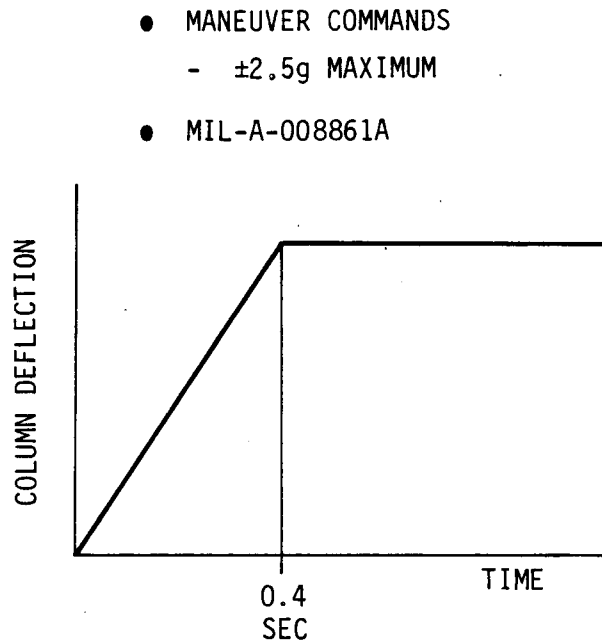
FIGURE 13

DAST ARW-2 MANEUVER INPUT FOR ACT SYSTEM DESIGN

44

The RSS system shall provide the intent of Level 1 flying qualities as defined in MIL-F-8785B (ASG) and summarized in Paragraph 3.2.3.3, as appropriate for the DAST research mission. The intent is to achieve required longitudinal drone stability with the RSS system and use the longitudinal AFCS as the drone control loop.

3.2.2.4 Primary AFCS. The primary AFCS shall provide the intent of Level 1 flying qualities in each axis as defined in MIL-F-8785B (ASG) as appropriate for the DAST research mission with the existing BQM-34E/F control surface authority. The flying qualities are summarized in Paragraph 3.2.3.3.

3.2.2.5 Backup AFCS. The backup AFCS shall be designed to provide minimum flying qualities necessary to return the drone to a safe Mid Air Recovery System (MARS) recovery in case of failure in the primary AFCS ground computer loop. Minimum flying qualities for the backup AFCS will be at least Level 3 as outlined in Paragraph 3.2.3.3.

3.2.2.6 ACS and AFCS Normal Operation. Normal operation shall be with all of the ACS and the primary AFCS operating. The AFCS and ACS shall become active (engage) three seconds after separation from the launch aircraft.

3.2.2.7 ACS and AFCS Abnormal Operation. The ACS systems shall remain operative when the AFCS switches to the onboard backup mode.

For failure of the GLA, MLA or FSS functions, the RSS function shall remain engaged and flight restrictions shall be applied.

For loss of the RSS function the automatic recovery sequence shall be initiated.

The backup AFCS must hold the drone in a recoverable attitude for up to 20 seconds in case of loss of control signal from either the ground pilot or the F-104 backup pilot.

3.2.3 System Synthesis Criteria.

3.2.3.1 Stability Margins. All ACS and AFCS functions shall be synthesized to meet MIL-F-9490D gain and phase margins at the design dive speed (V_D) as summarized on Figure 14. At $1.2V_D$ all modes shall be stable at nominal gain and phase.

MODE	GAIN MARGIN	PHASE MARGIN
f ≤ 0.06 HZ	±3.0 dB	±20°
MANEUVER	±4.5 dB	±30°
STRUCTURAL	±6.0 dB	±45°

FIGURE 14

DAST ARW-2 STABILITY MARGIN REQUIREMENTS

3.2.3.2 Reliability. Reliability and redundancy of the ACS shall be such that the overall probability of vehicle abort and loss is not significantly increased and is consistent with unmanned, limited time operation. System redundancy shall be utilized as required to achieve this goal.

3.2.3.3 Flying Qualities. The ACS and AFCS systems shall meet selected flying qualities of MIL-F-8785B (ASG) for a Class IV aircraft, Category B flight phase. The selected longitudinal and lateral-directional flying quality requirements to be used for design are summarized on Figure 15 and Figure 16.

3.2.3.4 Structural Safety Factor. A free flight safety factor of 1.5, consistent with manned transport criteria per FAR Part 25, shall be used for structural design.

3.2.3.5 Operational Environment. The active control system electronics shall be designed for the altitude, temperature and vibration environment specified in NASA-DFRC Process Specification 21-2 commensurate with 60,000 foot maximum test altitude.

3.2.3.6 Service Life. Design operational life of the active control system electronics shall be 100 hours, assuming a maximum of 50 flights over a five year period.

3.2.3.7 Electrical Power. Electrical power available for the wing control surfaces required by the ACS is approximately 43 amperes without modifications to the electrical system. The drone vehicle has 28 VDC electrical power.

3.2.3.8 Ground Computer and Telemetry. The AFCS and ACS shall be compatible with the ground computer and telemetry capabilities presented in Reference 1.

3.2.4 Critical Design and Test Conditions. The ACS and AFCS critical design conditions are shown on Figure 17. This figure shows the airspeed and Mach number for V_C, V_D and $1.2V_D$ that are representative of a transport aircraft. A flight test placard was set at Mach 0.86 because wind tunnel test data on the ARW-2 high aspect ratio supercritical wing was not available above Mach 0.81 to support the stability and control analysis.

The critical maneuver load design condition is the high angle of attack (+HAA) condition at sea level for maximum gross weight with testing at 10,000 feet. The difference in wing loads between the sea level condition and the test condition should be small because the upper left hand corner of the V-n diagram for sea level and 10,000 feet are almost identical. The lift coefficient at buffet does not change significantly with Mach number in the 0.3 to 0.4 range.

	LEVEL 1	LEVEL 3
PHUGOID MODE DAMPING	$\zeta_p > 0.04$	$T_2 > 55$ SECONDS
SHORT PERIOD DAMPING	$0.3 < \zeta_{sp} < 2.0$	$\zeta_{sp} > 0.15$
DUTCH ROLL DAMPING	$\zeta_d > 0.008$	$\zeta_d > 0.02$
DUTCH ROLL FREQUENCY (RAD/SEC)	$\omega_{n_d} > 0.4$	$\omega_{n_d} \gtrless 0.4$
DUTCH ROLL FREQUENCY - DAMPING PRODUCT (RAD/SEC)	$\zeta_d\omega_{n_d} > 0.15$	----
ROLL MODE TIME CONSTANT (SEC)	$\tau_R < 1.4$	$\tau_R < 10.0$
SPIRAL STABILITY-TIME TO DOUBLE AMPLITUDE (SEC)	$T_S > 20$	$T_S > 4$
LONGITUDINAL STATIC STABILITY	$\delta_S'/V > 0$	$\delta_S/V > 0$

FIGURE 15

SELECTED FLYING QUALITIES REQUIREMENTS, MIL-F-8785 CLASS IV, CATEGORY B
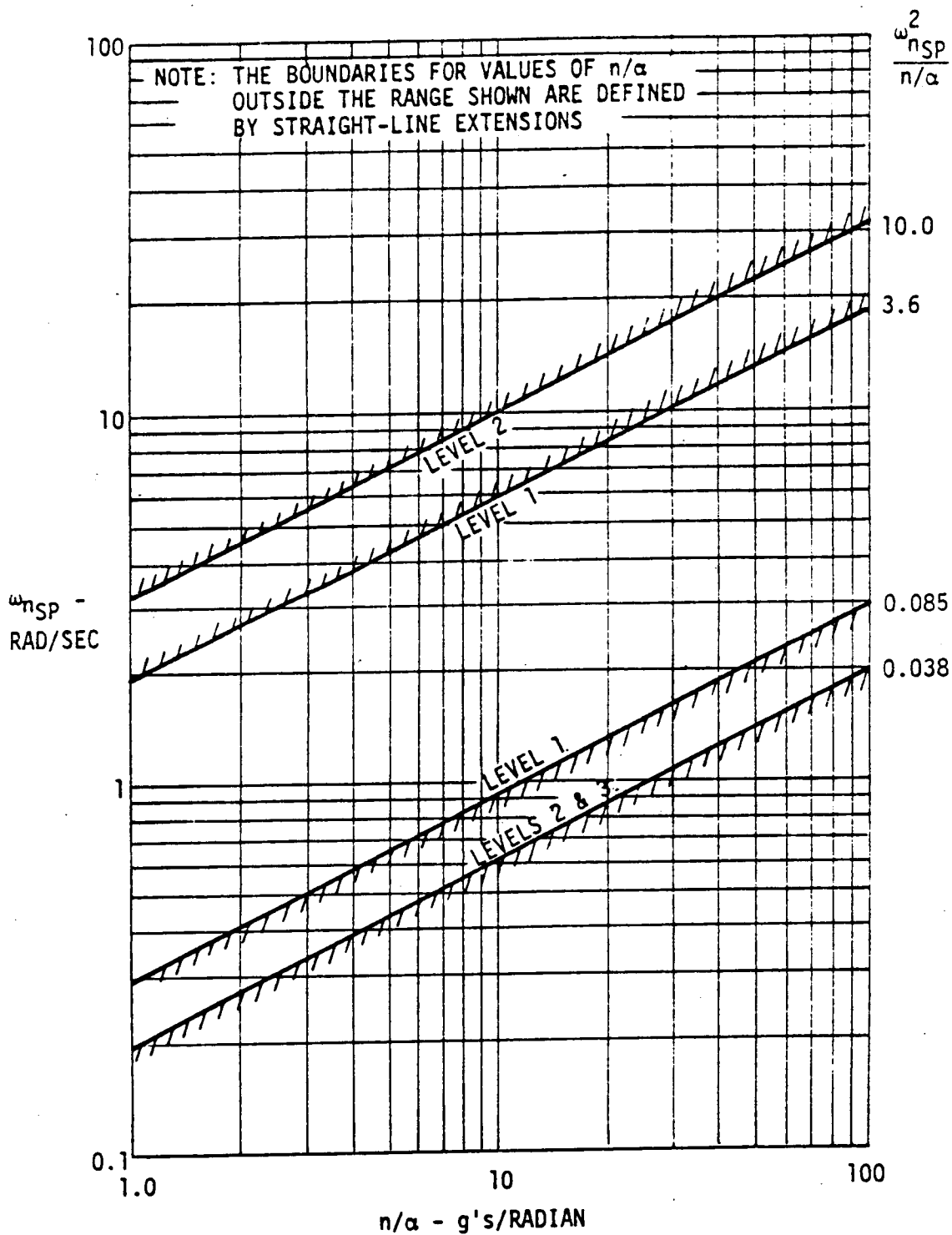
FIGURE 16

DAST ARW-2 SHORT-PERIOD REQUIREMENTS - CATEGORY B FLIGHT PHASE
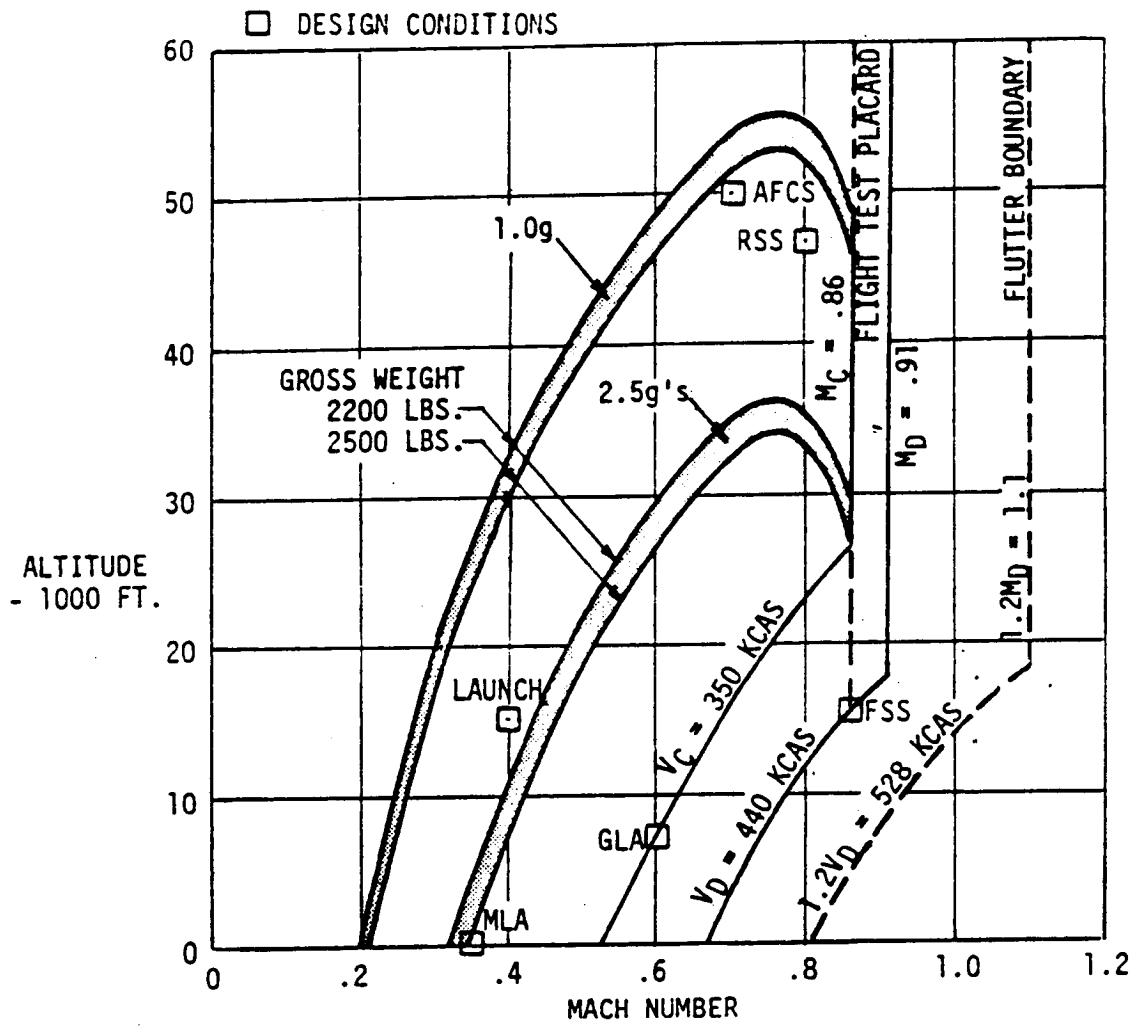
FIGURE 17

DAST ARW-2 OPERATIONAL FLIGHT ENVELOPE AND DESIGN CONDITIONS

The critical design and test condition for GLA is V_C (350 KCAS) at 7000 feet altitude.

The FSS is designed to be flutter free to 1.2 V_D at constant altitude and at constant Mach number. Testing shall be within the flight test envelope bounded by the placard at Mach 0.86 and V_D = 440 KCAS.

The primary RSS design and test condition is the Mach 0.8 cruise condition at 46,800 feet. The AFCS is required throughout the flight envelope.

The design C_L gross weight is 2350 pounds. This allows use of 150 pounds of fuel to launch and stabilize at the 46,800 foot test condition for load testing.

3.2.5 Flight Operation. The BQM-34E/F drone uses a Continental YJ69-T-406 engine with a rated static thrust of 1840 pounds at sea level. Characteristics of the drone engine are such that operation below 80 percent RPM is not recommended.

The DAST ARW-2 vehicle shall be launched from an inboard pylon on a B-52 aircraft.

The drone shall be installed on the launch vehicle pylon in an attitude so that it will have a -0.5g load factor at separation.

A single launch condition will be used for ACS and load testing.

Altitude:	15,000 feet
Mach Number:	0.4
Center-of-Gravity:	20 percent MAC
Airspeed:	100 KCAS
Gross Weight:	2500 Pounds

The ACS system shall be inoperative during captive flight. The AFCS and ACS systems will be designed to be inoperative for three seconds after separation from the launch aircraft.

The control surfaces added to the ARW-2 wing for the flutter suppression, maneuver load alleviation and gust load alleviation system shall be held in the faired position during separation of the drone from the launch aircraft. This requires that the hydraulic power supply unit and the servoactuator feedback electronics be turned on.

The DAST ARW-2 vehicle shall use an all movable horizontal tail surface as elevons for both pitch and roll control and a rudder on the vertical tail surface for yaw control. The ACS shall use wing control surfaces and tail surfaces as required. Capability shall be provided in the ACS electronics to use the wing control surfaces for roll control during separation, if required.

The ARW-2 vehicle shall be recovered by a helicopter using a Mid Air Recovery System (MARS). The RSS and AFCS shall remain active until the drag chute opens using a storage battery for electrical power.

50

4. AEROELASTIC AND DYNAMIC ANALYSIS

The final analysis cycle was conducted with small modifications to
structural stiffness and revised aerodynamics that match wind tunnel
test data of the 0.237 scale model. The revised aerodynamics, which
involved matching QSE stability derivatives and changes in control
surface modeling and effectiveness, significantly increased wing loads
at the gust load design condition. The revised structural stiffness did
not significantly affect wing loads. The airplane model also reflected
a relocation of fuselage ballast to shift the C.G. forward 12 percent
MAC at maximum gross weight.

Two different methods of incorporating aerodynamic effects into the
flexible EOM were utilized. One model was used for wing load analysis
and this model provided a close match of structural dynamic EOM to
elastically corrected wind tunnel data. The other model was used for
flutter analysis and provided an accurate description of airplane
structural vibration mode dynamics.

The revised airplane model predicted a 10 percent increase in the
critical load parameter of wing root vertical bending moment (WRVBM) at
the design gust condition and a 0.5 percent increase in WRVBM for design
maneuver. The previous analysis had predicted that the inboard section
of the wing was maneuver load critical; but due to the increased gust
load, the entire wing became gust load critical.

The increased gust load consequently resulted in a increased load level
with active gust load alleviation system, and a structural resizing
iteration cycle to increase wing strength was anticipated. However,
because the critical inboard section of the wing was previously maneuver
critical and because a large amount of conservatism had existed in the
previous design iteration stress analysis, a resizing iteration cycle
was not required. Additional stress analysis was completed which
included the load carrying capability of previously excluded wing
section redundant structural elements. The refined analysis indicated
positive safety margins at all critical stress points.

4.1 Structural Stiffness Update. As a result of the last stress
analysis in the previous study, some changes to the size of the front
and rear spars were required. Also, skin thickness at the attachment to
the spar and rib was revised. These changes were included in the wing
design, but had not been included in the analysis of wing structure and
ACS performance.

4.2 Aerodynamics for Wing Load Analysis. A technique for scaling
lifting surface theory aerodynamics to match test data was developed
during the last iteration as outlined in Section 5.5.2 of Reference 1.
In the previous iteration cycle, flexible EOM contained aerodynamic
effectiveness scaling which approximately matched rigid 0.237 scale

model tunnel data. For this analysis cycle, the EOM for wing load analyses were scaled to match QSE values for C_{L_α}, C_{M_α}, and $C_{M_{\delta\,STAB}}$ of Reference 4. This match provided close agreement of QSE and flexible EOM characteristics.

Aerodynamic scalers were defined for the forward body, wing and horizontal tail panels of Figure 18 using the iterative procedure shown on Figure 19. The scalers for the QSE match at each design or test Mach number are shown on Figure 20.

The wing control surface degrees of freedom in the loads analysis equations of motion were scaled through the use of scalers that match small surface planar doublet elastic C_{L_δ} to the QSE C_{L_δ}. The control surface effectiveness factors for the ARW-2 surfaces were assumed to be approximately the same as those for the smaller wind tunnel model surfaces. The effectiveness scalers for each Mach number are shown on Figure 21.

4.3 Aerodynamics for Flutter Analysis. Equations of motion for flutter analyses were developed using planar doublet aerodynamic influence matrices without scaling to match rigid body stability derivatives to either wind tunnel or QSE data. However, the wing control surface degrees of freedom were scaled to match the rigid C_{L_δ} values defined in the loads analysis EOM. The effectiveness scalers for flutter EOM are shown on Figure 22. Flutter boundary definitions and flutter suppression system analysis are presented in Paragraph 6.3.

4.4 Gust and Maneuver Loads. Total wing loads without the load alleviation systems and steady state 1g loads are shown on Figures 23 through 26 for gust and maneuver at the respective design conditions. Wing loads with the load alleviation systems are shown in Section 6.4.
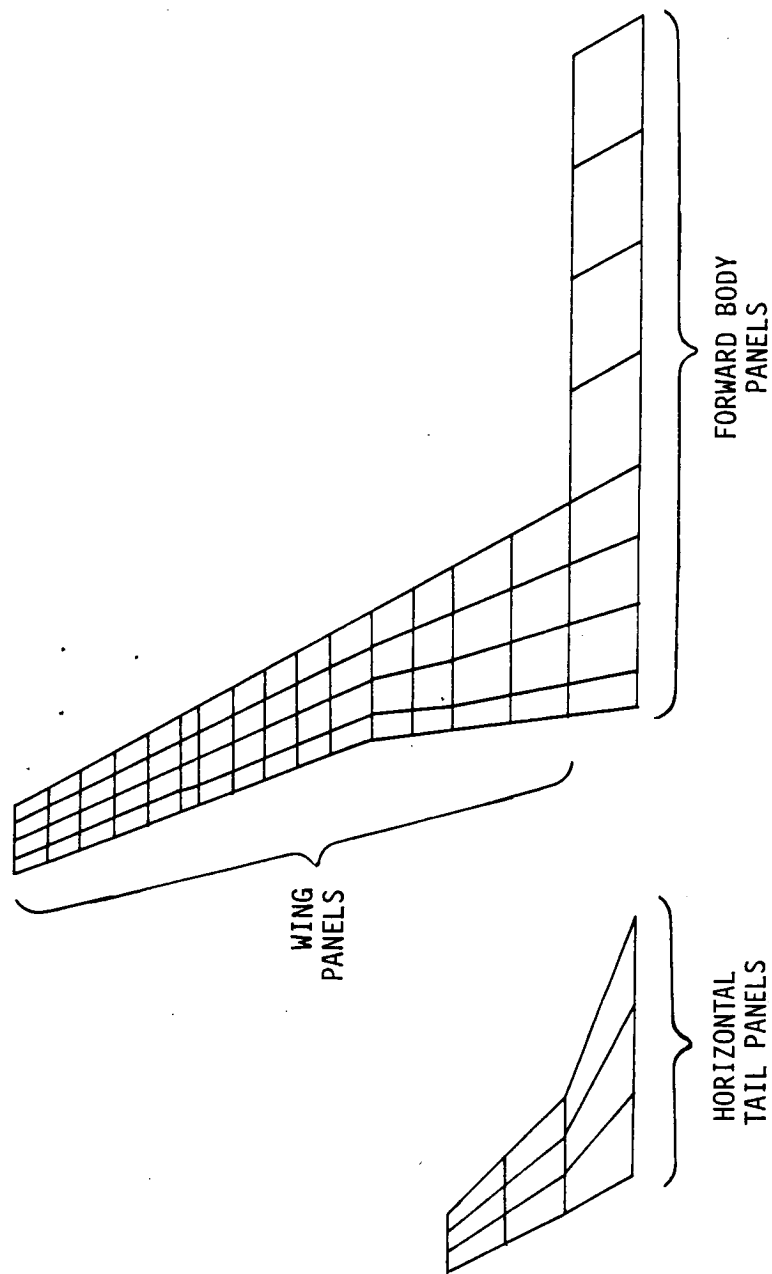
FIGURE 18

DAST ARW-2 AERODYNAMIC PANELS
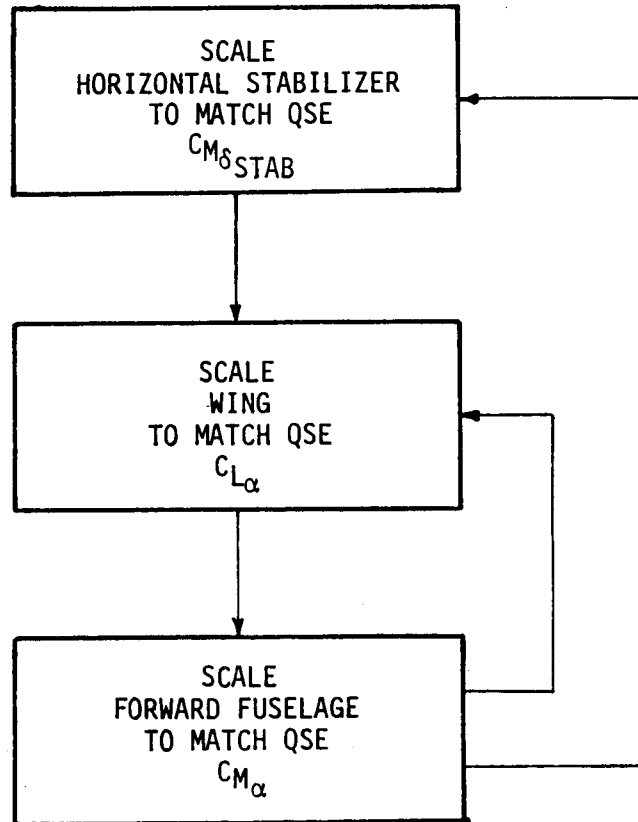
FIGURE 19

ITERATIVE PROCEDURE FOR MATCHING QSE STABILITY DERIVATIVES

54

MACH NO.	η_{FB}	η_{WG}	η_{HT}
0.35	0.855	1.047	0.937
0.40	0.868	1.020	0.938
0.60	0.880	1.064	0.969
0.70	1.035	0.933	0.945
0.80	0.785	1.150	0.971
0.86	1.021	1.040	0.954
0.91	1.000	1.000	0.950

FIGURE 20

AERODYNAMIC PANEL EFFECTIVENESS SCALERS

MACH NO.	INBOARD AILERON	OUTBOARD AILERON
0.35	0.852	0.643
0.40	0.882	0.667
0.60	0.745	0.645
0.70	0.931	0.800
0.80	0.571	0.500
0.86	0.518	0.514

FIGURE 21

WING CONTROL SURFACE EFFECTIVENESS SCALERS FOR LOAD ANALYSIS
EQUATIONS OF MOTION

55

MACH NO.	INBOARD AILERON	OUTBOARD AILERON
0.40	0.886	0.691
0.60	0.813	0.726
0.70	0.803	0.697
0.80	0.720	0.655
0.86	0.552	0.554

FIGURE 22

WING CONTROL SURFACE EFFECTIVENESS SCALERS FOR FLUTTER
ANALYSIS EQUATIONS OF MOTION
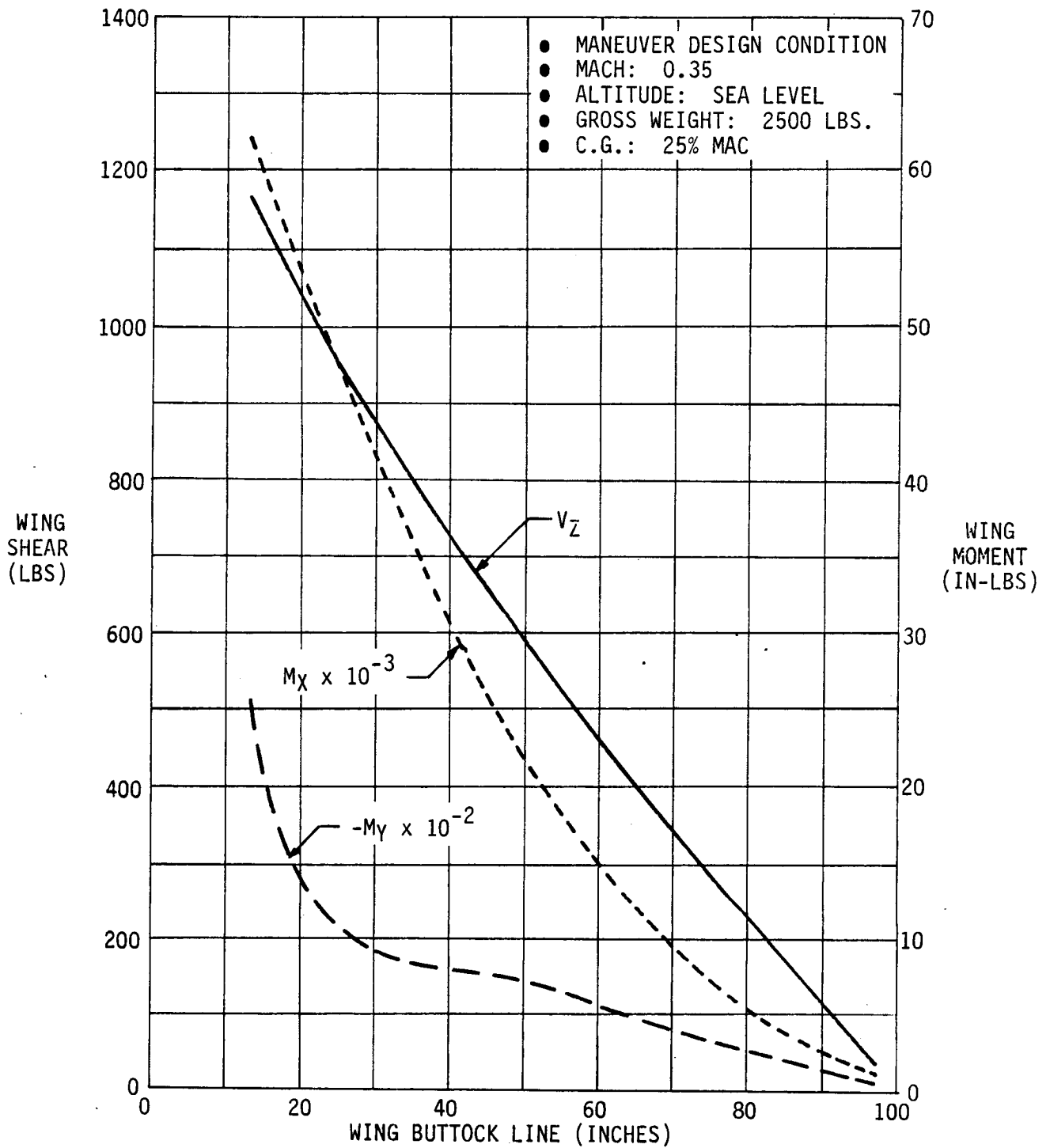
FIGURE 23

ARW-2 STEADY STATE (1g) WING LOADS AT THE MANEUVER DESIGN CONDITION
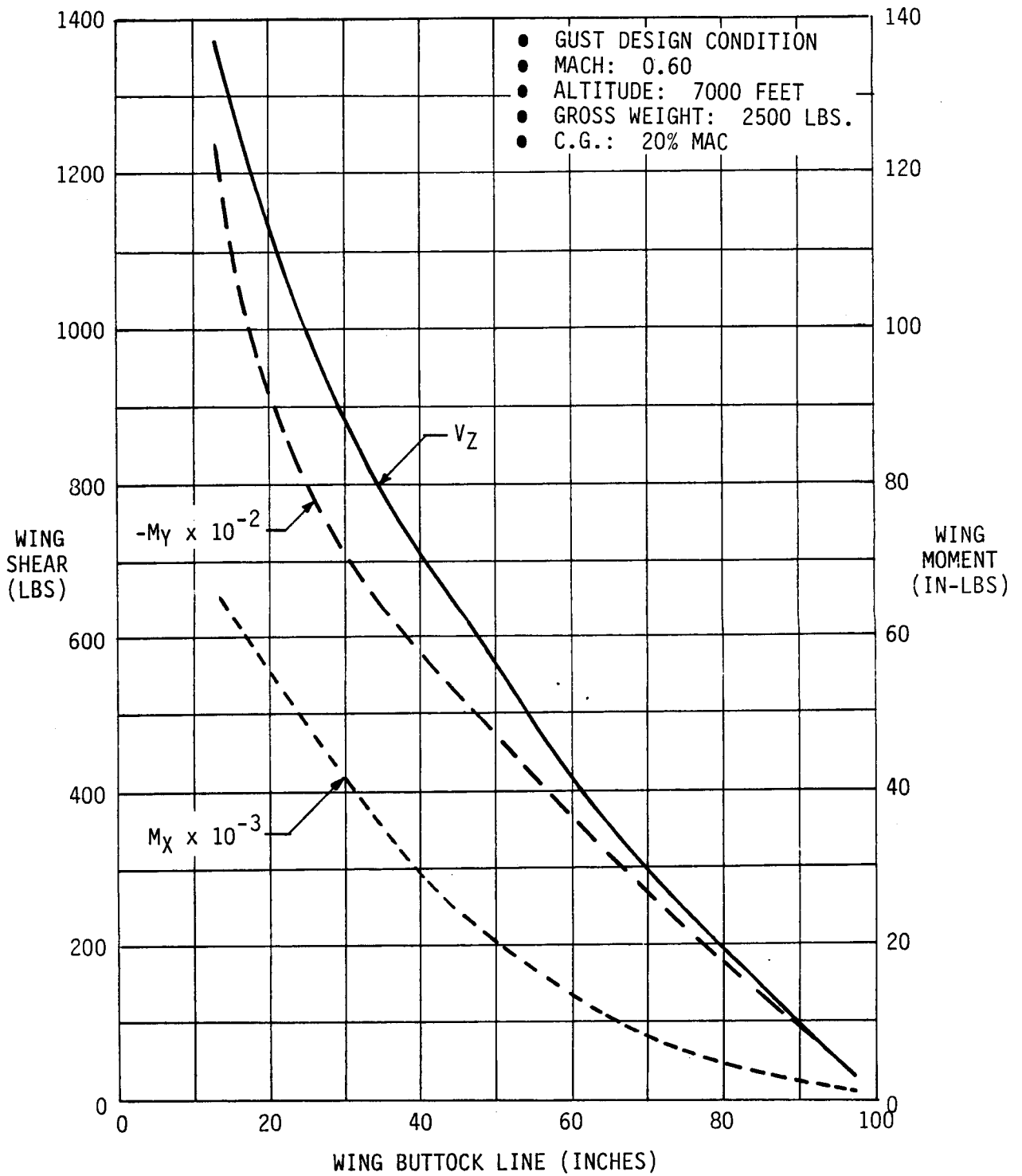
FIGURE 24

ARW-2 STEADY STATE (1g) WING LOADS AT THE GUST LOAD DESIGN CONDITION
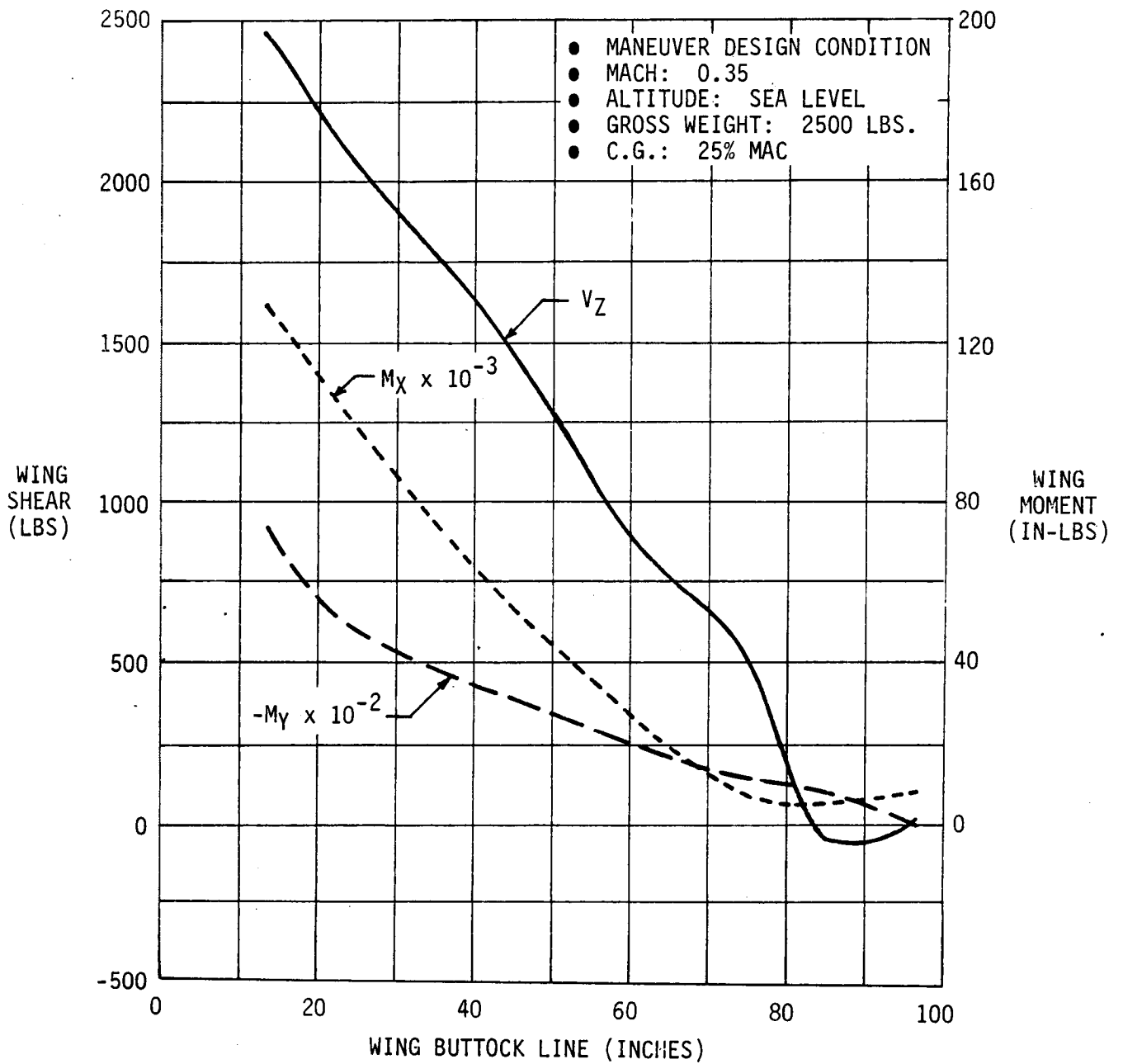
FIGURE 25

ARW-2 WING MANEUVER LOADS - WITHOUT ACS

59
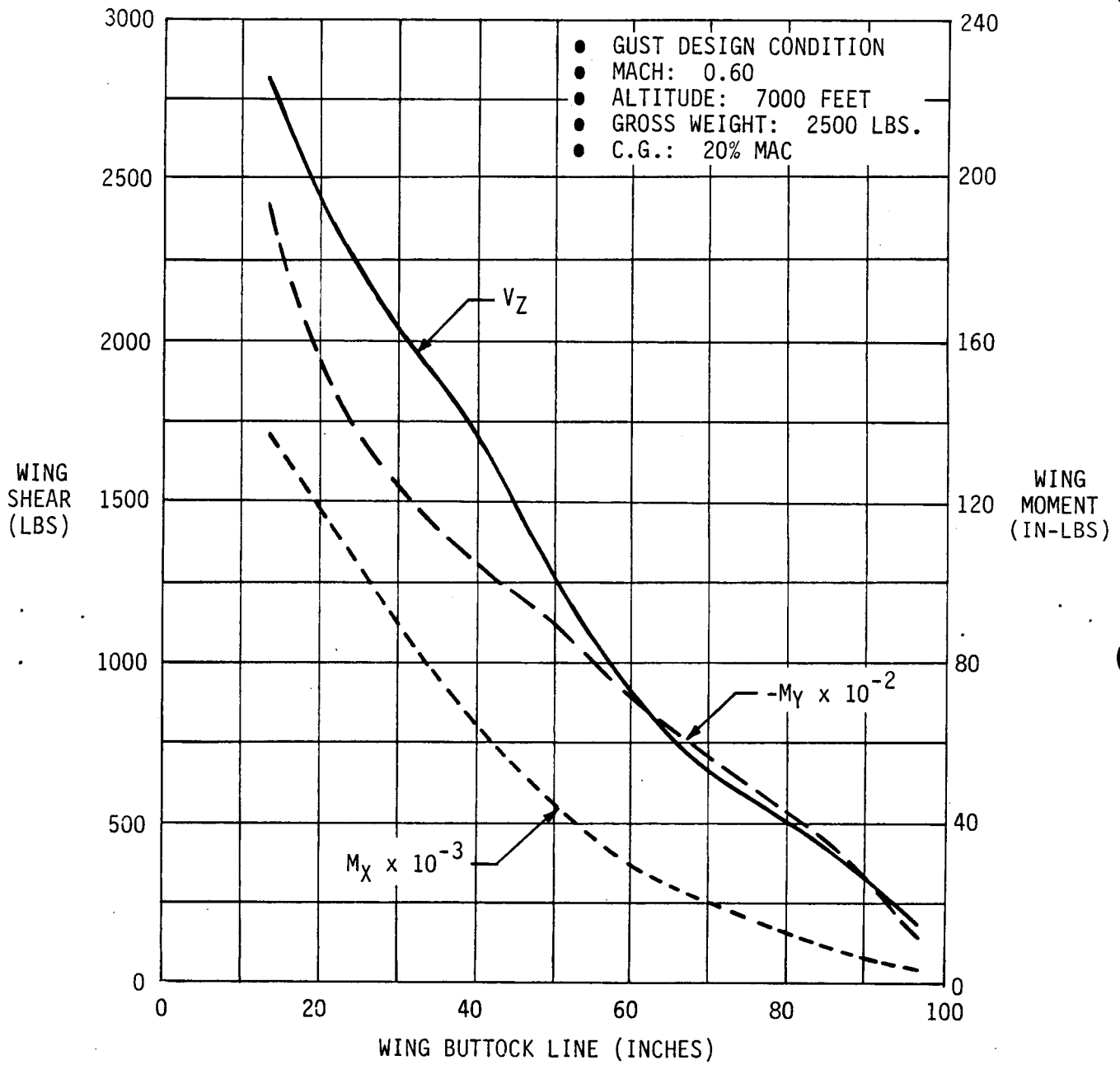
FIGURE 26

ARW-2 WING LOADS DUE TO GUST - WITHOUT ACS

5. STABILITY AND CONTROL ANALYSIS

An objective of this final design cycle iteration, prior to hardware implementation of the control systems, was to verify performance with airplane mathematical models containing elastically corrected wind tunnel test data for the 0.237 scale model. The only control systems evaluated with the latest aerodynamic data in the previous contract study were the lateral-directional systems discussed in Section 6.6.2. The data used in the previous contract study are documented in Reference 1.

The elastically corrected, 0.237 scale model tunnel data documented in Reference 4 was significantly different than the data available in the previous analysis. C.G. neutral points at the higher dynamic pressure conditions were significantly forward of the previous predictions. The neutral point varies over the flight range from 38.6 percent MAC at 1g cruise to 14.5 percent MAC at the maximum dynamic pressure condition.

Wing control surface tunnel data was corrected for revised size as well as elastic corrections.

Speed brake requirements for steady state flight with minimum engine RPM constraints were established. Speed brakes are required at launch and the maneuver load test condition.

Cruise trim drag was estimated for the range of C.G. positions to be controlled by the RSS system. The method of applying aerodynamic effectiveness scalers in the elastic structure EOM to match QSE aerodynamic coefficients as discussed in Section 4 was validated by the close agreement of QSE and elastic structure EOM dynamics.

5.1 QSE Stability Derivative Estimation. Quasi-static elastic aerodynamic data for the 0.237 scale model were generated by FLEXSTAB, a system of digital computer programs for predicting flexibility effects on airplane stability and control characteristics. QSE data for the DAST ARW-2 are contained in Boeing Document, D3-11542-1, DAST ARW-2 Piloted Simulator Aerodynamic Data based on 0.237 Scale Model Wind Tunnel Test Results, 7 March 1979.

Wind tunnel data for the wing control surfaces were not available at the time the QSE data were generated. After QSE data had been generated, wind tunnel tests were conducted with wing control surfaces. These test surfaces were smaller than the presently sized surfaces and elastic corrections for wing control surfaces were obtained from the digital programs that generated the elastic structure EOM. Two coefficients for each stability derivative were used to arrive at the QSE wing surface data. First, rigid control derivatives were estimated analytically for both wind tunnel test size surfaces and actual surface sizes. Ratios of actual to tunnel data were established from the estimate. These ratios are shown on Figure 27.

Rigid wing control surface derivatives with the scale factor of Figure 27 applied are shown on Figures 28 and 29.
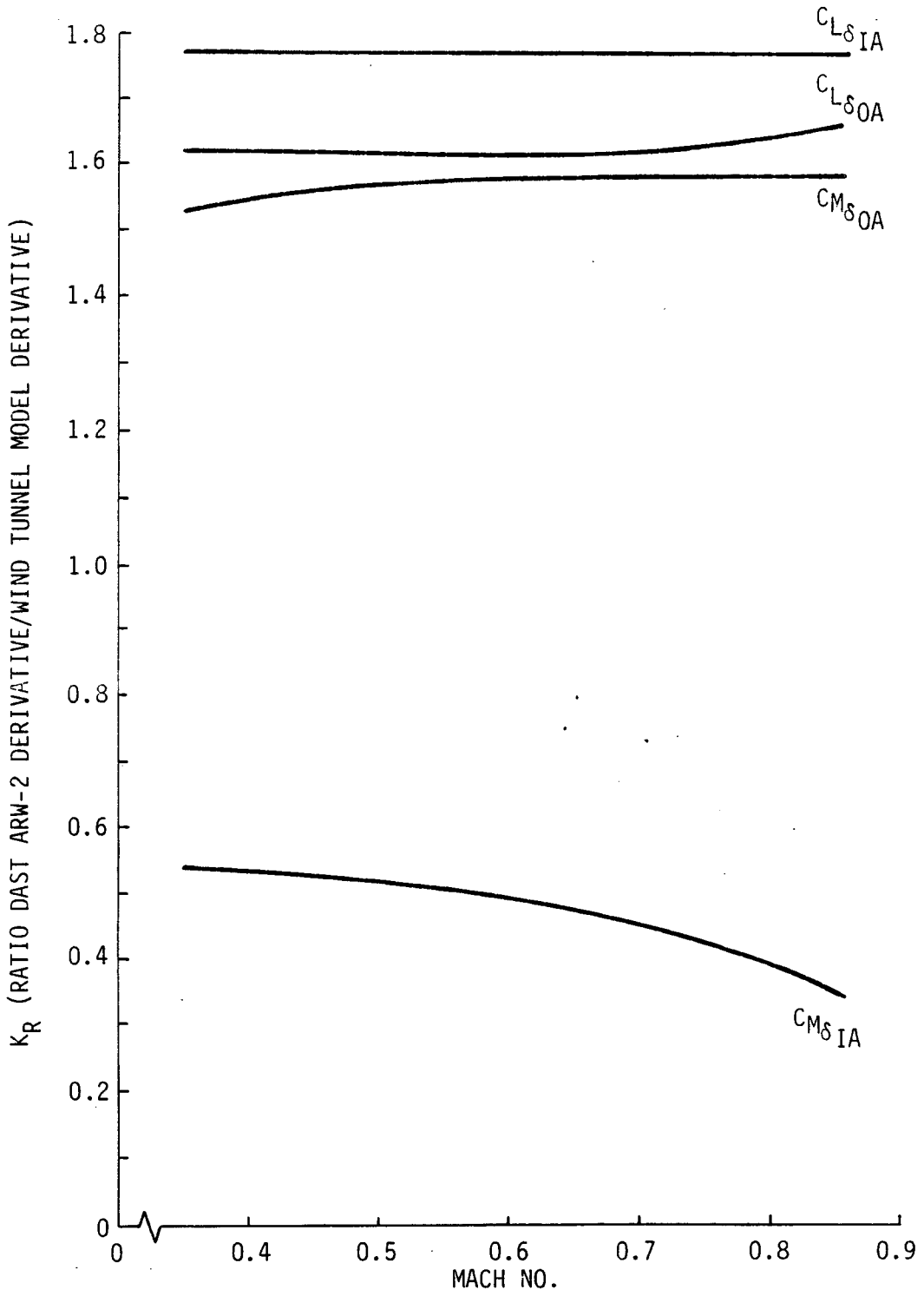
FIGURE 27

DAST ARW-2 WING CONTROL SURFACE SIZE CORRECTION RATIOS
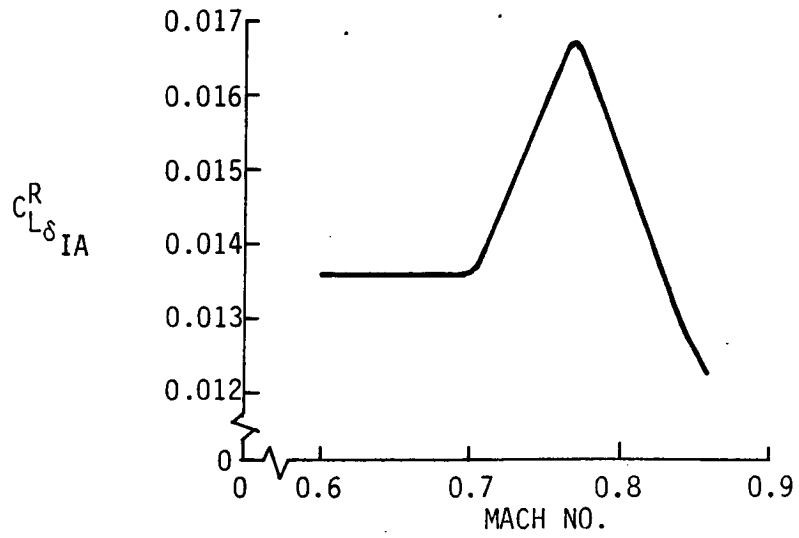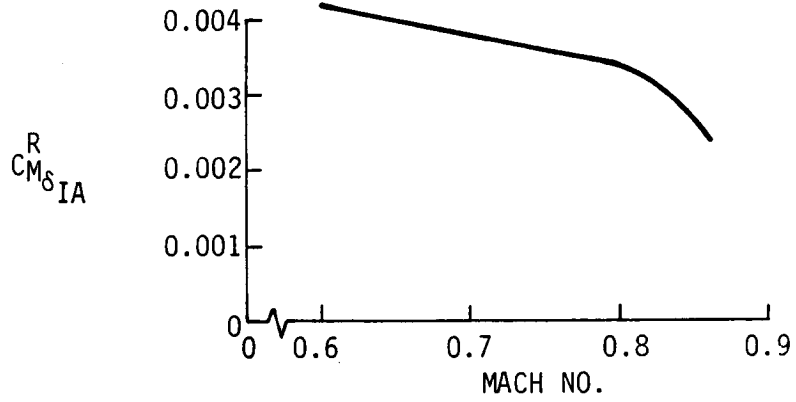
FIGURE 28

DAST ARW-2 INBOARD AILERON RIGID STABILITY DERIVATIVES

MACH NO.

$C_{M_\delta OA}^{R}$

$C_{L_\delta OA}^{R}$
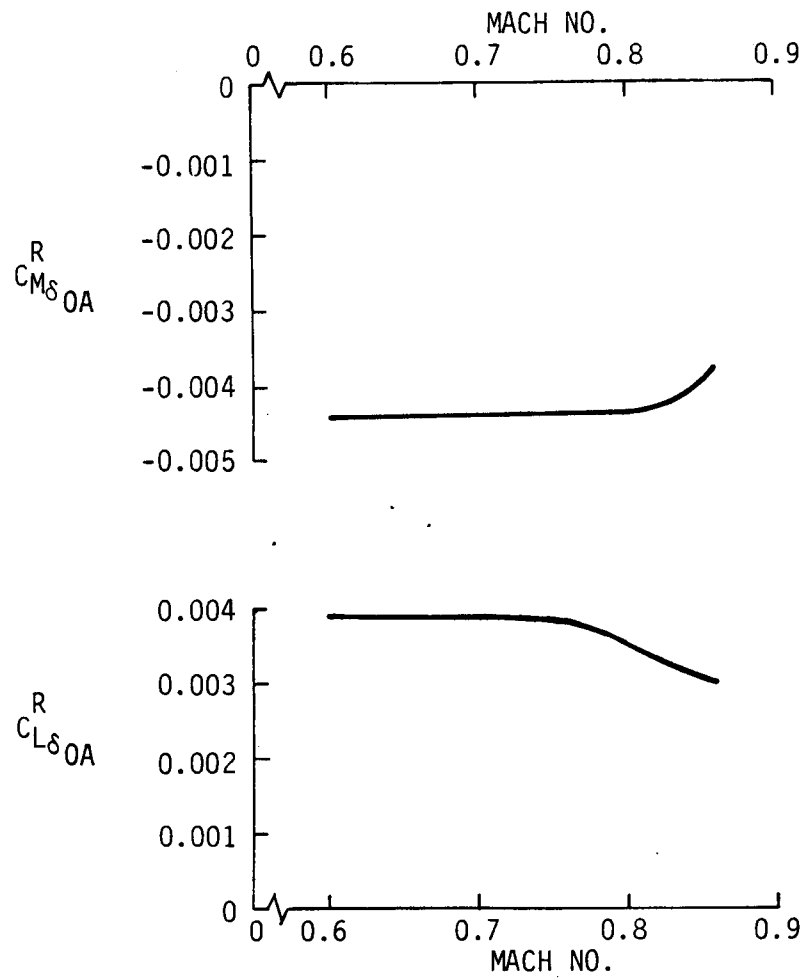
MACH NO.

FIGURE 29

DAST ARW-2 OUTBOARD AILERON RIGID STABILITY DERIVATIVES

Elastic correction factors for the actual surface sizes were computed as functions of dynamic pressure and Mach numbers. The elastic correction factors for the inboard and outboard lift and pitching moment coefficients are shown on Figures 30 and 31. Both correction factors above were applied to the rigid test derivatives to obtain the QSE surface data shown on Figures 32 through 35.

5.2 Speed Brake Requirements. Minimum thrust levels of the DAST vehicle engine requires that speed brakes be utilized at some test conditions. Aerodynamic drag data with speed brakes obtained from NASA Data Sheets for Wind Tunnel Test 833, June 1980 and thrust data generated by NASA DFRC are shown in Appendix A. Percent engine RPM to maintain steady-state flight test conditions as functions of speed brake setting is shown on Figure 36. Steady-state flight can be achieved at all design test conditions without speed brakes except MLA and launch. Fifty degrees speed brake is required at the MLA test condition and 55 degrees speed brake is required in the event a steady-state launch condition is to be maintained.

5.3 Neutral Point. Neutral points for the DAST ARW-2 design and test conditions, shown on Figure 37, were computed from the QSE aerodynamic data included in Appendix A and obtained from Boeing Document, D3-11542-1. Figure 37 shows the neutral points for 1g trimmed flight at each condition and also the neutral point for 1.2g flight at the cruise condition. Stability analysis was conducted at the 1.2g cruise condition due to the unstable characteristics of the pitching moment versus angle of attack at this point as shown on Figure 38.

The neutral points at some flight conditions are significantly forward of those obtained with the previous aerodynamic data estimates and the flight C.G. range was moved forward accordingly. The neutral point at launch is 29.7 percent MAC. A launch C.G. of 20 percent is selected to provide a stable air launch condition.

The C.G. range with fuel burn is from 20 to 32.8 percent MAC as shown on Figure 39. Neutral points at the maximum dynamic pressure condition and the 1.2g cruise condition of 14.5 and 16.7, respectively, and neutral points within the C.G. range at other flight conditions provide a broad range of stability characteristics both stable and unstable, which should be beneficial in flight test verification of the RSS system.

5.4 Minimum Trim Drag. DAST ARW-2 cruise trim drag, computed from the QSE data of Boeing Document D3-11542-1, is shown as a function of C.G. position on Figure 40. Minimum drag is well back of the selected flight C.G. range and is not attainable due to the highly unstable pitch characteristics at some flight conditions and available stabilizer authority. However, significant reduction in drag is obtained by operating at aft, unstable C.G. positions compared to operating at the most critical neutrally stable C.G. The RSS system, used to provide
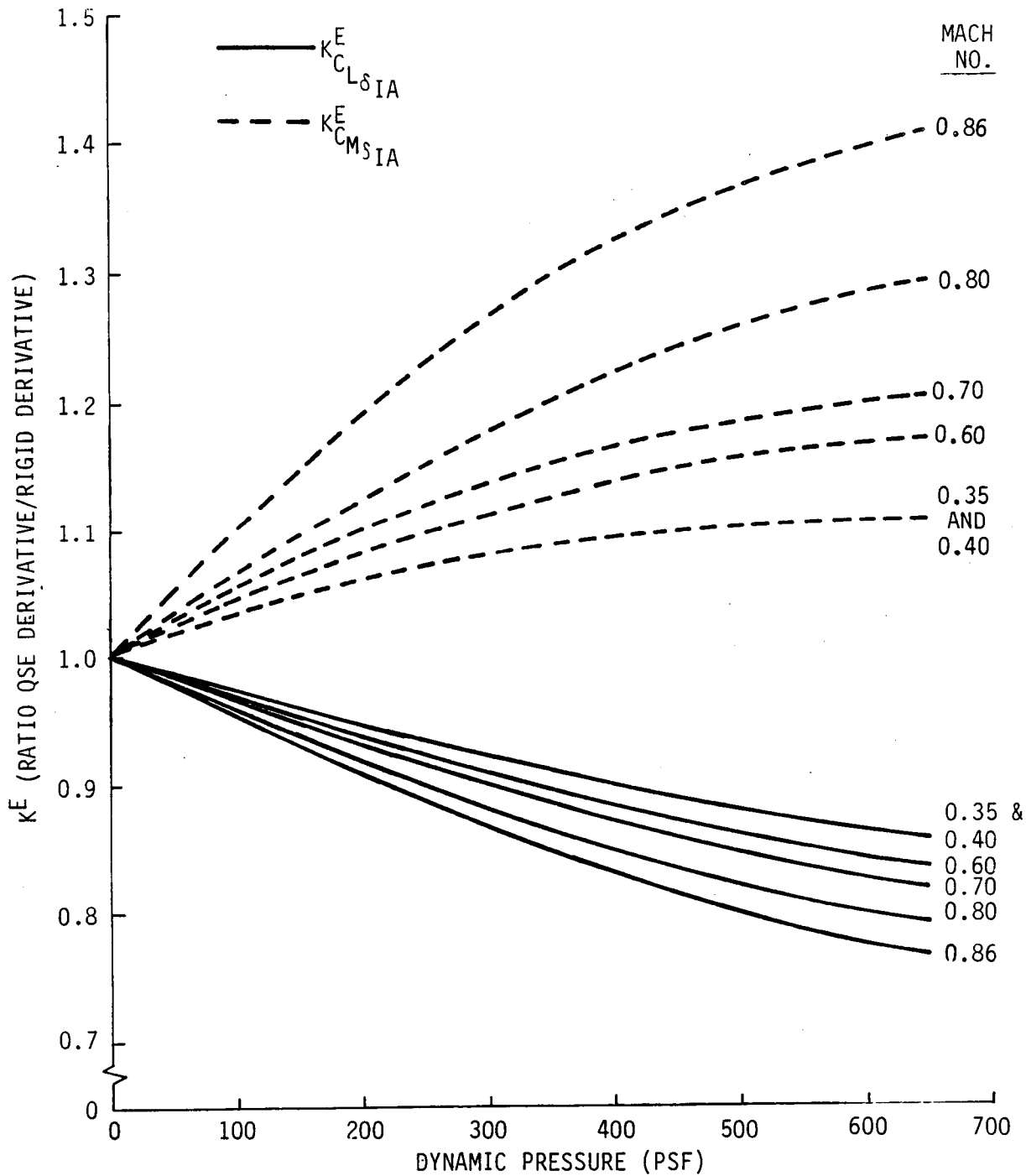
FIGURE 30

INBOARD AILERON ELASTIC CORRECTION FACTORS
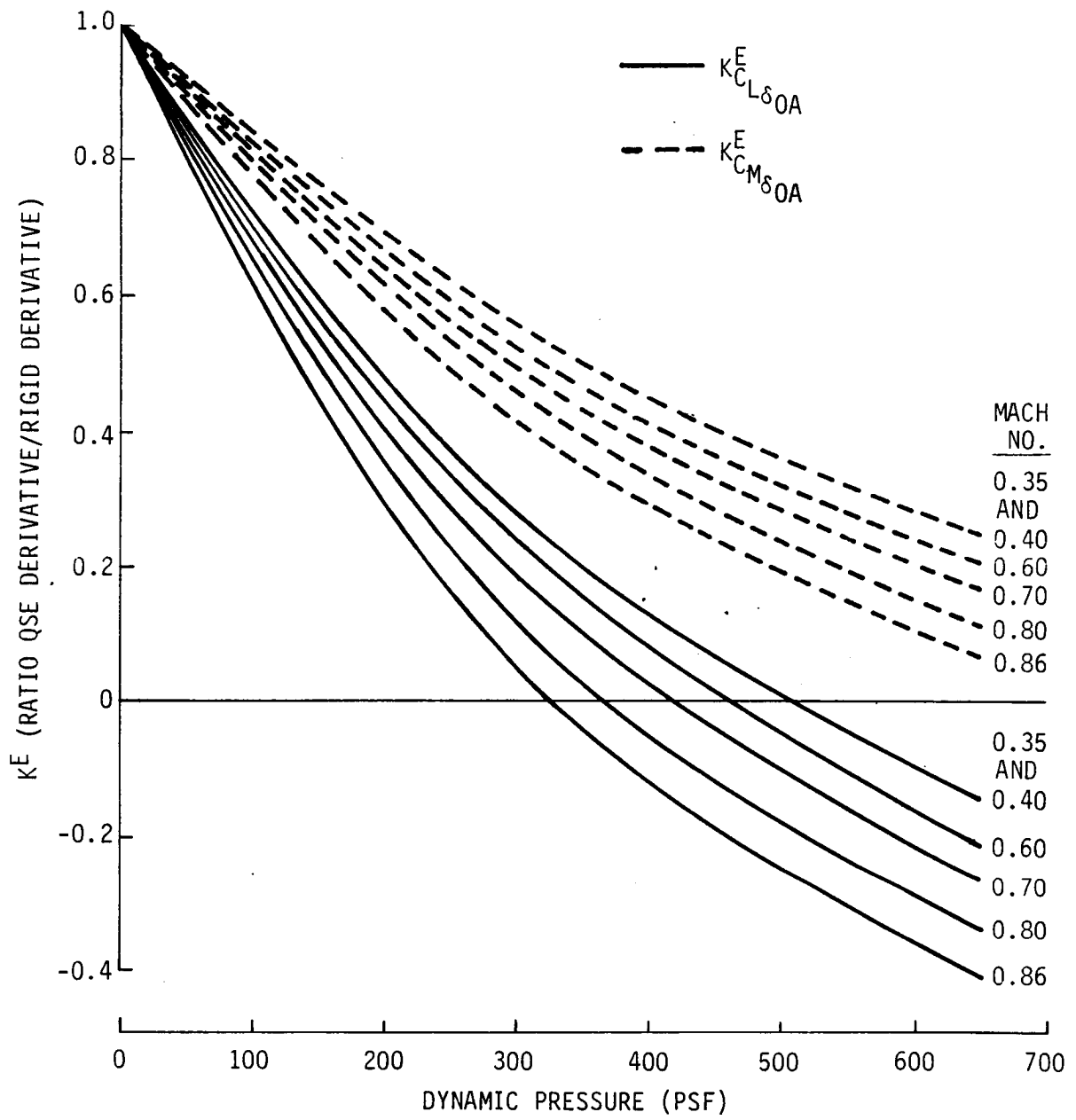
FIGURE 31

OUTBOARD AILERON ELASTIC CORRECTION FACTORS
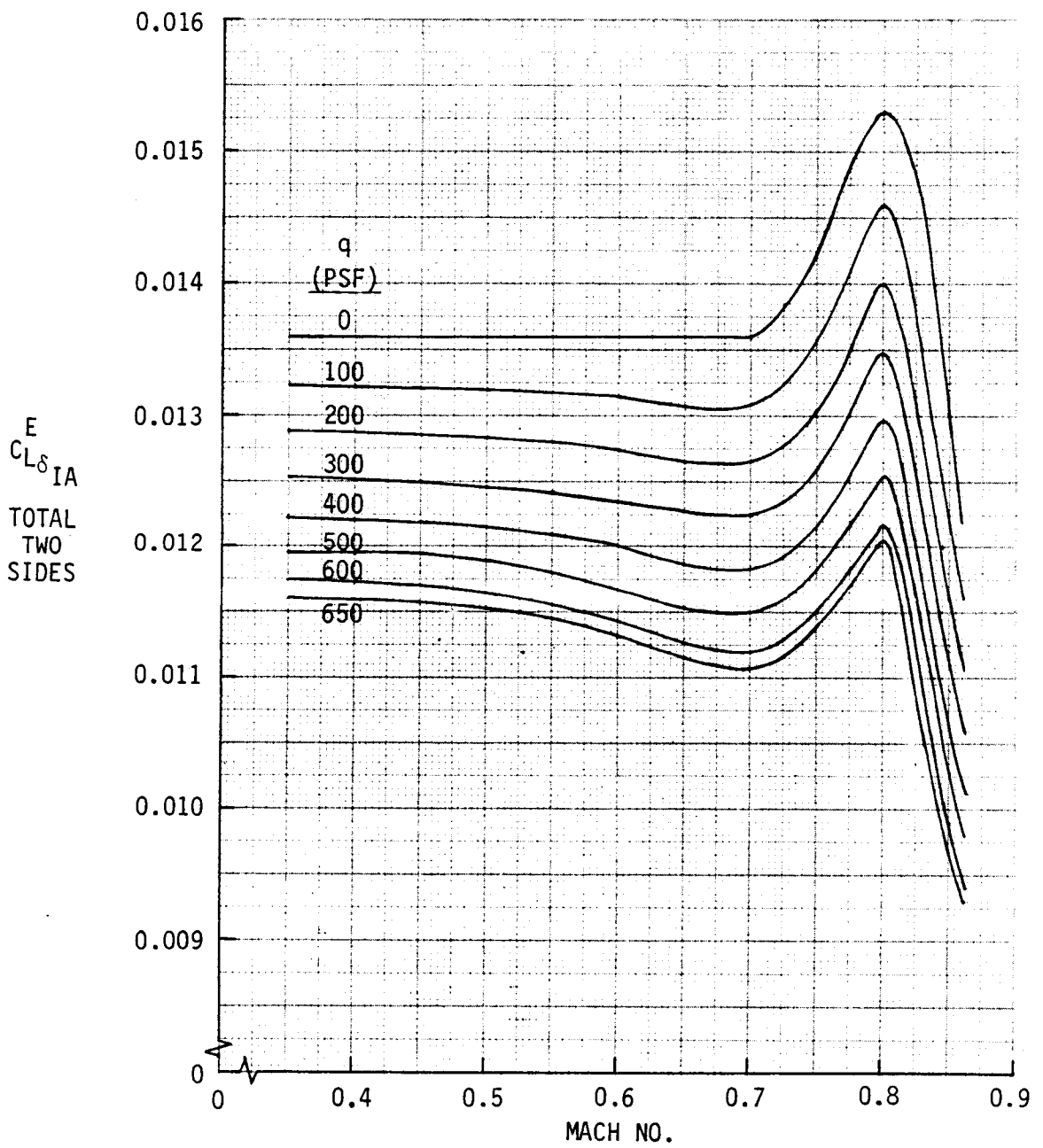
FIGURE 32

INBOARD AILERON QSE LIFT COEFFICIENT
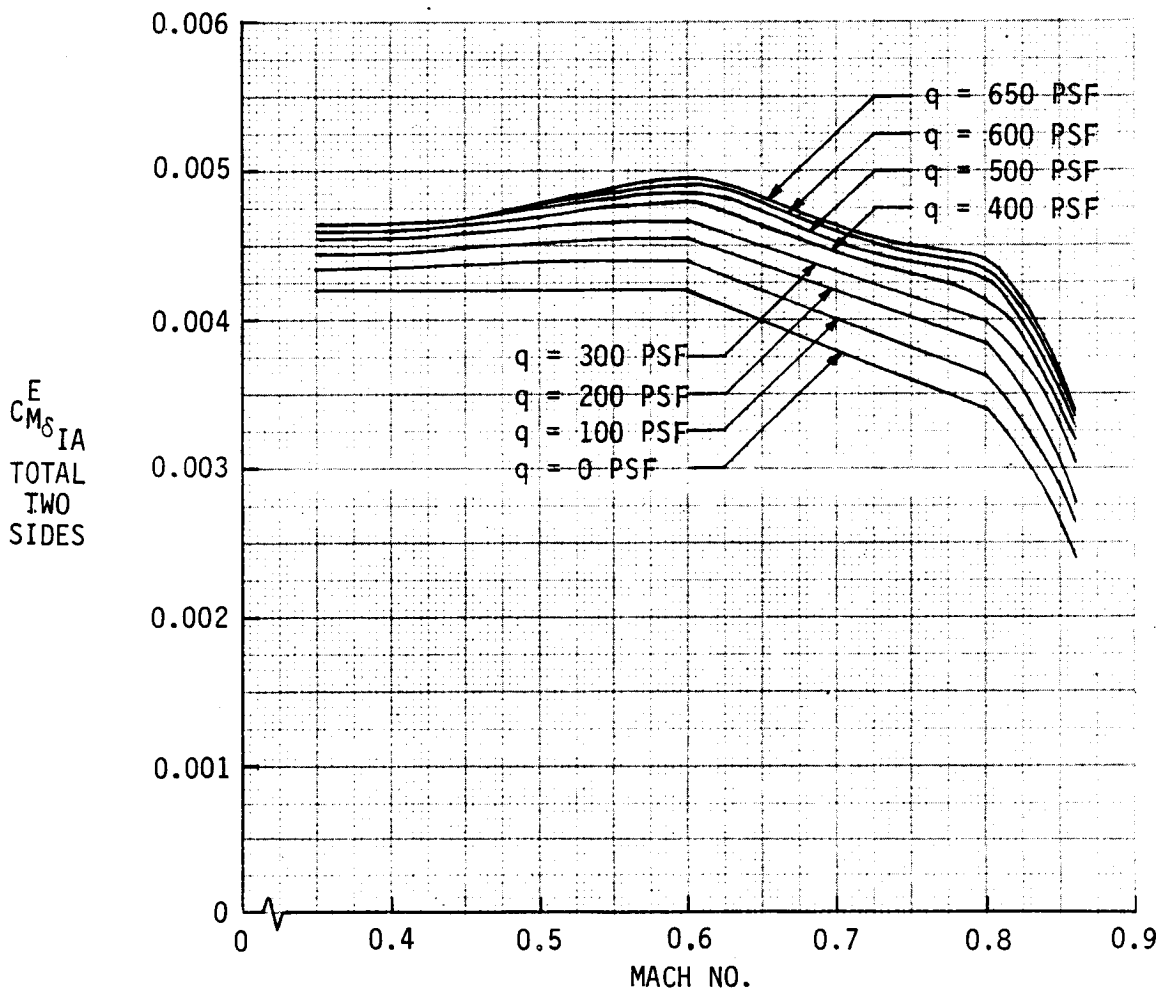
FIGURE 33

INBOARD AILERON QSE PITCHING MOMENT COEFFICIENT
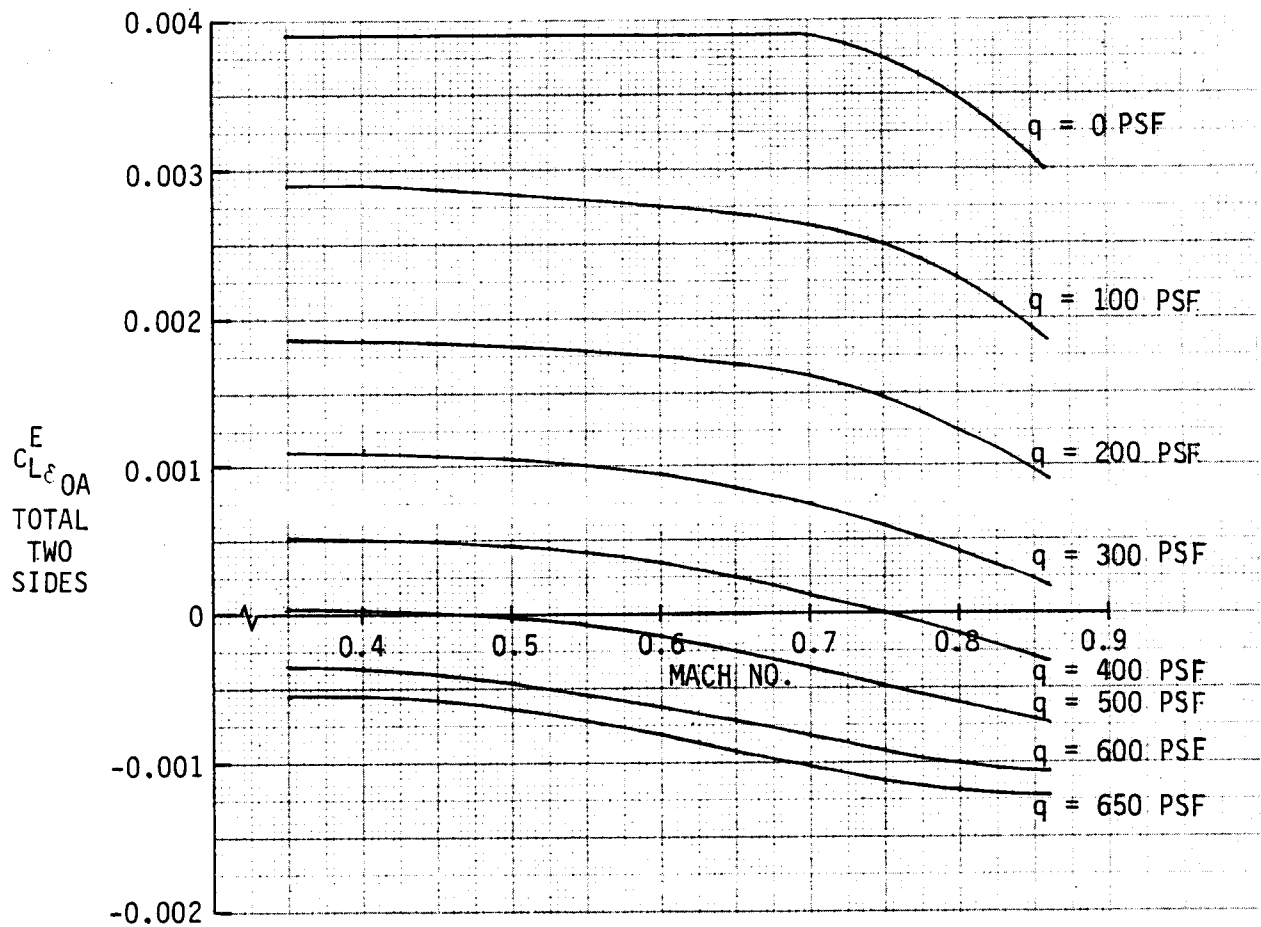
FIGURE 34

OUTBOARD AILERON QSE LIFT COEFFICIENT
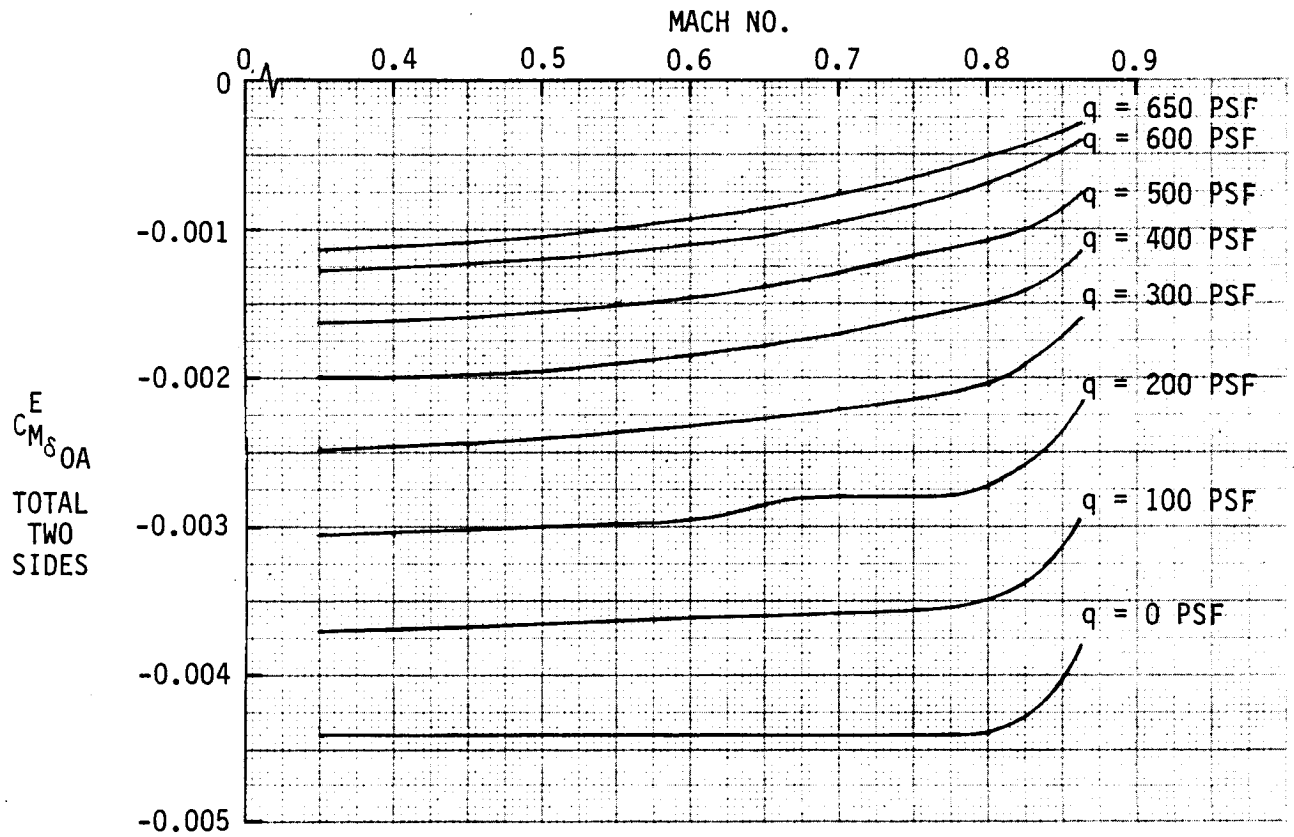
FIGURE 35

OUTBOARD AILERON QSE PITCHING MOMENT COEFFICIENT
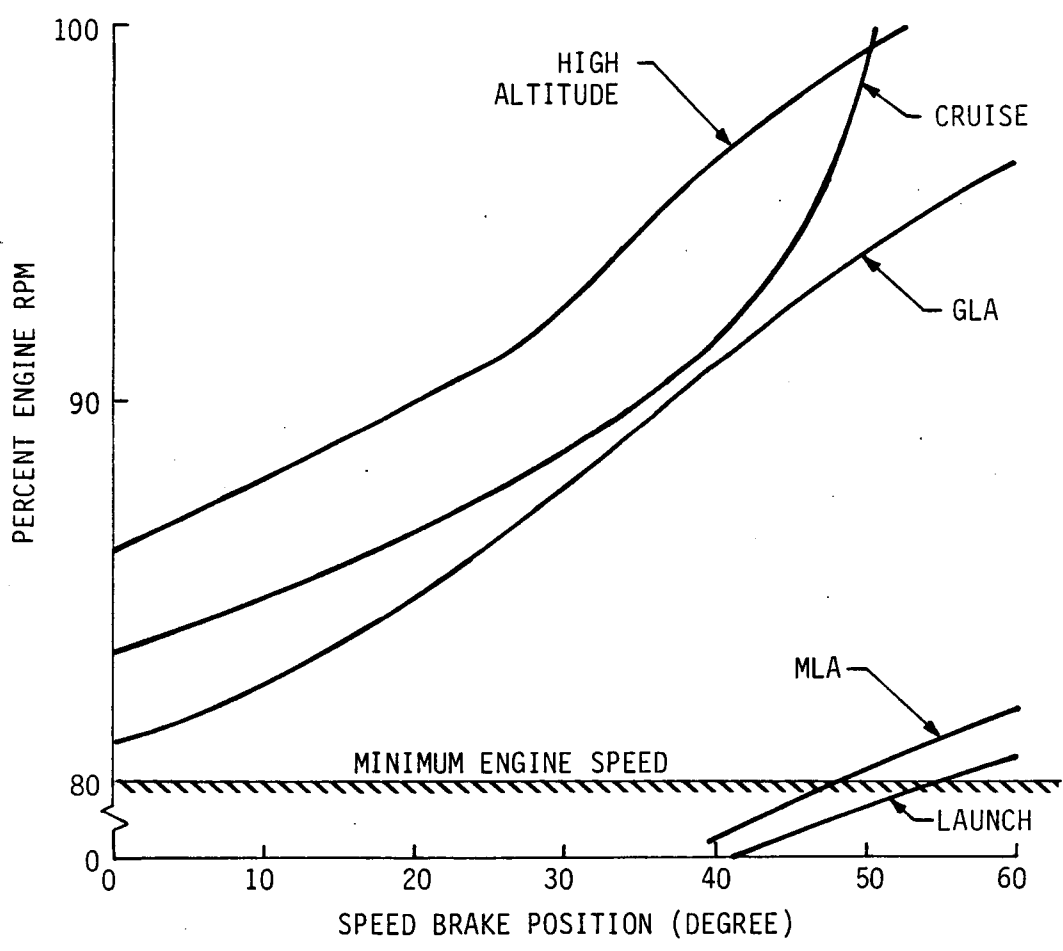
FIGURE 36

ENGINE RPM REQUIRED FOR STEADY STATE FLIGHT WITH SPEED BRAKE VARIATIONS

72

FLIGHT CONDITION			NEUTRAL POINT (PERCENT MAC)
CONDITION	MACH NO.	ALTITUDE (FEET)	
MANEUVER DESIGN	0.35	SEA LEVEL	30.0
MANEUVER TEST	0.42	10,000	28.9
LAUNCH	0.40	15,000	29.7
GUST DESIGN	0.60	7,000	27.2
GUST TEST	0.70	15,000	28.3
HIGH ALTITUDE	0.70	50,000	21.1
1g CRUISE	0.80	46,800	38.6
1.2g CRUISE	0.80	46,800	16.7
MAXIMUM q	0.86	15,000	14.5

FIGURE 37

DAST ARW-2 NEUTRAL POINTS

- MACH: 0.80
- ALTITUDE: 46,800 FEET
- GROSS WEIGHT: 2350 LBS.
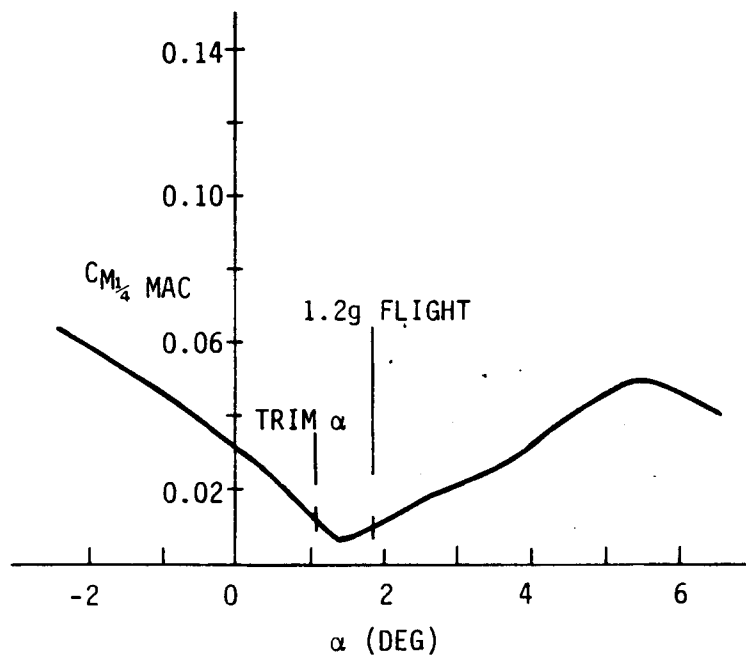
FIGURE 38

CRUISE CONDITION PITCH COEFFICIENT
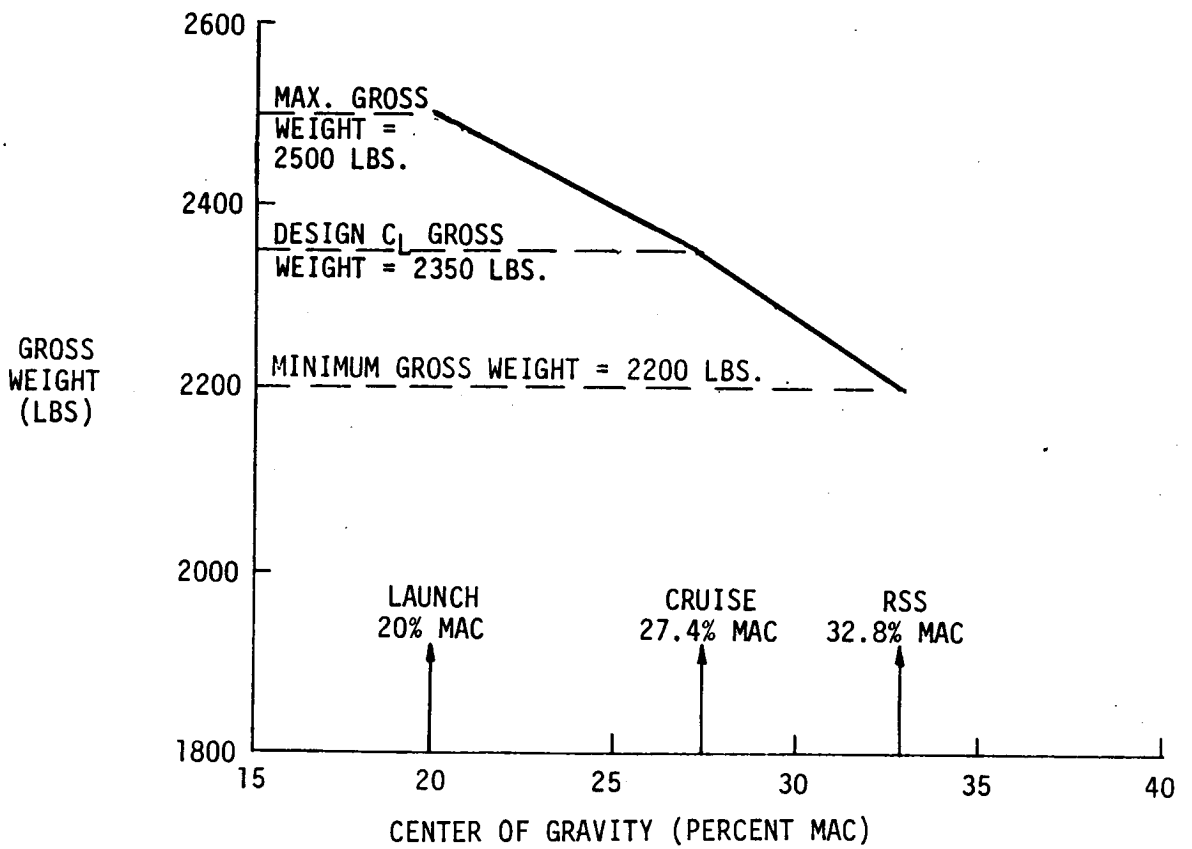
FIGURE 39

DAST ARW-2 CENTER OF GRAVITY VARIATION WITH FUEL USAGE

- MACH: 0.80
- ALTITUDE: 46,800 FEET
- GROSS WEIGHT: 2350 LBS.

CRITICAL NEUTRAL POINTS

MAXIMUM q⌐
CRUISE (1.2g)⌐

FLIGHT
C.G.
RANGE

CRUISE
DRAG
(LBS)

180 —
170 —
160 —
150 —

0   10   20   30   40   50   60

.C.G. (PERCENT MAC)
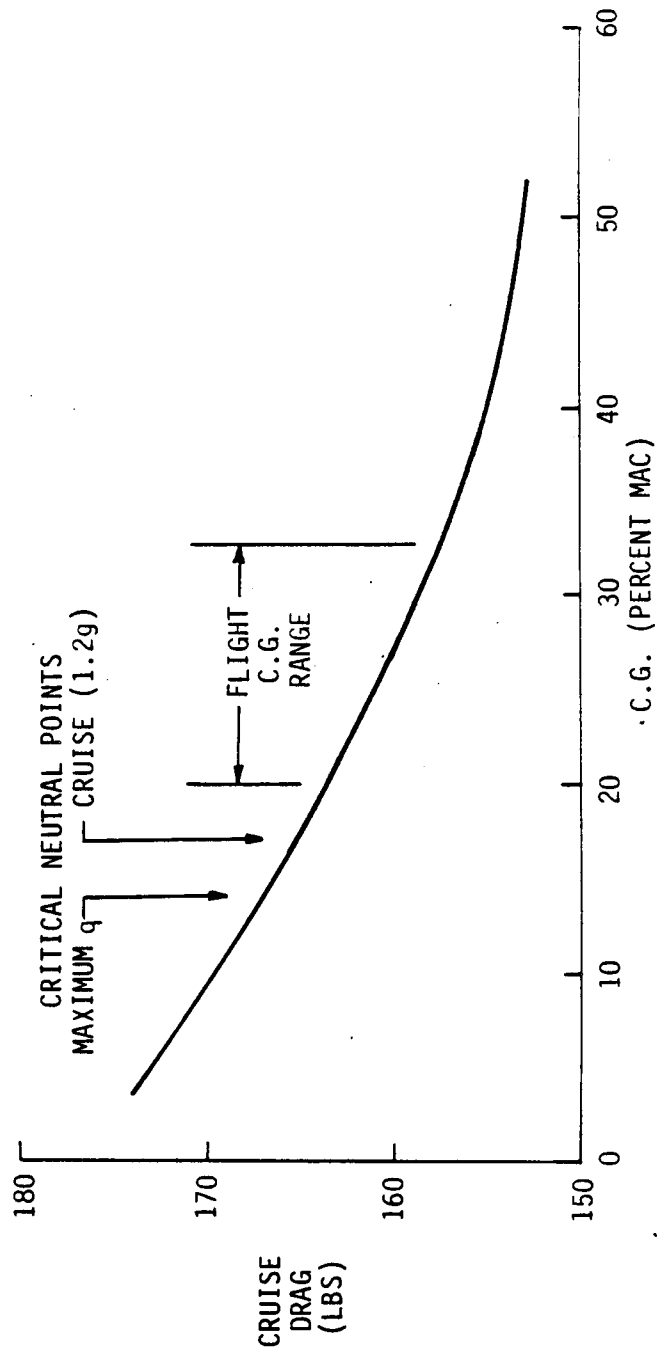
FIGURE 40

DAST ARW-2 TRIM DRAG VARIATION WITH C.G. POSITION

feedback controlled stability at the aft, unstable C.G. positions is discussed in Section 6.5.

5.5 Comparison of QSE and Flexible Equations of Motion. Both QSE and elastic EOM were used in the analysis and design of the ACS. As discussed in Section 4, the method of aerodynamically scaling the elastic EOM was modified to provide close agreement of the elastic EOM to QSE EOM. A comparison of QSE and elastic EOM characteristic roots at the design flight conditions is shown on Figure 41. At most conditions, a very close agreement exists. At the conditions where the least agreement exists, closing the system feedback loops reduces the difference in placement of the roots as shown on Figures 42 and 43.

CONDITION	QSE EQUATIONS		FLEXIBLE EQUATIONS	
	PHUGOID	SHORT PERIOD	PHUGOID	SHORT PERIOD
MLA DESIGN - MACH: 0.35 - ALT.: SEA LEVEL - C.G.: 20% MAC	$(S+0.0034 \pm j0.0701)$	$(S+0.7555 \pm j1.499)$	$(S+0.00339 \pm j0.1099)$	$(S+0.802 \pm j1.843)$
LAUNCH - MACH: 0.40 - ALT.: 15,000 FT. - C.G.: 20% MAC	$(S+0.0022 \pm j0.0614)$	$(S+0.513 \pm j1.276)$	$(S+0.00275 \pm j0.1034)$	$(S+0.545 \pm j1.557)$
GLA DESIGN - MACH: 0.60 - ALT.: 7,000 FT. - C.G.: 27.4% MAC	$(S+0.0075 \pm j0.1107)$	$(S+0.441)(S+1.988)$	$(S+0.0052 \pm j0.00558)$	$(S+1.11 \pm j1.1268)$
HIGH ALTITUDE - MACH: 0.70 - ALT.: 50,000 FT. - C.G.: 27.4% MAC	$(S+0.0004 \pm j0.0598)$	$(S-0.7448)(S+1.253)$	$(S+0.004 \pm j0.0686)$	$(S-0.717)(S+1.188)$
CRUISE - MACH: 0.80 - ALT.: 46,800 FT. - C.G.: 27.4% MAC	$(S+0.0064 \pm j0.0887)$	$(S+0.424 \pm j1.87)$	$(S+0.0024 \pm j0.058)$	$(S+0.395 \pm j2.06)$
MAXIMUM q - MACH: 0.86 - ALT.: 15,000 FT. - C.G.: 27.4% MAC	$(S+0.02)(S+0.2512)$	$(S-2.628)(S+5.693)$	$(S+0.0092 \pm j0.537)$	$(S-1.705)(S+4.467)$

FIGURE 41

COMPARISON OF QSE AND FLEXIBLE BASIC AIRPLANE CHARACTERISTIC ROOTS

- MACH: 0.60
- ALTITUDE: 7000 FEET
- C.G.: 27.4% MAC

- - - - QSE

———— ELASTIC

POINT "1" - OPERATING GAIN
(PREVIOUS RSS SYSTEM)
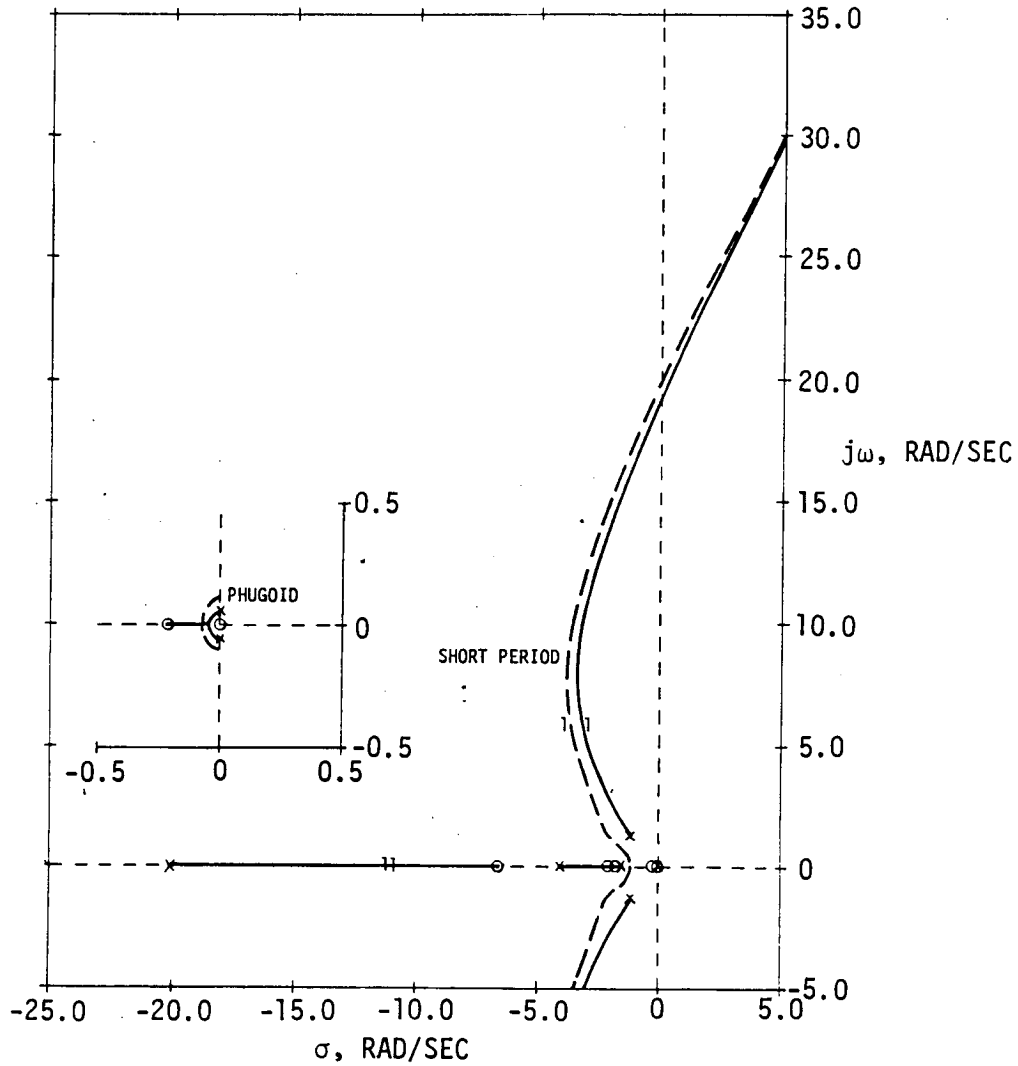
FIGURE 42

COMPARISON OF QSE AND FLEXIBLE MODEL RSS SYSTEM ROOT LOCUS AT
THE GLA DESIGN CONDITION

- MACH: 0.86
- ALTITUDE: 15,000 FEET
- C.G.: 27.4% MAC

- - - - QSE

———— ELASTIC

POINT "1" - OPERATING GAIN
(PREVIOUS RSS SYSTEM)
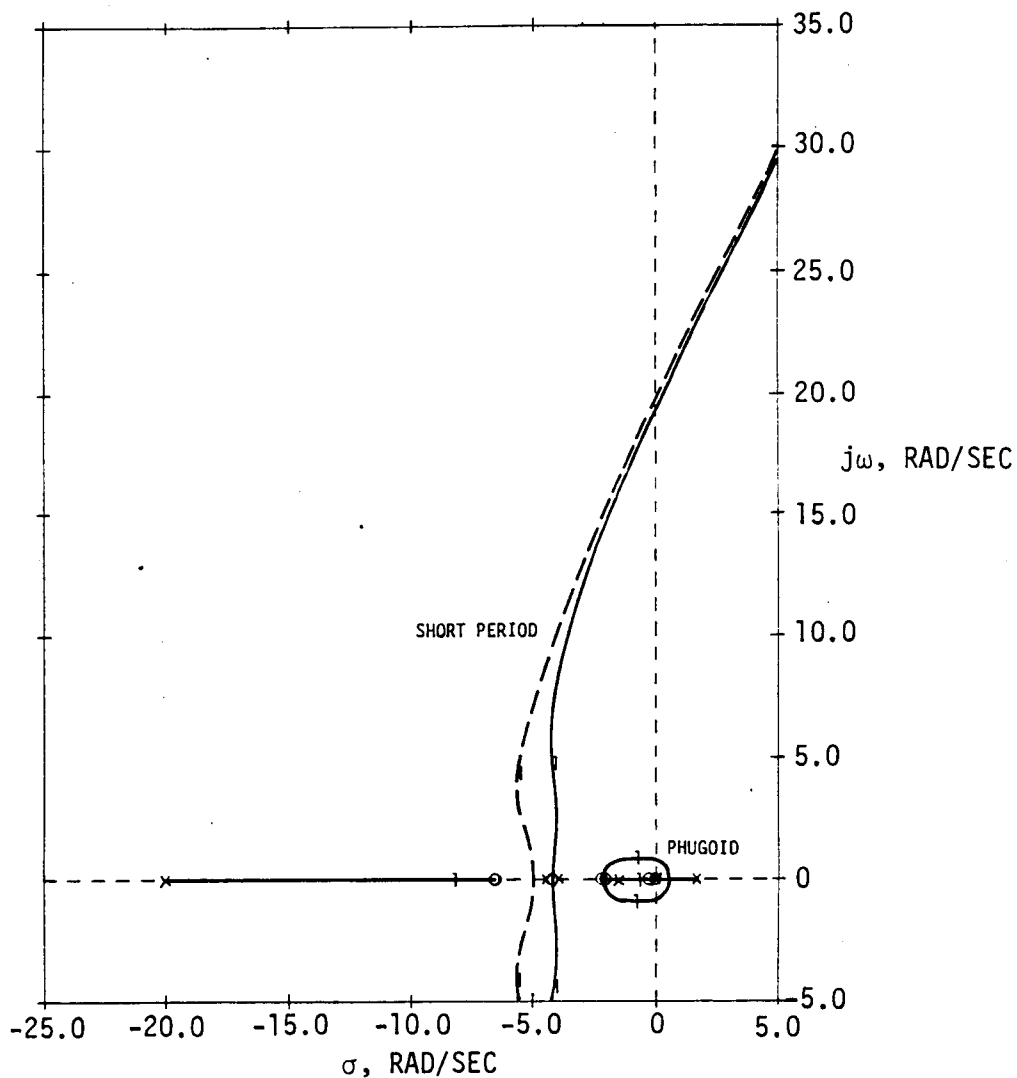
FIGURE 43

COMPARISON OF QSE AND FLEXIBLE MODEL RSS SYSTEM ROOT LOCUS AT
MAXIMUM DYNAMIC PRESSURE CONDITION

80

6. ACTIVE/AUTOMATIC FLIGHT CONTROL SYSTEMS SYNTHESIS

Active Control Systems (ACS) were synthesized as part of the integrated design of the DAST ARW-2 wing using conventional analytical techniques. This synthesis is described in detail in Reference 1. The ACS includes Gust Load Alleviation (GLA) and Maneuver Load Alleviation (MLA) to minimize wing structural strength, flutter suppression to suppress flutter up to 20 percent above design dive speed, and Relaxed Static Stability (RSS) to minimize trim drag.

In addition to the ACS, primary and backup Automatic Flight Control Systems (AFCS) were synthesized to provide longitudinal and lateral-directional dynamic stability. The primary AFCS, which will be implemented on the ground based computer, provides the intent of MIL-F-8785B Level 1 flying qualities. The backup AFCS provides qualities necessary to return the drone to a safe recovery area in case of failure in the primary AFCS ground computer loop. The AFCS for the lateral-directional axis provides Dutch roll damping, turn coordination, roll attitude command and conventional maneuver responses. The primary pitch AFCS and the RSS system provide angle of attack and vertical acceleration limiting through acceleration responses to operator pitch commands and also computes required MLA inboard aileron commands. The backup pitch AFCS limits angle of attack and produces a glide angle command system.

The synthesis conducted during the third design cycle iteration completed in this study and documented herein verified the structural and control system design with wind tunnel test data from the 0.237 scale ARW-2 model.

Brief summaries of synthesis and performance criteria used to design the ACS and AFCS and evaluate performance are presented in Paragraph 6.1 with more detailed presentation in Paragraph 3.2.

Servoactuator models were developed and synthesized with a goal to provide an analytical model that would more closely predict hardware test results. Because of some unpredictable nonlinear characteristics such as friction, changes in bulk modulus and minimum feedback relationships, the bandwidth predicted by analysis is difficult to realize with hardware; however a model was developed and finalized during testing. The model definitions, analysis and test results are presented in Paragraph 6.2.

Paragraph 6.3 discusses the Flutter Supression System (FSS) and its improvement in flutter speed. The FSS provides structural damping that meets FAR Part 25 to 1.2 V_D up to 15,000 feet altitude and 20 percent margin above the placard test speed.

Synthesis and performance evaluation of the gust and maneuver load alleviation systems are presented in Paragraph 6.4. Results indicate that the MLA and GLA systems reduce maximum wing design loads by approximately 18 percent.

The use of an RSS system to provide stability and flying qualities at reduced trim drag is presented in Paragraph 6.5. Although minimum trim drag cannot be achieved, the RSS system permits flight at aft unstable C.G. positions to take advantage of reduced trim drag.

The primary and backup AFCS were reevaluated using revised aerodynamics and physical properties and the results are discussed in Paragraph 6.6. The longitudinal primary AFCS was revised to be more compatible with larger variations in aerodynamic characteristics at different flight conditions.

Paragraph 6.7 discusses the evaluation of control authority of the DAST stabilizer configuration. Analysis indicates more positive stabilizer authority is desirable.

Control system compatibility is discussed in Paragraph 6.8 and analysis indicates that system capability is satisfactory and no airplane mode destabilization exceeds requirements.

Computer implementation of the ground based control systems is discussed in Paragraph 6.9. Flow diagrams and difference equations are presented in this discussion.

6.1 Performance and Synthesis Criteria. The GLA and MLA systems were to be critical systems minimizing structural strength and stiffness by reducing wing root bending moment by approximately 20 percent.

The ARW-2 wing without FSS was to exhibit flutter within the flight envelope. With FSS the flutter boundary was to be extended to 1.2 V_D.

The goal of the RSS system was to provide stability and flying qualities as required to operate the drone with center of gravity at the minimum trim drag condition. A stable launch condition was required with an inoperative RSS system.

Flying quality criteria were per MIL-F-8785B for a Class IV, Category B, aircraft. The ACS and AFCS were to provide the intent of Level 1 flying qualities in the primary mode and Level 3 flying qualities in the backup mode (primary mode inoperative).

The wing control surfaces were to be typical of a transport design, trailing edge surfaces with similar effectivenesses and locations. All ACS systems were to be compatible and capable of operating simultaneously as one system.

82

Minimum stability margins taken from MIL-F-9490D are given on Figure 14.

The design gust velocity envelope and ramp type maneuver used to design the GLA and MLA systems are presented on Figures 12 and 13. The design peak gust level was 62 ft/sec except the design gust level for the FSS synthesis was 12 ft/sec peak (6 ft/sec RMS at 2σ level). Design limit wing maneuver loads were determined for maneuvering load factors of +2.5 and -1.0 per FAR Part 25.

Electrical power available for the ACS wing control surface servoactuators was 43 amperes at 28 VDC.

Control surface maximum displacement and rate requirements are shown on Figure 44. Analysis was conducted to determine maximum control activity in random turbulence to determine these displacement and rate requirements. A Von Karman spectrum with a characteristic gust scale length of 2500 feet was used to represent the random atmospheric turbulence characteristics. Aileron RMS displacement and rate per unit gust at the design and test conditions were determined. The results of the Power Spectral Density (PSD) symmetric analysis for the outboard ailerons at the FSS test condition are shown on Figure 45. The contributions from antisymmetric are negligible and are not shown.

The servoactuator requirements are summarized and presented on Figure 46. These requirements are based on estimated hinge moments and PSD analysis. Also shown on this figure are NASA actuator test results for comparison to the requirements.

6.2 Servoactuator Models. Math models were developed and used during previous NASA contracts. Test results did not compare favorably with results obtained from analysis. These analyses results are documented in References 2 and 3 and the test results are documented in Appendix B. A model is required that can predict the implemented servoactuator performance, however, because of some unpredictable nonlinear characteristics such as friction, changes in bulk modulus and pressure feedback relationships, the bandwidth predicted by analysis is difficult to realize with hardware. The effort to derive a workable model is described by the following paragraphs. The final result eliminates pressure feedback and limits the servoactuators to a 50 Hz bandwidth which provides reasonably predictable test results.

6.2.1 Initial Servoactuator Model. The closed loop servoactuator dominant frequency mode predicted by analysis was approximately 110 Hz, however, the dominant mode obtained during hardware testing was approximately 70 Hz. A comparison of analysis and test results using the DAST ARW-1 parameters is shown on Figure 47. Further testing indicated that hydraulic line lengths had little effect upon the closed loop bandwidth as shown by the frequency responses of Figure 48 although hydraulic frequencies and loop stability are affected by line lengths.

MANEUVER

SURFACE	DISPLACEMENT (DEGREES)	RATE (DEG/SEC)
INBOARD AILERON	20	50
OUTBOARD AILERON	15	29
STABILIZER (FROM TRIM)	4	8

GUST

SURFACE	GLA DESIGN 62 FPS PEAK GUST DISPLACEMENT (DEGREES)	GLA DESIGN 62 FPS PEAK GUST RATE (DEG/SEC)	GLA TEST 10 DEG. PEAK INBD. AIL. DISPLACEMENT (DEGREES)	GLA TEST 10 DEG. PEAK INBD. AIL. RATE (DEG/SEC)	FSS DESIGN .12 FPS PEAK GUST DISPLACEMENT (DEGREES)	FSS DESIGN .12 FPS PEAK GUST RATE (DEG/SEC)
OUTBOARD AILERON	12.7	146	8*	85*	5.9	640
STABILIZER (FROM TRIM)	3.05	97	1.8*	60*	0.6	17.2
INBOARD AILERON	---	---	10	114	---	---

*ESTIMATE BASED ON RATIO (AILERON EXCITATION/GUST EXCITATION) * GUST VALUE

FIGURE 44

CONTROL SURFACE MAXIMUM DISPLACEMENT AND RATE REQUIREMENTS

- SYMMETRIC
- MACH: 0.86
- ALTITUDE: 15,000 FEET
- FSS, GLA AND RSS ON
- 12 FT/SEC PEAK VERTICAL GUST
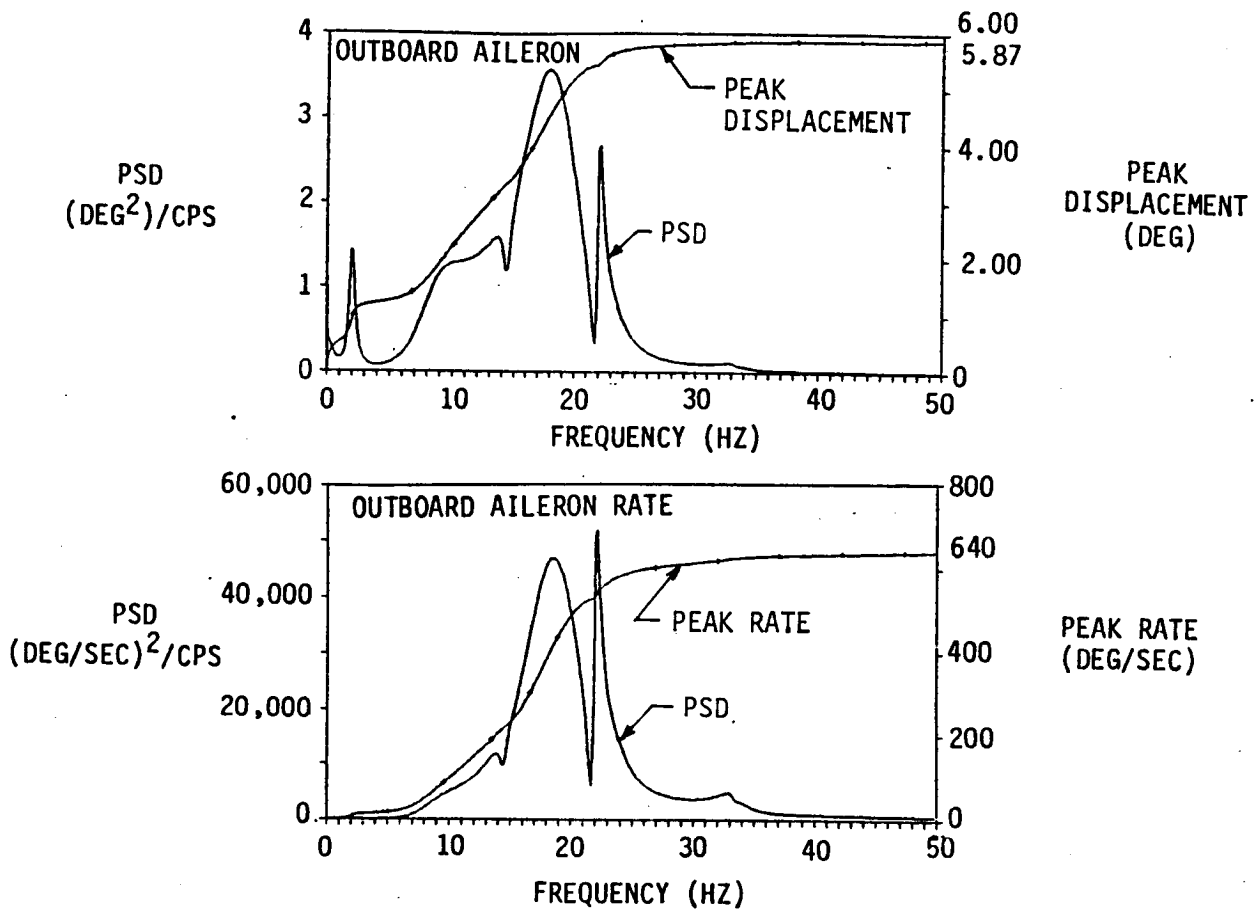
FIGURE 45

SYMMETRIC OUTBOARD AILERON DISPLACEMENT AND RATE REQUIREMENTS

REQUIREMENT	UNIT	INBOARD AILERON INBOARD SEGMENT	INBOARD AILERON OUTBOARD SEGMENT	OUTBOARD AILERON
HINGE MOMENT	IN-LB	430	430	230
DEFLECTION	DEG.	T.E.D.: 20 T.E.U.: 10	T.E.D.: 20 T.E.U.: 10	±15
RATE	DEG/SEC	114*	114*	640

*REQUIRED FOR GUST SIMULATION

NASA TEST RESULTS **

ACTUATOR	LEAKAGE (CIS)	MAXIMUM TORQUE (IN-LB)	FRICTION TORQUE (IN-LB)
INBOARD	0.02	500	35
OUTBOARD	0.03	300	42

**AFTER RUN-IN ±10° DISPLACEMENT @ 10 HZ FOR 30 MINUTES

FIGURE 46

SERVOACTUATOR REQUIREMENTS
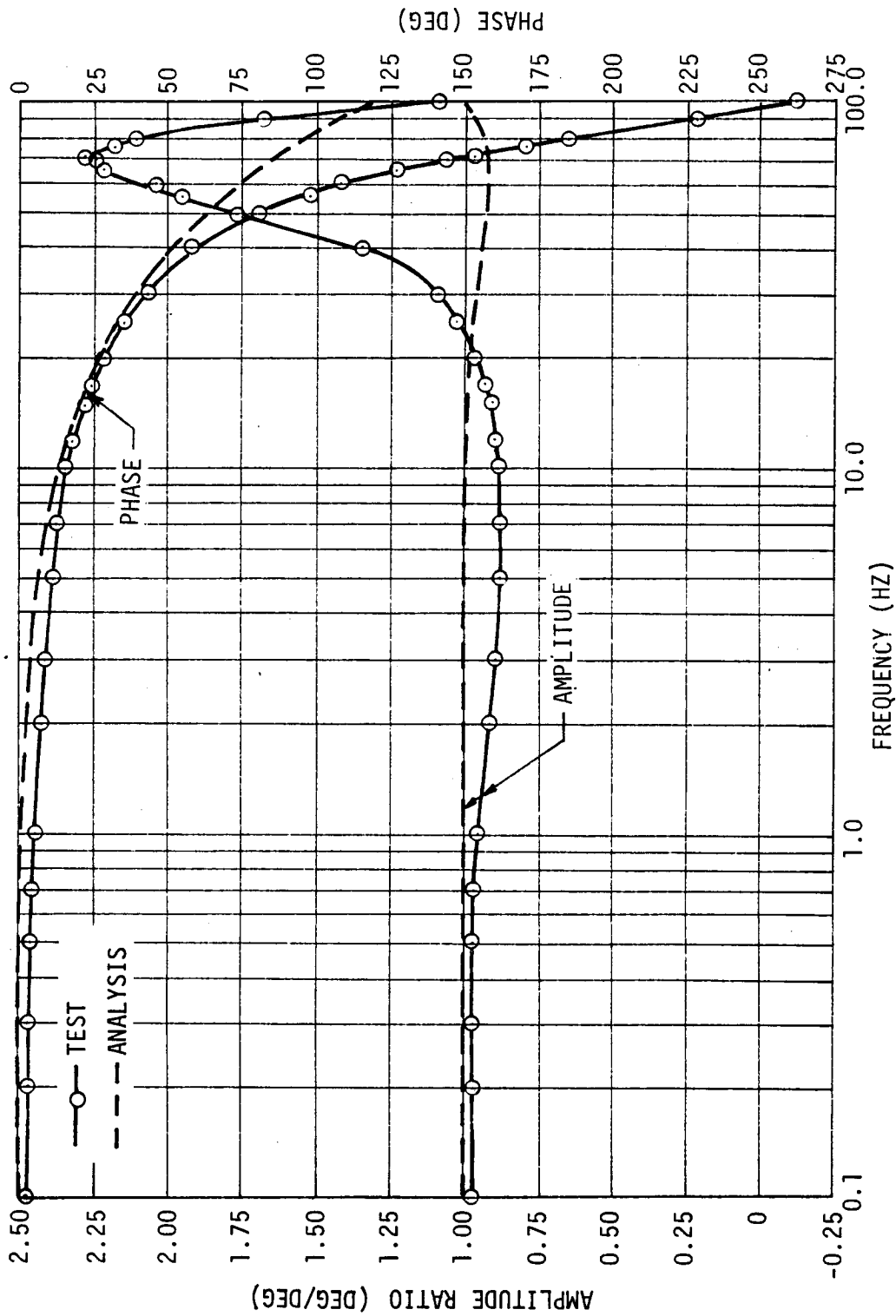
FIGURE 47

DAST ARW-1 SERVOACTUATOR FREQUENCY RESPONSE (ANALYSIS AND TEST)
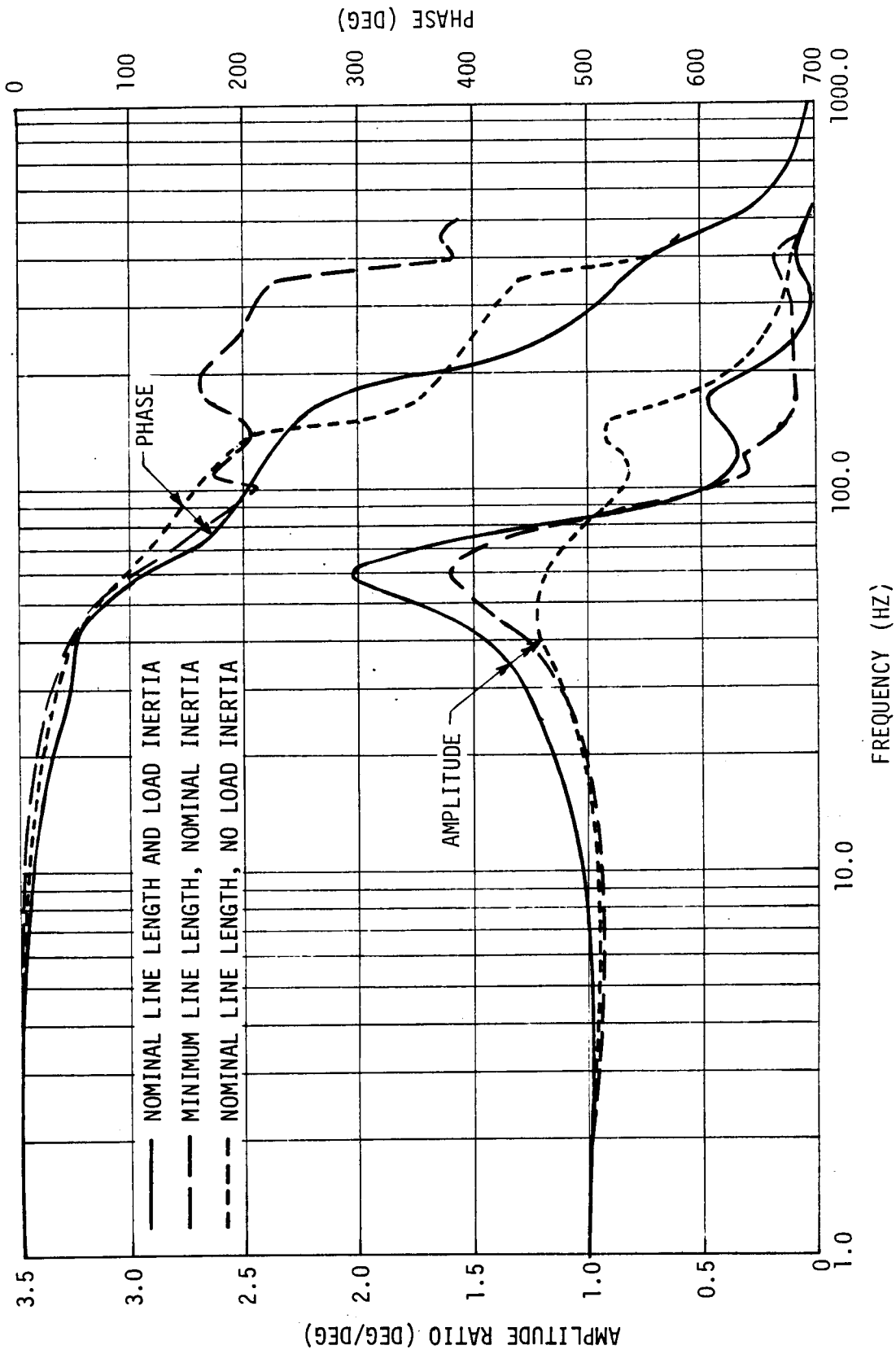
FIGURE 48

DAST ARW-1 ACTUATOR DISPLACEMENT FREQUENCY RESPONSE TEST DATA

88

A low frequency dominant mode was always evident during servoactuator testing but not identified in analysis. A study was made in an attempt to determine this anomaly. A servo valve represented by the transfer function as developed in Reference 4 is shown on Figure 49 and includes a first order lag associated with the servovalve closed loop. Servovalve parameters were selected and used in this transfer function to provide a good curve-fit to servoactuator test data and the results are shown on Figure 50.

A baseline actuator was synthesized from ARW-1 data and these techniques were used to develop the ARW-2 servoactuator math model as shown by the block diagram on Figure 51 and the parameters listed on Figure 52.

The parameters of a Moog Series 30 servovalve were used to synthesize the servoactuator as shown by the root locus on Figure 53 and the resulting frequency response is shown on Figure 54.

A wider bandwidth servovalve selected for analysis in an effort to improve servoactuator bandwidth did not increase the actuator bandwidth appreciably but did improve performance because the first order lag associated with the servovalve closed loop crossover frequency was moved from 640 to 1250 radians. A Hydraulic Research Model AR-25 servo valve was selected for hardware implementation because it is a direct replacement for the Moog Series 30 and its crossover frequency is 1000 radians. The AR-25 servovalve frequency response and transfer function are shown on Figure 55. The resulting servoactuator frequency response is shown on Figure 56 and indicates that a nearly flat response to 80 Hz can be realized.

6.2.2 Servoactuator Bench Tests. Testing was accomplished on a breadboard of the DAST ARW-2 outboard and inboard aileron servoactuator. The breadboard included hydraulic line lengths, load inertias and electronics equivalent to the ARW-2 design.

The objectives of the bench testing were to verify the synthesized servoactuator model and select the final gains required for good closed loop stability. A favorable test and analysis comparison of the servoactuator dominant modes would ensure confidence that the analysis model could accurately predict the hardware response. The surface actuator mode is determined during test by closing only the position loop and increasing the loop gain until the system is just unstable. The servo valve mode is then determined by closing the pressure loop with position loop closed at nominal gain and increasing pressure feedback gain until system again goes unstable. A summary of these results is shown on Figure 57 which compares analysis and test results using both the Series 30 and Model AR-25 servovalves.

Extensive closed loop testing was accomplished, however desired performance could not be realized with the pressure feedback loop

$$\frac{Q_V}{V_C} = \frac{K_V K_A}{((S/\omega_C) + 1)((S^2/\omega_0^2) + (2\delta_0/\omega_0) + 1)}$$

Where: Q_V = Servovalve no-load flow, inch^3/sec

V_C = D-C valve flow command, volts

K_V = Servovalve no-load flow gain constant, inch^3/sec/ma

K_A = Current drive gain constant, ma/volt

ω_0 = Natural frequency of spring-mass resonance of torque motor, rad/sec

ω_C = Crossover frequency of spool position closed loop, rad/sec.

FIGURE 49

SERVOVALVE TRANSFER FUNCTION
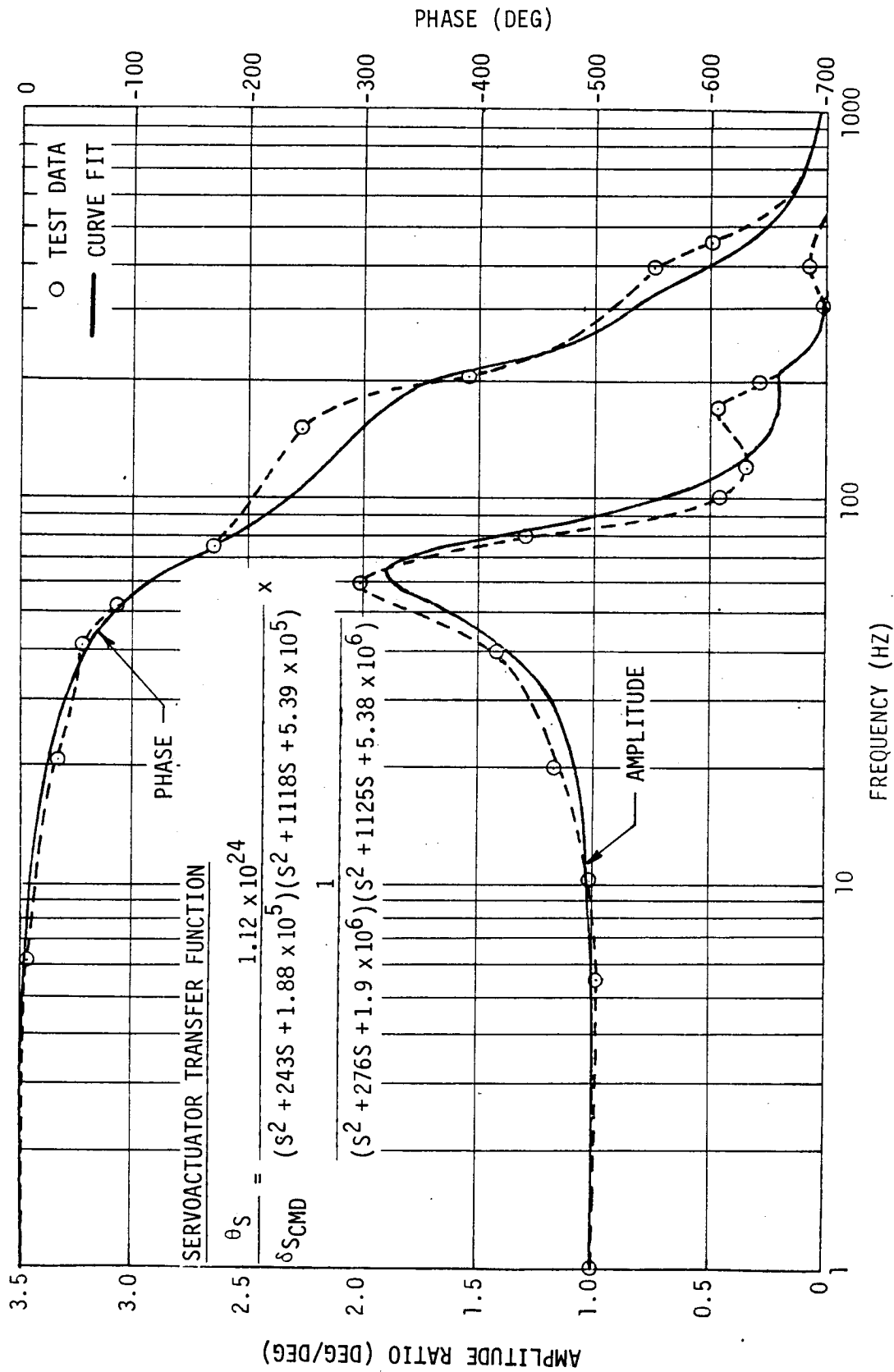
FIGURE 50

DAST ARW-1 TEST AND ANALYSIS DATA COMPARISON

The figure contains the following labeled content:

PHASE (DEG)

AMPLITUDE RATIO (DEG/DEG)

FREQUENCY (HZ)

o TEST DATA
— CURVE FIT

SERVOACTUATOR TRANSFER FUNCTION

$$\frac{\theta_S}{\delta_{S_{CMD}}} = \frac{1.12 \times 10^{24}}{(S^2 + 243S + 1.88 \times 10^5)(S^2 + 1118S + 5.39 \times 10^5)} \times$$

$$\frac{1}{(S^2 + 276S + 1.9 \times 10^6)(S^2 + 1125S + 5.38 \times 10^6)}$$

PHASE

AMPLITUDE
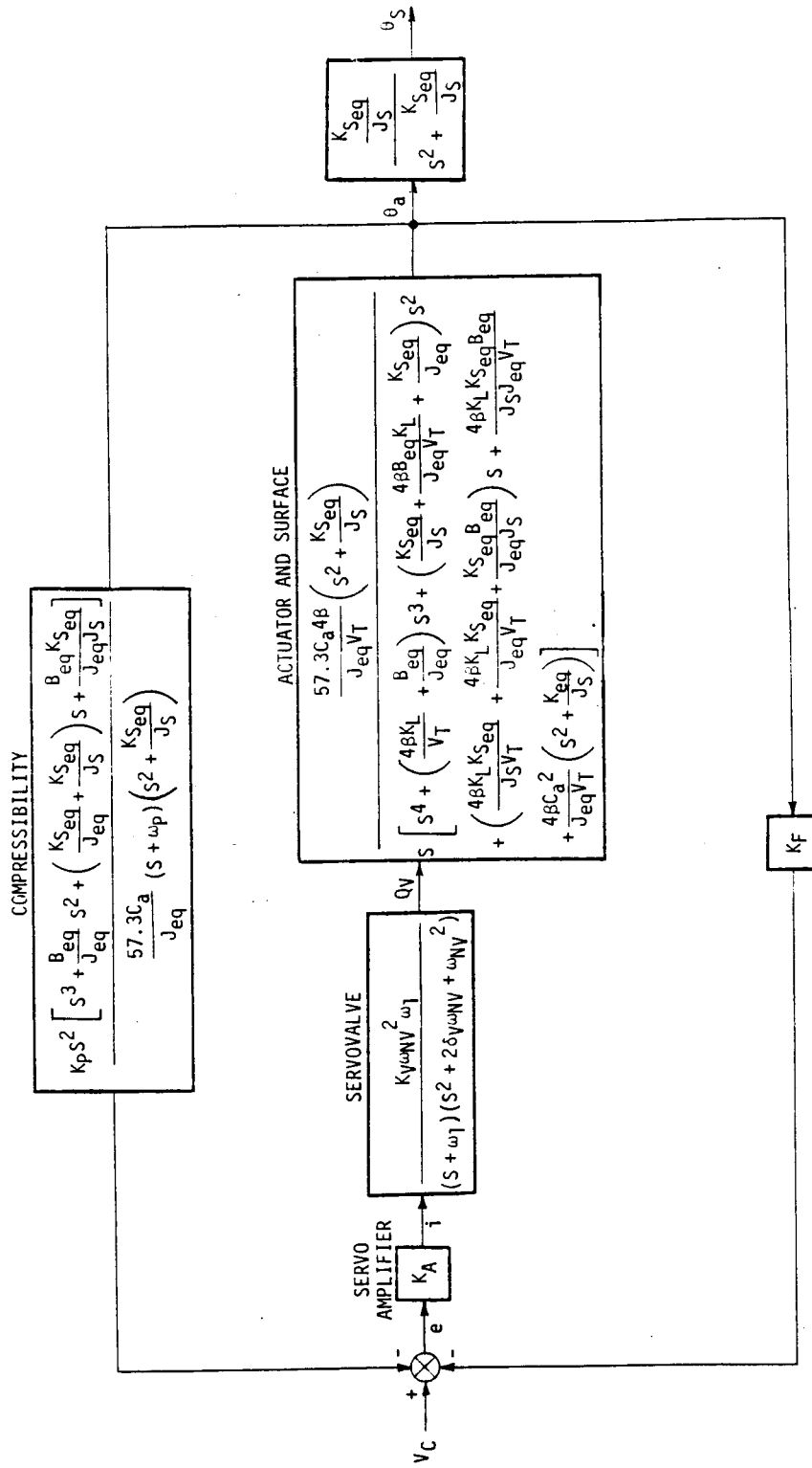
FIGURE 51

DAST ARW-1 AND DAST ARW-2 HYDRAULIC ACTUATOR MODEL WITH SURFACE COMPLIANCE AND ACTUATOR LEAKAGE

PARAMETER DESCRIPTION	INBOARD AILERON		OUTBOARD AILERON
	INBOARD SEGMENT	OUTBOARD SEGMENT	
B_{eq} - EQUIVALENT ACTUATOR-SURFACE DAMPING, (IN-LB)/(RAD/SEC)	4.0	4.0	4.0
β - HYDRAULIC OIL BULK MODULUS, PSI	60,000	60,000	60,000
C_a - ACTUATOR COEFFICIENT, IN^3	0.3185	0.3185	0.2074
δ_v - SERVOVALVE FIRST STAGE DAMPING RATIO	0.240	0.240	0.240
J_{eq} - EQUIVALENT ACTUATOR INERTIA, IN-LB-SEC^2	5.987×10^{-4}	1.005×10^{-3}	2.383×10^{-3}
J_S - SURFACE INERTIA, IN-LB-SEC^2	1.084×10^{-2}	1.581×10^{-2}	6.289×10^{-3}
K_A - SERVOVALVE DRIVER AMPLIFIER GAIN CONSTANT, ma/V	30.1	20.1	5.0
K_F - POSITION FEEDBACK GAIN CONSTANT, V/DEG	0.5	0.5	0.5
K_L - ACTUATOR INTERNAL LEAKAGE, IN^3/SEC/PSI	2.57×10^{-5}	2.57×10^{-5}	7.44×10^{-5}
K_{NL} - SERVOVALVE NO-LOAD FLOW GAIN CONSTANT, IN^3/SEC/ma	0.110	0.110	0.529
K_p - PRESSURE FEEDBACK GAIN CONSTANT, V/PSI	0.00247	0.00610	0.00588
$K_{S_{eq}}$ - EQUIVALENT ACTUATOR-SURFACE COMPLIANCE, (IN-LB)/RAD	11850.0	6942.0	5571.0
$K_A K_V K_F$ - POSITION LOOP GAIN CONSTANT, IN^3/SEC/DEG	1.353	0.904	1.334
$K_A K_V K_p$ - PRESSURE LOOP GAIN CONSTANT, IN^3/SEC/PSI	0.00667	0.01327	0.01568
P_L - HYDRAULIC LOAD PRESSURE, PSI*	500.0	500.0	500.0
P_S - HYDRAULIC SUPPLY PRESSURE, PSI	1500.0	1500.0	1500.0
V_T - TOTAL ENTRAPED HYDRAULIC OIL VOLUME, IN^3	0.784	1.316	3.120
W_1 - SERVOVALVE POSITION LOOP FIRST ORDER BREAK, RAD/SEC	670.0	670.0	1256.0
W_{N_V} - SERVOVALVE FIRST STAGE RESONANCE, RAD/SEC	1056.0	1056.0	2513.0
W_p - WASHOUT BREAK FREQUENCY, RAD/SEC	10.0	10.0	10.0

*ASSUMED 500 PSI TO CALCULATE K_V FROM $K_V = K_{NL}\sqrt{1 - P_L/P_S}$

$\dot{\theta}_a = 8K_V \times 57.3/C_a$ Deg/Sec

FIGURE 52

DAST ARW-2 SERVOACTUATOR PARAMETERS
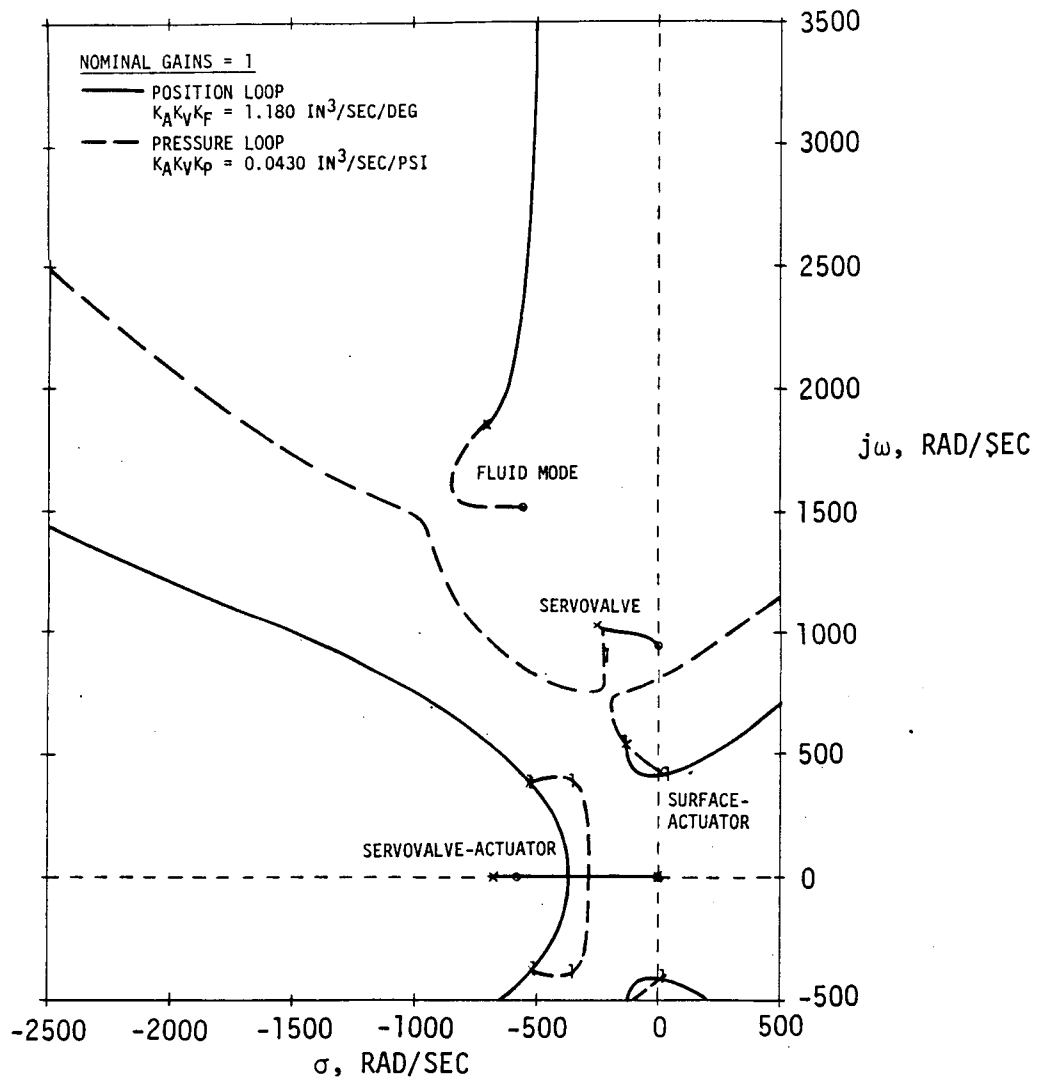
FIGURE 53

DAST ARW-2 OUTBOARD SERVOACTUATOR WITH SERIES 30 SERVOVALVE ROOT LOCUS

PHASE (DEG)

FREQUENCY (HZ.)

AMPLITUDE RATIO (DEG/DEG)
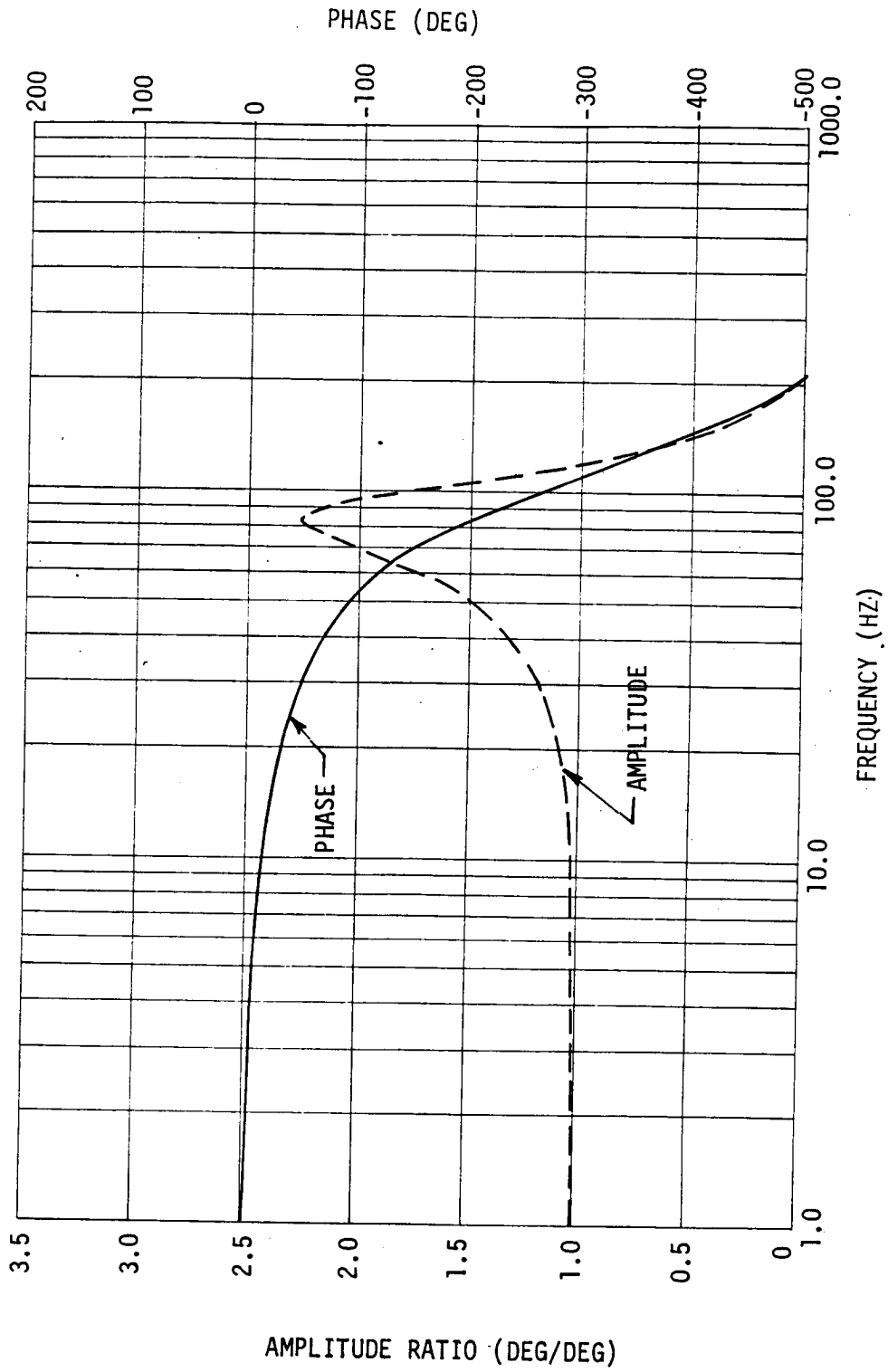
FIGURE 54

DAST ARW-2 OUTBOARD SERVOACTUATOR WITH SERIES 30 SERVOVALVE FREQUENCY RESPONSE
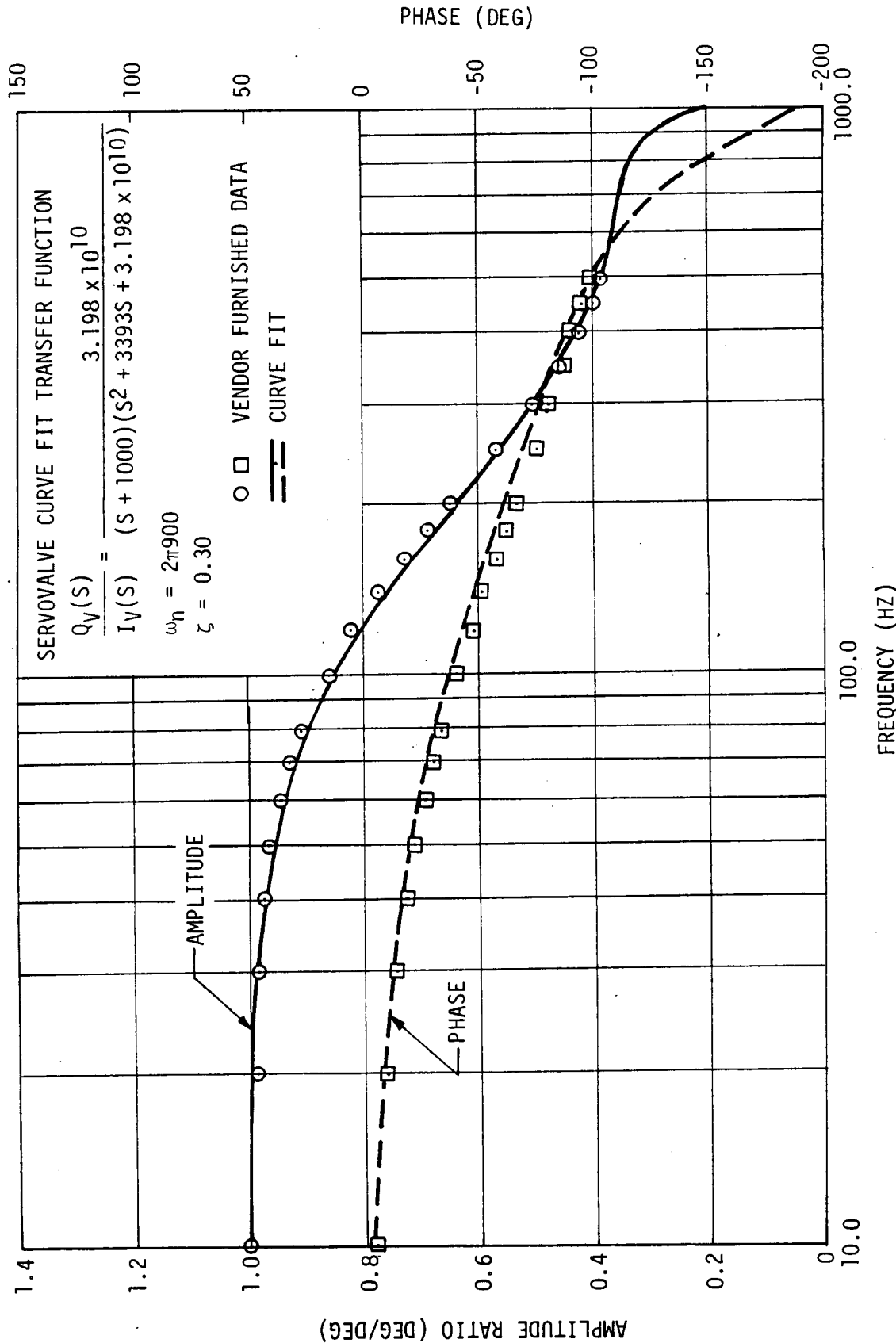
FIGURE 55

HYDRAULIC RESEARCH SERVOVALVE MODEL AR-25 (SPECIAL)

The figure contains the following annotations:

SERVOVALVE CURVE FIT TRANSFER FUNCTION

$$\frac{Q_V(S)}{I_V(S)} = \frac{3.198 \times 10^{10}}{(S+1000)(S^2 + 3393S + 3.198 \times 10^{10})}$$

$\omega_n = 2\pi 900$

$\zeta = 0.30$

○ □ VENDOR FURNISHED DATA

━━ CURVE FIT

AMPLITUDE

PHASE

Axis labels:
PHASE (DEG)
AMPLITUDE RATIO (DEG/DEG)
FREQUENCY (HZ)

PHASE (DEG)

AMPLITUDE RATIO (DEG/DEG)

25 PERCENT INCREASE IN
PRESSURE FEEDBACK GAIN

PHASE

AMPLITUDE

SERVOACTUATOR TRANSFER FUNCTION

$$\frac{\theta_S}{\theta_{CMD}} = \frac{5.89 \times 10^{23}}{(S^2 + 185.3S + 2.191 \times 10^5)(S^2 + 818.4S + 3.384 \times 10^5)}$$

$$\times \frac{1}{(S^2 + 510.1S + 2.151 \times 10^6)(S^2 + 1446.3S + 3.74 \times 10^6)}$$

FREQUENCY (HZ)

FIGURE 56

DAST ARW-2 OUTBOARD SERVOACTUATOR WITH MODEL AR-25 SERVOVALVE

97

MODE	ANALYSIS FREQUENCY		TEST FREQUENCY	
	SERIES 30	AR-25	SERIES 30	AR-25
SURFACE-ACTUATOR	76-82 HZ	95-100 HZ	72-76 HZ	80-92 HZ
SERVOVALVE	120-160 HZ	350-400 HZ	115-120 HZ	350-355 HZ

FIGURE 57

SERVOACTUATOR DOMINANT MODES COMPARISON WITH SERIES 30 AND AR-25 SERVOVALVES

closed. It was suspected that the pressure loop was influenced by actuator friction which caused a decrease in amplitude with an increase in frequency until at some frequency the effect of friction became less evident resulting in an increase in gain which caused stability problems at the actuator dominant frequency mode. The effect of friction can be seen from the responses shown on Figure 58. These results show that by increasing the break frequency of the washout in the pressure feedback loop, friction is less effective in reducing output amplitude at lower frequencies, however, the peak responses at the actuator dominant mode are very sensitive to input command amplitude indicating that other non-linearities in the servoactuator may be affected.

Pressure feedback reduces bandwidth and depends upon a lightly damped position loop to extend the bandwidth. Pressure feedback also causes the actuator performance to be more sensitive to changes within the servo loop. For example, friction, hydraulic bulk modulus, supply and load pressures can destabilize servovalve performance as described in Reference 4.

6.2.3 Final Servoactuator Model. Pressure feedback was eliminated and notch filters were added to limit the actuator bandwidth. Position loop gain was adjusted to give optimum performance with phase and gain margins greater than ± 45 degrees and ± 6 dB, respectively. The curve labeled "Test" shown on Figure 59 is the resulting frequency response for the outboard servoactuator. Similar results were obtained for the inboard servoactuators.

The solid curve on Figure 59 represents the result of a curve-fit to the test data. During the flight worthiness testing, frequency responses were again obtained and the outboard actuator response is shown by the curve identified as "Final Implementation" which compares favorably with the other responses shown on this figure. The transfer function for this curve-fit shown on this figure was used as the actuator model to update the flutter analysis described in Section 6.3.

The frequency responses on Figure 60 show the effect of including the band limiting notch filters and only a 17-degree increase in phase lag at 20 Hz results. This additional phase shift does not reduce the flutter suppression stability margins below the specified requirements. Figures 61 and 62 show that the outboard servoactuators are no-load velocity limited above 10 Hz and the inboard servoactuators are no-load velocity limited above 2 Hz.

Maximum surface displacements and rates are shown on Figure 63. The static and maximum hinge moments for the outboard ailerons at the FSS condition are 225 in-lb and 280 in-lb respectively at zero degrees and 15 degrees deflection.

99
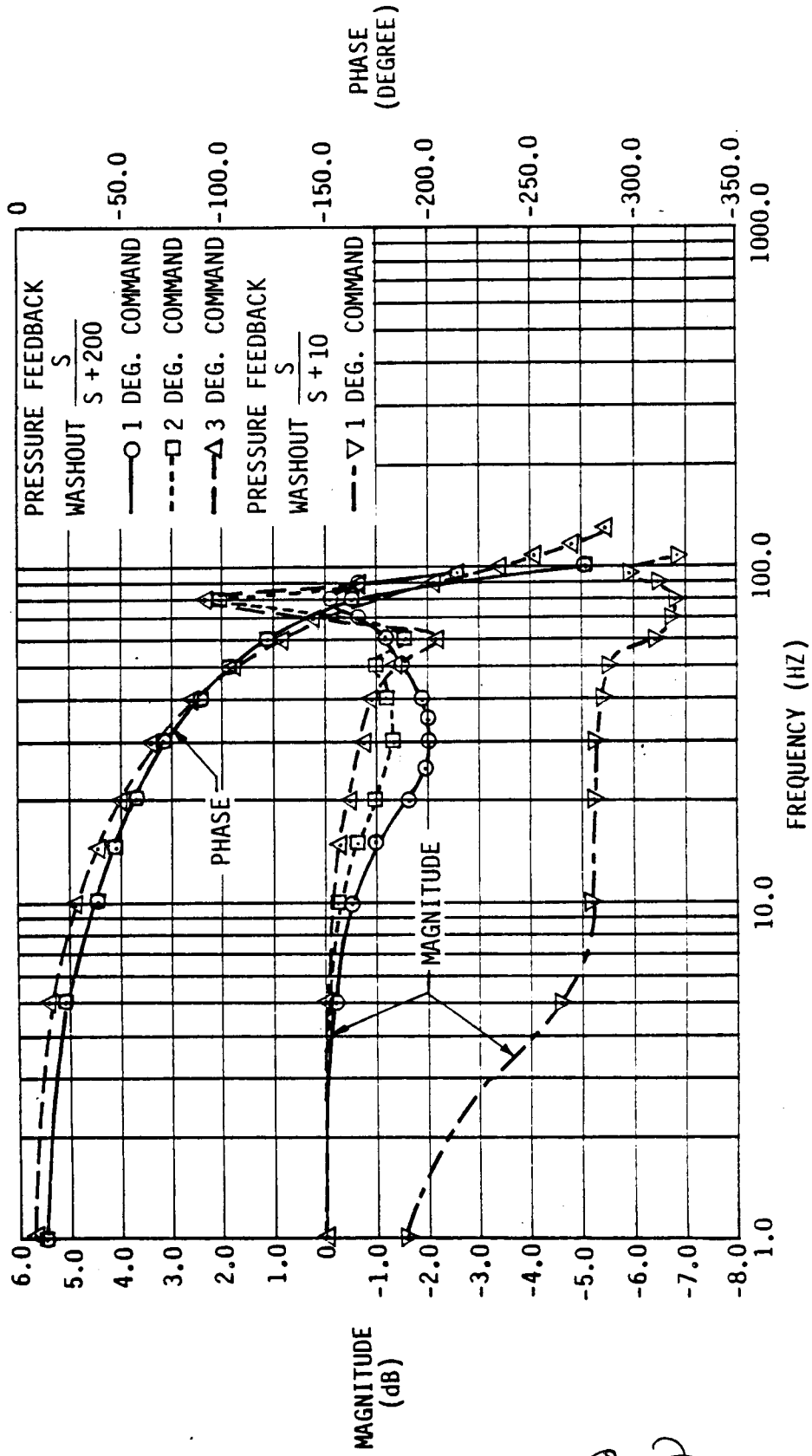
FIGURE 58

OUTBOARD SERVOACTUATOR RESPONSES (AR-25 SERVOVALVE)

C-2

ACTUATOR TRANSFER FUNCTION

$$\frac{4.046 \times 10^{12}(S^2 + 28.6S + 477.5^2)}{(S + 180)(S^2 + 251S + 314^2)(S^2 + 229S + 2.28 \times 10^5)(S^2 + 286S + 477.5^2)}$$
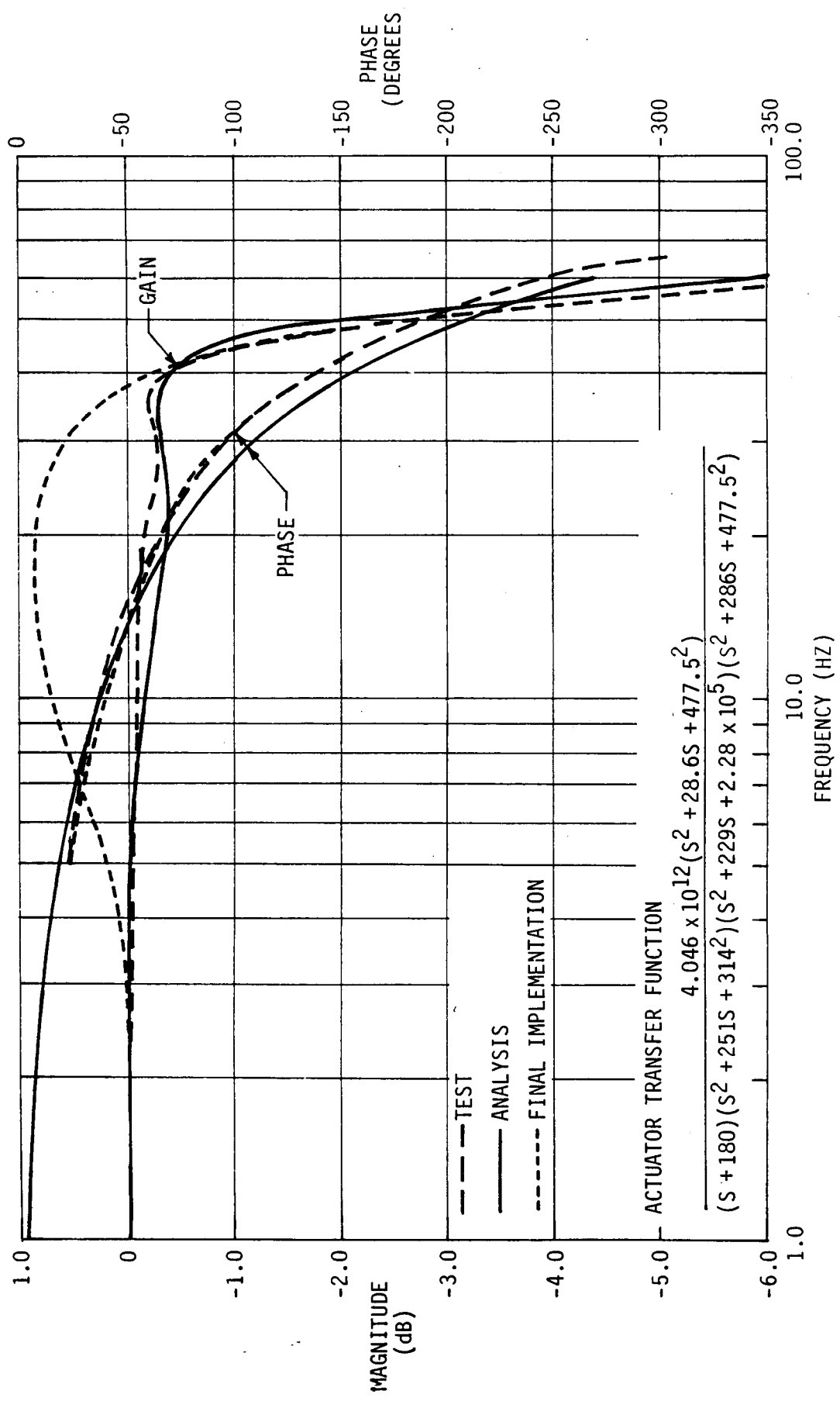
FIGURE 59

OUTBOARD SERVOACTUATOR ANALYSIS AND TEST RESPONSE COMPARISONS

101
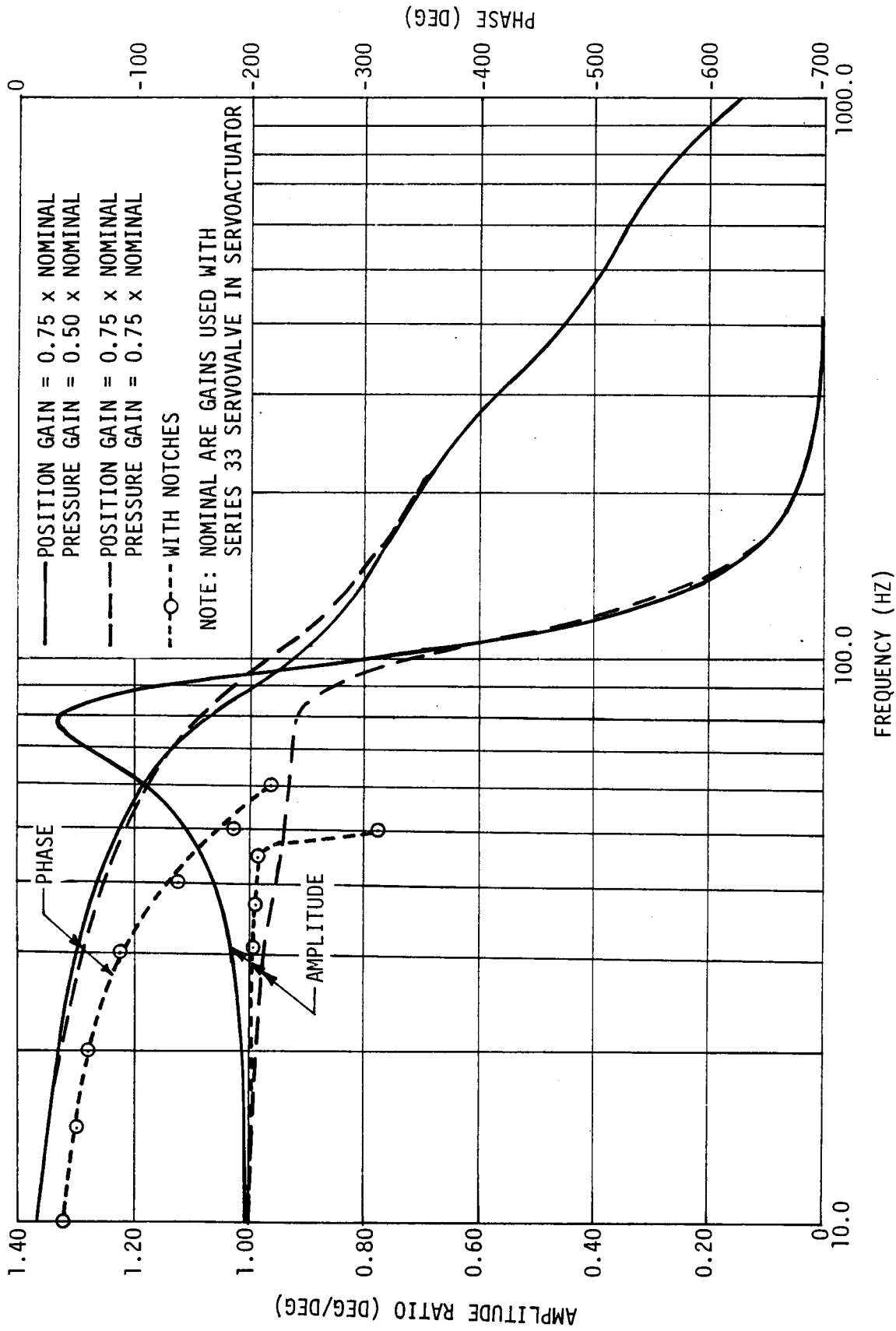
FIGURE 60

DAST ARW-2 OUTBOARD SERVOACTUATOR WITH MODEL AR-25 SERVOVALVE
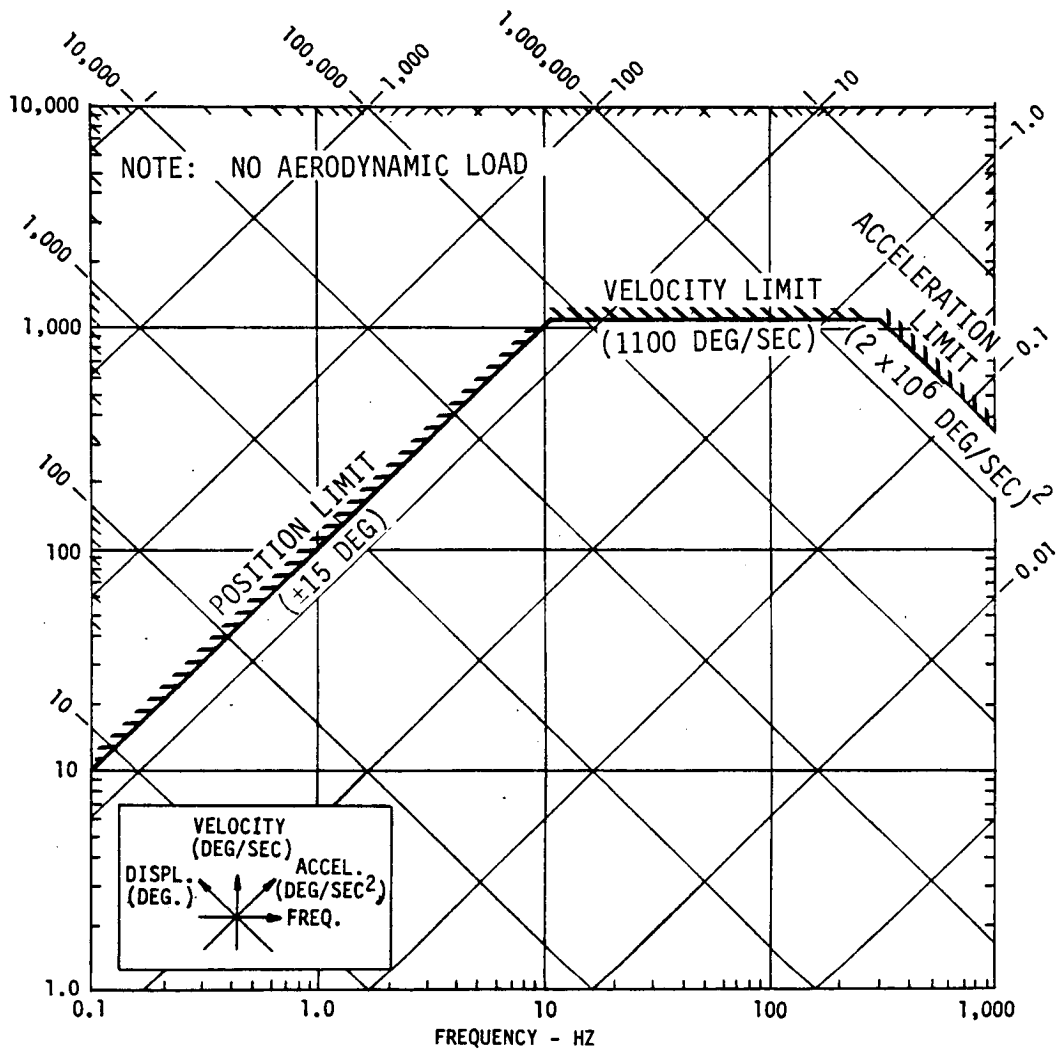
FIGURE 61

ARW-2 OUTBOARD SERVOACTUATOR PERFORMANCE
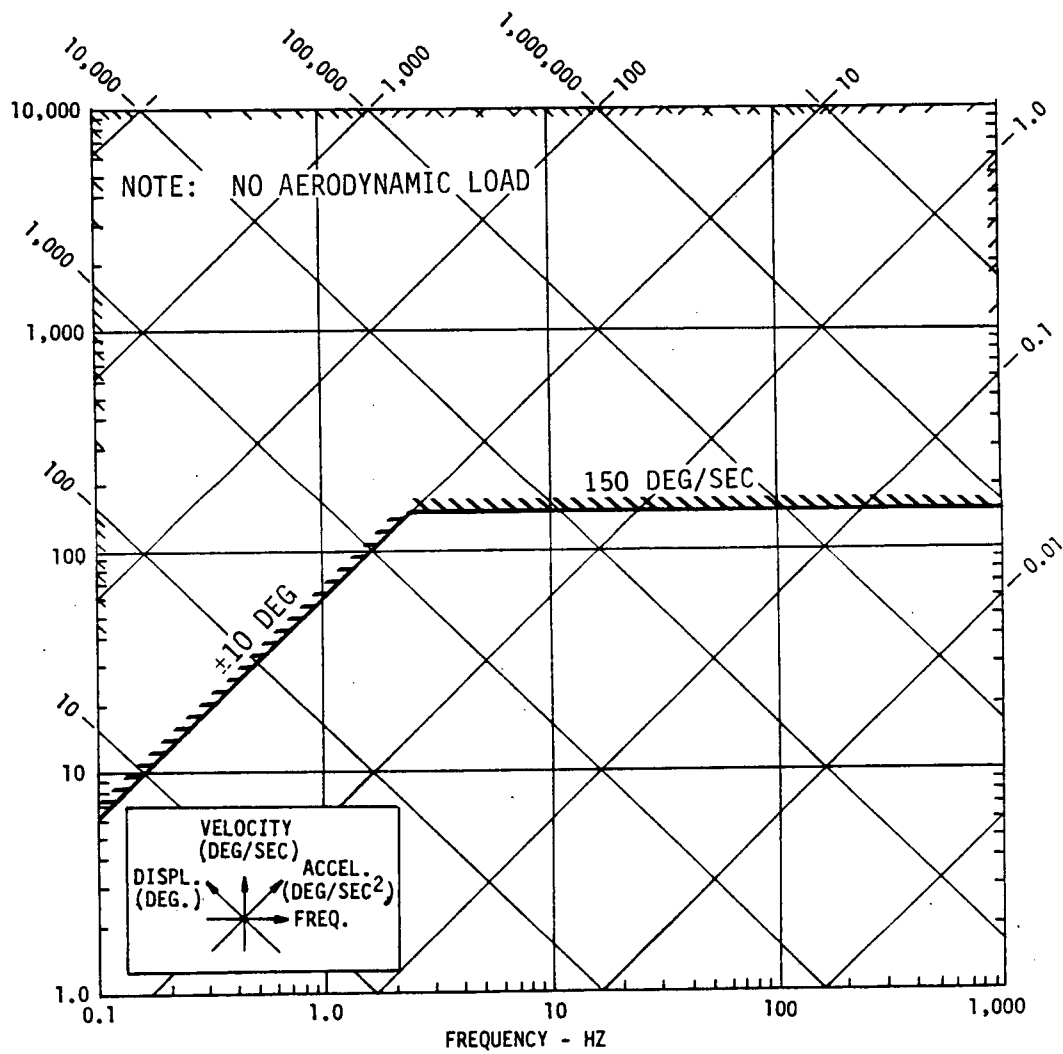
FIGURE 62

ARW-2 INBOARD SERVOACTUATOR PERFORMANCE

SURFACE	DISPLACEMENT (DEGREES)	MAXIMUM ACTUATOR RATES (DEG/SEC)		
		NO-LOAD	STATIC HINGE MOMENT [1]	MAXIMUM HINGE MOMENT [2]
INBOARD AILERON INBOARD SEGMENT	T.E.D.: 20 T.E.U.: 10	150	125 (GLA)	99 (GLA)
INBOARD AILERON OUTBOARD SEGMENT		150	102 (GLA)	40 (GLA)
OUTBOARD AILERON	±15	1100	615 (FSS)	370 (FSS)
STABILIZER	+7 -12	80	---	---

[1] AT ZERO DEGREES AILERON DEFLECTION

[2] AT MAXIMUM AILERON DEFLECTION

FIGURE 63

MAXIMUM SURFACE DISPLACEMENTS AND RATES

105

The loaded rate capability of the outboard ailerons is shown on Figure 64 to be 615 degrees per second at zero degrees deflection and 370 degrees per second at maximum deflection of 15 degrees. A peak displacement of approximately 4.25 degrees and a peak rate of approximately 200 degrees per second are required at 18 Hz can be determined from the results shown on Figure 45. From this data the maximum no-load rate requirement of 955 degrees per second was selected for testing; however, a no-load rate in excess of 1000 degrees per second was obtained. Similar rationale was used for all actuators which verify that the servoactuators meet rate and stability requirements as implemented for all flight conditions. These rates and displacements should however be verified during flight testing.

6.3 Flutter Suppression System Synthesis. Analysis was conducted in this study to finalize the synthesis of a FSS for the DAST ARW-2 drone configuration. Analysis was conducted previously in iterations one and two of the integrated design study (Reference 1), which identified a wing ballast configuration that produced a flutter boundary 9 or 10 percent below design dive speed V_D. Preliminary symmetric and antisymmetric flutter suppression systems were synthesized during the integrated design cycles for this configuration. A summary of the integrated design study results is presented in Paragraph 6.3.1. The conditions analyzed during this synthesis are shown on Figure 65.

Final synthesis was conducted using the mathematical models described in Paragraph 6.3.3. EOM were updated to reflect the 0.237 scale ARW-2 model wind tunnel test results and contain unscaled fuselage and wing structural elastic modes in addition to the scaled rigid body modes. The update of these EOM and finalization of the FSS were accomplished in the third iteration of the integrated design as documented herein. A performance evaluation was conducted on the final FSS and is described in Paragraph 6.3.4.

6.3.1 Integration Design Study. This paragraph summarizes results of iteration one and two of the integrated design study documented in Reference 1. In this study preliminary design of a flutter suppression system for the DAST ARW-2 drone was accomplished.

6.3.1.1 Configuration. During the course of the integrated design study, several configurations were modeled and analyzed. The final configuration included a 2 pound mass added to the leading edge of the rib at Wing Buttock Line (WBL) 98.9. This configuration exhibited symmetric and antisymmetric flutter modes that were similar in nature and produced an open loop flutter boundary approximately 10 percent below design dive speed (V_D), as shown on Figure 66. The outboard aileron selected for flutter suppression was sized as described in Reference 1 to have an 18 inch span.

NOTE: THIS CURVE DOES NOT
INCLUDE INERTIA LOAD.
INERTIA RATE DROPS
BY 20°/SEC AT 4.5 DEG.
AMPLITUDE AT 18 HZ.
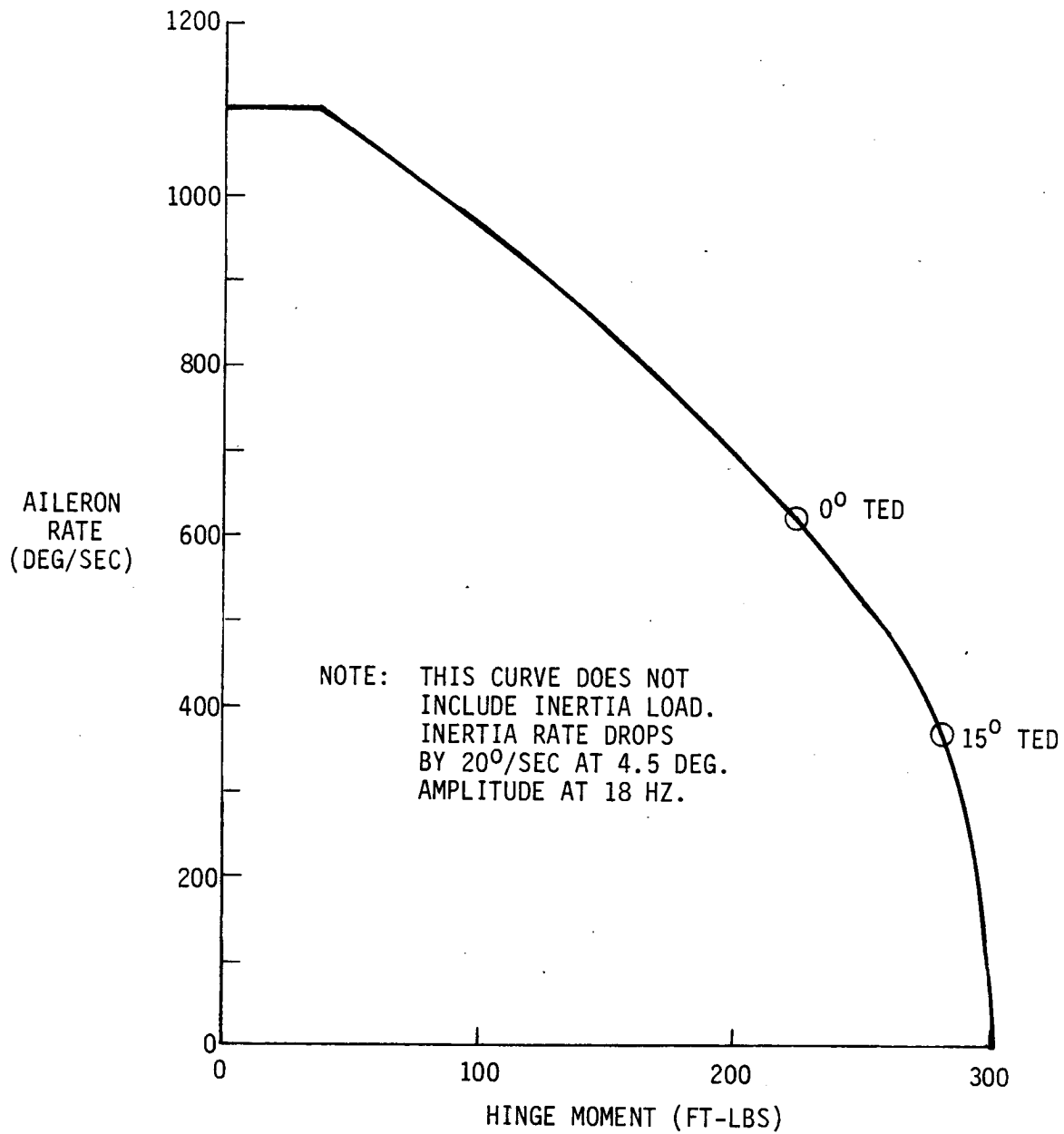
FIGURE 64

OUTBOARD AILERON RATE VERSUS HINGE MOMENT

MACH	ALTITUDE (FEET)	MACH	ALTITUDE (FEET)
0.60	7,000 12,000 15,000 18,000 25,000	0.83	3,000 12,000 15,000 16,000 17,000 18,000 20,000 25,000
0.70	12,000 15,000 18,000 25,000 50,000	0.86	2,000 4,250 8,000 12,000 15,000 18,000 25,000
0.80	2,000 10,000 12,000 13,000 15,000 17,000 18,000 25,000 46,800	0.91	6,000 8,000 10,000 12,000 15,000 18,000 25,000

FIGURE 65

DAST ARW-2 FLIGHT CONDITIONS ANALYZED
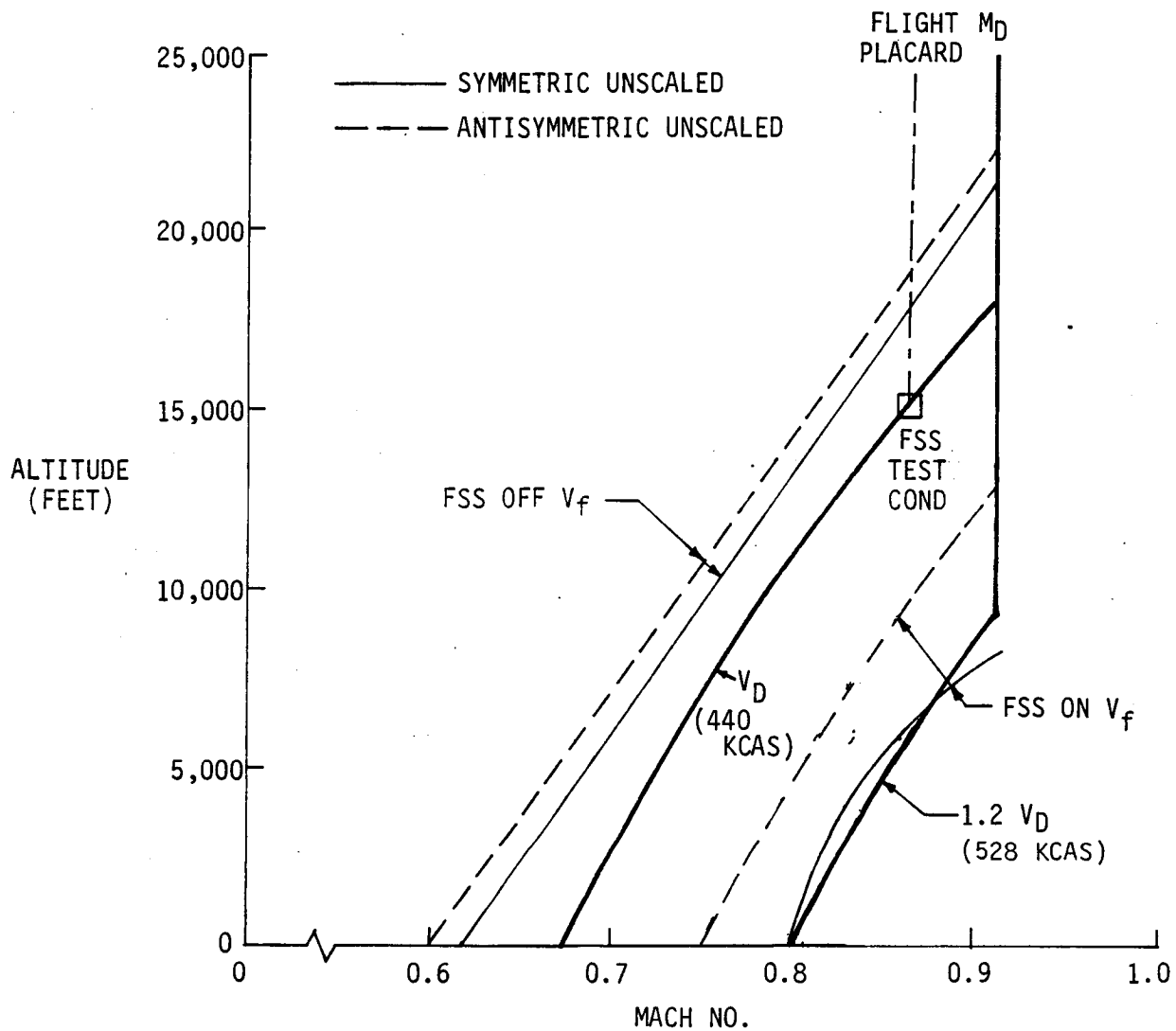
FIGURE 66

FLUTTER BOUNDARY FOR THE FINAL (ITERATION 3) FSS CONFIGURATION
WITHOUT ANTISYMMETRIC GAIN SCHEDULING

6.3.1.2 FSS Definition. The FSS system synthesized as described in Reference 1 to suppress the symmetric and antisymmetric flutter modes is shown in the block diagram on Figure 67. The system uses the difference of vertical accelerations at WBL 84 on the rear spar and WBL 82 on the front spar on the left and right wing panels summed to drive 18-inch span outboard ailerons through appropriate shaping filters. Both shaping filters had variable gains and filter first order break frequencies to adapt the system to the flight conditions at which the system must operate.

6.3.1.3 Actuator Dynamics. The servoactuator model used through the analysis was:

$$\frac{\theta_S}{\theta_{CMD}} = \frac{6.583 \times 10^4 \ (DEG/DEG)}{(S+401)(S^2+1681.8S+1.028 \times 10^6)(S^2+654.7S+1.597 \times 10^6)}$$

The actuator dynamic representation was to be updated during design cycle iteration three in an effort to more closely match the dynamics observed during hardware tests.

6.3.1.4 Results. The results of the integrated design study (Reference 1) showed that the FSS system actively suppressed the flutter mode which was composed primarily of first wing vertical bending and first torsion elastic modes. The third iteration included updated EOM based on the 0.237 scale ARW-2 model wind tunnel test results and an updated actuator model that is documented herein.

6.3.2 System Criteria. Criteria used during the FSS synthesis guided the form of the final system. The criteria included constraints on the system, such as type of sensors, size of surfaces, complexity of shaping filters and implementation and synthesis criteria which set performance goals such as stability margins and model damping.

6.3.2.1 Constraints. Constraint criteria ultimately affect performance of a system but do not specify any particular system performance. All constraints imposed were either directly or indirectly attributable to the integrated design study results. Constraints that were a direct result of the integrated design study were intended to minimize duplication of analysis already performed or those considered adequate and frozen by interation two such as surface size, while the indirect constraints were to improve the system performance.

The control surfaces were selected in iteration two (Reference 1) to have a span of 18 inches with approximately 23 percent chord. With conventional airplane design, the control surfaces are usually a constraint, however, using integrated design methodology, the control surfaces selected for FSS were adequate to suppress flutter throughout the flight envelope.

110

SYMMETRIC FILTER

$$\frac{81,150 K_S S (S^2 + 40S + 196^2)(S^2 + 220S + 456^2)}{(S+2)(S+D_S)(S+250)(S^2+100S+196.5^2)(S^2+400S+520^2)}$$

$K_S = 0.217(1.61-M)(Q-0.15)$

$D_S = 735 - 833.3M + 22.93Q$

ANTISYMMETRIC FILTER

$$\frac{65,260 K_A S (S+140)^2 (S^2+160S+330^2)}{(S+2)(S+D_A)(S^2+160S+161^2)(S^2+560S+456^2)(S+240)}$$

$K_A = 1.4 - 0.096Q$

$D_A = 850 \ (1 - M)$

$\ddot{Z}$ + DOWN
δ_A + TED
$Q \sim PSI$

RIGHT
WING
ACTUATOR

δ_{AIL} (DEG)

LEFT
WING
ACTUATOR

δ_{AIL} (DEG)

g's

g's

$\ddot{Z}_{WBL\ 84}$ REAR SPAR

RIGHT WING

$\ddot{Z}_{WBL\ 82}$ FRONT SPAR

$\ddot{Z}_{WBL\ 84}$ REAR SPAR

LEFT WING

$\ddot{Z}_{WBL\ 82}$ FRONT SPAR

FIGURE 67

DAST ARW-2 SECOND ITERATION FSS BLOCK DIAGRAM

111

Other constraints were considered during the finalization of the FSS system. Actuator compensation to reduce phase shifts induced when the pole-zero cancellation is imperfect was minimized and used only after sensitivity analysis verified that an anticipated pole-zero mismatch had minimal effect on FSS performance. Sensitivity analysis is described in Paragraph 6.3.5.

The control laws should have as large as possible roll off to reduce coupling with high frequency modes and to reduce susceptibility to high frequency noise. This was accomplished with shaping filters in the servoactuator drive electronics as described in Paragraph 6.2.3.

The control laws should have as low gain as possible at low frequencies to reduce coupling with rigid body and filter modes. This was verified by compatibility analysis as described in Paragraph 6.8.

6.3.2.2 Synthesis Criteria. Synthesis criteria specify desired performance of the system. The synthesis criteria used in the FSS development are discussed in the following paragraph.

The FSS should provide mode damping so that the wing is free from divergence and flutter at all speeds up to 120 percent of the design dive speed, V_D. These requirements, minimum flight altitude of 10,000 feet and the test envelope are shown on Figure 68. The gain and phase requirements are shown on Figure 69. The FSS should exhibit MIL-F-9490D stability margins at V_D as given on Figure 70. The FSS should not degrade damping of any mode to below a damping ratio of 0.01 (except the flutter mode) and should not significantly reduce damping of any mode with damping ratio below 0.01. The FSS should be capable of operating in 6 feet/second RMS (at 2σ level) random turbulence with 12 feet/second peaks.

6.3.3 Final Flutter Suppression System. The form of the integrated design FSS was used as the starting point in the final system synthesis. The EOM used in the analysis reflected the 0.237 scale ARW-2 wind tunnel test results with scaled structural modes and unscaled rigid body modes. The integrated design study results including sensor types and the systems criteria are discussed in Reference 1 and summarized above.

6.3.3.1 Configuration. The final DAST ARW-2 wing configuration is shown on Figure 71. The 2 pound ballast is located at the leading edge of the rib at WBL 98.9 and the outboard 18 inch, 23 percent chord, trailing edge control surface is located between WBL 89.7 and WBL 107.7. The accelerometer positions are shown on Figure 6 to illustrate the physical relationship of the various components.

The mathematical model included all the above components and fuselage and empennage structural elastic modes. These modes account for wing-body and wing-wing coupling which might affect the flutter modes.

112
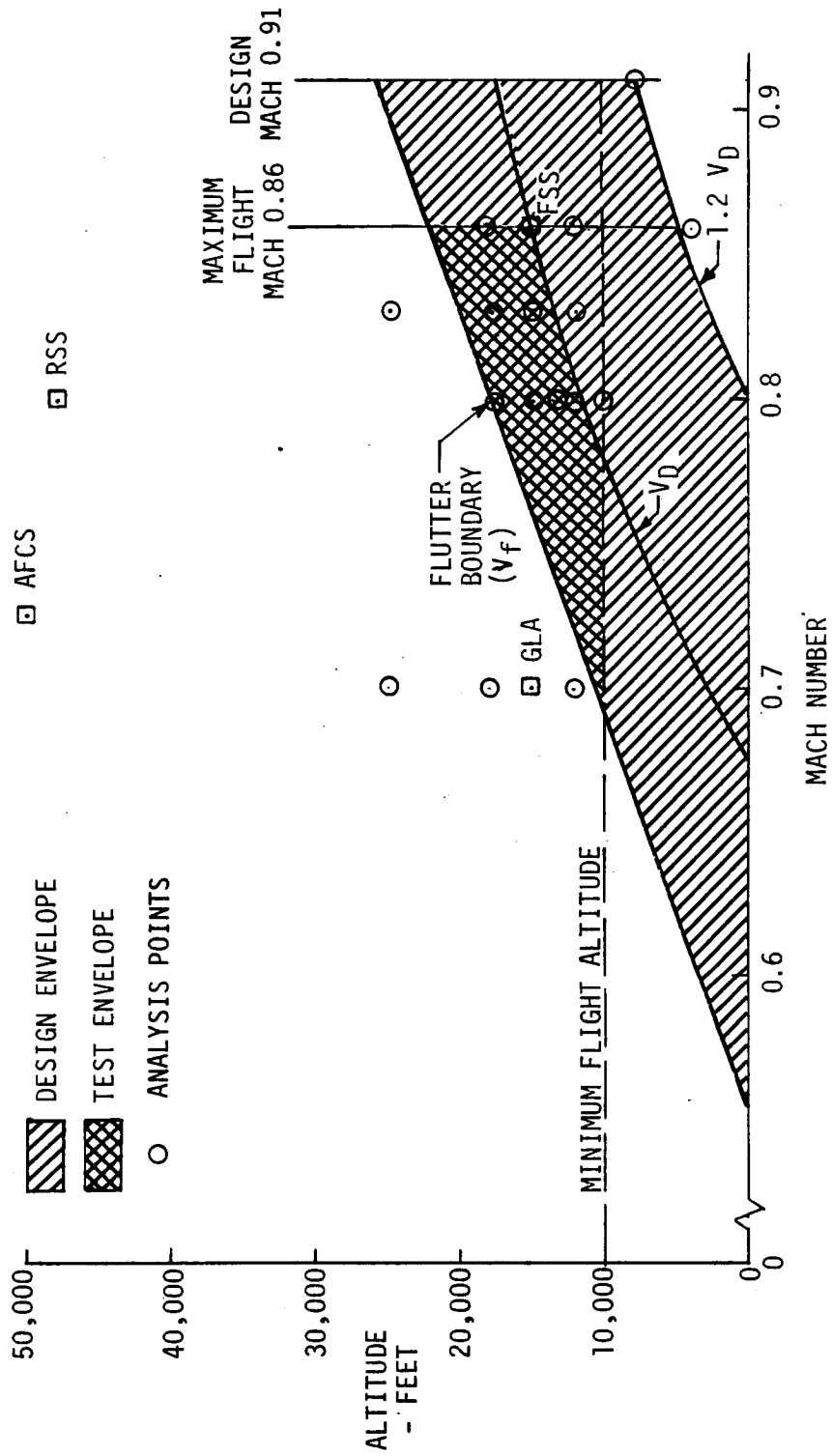
FIGURE 68

DAST ARW-2 FLUTTER SUPPRESSION TEST AND DESIGN ENVELOPE

NOTE: Design dive velocity (V_D) = 440 KCAS
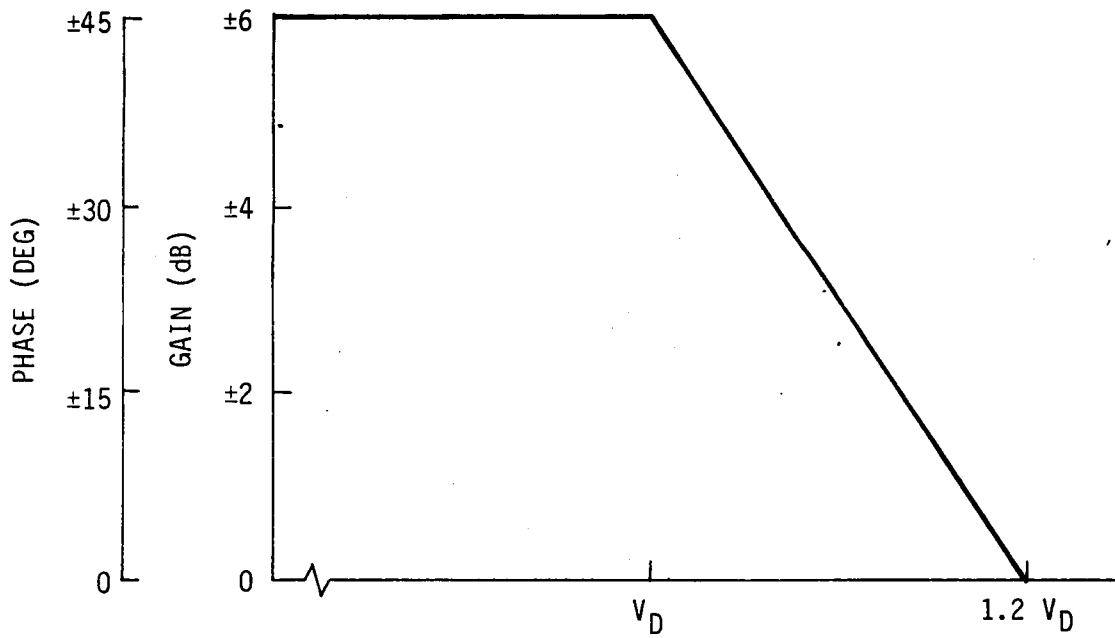
FIGURE 69

DAST ARW-2 FLUTTER SUPPRESSION SYSTEM GAIN AND PHASE REQUIREMENTS

MODE	GAIN	PHASE
FREQUENCY $\leq$ 0.06 HZ	±3.0 dB	±20 DEG.
0.06 HZ $\leq$ FREQUENCY $\leq$ FIRST STRUCTURAL MODE	±4.5 dB	±30 DEG.
ALL STRUCTURAL MODES	±6.0 dB	±45 DEG.

FIGURE 70

MIL-F-9490D STABILITY MARGINS

SURFACE	PERCENT CHORD
INBOARD	15
OUTBOARD	23
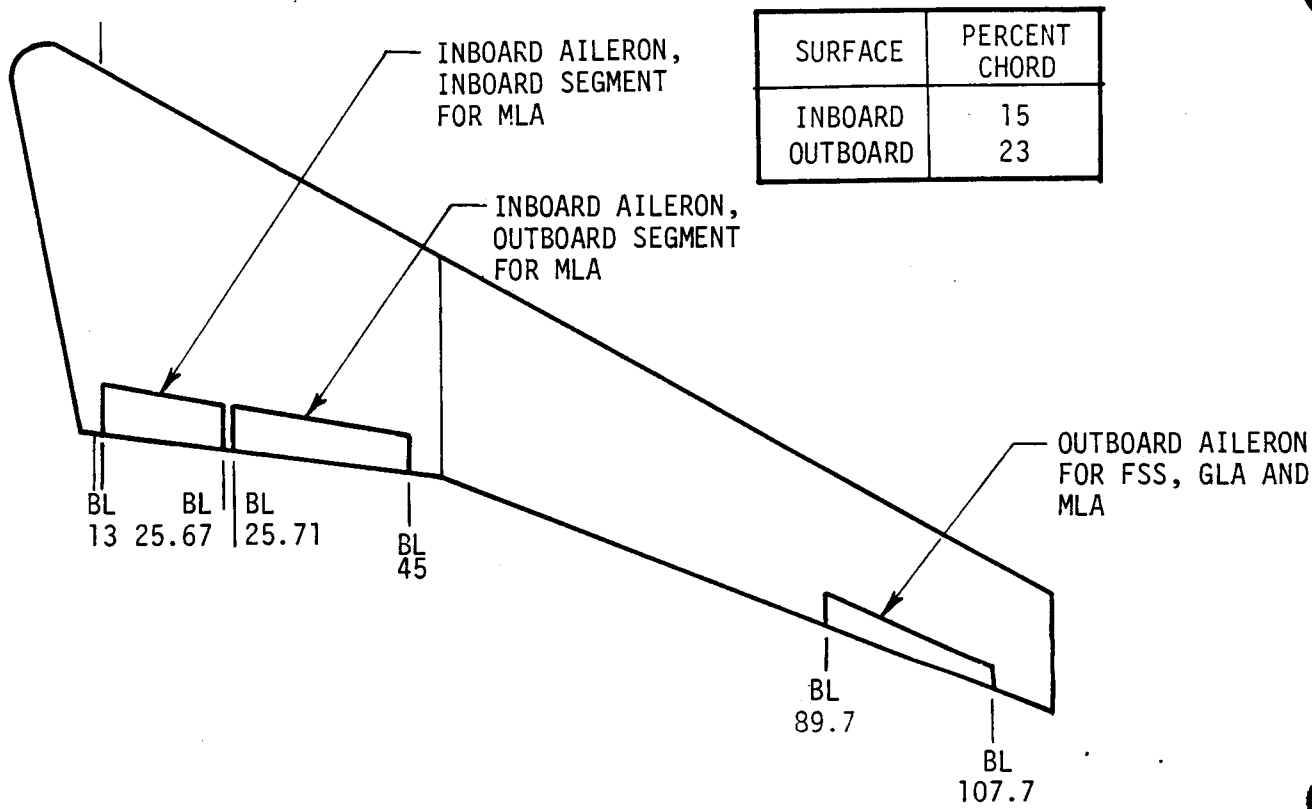
FIGURE 71

CONTROL SURFACE DEFINITION - FINAL DESIGN ITERATION

6.3.3.2 Servoactuator Model. The transfer function for the servoactuator was defined through analysis and bench testing described in Paragraph 6.2. The simplified transfer function of the servoactuator for the no-load condition is:

$$\frac{\delta_{AIL}}{\delta_{CMD}} = \frac{4.046 \times 10^{14}(S^2 + 28.6S + 477.5^2)}{(S + 180)(S^2 + 251S + 314^2)(S^2 + 229S + 477.5^2)(S^2 + 286S + 477.5^2)}$$

Servoactuator dynamics vary with hinge moment as discussed in Paragraph 6.3.5.2.4. The no-load transfer function was used during the synthesis study. The effect of maximum resisting and maximum aiding hinge moment variation in actuator dynamics of FSS performance was evaluated for a purely analytical actuator model.

6.3.3.3 Sensor Location. Sensor type and control surface size and location were fixed in the integrated design study (Reference 1) leaving sensor location and orientation to be defined if affected by the updated EOM. Zero locus techniques were used to select these two parameters to satisfy two primary goals. Coupling with the flutter mode was to be maximized while minimizing adverse coupling with other structural and rigid body modes.

To establish sensor locations, the selection process must be an integral part of the overall FSS synthesis as shown on Figure 72. This method was used in an iterative manner to establish sensor locations based upon closed-loop system results.

During the integrated design analysis described in Reference 1, the difference of two vertical accelerometer signals on the front and rear spar at the WBL 82 and WBL 84, respectively, was selected to synthesize the FSS. Initial third iteration FSS synthesis with updated EOM utilized these locations, however, both symmetric and antisymmetric flutter requirements could not be met and the sensor position methodology of Figure 72 was implemented.

Effects of varying locations and spanwise orientation of the two vertical accelerometers along the front and rear spar were evaluated using the above described methodology with results shown on Figures 73 and 74. These zero root loci, subsequent closed loop flutter analysis described in Paragraph 6.3.3.4 and sensor location sensitivity described in Paragraph 6.3.5.1 show that vertical accelerometers located at WBL 82 on front spar and WBL 84 on rear spar offer best results for symmetric FSS and vertical accelerometers located at WBL 92 on both front and rear spars offer best results for antisymmetric FSS. These sensor locations were used to finalize the FSS system. The front spar location WBL 80 was not selected, although it appears, as shown on Figure 73, to be a better selection, because this zero location retards movement of the flutter mode to the left more than the selected WBL 82.

117
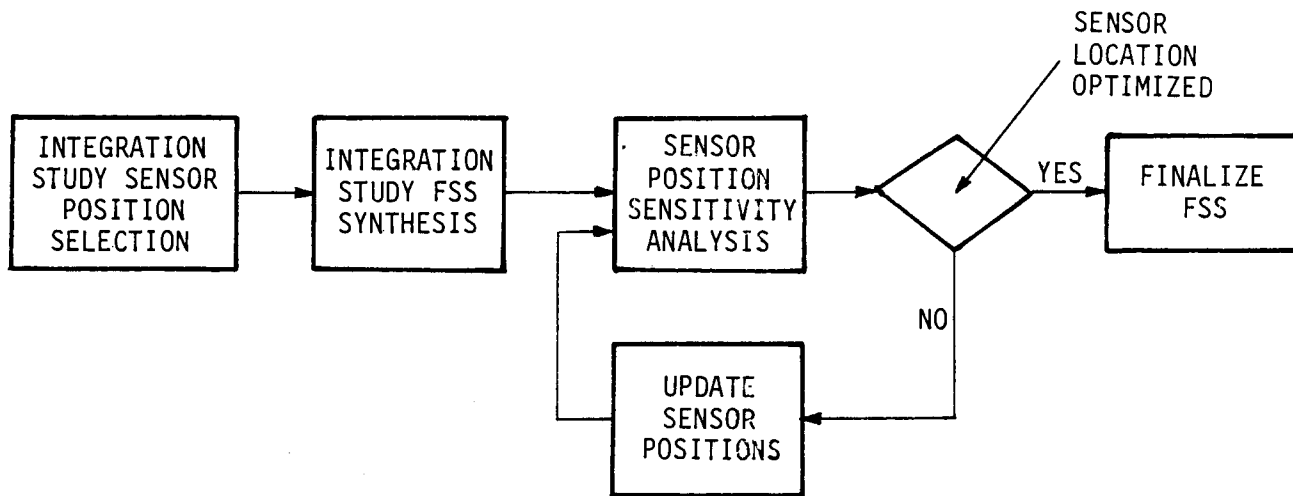
FIGURE 72

SENSOR POSITION SELECTION METHODOLOGY

FIGURE 73

SYMMETRIC SENSOR ZERO ROOT LOCI AND FLUTTER MODE DAMPING

FLUTTER
MODE
DAMPING
RATIO

0.10

0.05

0

0   90   92   94
FRONT SPAR SENSOR LOCATION (WBL)
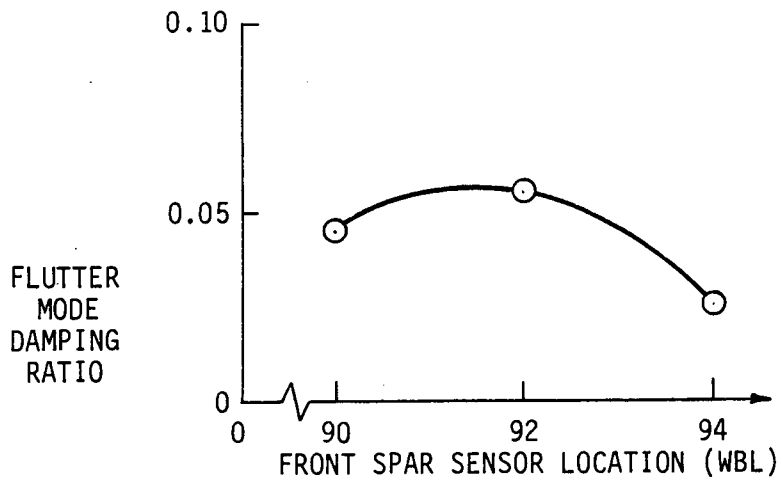
| SYMBOL | SENSOR LOCATION | |
	REAR SPAR	FRONT SPAR
□	WBL 94	WBL 92
△	WBL 92	WBL 92
○	WBL 90	WBL 94

jω (RAD/SEC)

140

130

LOCATION SELECTED

✕ FLUTTER MODE

120

-30   -20   -10   0   10   20
σ (RAD/SEC)
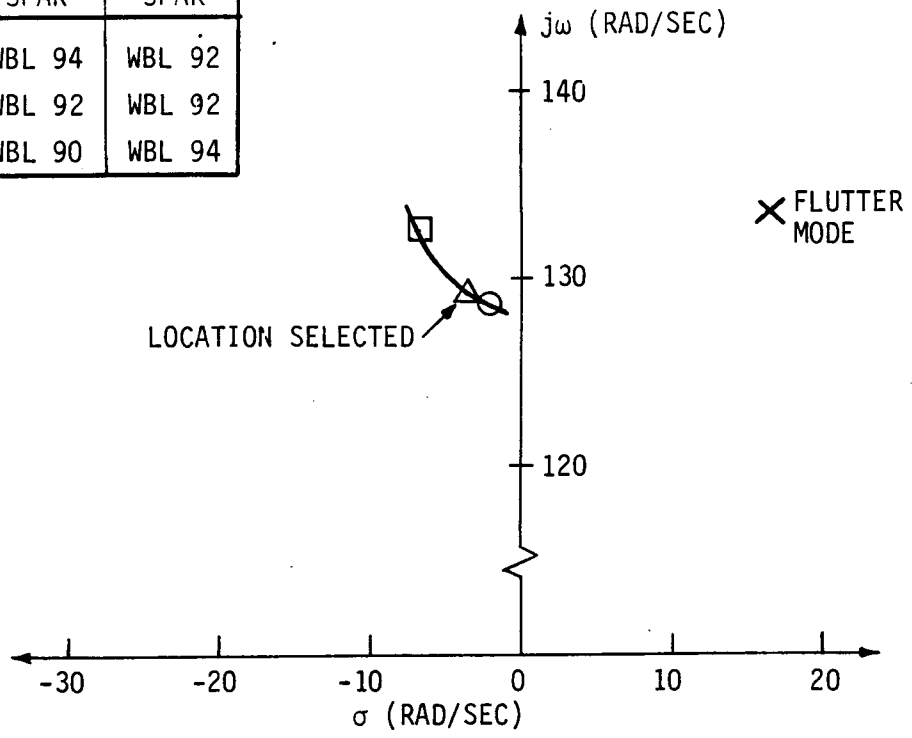
FIGURE 74

ANTISYMMETRIC SENSOR ZERO ROOT LOCI AND FLUTTER MODE DAMPING

120

6.3.3.4 Filter Definition. The FSS filter configuration was finalized using accelerometer locations described in Paragraph 6.3.3.3 and an actuator transfer function which was curve-fit to the laboratory bench test results described in Paragraph 6.2.2.

The flutter suppression filters were synthesized using root locus techniques in an iterative method shown on Figure 75. The synthesis began with definition of filters at the flutter suppression design condition, Mach 0.86 at 15,000 feet. The filters were then evaluated at other conditions and adjustments made as necessary to meet the requirements.

The region in the flight envelope in which the FSS is required to stabilize the flutter modes is shown on Figure 68 by the shaded area. The flight envelope was selected as shown on this figure by the cross-hatched area. The placard set at 0.86 Mach during the integrated design study could not be increased to 0.91 Mach because of thrust limitations.

The final filters developed in the third design iteration shown on Figure 76 utilize washout filters of $S/(S + 2)$ to eliminate low frequency and steady-state commands to the control surfaces.

6.3.3.4.1 Synthesis. Synthesis was initiated using the form of the iteration two filters with an analytical model of the servoactuator. Servoactuator compensation was included during the synthesis procedure. Sensor locations were selected using this FSS model and these sensor locations were verified with the final filters and actuator. After laboratory bench tests had been run, a transfer function which had been curve-fit to the laboratory results was included in the synthesis procedure in place of the analytical model. The inclusion of the dynamics of the servoactuator determined by test led to the synthesis of the final FSS filters shown on Figure 76. The actuator transfer function is also shown on this figure and the FSS is shown as implemented to receive sensor signals from both wings.

The frequency response of the symmetric and antisymmetric shaping filters with and without the actuator is shown on Figure 77 and Figure 78 respectively. Root locus plots for the symmetric and antisymmetric system at 0.86 Mach, 15,000 feet, are shown on Figures 79 and 80 respectively. Additional root locus analysis verifying FSS stability throughout the flight envelope was conducted and has been presented at the design reviews and critical conditions are included in Appendix C.

6.3.3.4.2 Parameter Scheduling. Scheduling of gains or time constants was not required to meet the gain and phase margins at the design flight condition for either symmetric or antisymmetric modes. Symmetric scheduling is not required at the 0.91 Mach condition. Gain scheduling is required at the 0.91 Mach condition for the antisymmetric FSS. The gain schedule is shown on Figure 81. Scheduling is not required for the flight envelope and is not implemented for flight test.
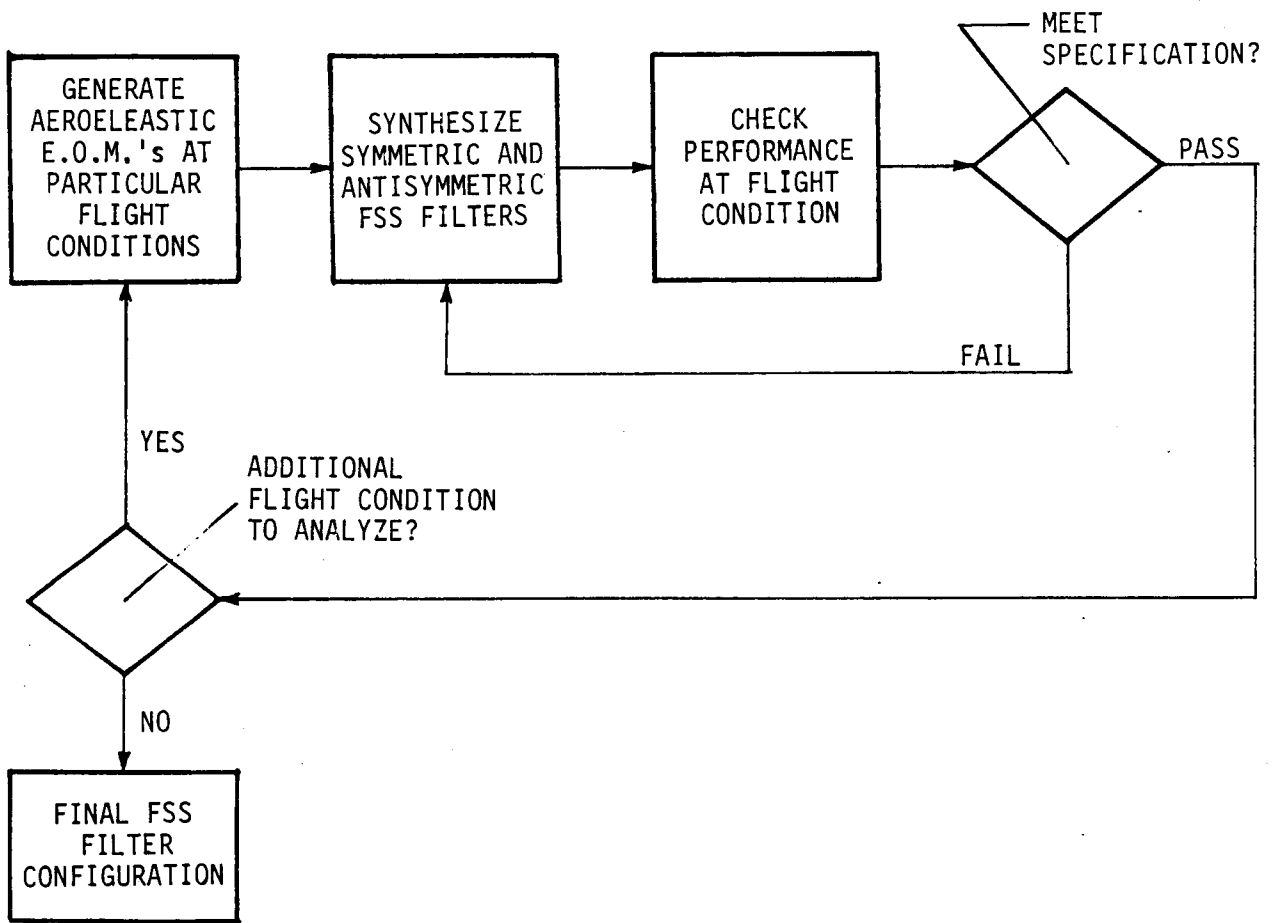
FIGURE 75

FLUTTER SUPPRESSION SYSTEM FILTER SYNTHESIS PROCEDURE

RIGHT WING ACTUATOR δ_{AIL} (DEG)

4.01 DEG/g, -150.5 DEG @ 18 HZ. SYMMETRIC

LEFT WING ACTUATOR δ_{AIL} (DEG)

3.15 DEG/g, -143 DEG @ 21 HZ ANTISYMMETRIC

INPUT TO BOTH WING ACCELEROMETERS

SYMMETRIC FILTER

$$\frac{155.5 S^3 (S^2 + 232S + 123^2)(S^2 + 147.2S + 85^2)(S^2 + 30S + 470^2)(S^2 + 63.2S + 158^2)(S + 182)(S^2 + 251S + 314^2)}{(S+2)^3(S+200)(S^2+180S+99^2)(S^2+61.37S+85^2)(S+1750)^2(S+150)^2(S+640)^2}$$

ACTUATOR

$$\frac{4.046 \times 10^{12}(S^2 + 28.6S + 477.5^2)}{(S+180)(S^2+251S+314^2)(S^2+229S+477.5^2)(S^2+286S+477.5^2)}$$

ANTISYMMETRIC FILTER

$$\frac{178.4 S^3 (S^2 + 232S + 123^2)(S^4 + 190.52S + 110^2)(S^2 + 20S + 455^2)(S^2 + 84S + 180^2)(S + 182)(S^2 + 251S + 314^2)}{(S+2)^3(S+316)(S^2+180S+99^2)(S^2+79.4S+110^2)(S+1750)^2(S+150)^2(S+640)^2}$$

$\ddot{Z}$ + DOWN

δ_A + TED

NOTE: HARDWARE IMPLEMENTED GAINS AND FILTERS ARE SHOWN

$\ddot{Z}_{WBL\ 84}$ REAR SPAR
$\ddot{Z}_{WBL\ 82}$ FRONT SPAR
RIGHT WING

$\ddot{Z}_{WBL\ 84}$ REAR SPAR
$\ddot{Z}_{WBL\ 82}$ FRONT SPAR
LEFT WING

$\ddot{Z}_{WBL\ 92}$ REAR SPAR
$\ddot{Z}_{WBL\ 92}$ FRONT SPAR
LEFT WING

$\ddot{Z}_{WBL\ 92}$ REAR SPAR
$\ddot{Z}_{WBL\ 92}$ FRONT SPAR
RIGHT WING

FIGURE 76

FINAL DAST ARW-2 FLUTTER SUPPRESSION SYSTEM

FIGURE 77

SYMMETRIC FREQUENCY RESPONSE OF FSS SHAPING FILTER

124
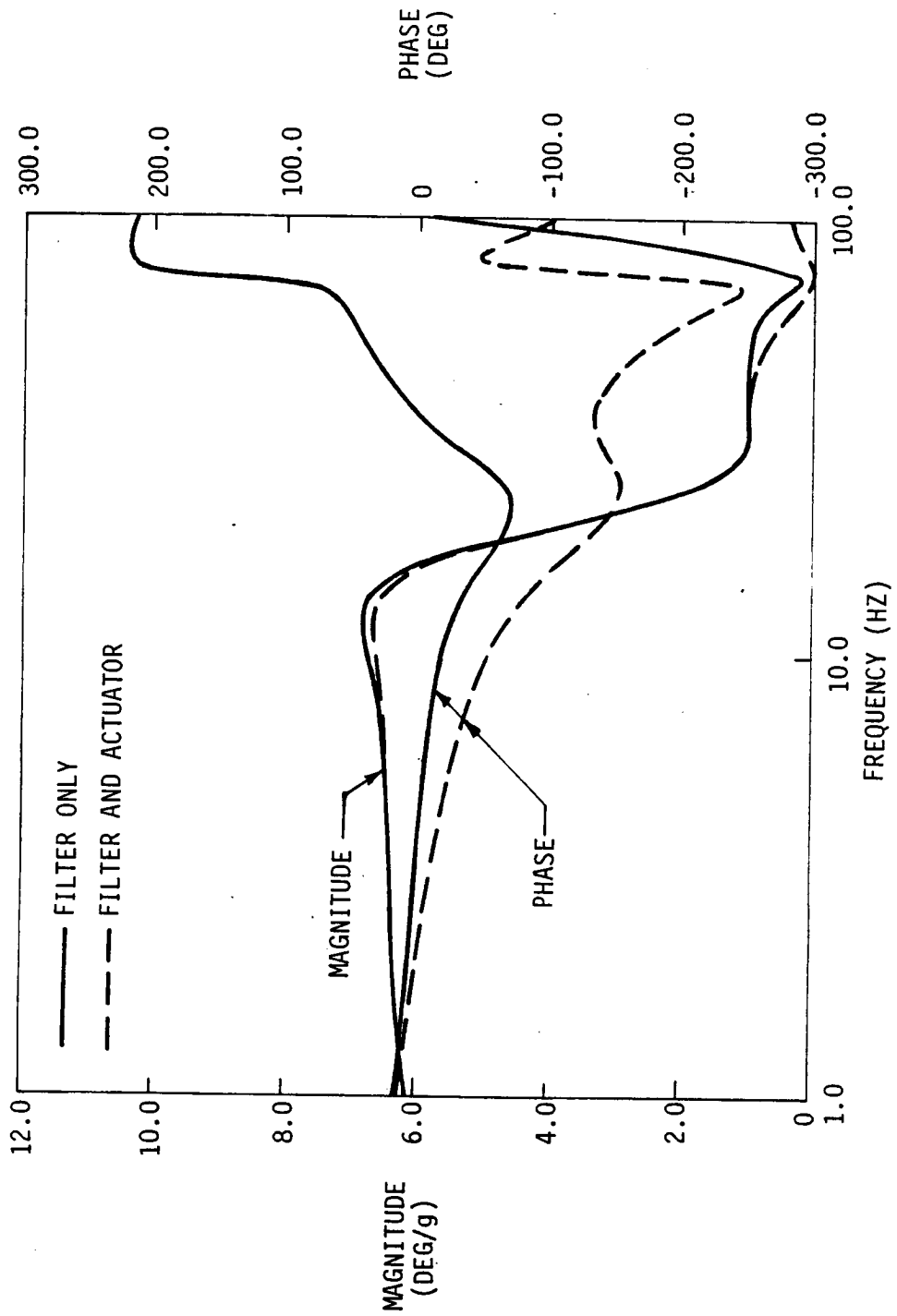
FIGURE 78

ANTISYMMETRIC FREQUENCY RESPONSE OF FSS SHAPING FILTER
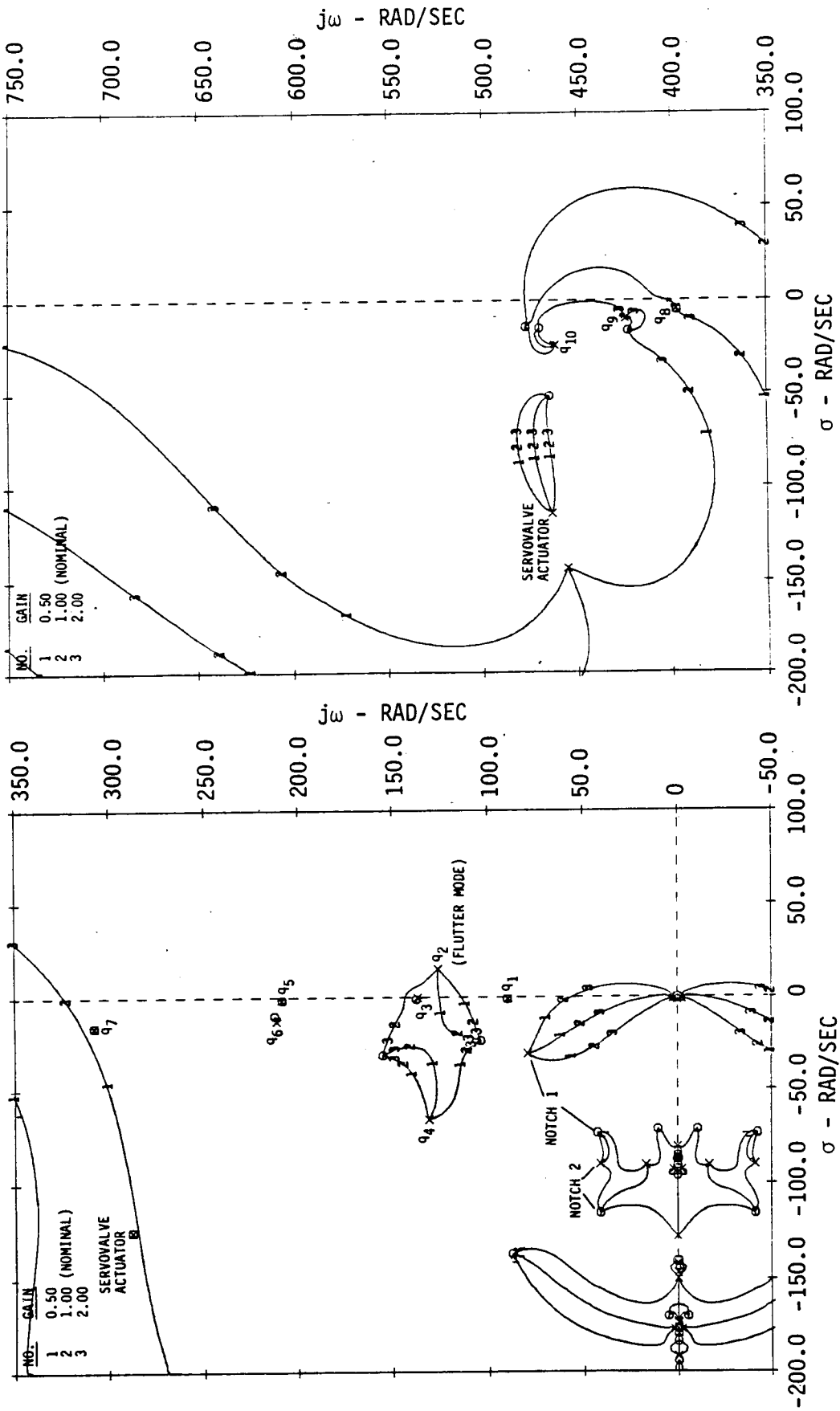
FIGURE 79

DAST ARW-2 PHASE-GAIN ROOT LOCUS OF SYMMETRIC FSS, NOMINAL SYSTEM

126
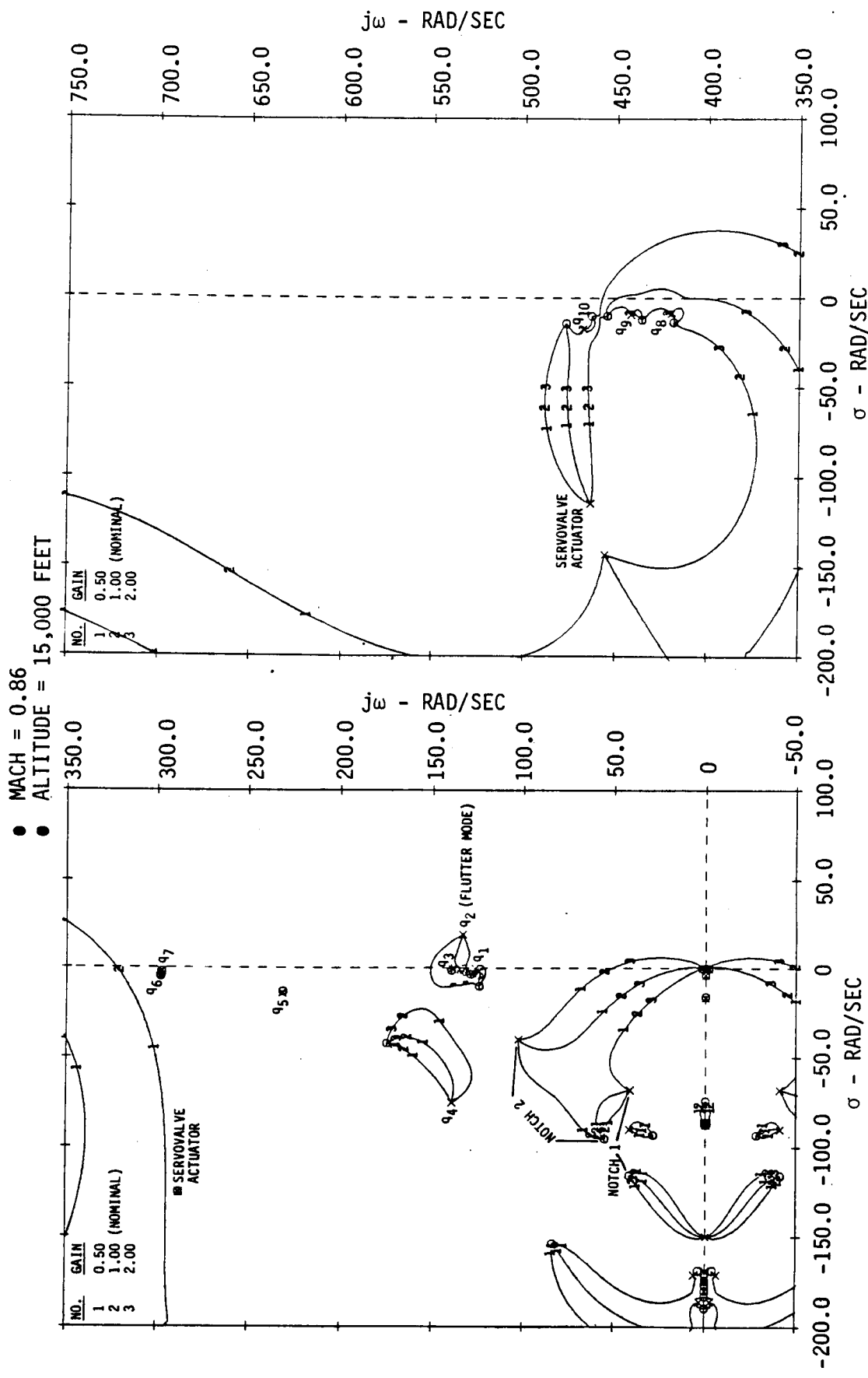
FIGURE 80   DAST ARW-2 PHASE-GAIN ROOT LOCUS OF ANTISYMMETRIC FSS, NOMINAL SYSTEM

● MACH = 0.86
● ALTITUDE = 15,000 FEET

127
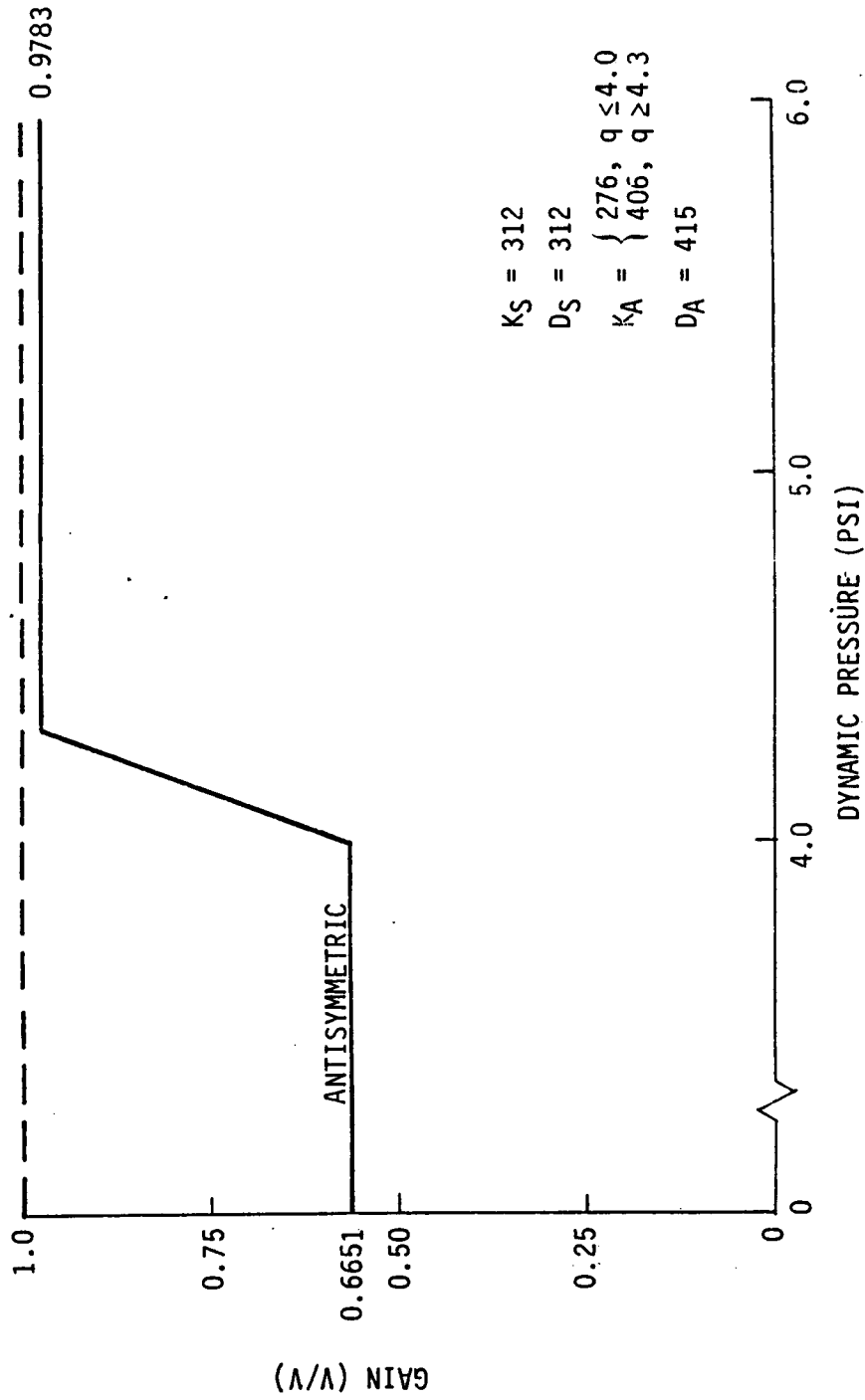
FIGURE 81

ANTISYMMETRIC SCHEDULER

6.3.4 Flutter Suppression System Performance. Analysis was conducted to evaluate performance and sensitivity of the flutter suppression system and compatibility of the system with gust load alleviation, maneuver load alleviation, relaxed static stability and automatic flight control systems. Performance evaluation consisted of analysis to establish the ability of the FSS to stabilize the flutter mode and not degrade stability of the other structural modes throughout the flutter envelope to a damping ratio of less than 0.01, except when the unaugmented model damping ratio is below 0.01. The flutter suppression system definition used for the performance evaluation is presented in Paragraph 6.3.3.4.

Analysis was also conducted to define sensitivity of the FSS to various expected system variations and these sensitivity studies are described in Paragraph 6.3.5.

Effects of the FSS on rigid body modes and effects of the GLA, MLA, RSS and AFCS on the flutter modes were examined to determine if the systems were compatible. System compatibility is discussed in Paragraph 6.8. All systems are compatible.

6.3.4.1 Stability. Analysis was conducted to determine stability characteristics of the DAST ARW-2 vehicle with the FSS over the entire flutter envelope. This analysis included determination of damping and frequency of the flutter mode and other structural elastic modes with the FSS operating and the evaluation of stability margins of the system. A list of all flight conditions analyzed is presented on Figure 65.

6.3.4.1.1 Damping and Frequency Evaluation. Closed loop damping and frequency were determined for each of the rigid body and structural elastic modes with the FSS engaged. The resulting flutter boundaries with the systems operating are shown on Figure 66. Both systems exceed design goals. The higher closed loop symmetric flutter boundary is due to the higher loop gain.

Damping ratios and frequencies with the FSS on and off are presented for the symmetric and antisymmetric systems at Mach 0.86 and 15,000 feet altitude on Figures 82 and 83 respectively. This data shows that the FSS does not reduce mode damping ratio to below 0.01 or degrade damping of modes with damping ratios below 0.01.

Flutter mode damping ratios versus Mach number at a constant altitude of 15,000 feet is shown for the symmetric and antisymmetric systems on Figures 84 and 85, respectively. These plots illustrate the violence of the flutter modes and the capability of the FSS to stabilize the modes to 1.2 V_D. Flutter mode damping ratio versus altitude at Mach 0.86 is shown for both on Figure 86 and 87.

- MACH = 0.86
- ALTITUDE = 15,000 FEET
- UNSCALED EOM

MODE	OPEN LOOP		CLOSED LOOP	
	DAMPING (ζ)	FREQUENCY (HZ)	DAMPING (ζ)	FREQUENCY (HZ)
PHUGOID	0.2067	0.0071	0.2067	0.0071
SHORT PERIOD	0.5077	0.4470	1.0000	0.2479
q_1 (FLUTTER MODE)	0.0105	14.235	0.0126	14.2748
q_2	-0.1190	20.137	0.1791	18.4863
q_3	0.0024	21.715	0.0094	21.8349
q_4	0.4521	23.349	0.1899	22.8006
q_5	0.0084	33.241	0.0083	33.1778
q_6	0.0619	33.711	0.0480	33.8741
q_7	0.05265	49.051	0.0526	49.0513
q_8	0.0118	63.182	0.0110	63.2372
q_9	0.0238	67.556	0.0222	67.4680
q_{10}	0.0524	73.600	0.0525	73.6068
SERVOVALVE ACTUATOR	0.3997	49.975	0.3997	49.9746
	0.2398	75.996	0.1659	75.0067
ACTUATOR NOTCH	0.2995	75.996	0.2338	99.1921
FILTER	1.0000	101.859	1.0000	83.4313
FILTER	1.0000	32.149	1.0000	30.9143
FILTER	1.0000	23.873	1.0000	22.4560
FILTER	1.0000	0.3183	1.0000	0.2479
NOTCH 1	0.9089	15.760	0.8660	13.5282
NOTCH 2	0.3610	13.528	0.2824	8.5497

FIGURE 82

DAST ARW-2 SYMMETRIC ELASTIC MODE DAMPING AND FREQUENCY

● MACH = 0.86
● ALTITUDE = 15,000 FEET
● UNSCALED EOM

MODE	OPEN LOOP		CLOSED LOOP	
	DAMPING (ζ)	FREQUENCY (HZ)	DAMPING (ζ)	FREQUENCY (HZ)
DUTCH ROLL	0.1013	0.2940	0.1093	0.2938
q_1 (FLUTTER MODE)	0.0032	20.1276	0.0323	19.7278
q_2	-0.1372	21.4575	0.0713	21.9226
q_3	0.0040	22.1686	0.0107	22.2626
q_4	0.4735	25.1816	0.2325	26.6431
q_5	0.0602	36.8933	0.0556	36.8799
q_6	0.0487	44.0945	0.0487	44.0945
q_7	0.0077	47.3698	0.0078	47.3650
q_8	0.0214	66.9585	0.0212	66.9456
q_9	0.0209	70.4047	0.0208	70.4031
q_{10}	0.0367	74.5435	0.0361	74.6541
SERVOVALVE ACTUATOR	0.3997	49.9746	0.3997	49.9746
	0.2398	75.9964	0.1254	78.3808
ACTUATOR NOTCH	0.2995	75.9964	0.1139	61.1523
FILTER	1.0000	101.8590	1.0000	76.3762
FILTER	1.0000	49.6563	1.0000	55.4267
FILTER	1.0000	0.3183	0.1093	0.2939
FILTER	1.0000	278.5212	0.1709	282.6790
FILTER	1.0000	23.8732	0.9547	19.6087
NOTCH 1	0.9089	15.7601	0.9574	15.5153
NOTCH 2	0.3610	17.5070	0.3177	7.7501

FIGURE 83

DAST ARW-2 ANTISYMMETRIC ELASTIC MODE DAMPING AND FREQUENCY
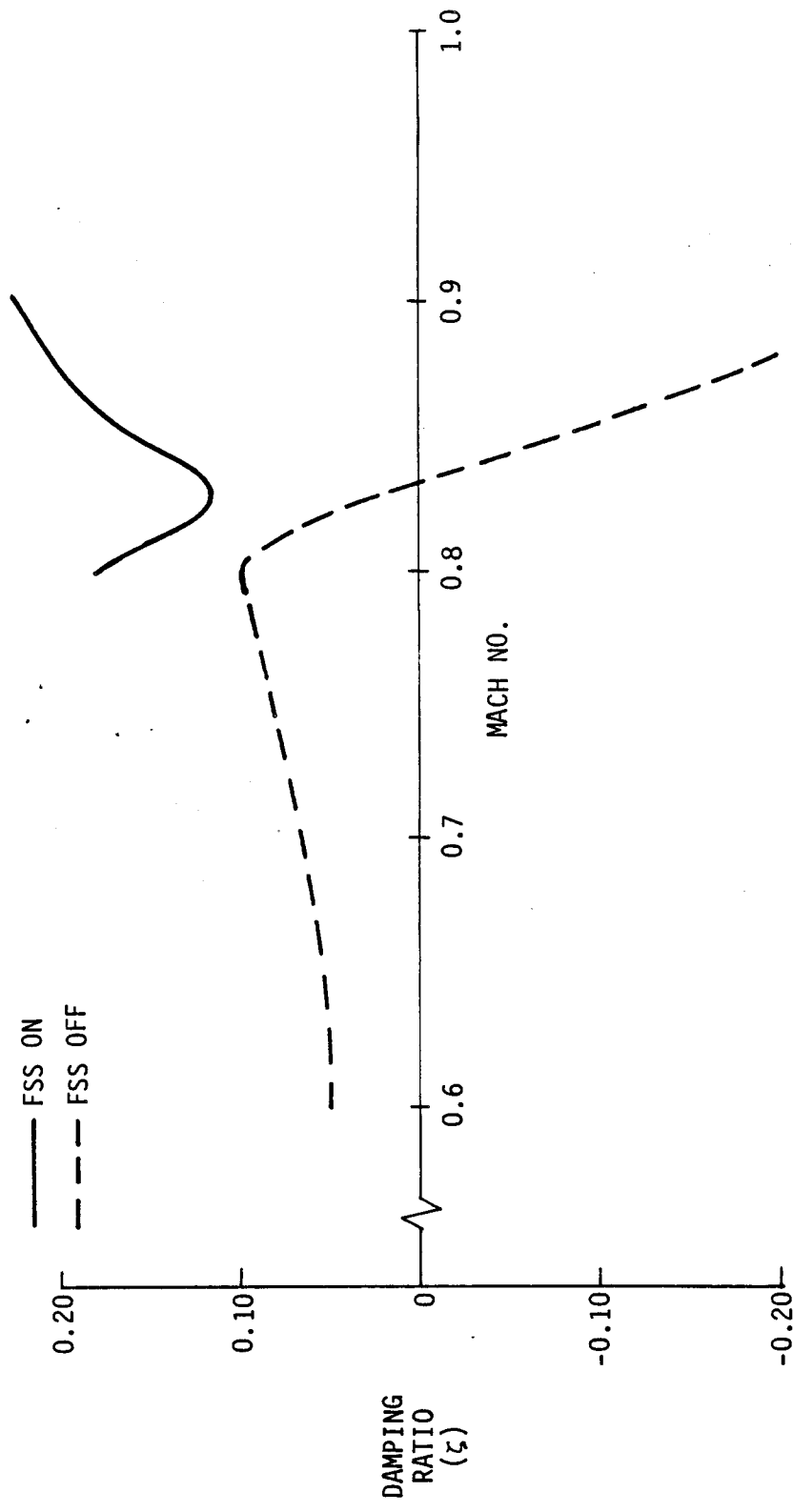
FIGURE 84

DAST ARW-2 SYMMETRIC FLUTTER MODE DAMPING, ALTITUDE: 15,000 FEET
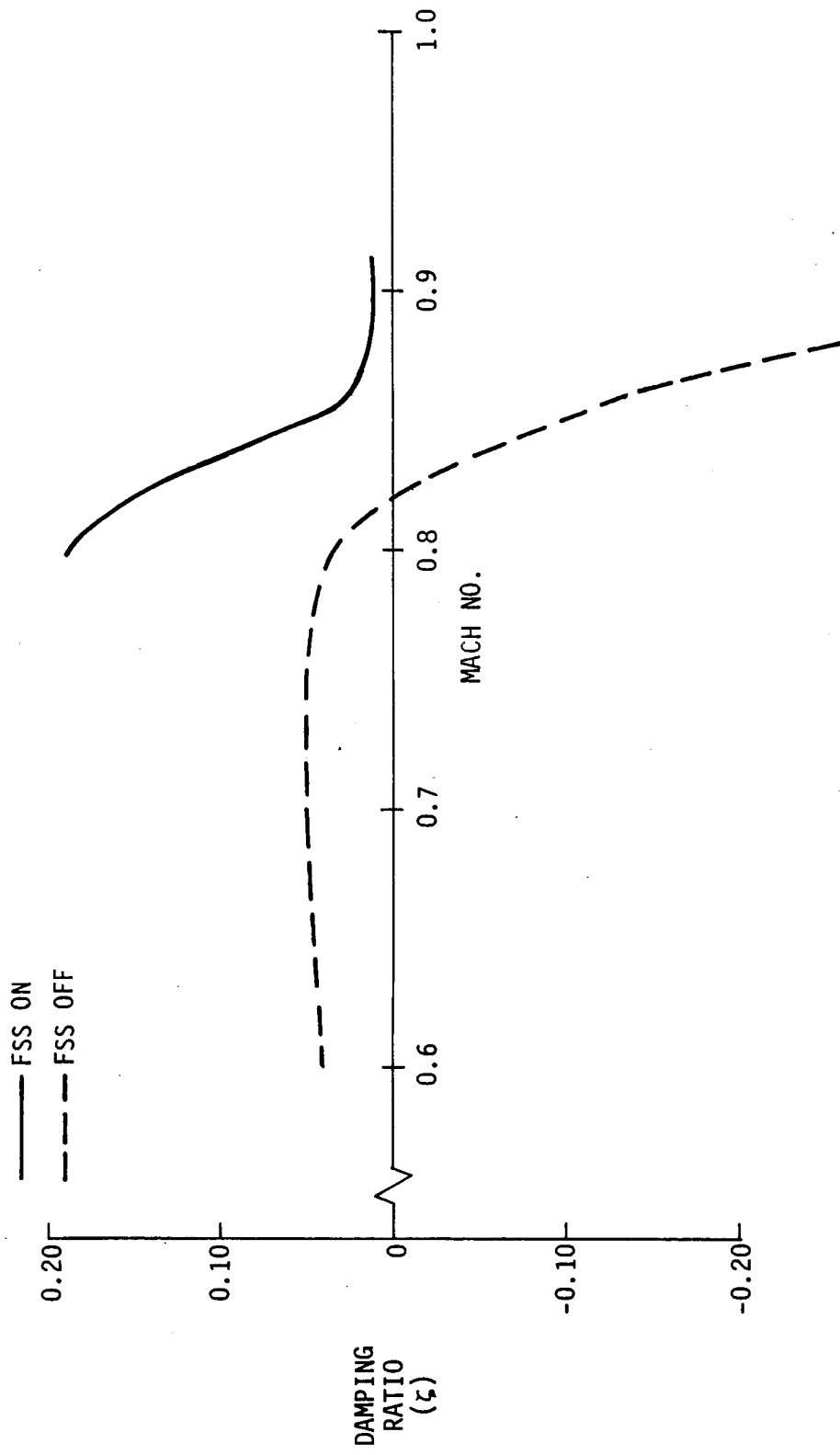
FIGURE 85

DAST ARW-2 ANTISYMMETRIC FLUTTER MODE DAMPING, ALTITUDE: 15,000 FEET

133
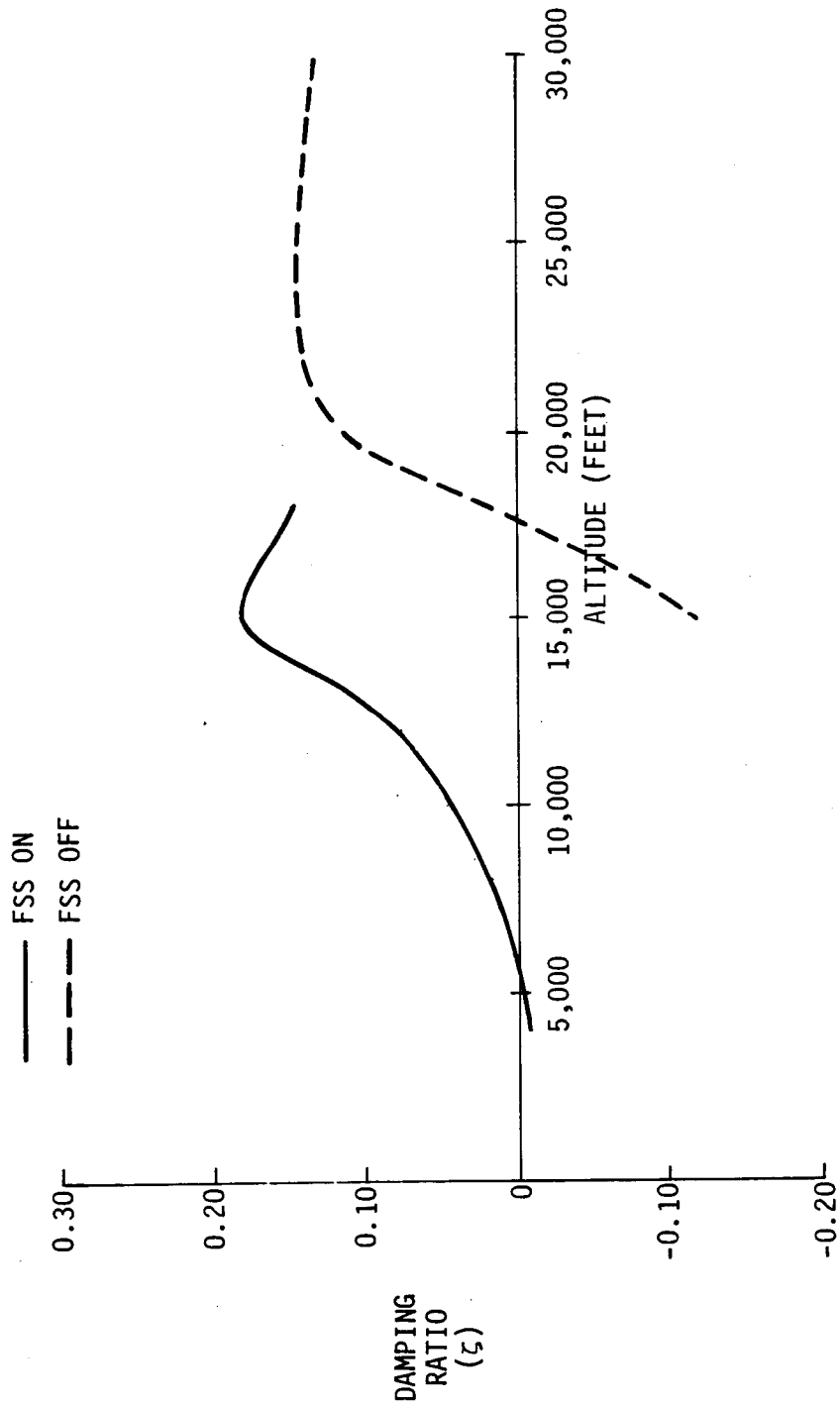
FIGURE 86

DAST ARW-2 SYMMETRIC FLUTTER MODE DAMPING, MACH: 0.86
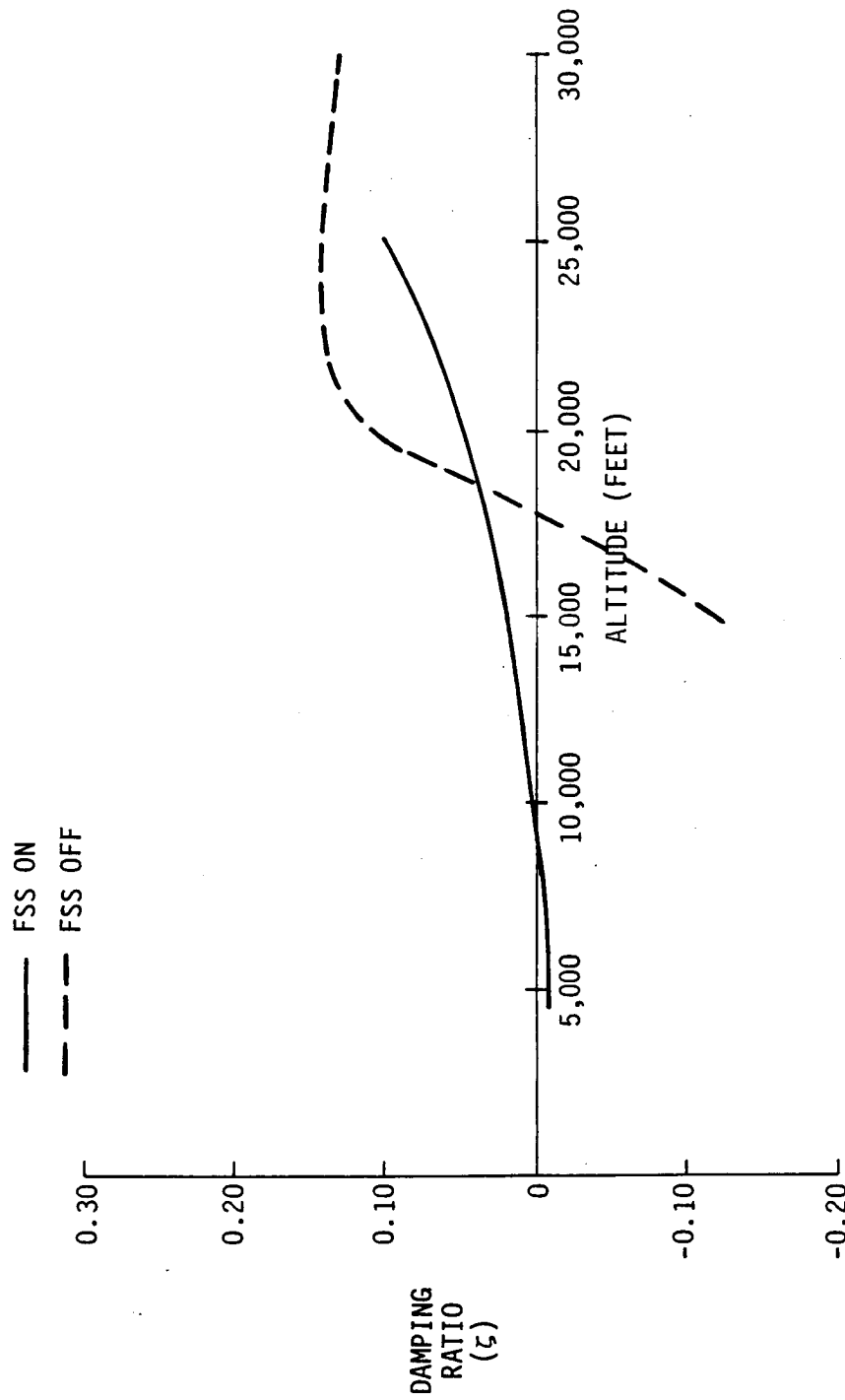
FIGURE 87

DAST ARW-2 ANTISYMMETRIC FLUTTER MODE DAMPING, MACH: 0.86

135

6.3.4.1.2 Stability Margins. Analysis was conducted to demonstrate the FSS meets stability margin requirements shown on Figure 70. Figures 79 and 80 show the nominal FSS has a greater than ±6.0 dB gain margins and ±45 degrees phase margins at the design condition. Nominal refers to a system without gain or parameter scheduling. When compared to the phase and gain requirements shown on Figure 69 and the flutter suppression envelope shown on Figure 68, Figures 88 through 92 show that the symmetric subsystem does not require gain or time constant scheduling, while Figure 93 shows the antisymmetric subsystem requires gain scheduling to meet the gain and phase margin requirements at the 0.91 Mach, 15,000 feet condition. Figures 93 through 97 show that the antisymmetric system meets the phase and gain requirements shown on Figure 69 with the implementation of the scheduler shown on Figure 81.

6.3.4.2 Control Surface Requirements. Analysis was conducted to determine maximum control surface activity in random turbulence to verify that the servoactuator system components selected in iteration two design study were adequate for the updated FSS. The results of this analysis are discussed in Section 6.1 and shown on Figures 45 and 46.

6.3.4.2.1 A Simulated Gust Excitation Generator. Outboard control surface response to a random noise generator is included in the Drone Active Control Electronics (DACE) unit to simulate a gust environment as described in Paragraph 7.4.9. The generator output signal is input to the inboard ailerons for airplane excitation. The outboard ailerons will respond to inboard aileron displacements and rates when the FSS is engaged and the frequency response results are shown on Figures 98, 99, and 100 which show very little outboard aileron response to inboard excitation below 5 Hz. Figure 101 shows very little inboard response to the random noise generator input above 5 Hz, therefore no inputs to FSS at the flutter frequencies are expected.

6.3.5 FSS Sensitivity. Analysis was conducted to determine sensitivity of the FSS to variations of system parameters. The sensitivity studies included sensor location, notch filter changes in Q and frequency, servoactuator dynamics, hinge moment effects, parameter scheduling and phase and gain changes.

Results of the sensitivity studies show that the FSS provides stability in the flight envelope as implemented without scheduling and will provide stability to 1.2 times the design dive speed with gain scheduling of the antisymmetric filter. The flight conditions analyzed are shown on Figure 65 and the critical phase-gain root loci are shown on Figures 79 and 80, on Figures 88 through 97 and in Appendix C. See Appendix D for sensitivity results.

The airplane is relatively insensitive to small changes in stability derivatives and the ACS tends to increase frequency and damping of the fuselage mode.

Hinge moments change gain and phase of the servoactuators and should be further evaluated during ground and flight test.

136
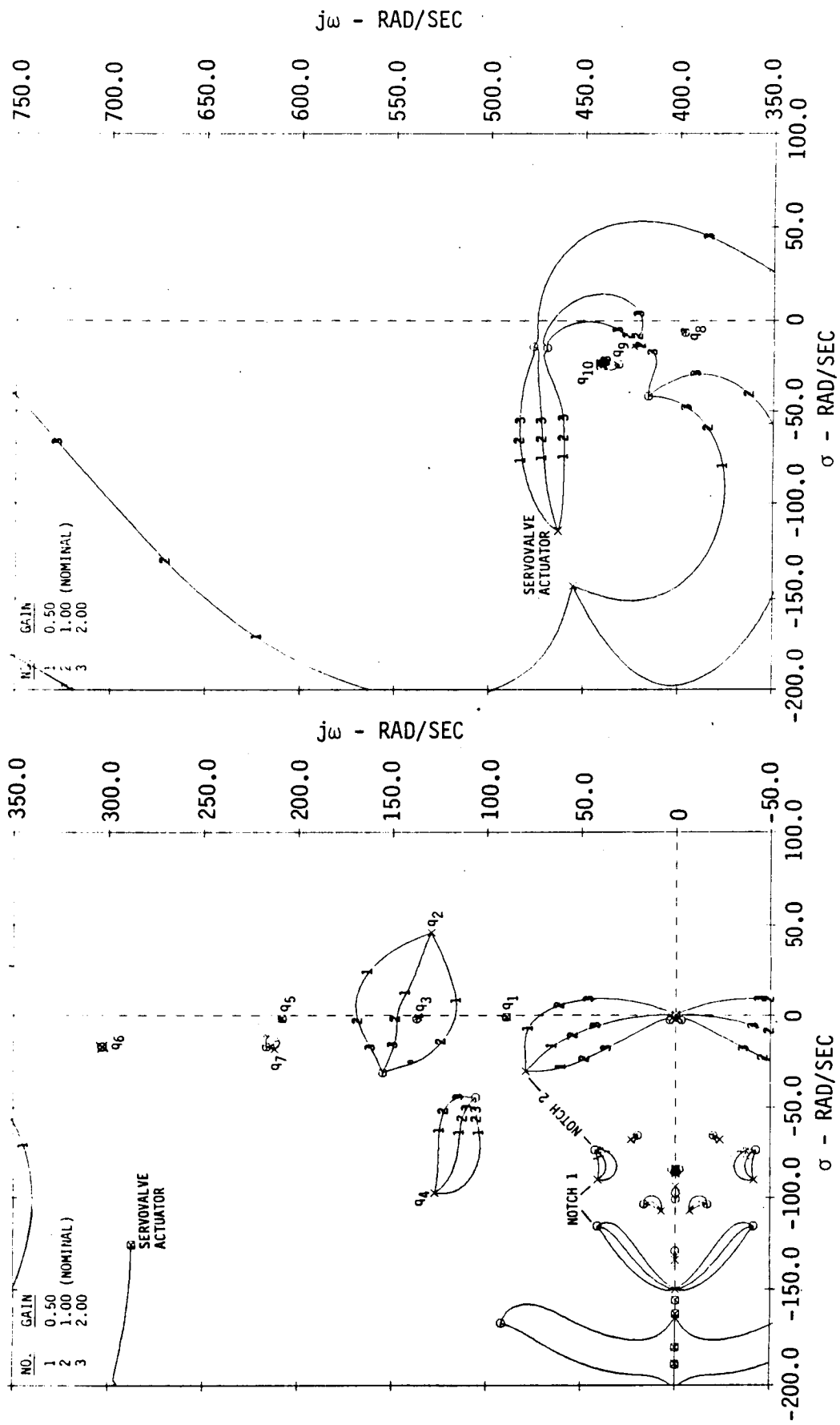
FIGURE 88

DAST ARW-2 PHASE-GAIN ROOT LOCUS OF SYMMETRIC FSS, NOMINAL SYSTEM
AT MACH 0.8 AND 2,000 FEET ALTITUDE
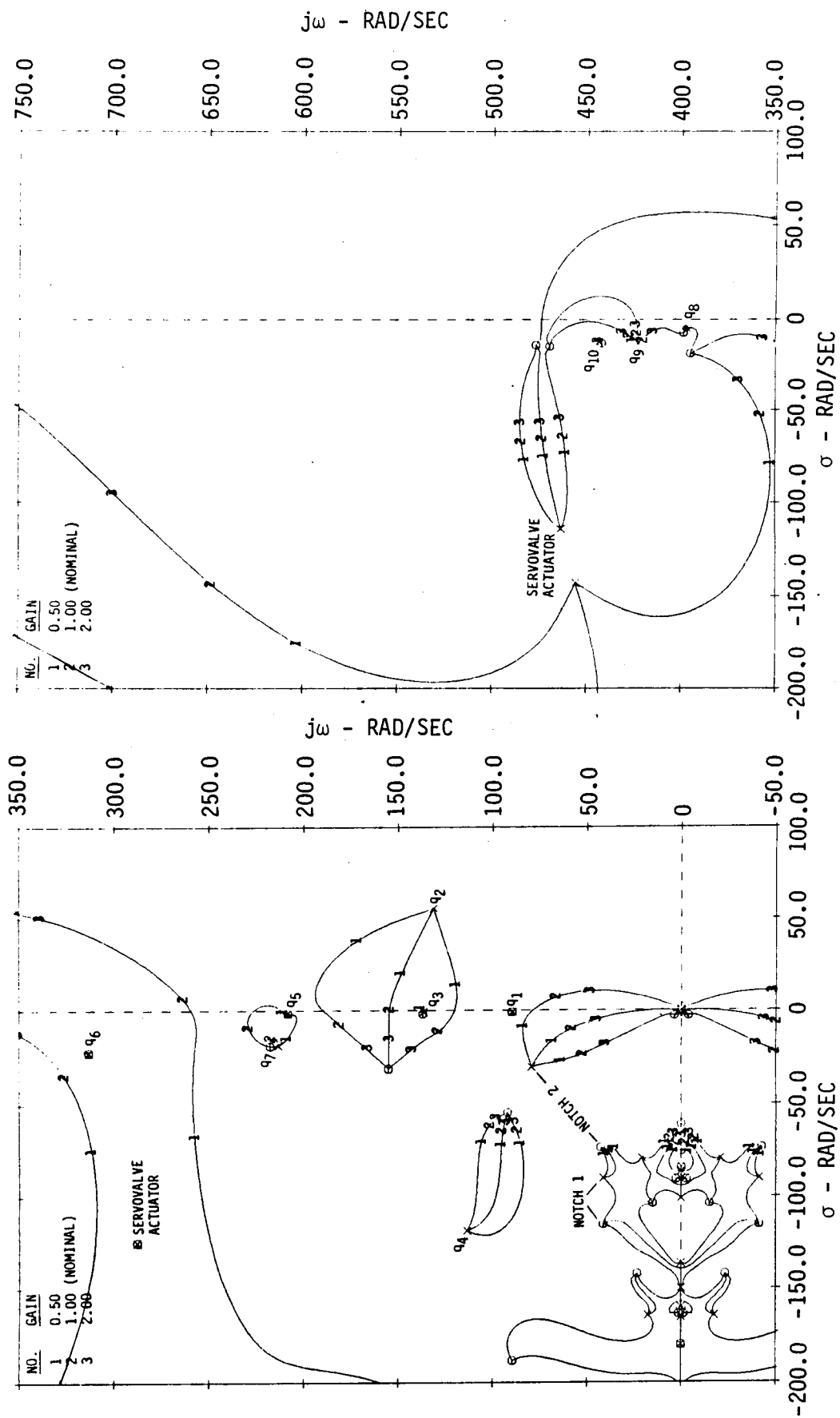
FIGURE 89

DAST ARW-2 PHASE-GAIN ROOT LOCUS OF ANTISYMMETRIC FSS, NOMINAL SYSTEM
AT MACH 0.83 AND 3,000 FEET ALTITUDE

138
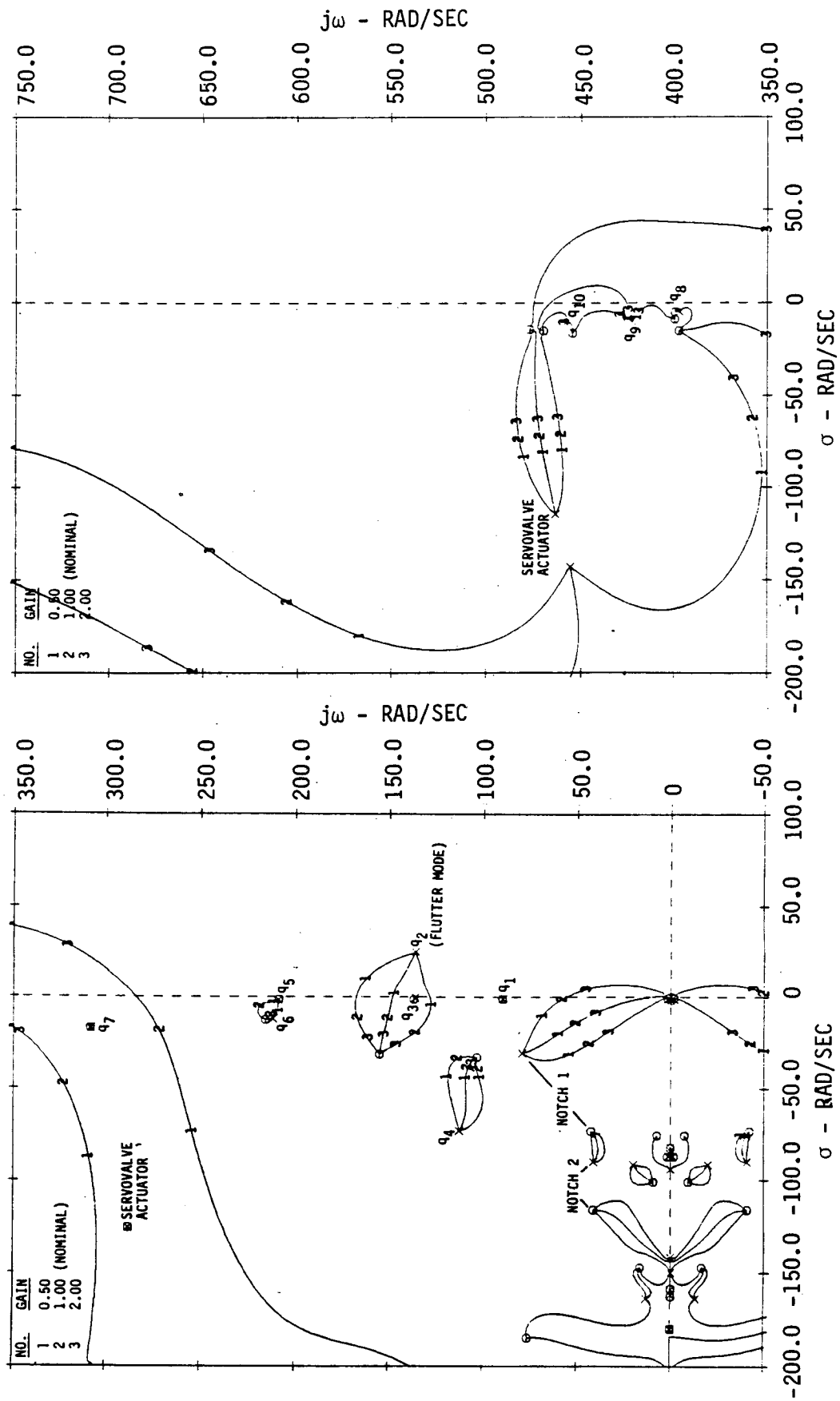
FIGURE 90

DAST ARW-2 PHASE-GAIN ROOT LOCUS OF SYMMETRIC FSS, NOMINAL SYSTEM
AT MACH 0.83 AND 12,000 FEET ALTITUDE
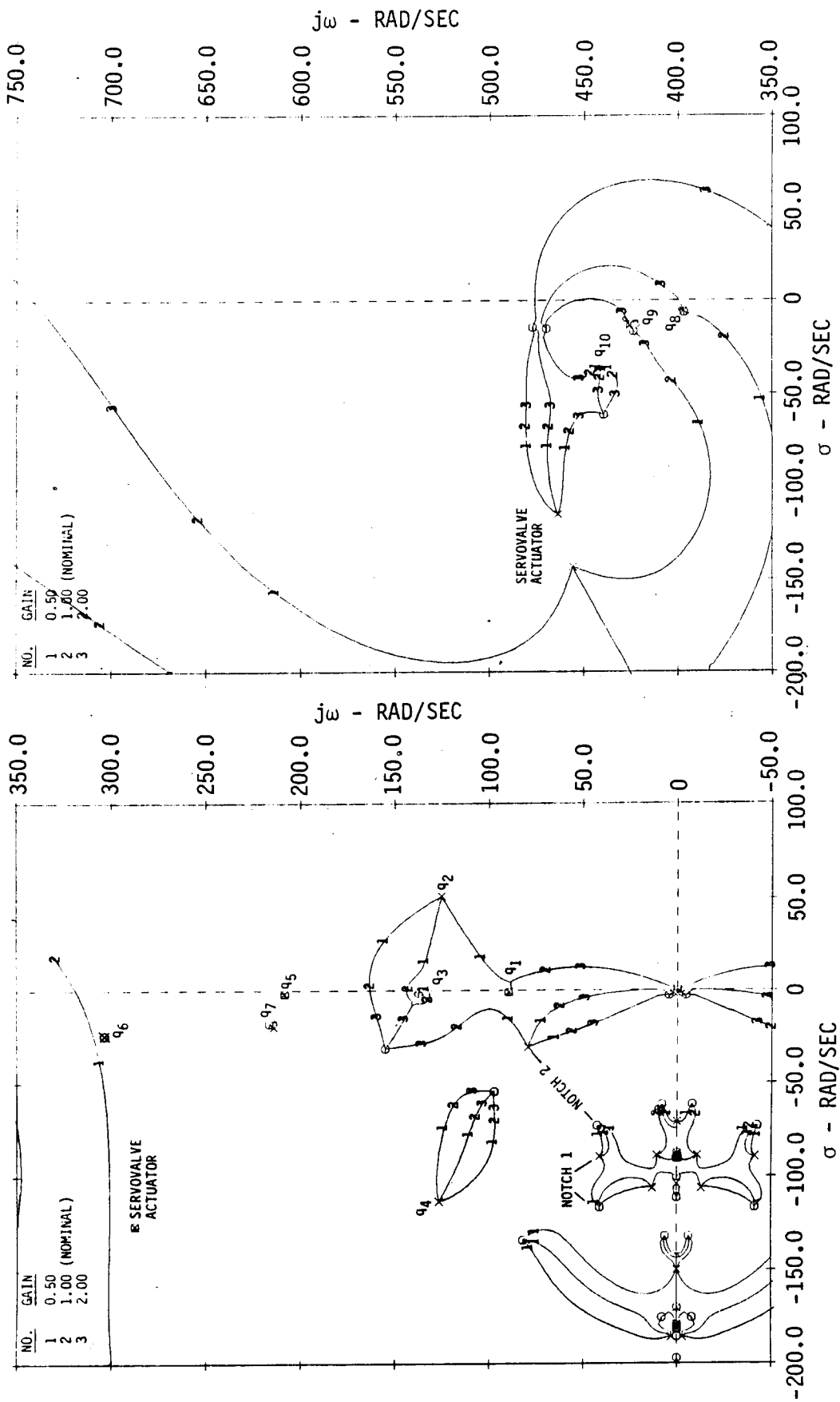
FIGURE 91

DAST ARW-2 PHASE-GAIN ROOT LOCUS OF SYMMETRIC FSS, NOMINAL SYSTEM
AT MACH 0.86 AND 4,250 FEET ALTITUDE
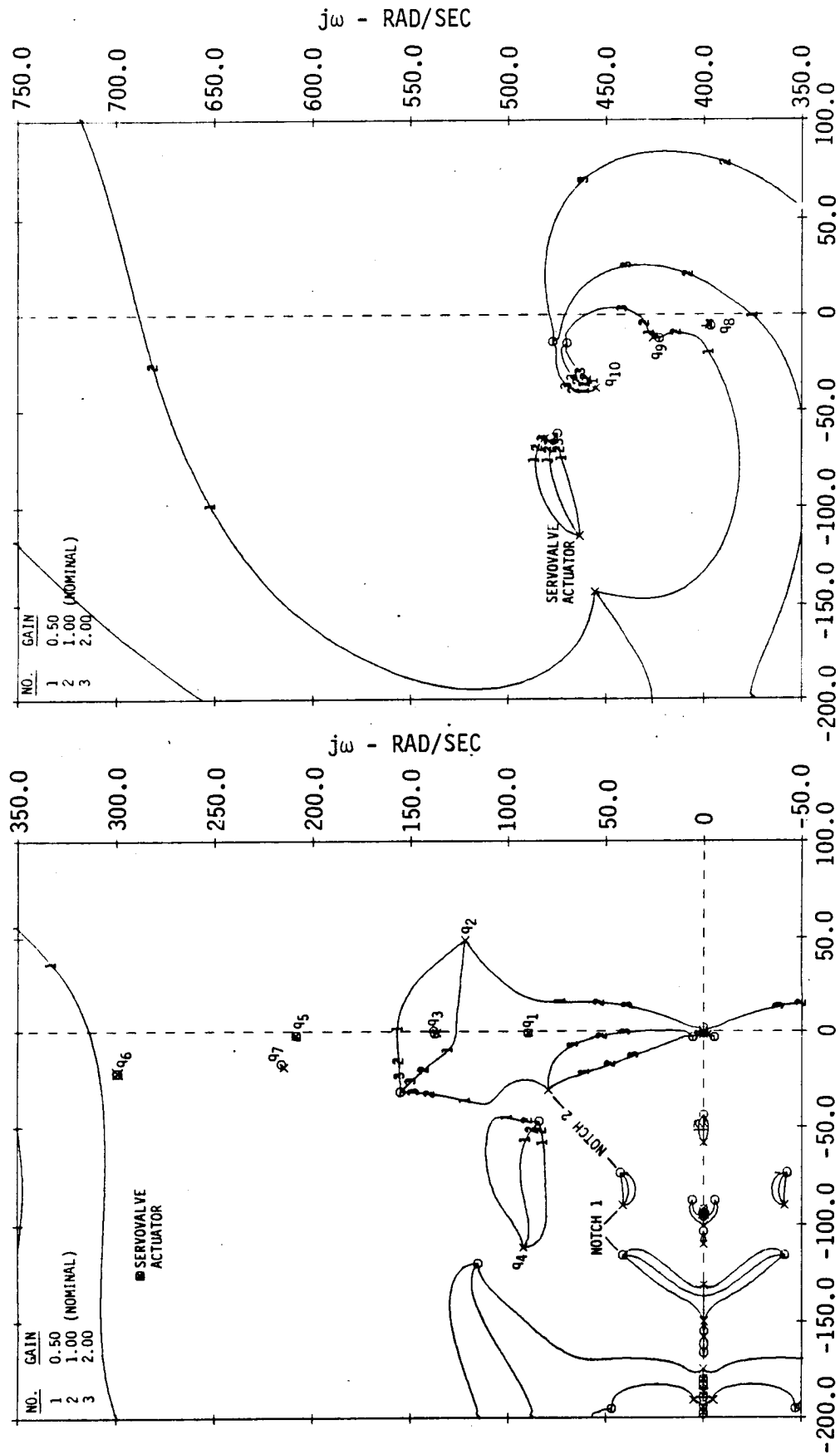
DAST ARW-2 PHASE-GAIN ROOT LOCUS OF SYMMETRIC FSS, NOMINAL SYSTEM
AT MACH 0.91 AND 8,000 FEET ALTITUDE
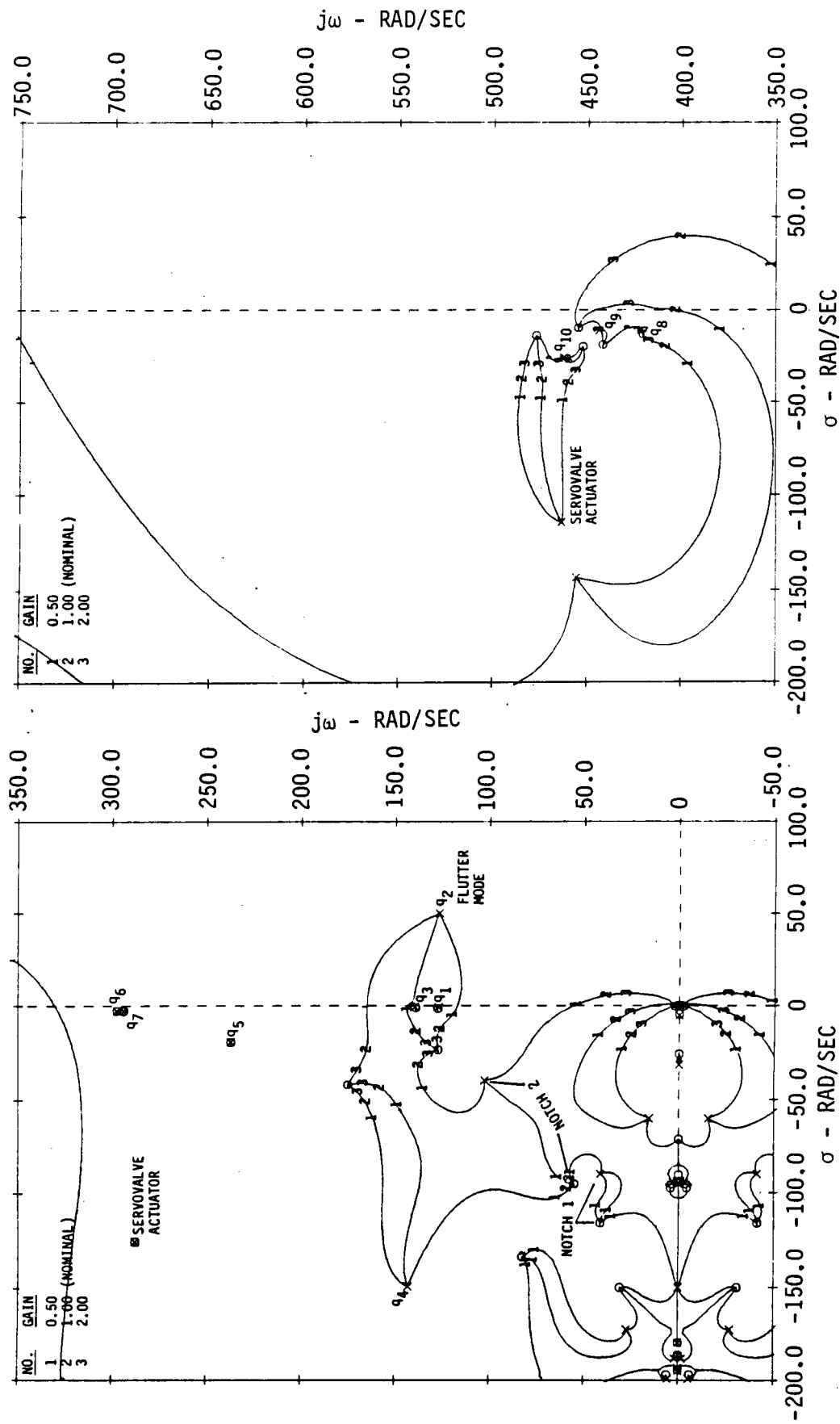
FIGURE 92

FIGURE 93

DAST ARW-2 PHASE-GAIN ROOT LOCUS OF ANTISYMMETRIC FSS WITH PARAMETER SCHEDULING
AT MACH 0.91 AND 8,000 FEET ALTITUDE

142
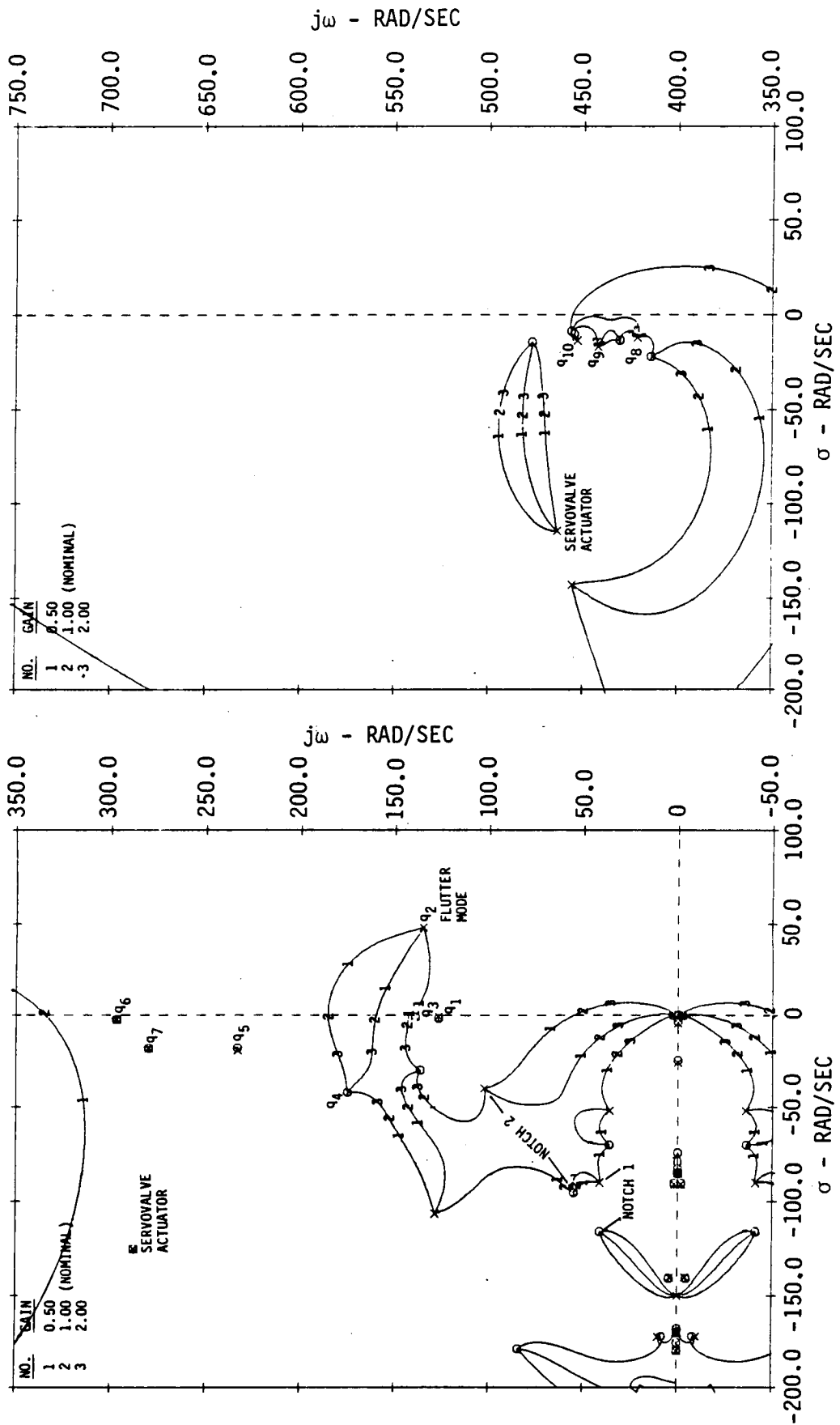
FIGURE 94

DAST ARW-2 PHASE-GAIN ROOT LOCUS OF ANTIYSMMETRIC FSS WITH PARAMETER SCHEDULING
AT MACH 0.8 AND 2,000 FEET ALTITUDE

143
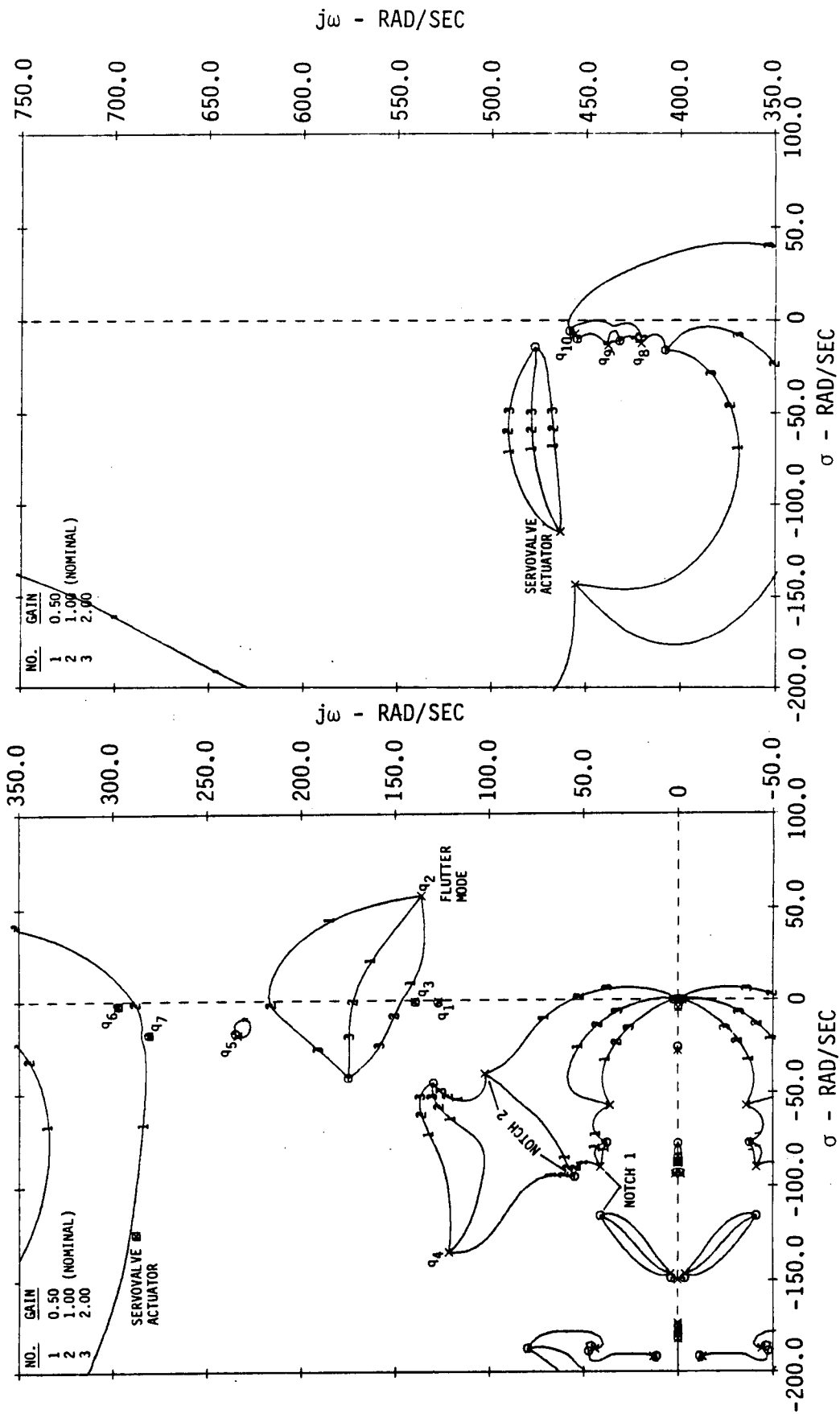
FIGURE 95

DAST ARW-2 PHASE-GAIN ROOT LOCUS OF ANTISYMMETRIC FSS WITH PARAMETER SCHEDULING
AT MACH 0.83 AND 3,000 FEET ALTITUDE

144
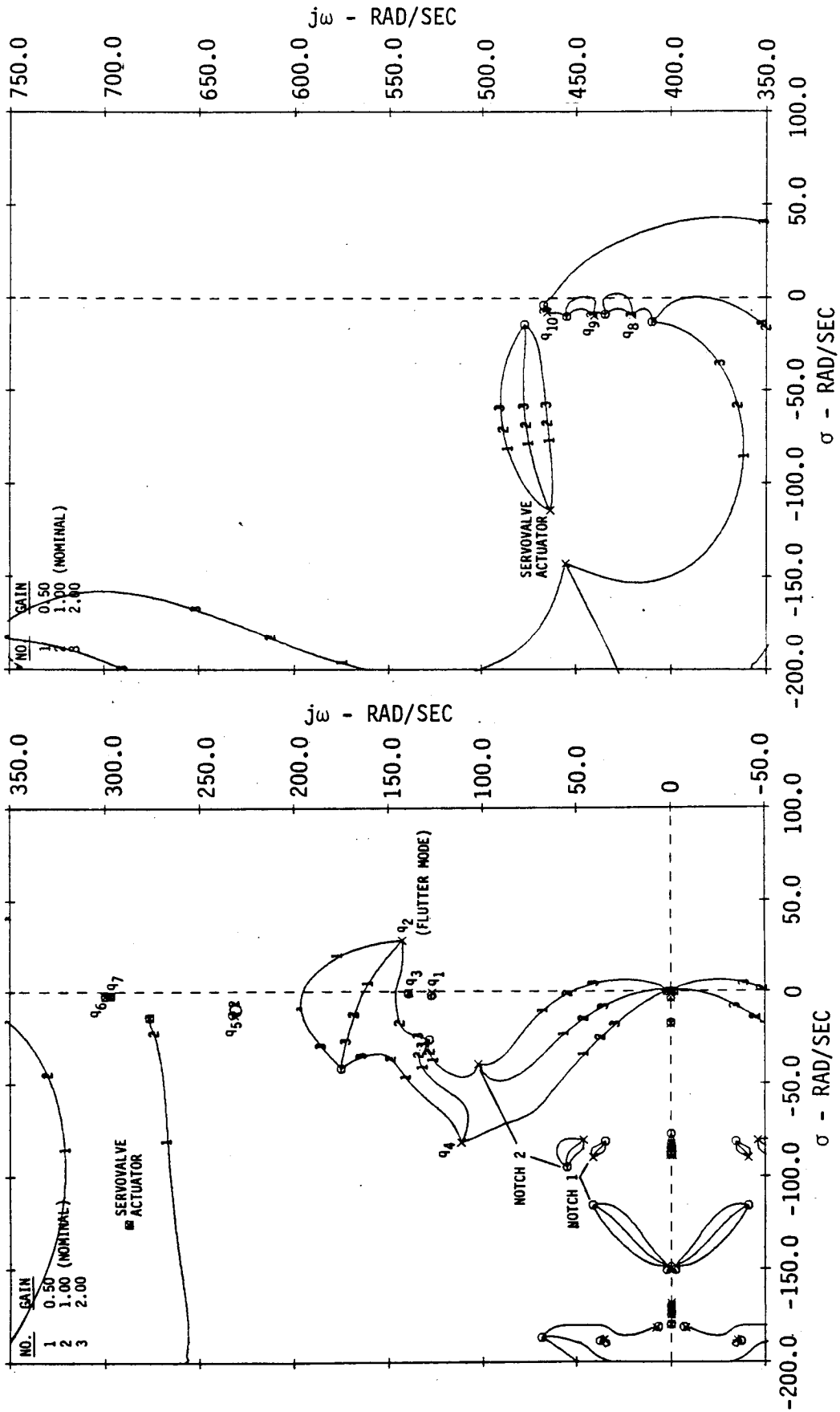
FIGURE 96

DAST ARW-2 PHASE-GAIN ROOT LOCUS OF ANTISYMMETRIC FSS, NOMINAL SYSTEM
AT MACH 0.83 AND 12,000 FEET ALTITUDE
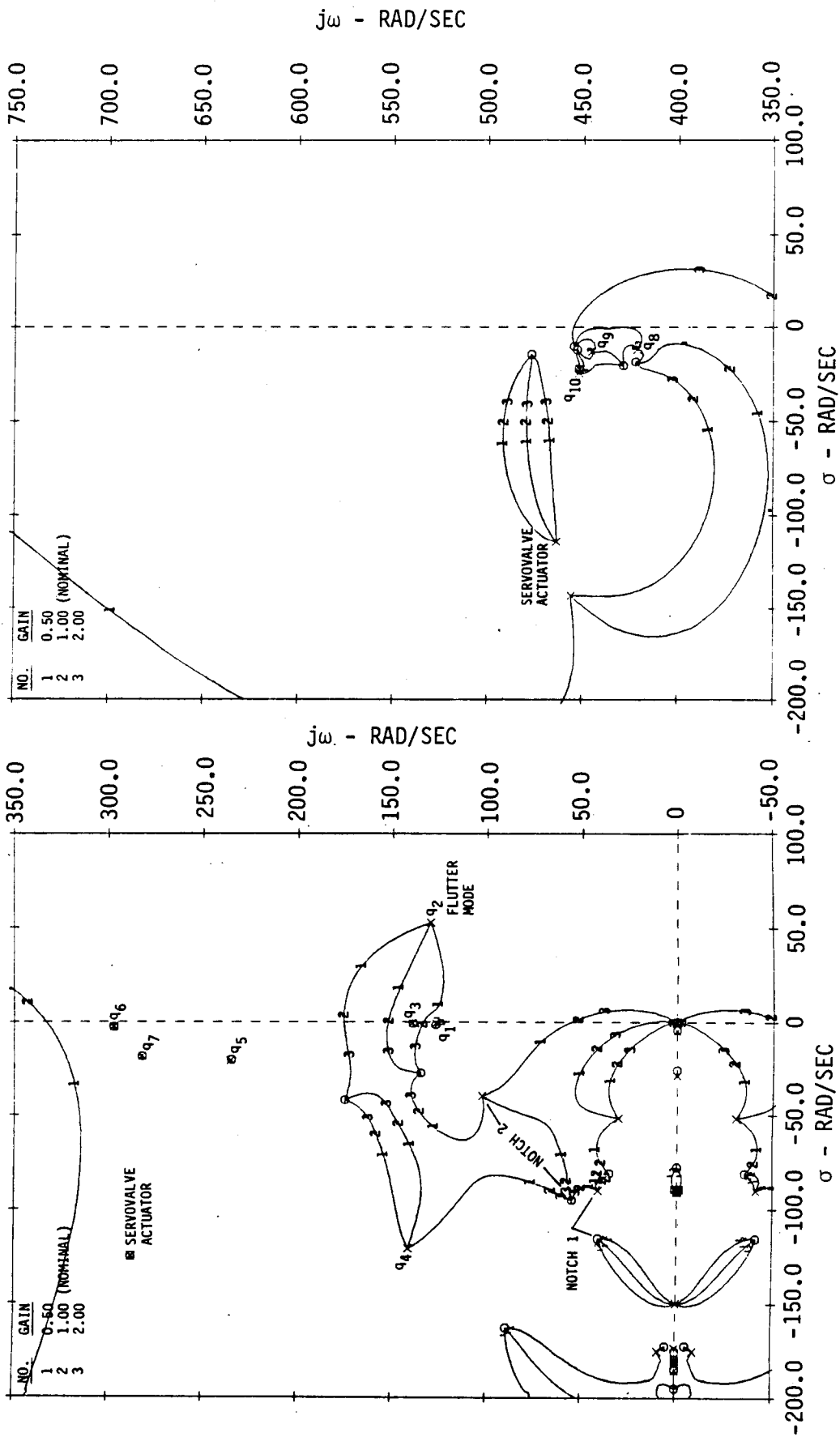
FIGURE 97

DAST ARW-2 PHASE-GAIN ROOT LOCUS OF ANTISYMMETRIC FSS WITH PARAMETER SCHEDULING
AT MACH 0.86 AND 4.250 FEET ALTITUDE
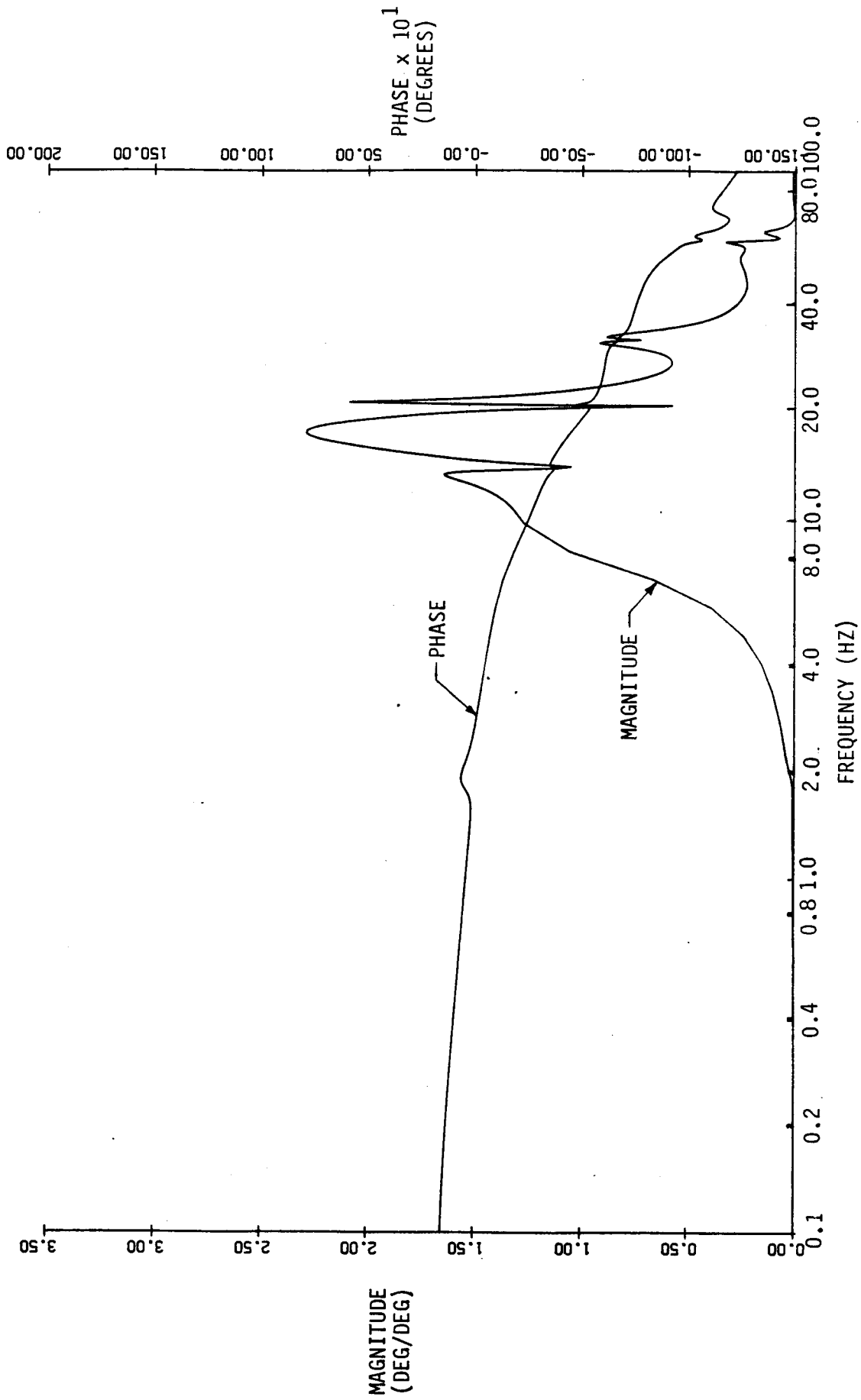
FIGURE 98

DAST ARW-2 OUTBOARD AILERON DISPLACEMENT RESPONSE TO INBOARD AILERON INPUT
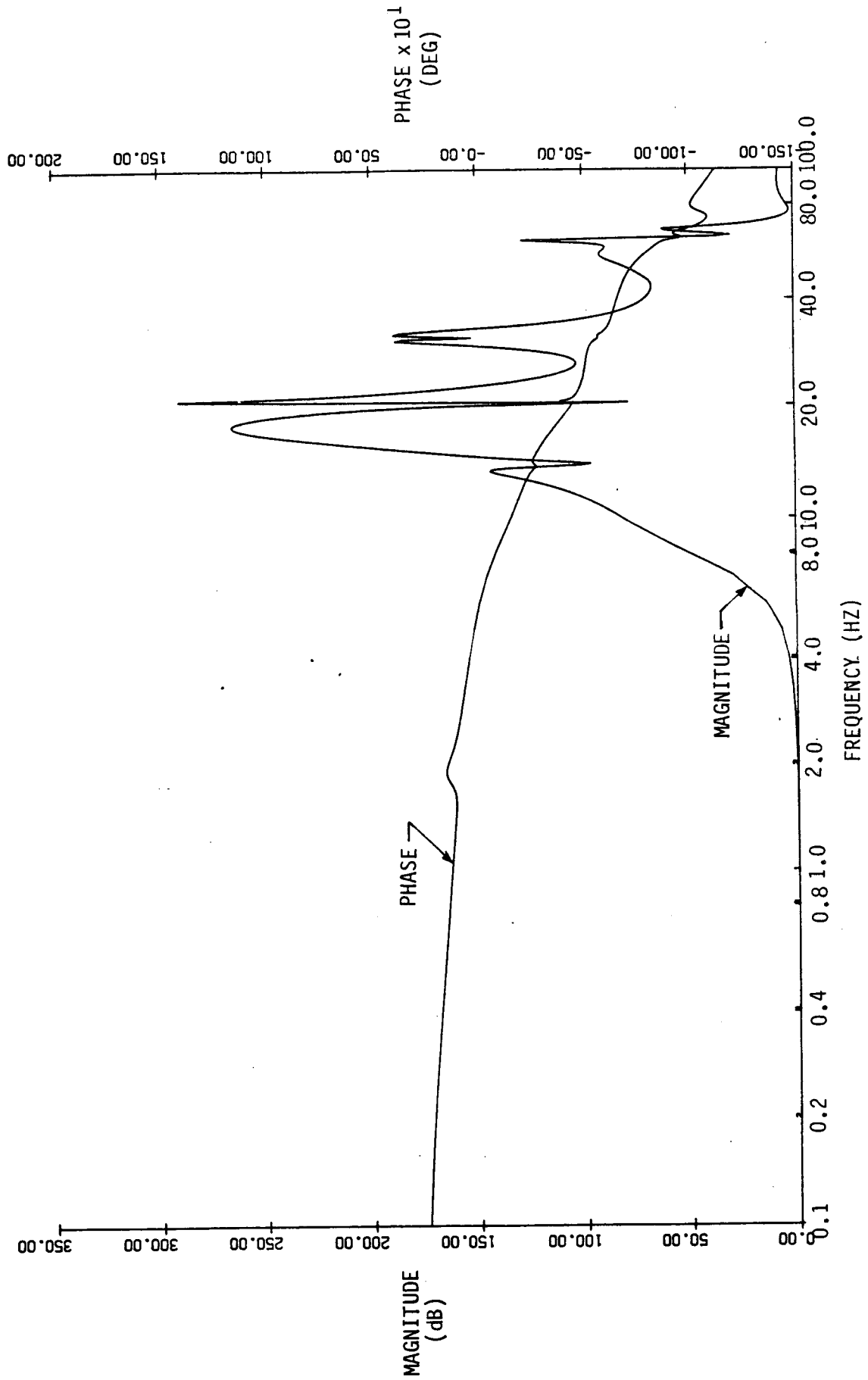
FIGURE 99

DAST ARW-2 OUTBOARD AILERON RATE RESPONSE TO INBOARD AILERON INPUT

148

PHASE x10^1
(DEG)
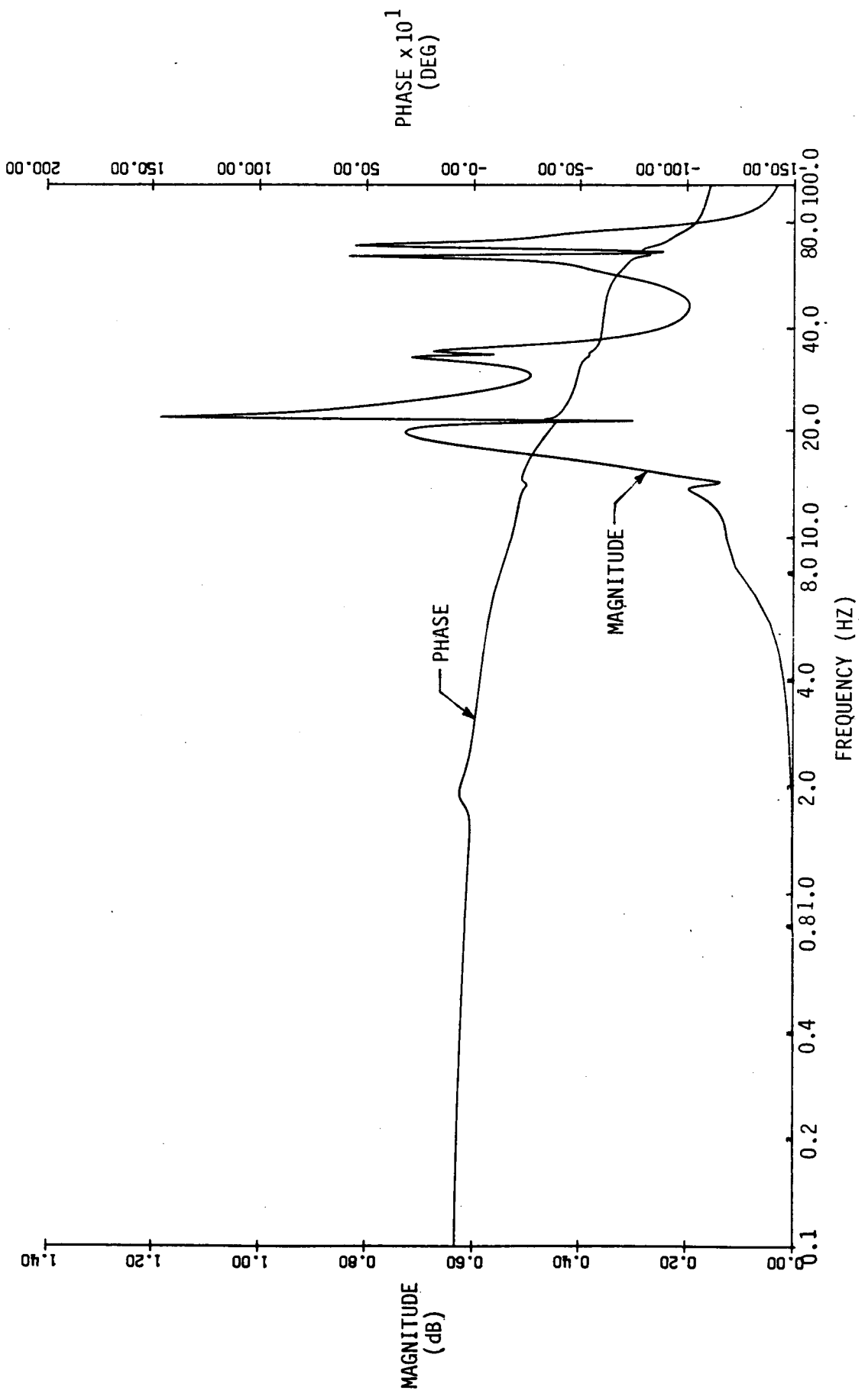
DAST ARW-2 FSS SENSOR ACCELERATION RESPONSE TO INBOARD AILERON INPUT

FIGURE 100

FREQUENCY (HZ)

MAGNITUDE
(dB)

PHASE

MAGNITUDE

149
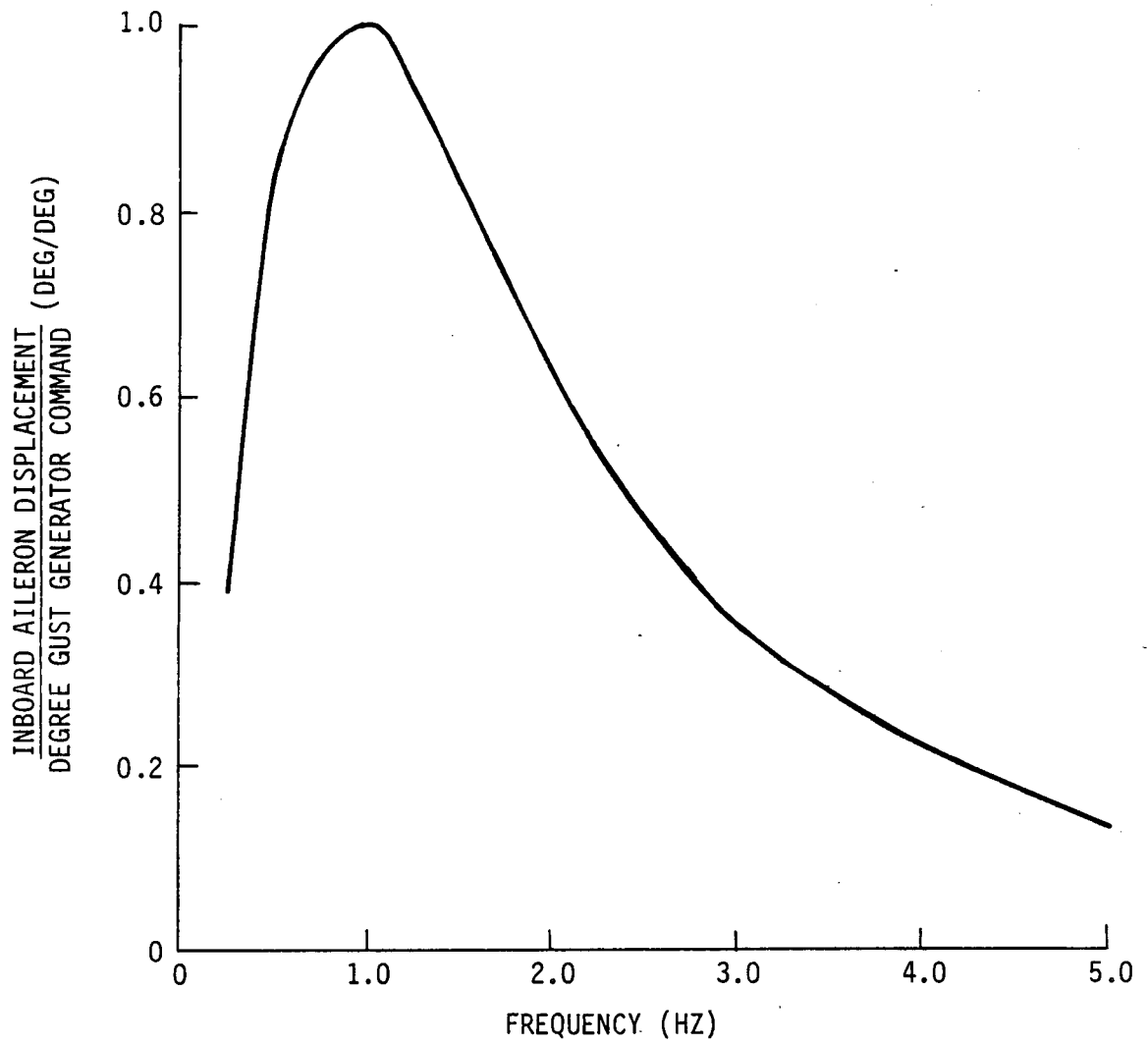
FIGURE 101

INBOARD AILERON DISPLACEMENT RESPONSE TO GUST GENERATOR INPUT

6.3.5.1 Sensor Location. The effects of varying sensor locations are discussed in Paragraph 6.3.3.3. The results of the sensitivity study indicates that sensor location is relatively critical and the sensors should be installed within 0.5 inch of the analyzed locations. Figures 72 and 73 of Appendix D summarize this sensitivity study.

6.3.5.2 Servoactuator Dynamics. Several sensitivity studies were made to determine how system stability is affected by parameter changes within the actuator loop. These studies were conducted using analytical models and included servoactuator loop sensitivity to changes in servo valve models, surface-actuator mode compensation pressure feedback gain reduction, and hinge moment.

Sensitivity studies were not made on the final actuator model derived from testing; however, the results are valid and are presented as insight to guide future actuator evaluations.

6.3.5.2.1 Servovalve Models. Three servovalve models were evaluated which included a Moog Series 30, a Moog Series 31, and a Hydraulic Research Model AR-25. A servovalve with a wide bandwidth is desirable for improved system performance. The Series 31 was discarded because of cost and circuit complexity. The AR-25 servovalve was selected because it is a direct replacement for the Moog Series 30 but has a wider bandwidth as described in Paragraph 6.2. FSS performance improved resulting from the increased servovalve bandwidth even though the closed loop actuator bandwidth did not increase appreciably. Figures 102 and 103 compare servovalve results.

6.3.5.2.2 Surface-Actuator Mode Compensation Filter. During synthesis, a filter was added to the symmetric FSS to cancel the surface-actuator mode (ω_n) and improve FSS performance. The form of this filter is:

$$G_F = \frac{s^2 + 2\delta\omega_n S + \omega_n}{(S + \omega_n)^2}$$

System sensitivity to removing and varying filter parameters was evaluated. The effects of removing the actuator compensation destabilized airplane modes and these modes were difficult to stabilize. Figures 104 and 105 show these effects on symmetric FSS. Removing the antisymmetric compensating filter decreased the lead phase margin to 40 degrees as shown by the result presented on Figure 106 as compared to Figure 107.

Since removing the compensating filter caused adverse effects, implying that the filter should remain in, an evaluation was made to determine the effects of changing parameters within the filter. The compensating surface-actuator filter mode frequency was changed plus and minus 20 percent of the nominal value. The results are summarized on Figure 108 for the symmetric FSS and indicate that the FSS is relatively insensitive to filter parameter changes. The filters are implemented with the highest grade of components which are relatively insensitive to environmental changes. Figures 88 and 89 showing the root locus of this sensitivity analysis can be found in Appendix D.
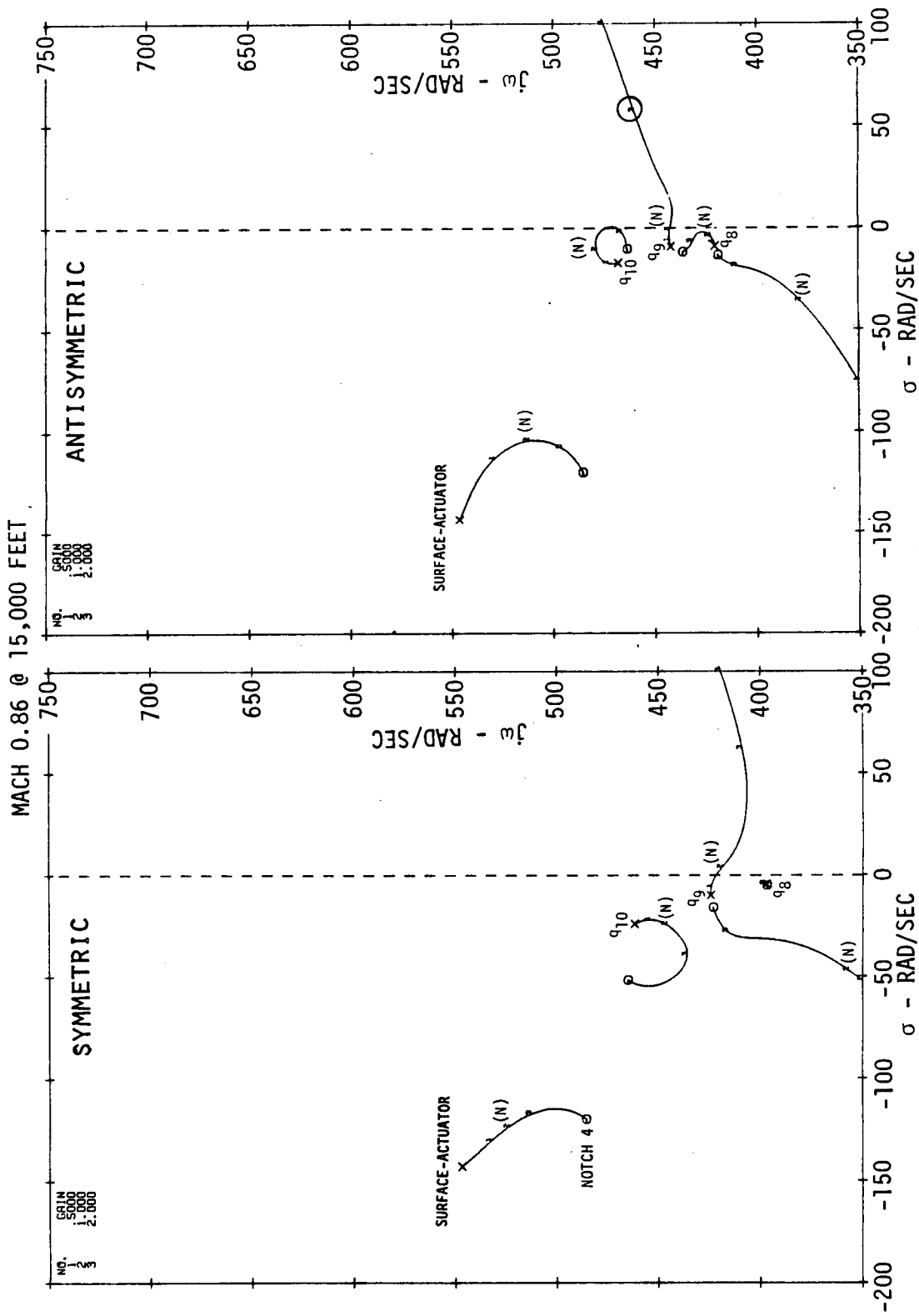
MACH 0.86 @ 15,000 FEET

FIGURE 102

ROOT LOCUS OF SYMMETRIC AND ANTISYMMETRIC FSS WITH SERIES 30 SERVOVALVE

152
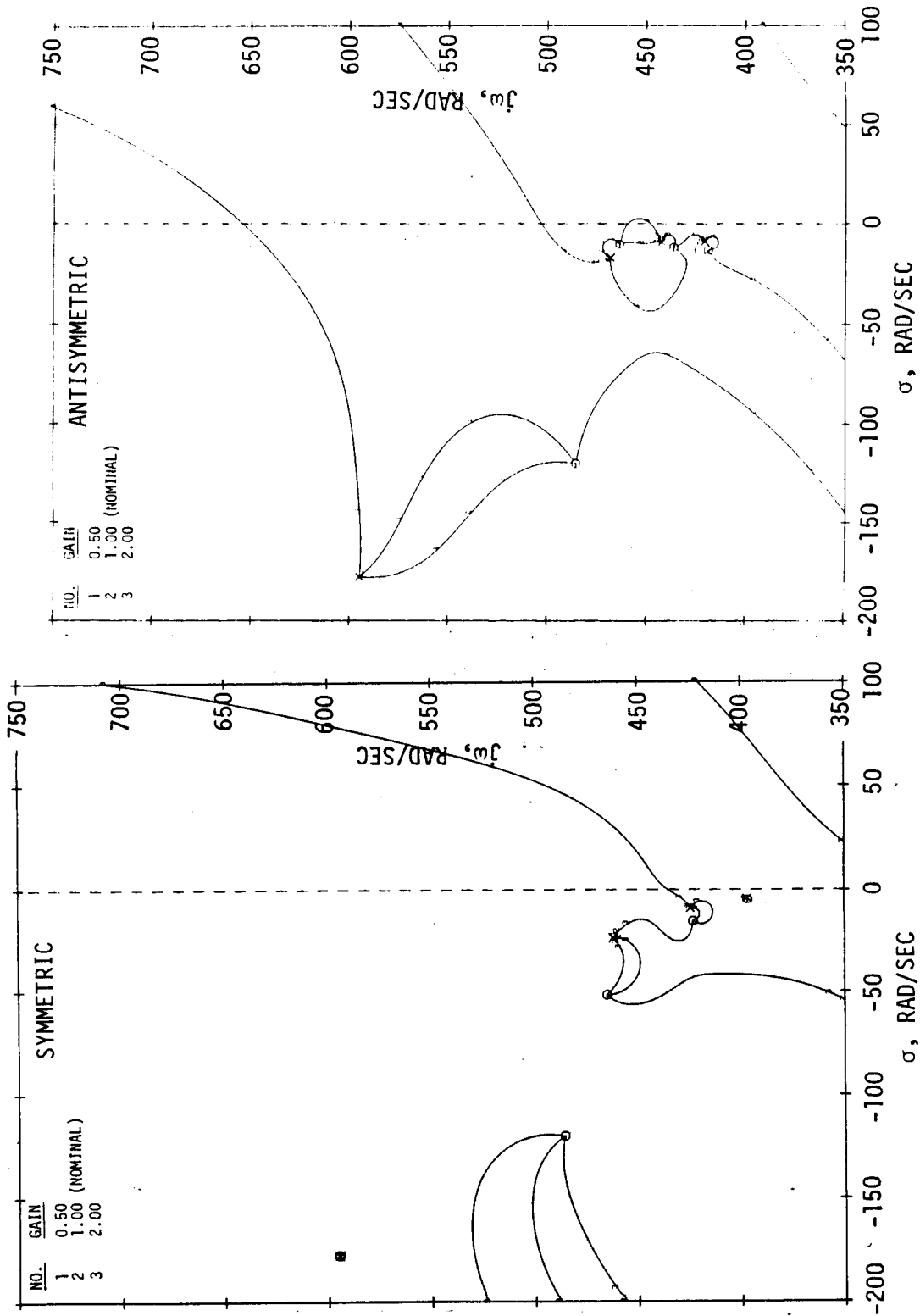
FIGURE 103

PHASE-GAIN ROOT LOCUS OF SYMMETRIC AND ANTISYMMETRIC FSS WITH AR-25 SERVOVALVE

153
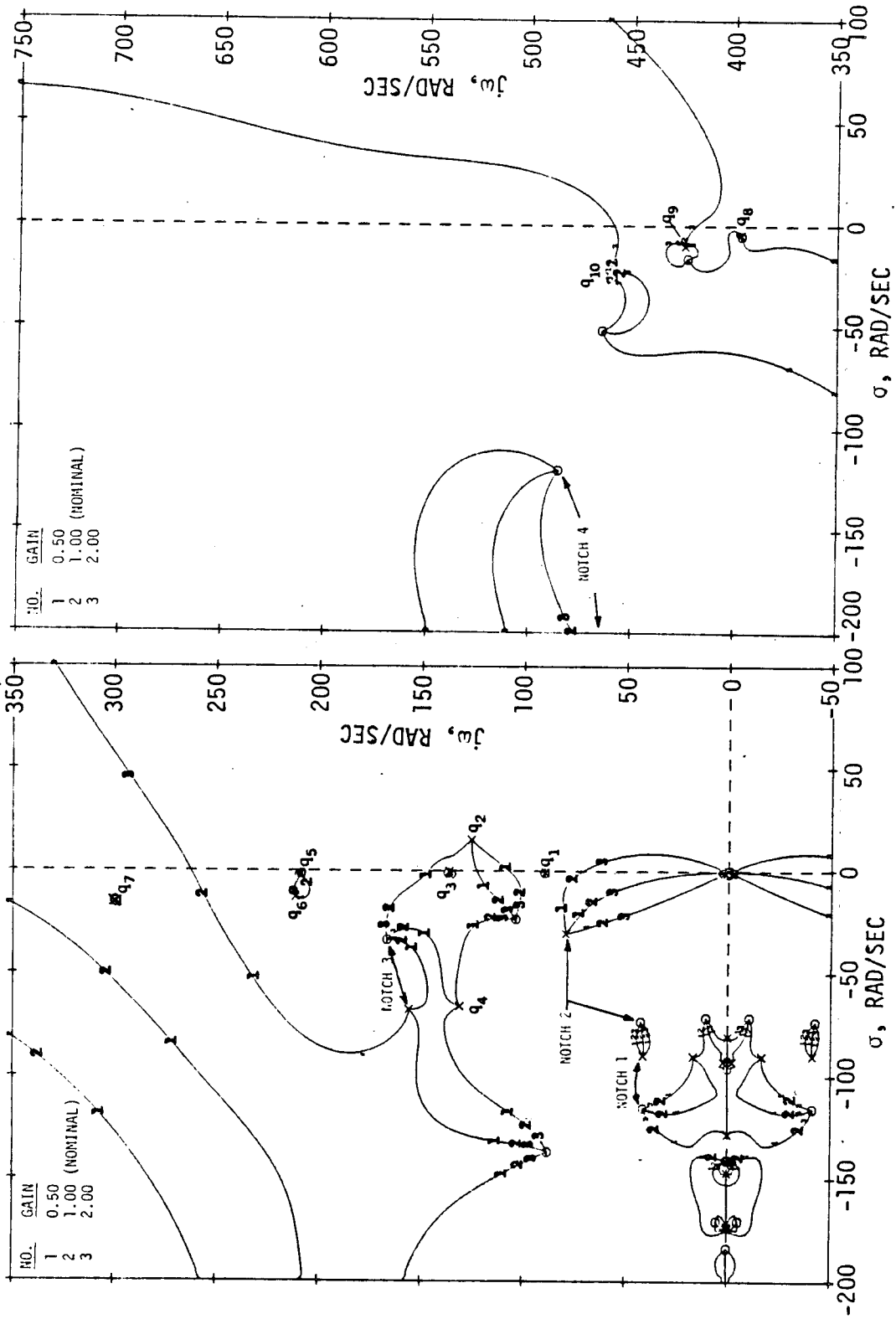
FIGURE 104

PHASE-GAIN ROOT LOCUS OF SYMMETRIC FSS - NOMINAL SYSTEM

154

● MACH = 0.86
● ALTITUDE = 15,000 FEET
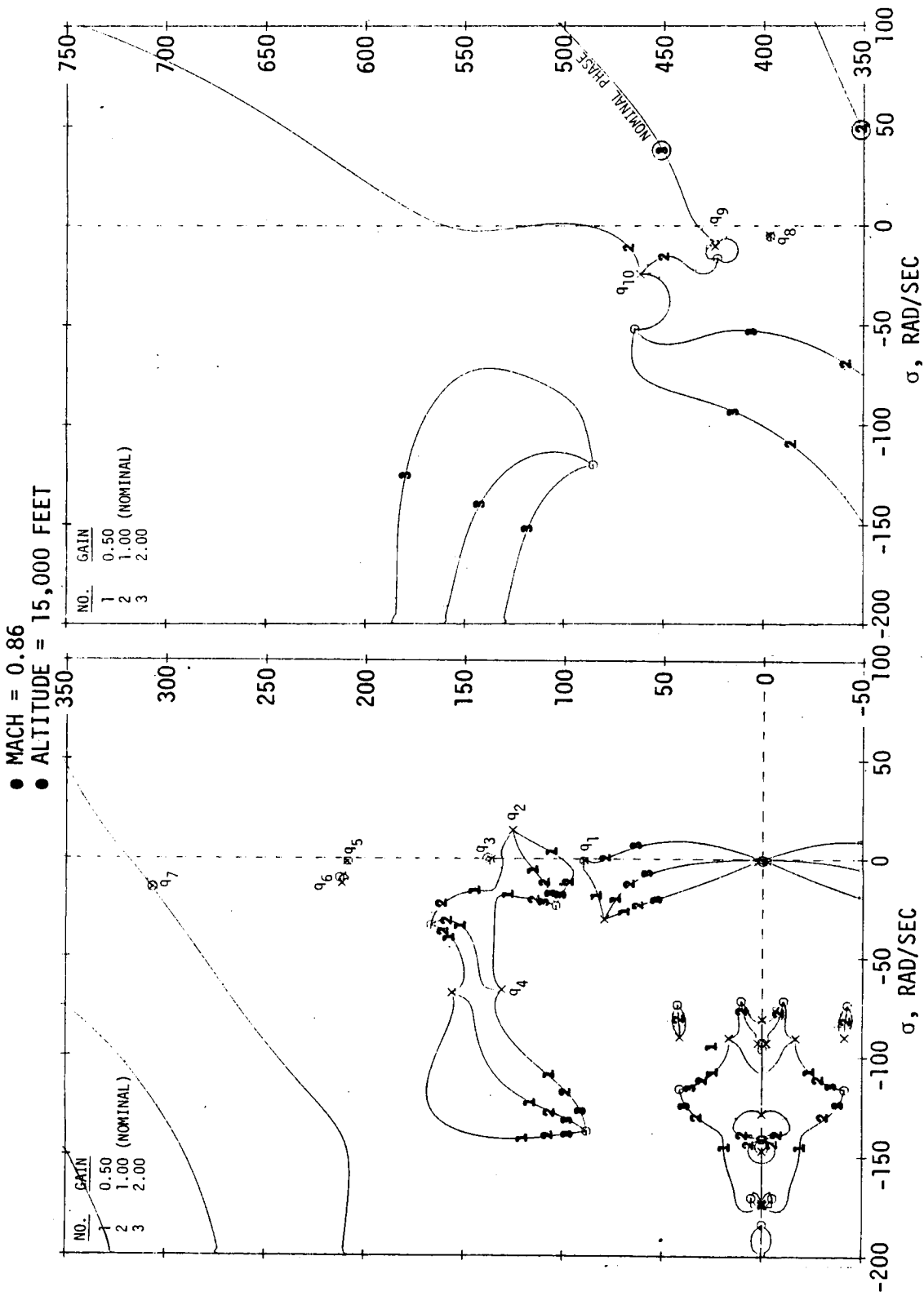
FIGURE 105

PHASE-GAIN ROOT LOCUS OF SYMMETRIC FSS – EFFECTS OF UNCOMPENSATING ACTUATOR

155
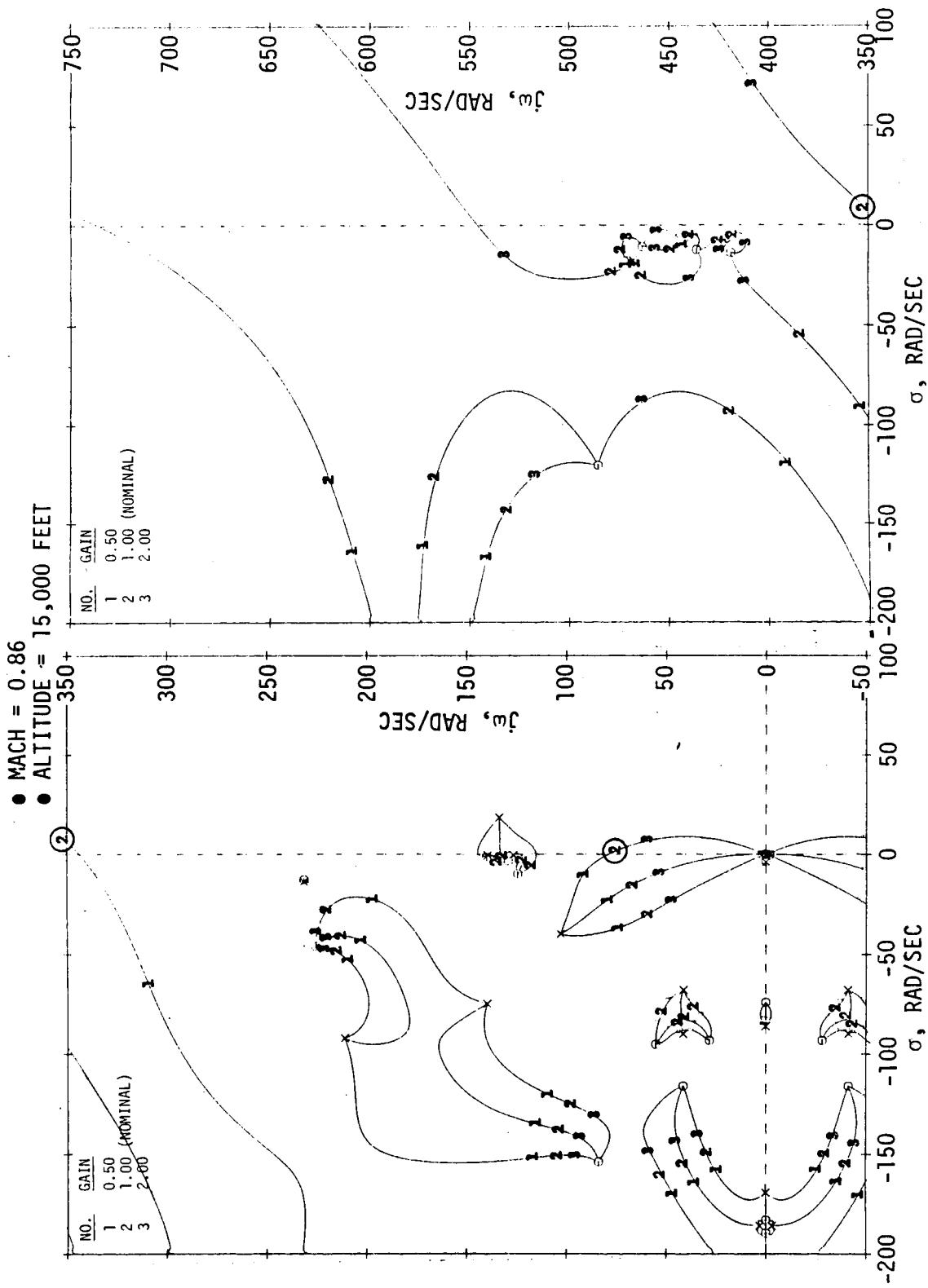
FIGURE 106

PHASE-GAIN ROOT LOCUS OF ANTISYMMETRIC FSS – EFFECTS OF UNCOMPENSATING ACTUATOR

156

PHASE-GAIN ROOT LOCUS OF ANTISYMMETRIC FSS – NOMINAL SYSTEM

FIGURE 107

157
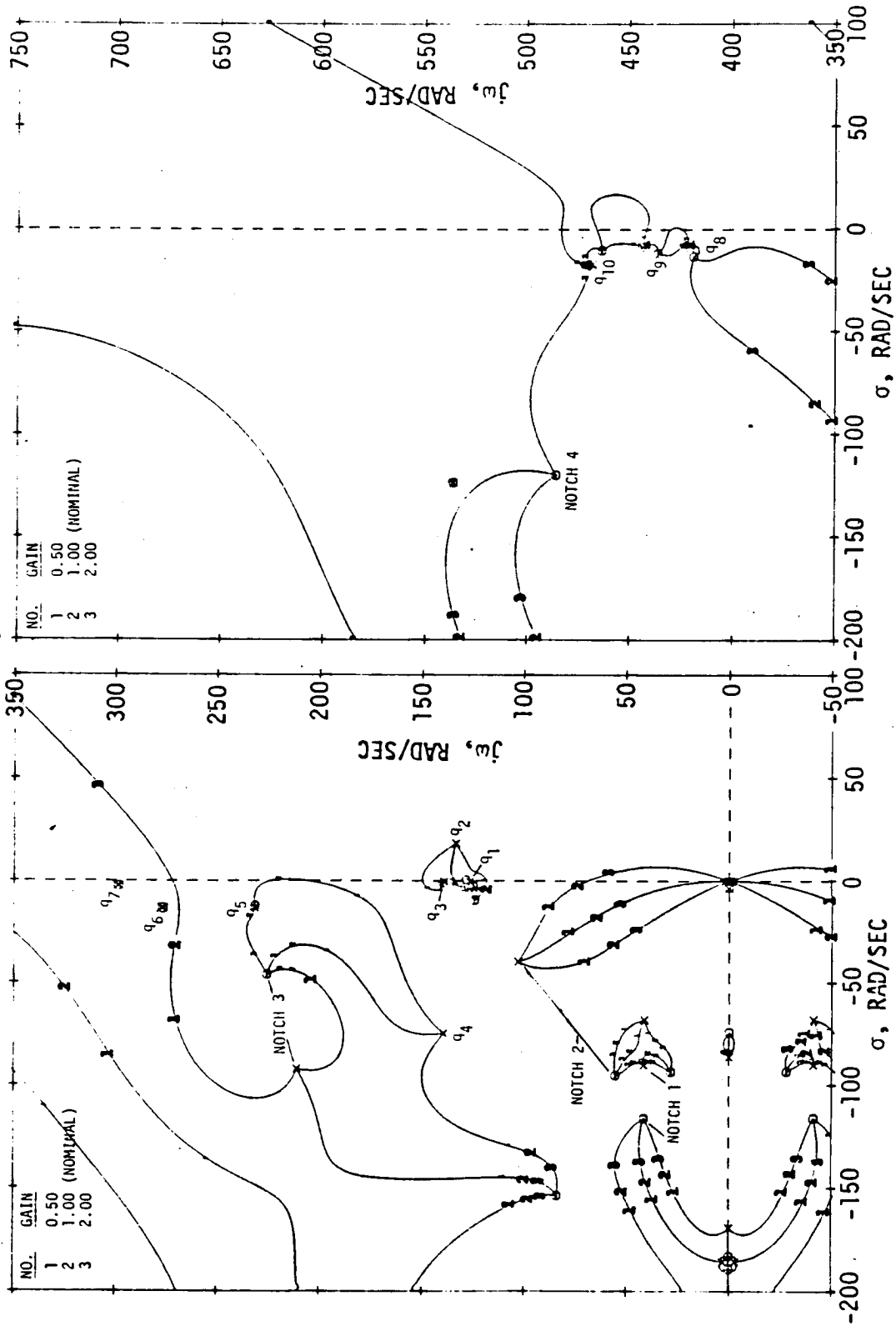
- MACH = 0.86
- ALTITUDE = 15,000 FEET
- WITHOUT FSS WASHOUT

| MODE | OPEN LOOP | | CLOSED LOOP DAMPING RATIO (ζ) - NOMINAL GAIN | | | | | |
| | | | +45 DEGREES | | NOMINAL | | -45 DEGREES | |
	FREQUENCY (HZ)	DAMPING RATIO (ζ)	20% INCREASE	20% DECREASE	20% INCREASE	20% DECREASE	20% INCREASE	20% DECREASE
q_1	14.2	0.0105	0.0126	0.0126	0.0126	0.0126	0.0126	0.0126
q_2	20.1	-0.1190	0.1074	0.1098	0.1344	0.1396	0.1138	0.1152
q_3	21.7	0.0024	0.0094	0.0094	0.0094	0.0094	0.0094	0.0094
q_4	23.3	0.4521	0.7878	0.7908	0.1813	0.1759	0.1995	0.2043
q_5	33.2	0.0084	0.0083	0.0083	0.0083	0.0083	0.0083	0.0125
q_6	33.7	0.0619	0.0480	0.0480	0.0480	0.0490	0.0342	0.0222
q_7	49.1	0.0527	0.0565	0.0565	0.0565	0.0565	0.0565	0.0565
q_8	63.2	0.0118	0.0120	0.0119	0.0118	0.0119	0.0119	0.0121
q_9	67.6	0.0238	0.0228	0.0162	0.0175	0.0185	0.0224	0.0239
q_{10}	73.6	0.524	0.0426	0.0457	0.0478	0.0555	0.0552	0.0602

FIGURE 108

SYMMETRIC FSS SENSITIVITY TO SURFACE-ACTUATOR MODE FREQUENCY CHANGE

6.3.5.2.3 Pressure Feedback. Pressure feedback was used in the servoactuator closed loop synthesis prior to removal during bench testing. The effects of pressure feedback gain sensitivity on FSS stability were analyzed by reducing the gain by 30 percent and little decrease in stability was noted, however the antisymmetric lag phase margin was reduced to 40 degrees. The results are shown on Figures 93 thru 96 in Appendix D.

Pressure feedback affects the closed loop actuator response in several ways as was evident during bench testing. The nonlinearities associated with actuator friction are much more prominent when pressure feedback is used. The pressure feedback loop measures the force required to overcome friction thereby decreasing the loop gain at low frequencies. The effects of friction diminish with increase in frequency effectively returning the loop to nominal gain. Therefore when enough pressure feedback is used to damp the actuator at the resonant frequency, the loop gain at low frequencies is inadequate.

6.3.5.2.4 Hinge Moment Effects. The hinge moment changes due to aerodynamic forces during flight affect the gain and phase margins of the servoactuator loop. These results are summarized by Figure 109 as the hinge moment is varied and shown in Appendix D on Figures 97 through 104. Figure 110 is included here to show that the antisymmetric FSS does not require compensation to cancel the surface-actuator mode as did the symmetric FSS. The FSS was synthesized using the no-load hinge moment actuator transfer function. Following servoactuator sensitivity analysis, conclusions are summarized as follows:

- Series 31 or AR-25 Servovalves may be used

- Symmetric FSS requires Actuator compensation

- Relatively insensitive to ±20 percent frequency change of surface-actuator mode

- Uncompensating antisymmetric FSS reduces phase margin to ±40 degrees

- Thirty percent reduction in pressure feedback gain reduces antisymmetric FSS phase margin to ±40 degrees

- Increased hinge moments decrease servoactuator gain resulting in FSS gain reduction

6.3.5.3 Parameter Scheduling. The ARW-2 is thrust limited to 0.87 Mach and scheduling below these speeds is not required. Sensitivity to variations in antisymmetric gain scheduling was not performed because the antisymmetric subsystem meets the required gain and phase margins within the realizable flight envelope without gain scheduling. Parameter or gain scheduling is not required for the symmetric axis for any Mach number within the scope of the analysis performed. FSS scheduling is discussed in Paragraph 7.4.3.

HINGE MOMENT	PHASE	GAIN
NO LOAD	-38.8 DEG.	+0.19 dB
MAXIMUM AIDING - 230 IN-LBS.	-23.9 DEG.	+0.62 dB
STATIC - 150 IN-LBS.	-61.8 DEG.	-2.00 dB
MAXIMUM RESISTING	-68.6 DEG.	-3.04 dB

FIGURE 109

HINGE MOMENT SENSITIVITY
OUTBOARD SERVOACTUATOR GAIN AND PHASE RESPONSE @ 23.8 HZ

MACH = 0.86
ALTITUDE = 15,000 FEET
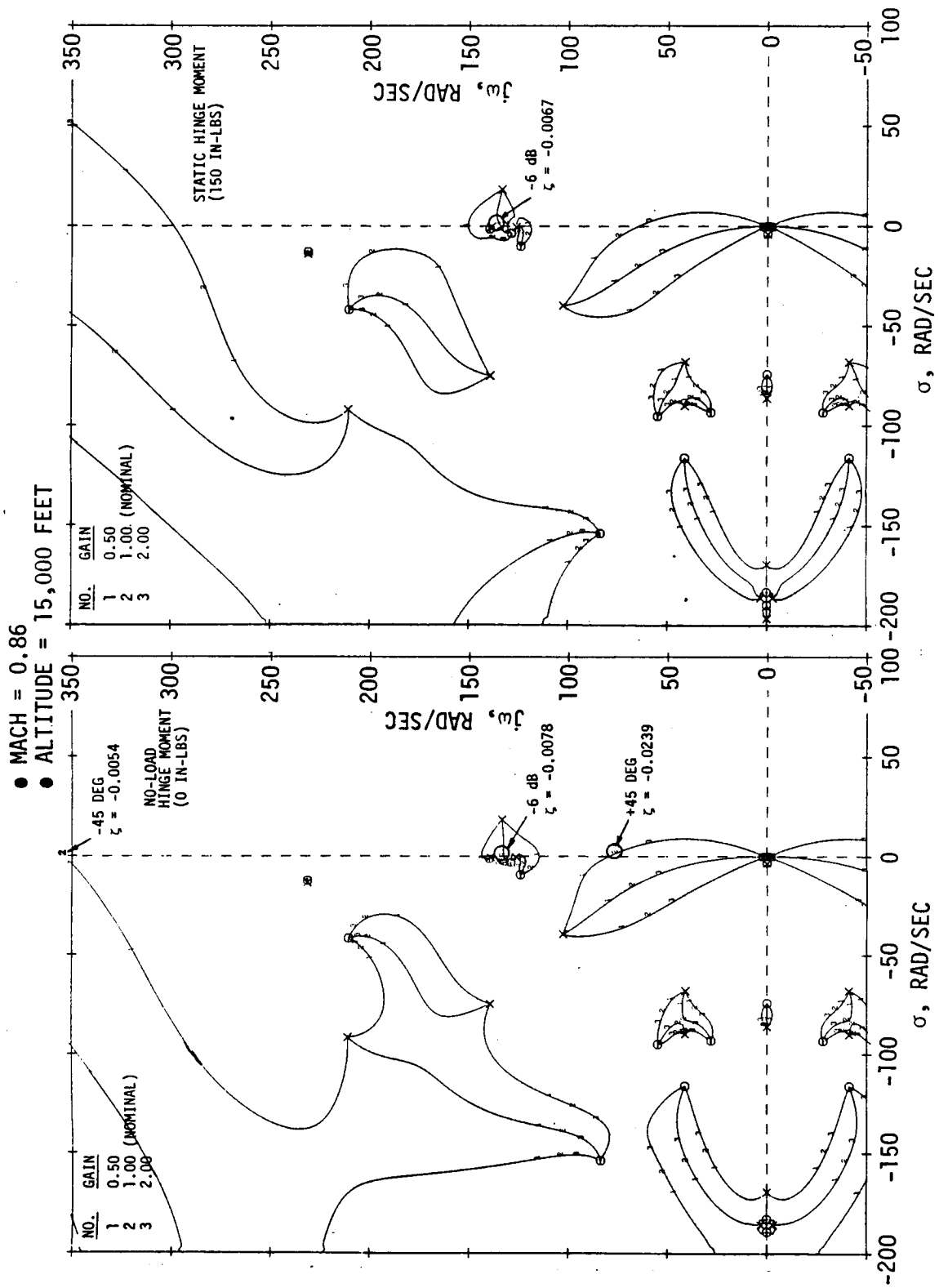
FIGURE 110

EFFECT OF HINGE MOMENT ON ANTISYMMETRIC FSS, UNCOMPENSATED ACTUATOR

161

6.3.5.4 Gain and Phase Sensitivity. The FSS has without parameter scheduling at least +45 degrees phase margin and +6 dB gain margin at the design condition of 0.86 Mach and 15,000 feet altitude.

Figures 82 and 83 show the open and closed loop symmetric and antisymmetric mode damping and frequencies at nominal gain and phase. These figures show that the FSS meets the damping requirements that no degradation in structural mode damping shall be below a damping ratio of 0.01 except when the unaugmented mode damping is less than 0.01. Comparable data at other flight conditions are shown on Figures 38 through 47 found in Appendix C. Figure 84 and 85 show the symmetric and antisymmetric flutter mode damping as a function of Mach number at a constant altitude of 15,000 feet. Symmetric and antisymmetric flutter mode damping as a function of altitude and a constant Mach number are shown on Figures 86 and 87 respectively. Similar data is presented in Appendix C on Figures 48 through 59 at other analyzed Mach number and altitudes.

6.3.6 Systems Compatibility. Flutter suppression system compatibility with the load alleviation systems, the relaxed static stability system and the AFCS were verified by determining the effects of the FSS on rigid body modes, and the ACS and AFCS systems on the flutter mode.

System compatibility was verified by linear system analysis and six Degree of Freedom (6 DOF) simulation analysis. Structural dynamic and QSE EOM were used in the analysis to determine the effect of each system coupling. A summary of FSS system compatibility study is shown on Figure 111 by presenting the effect on mode damping with various system loop closures.

The block diagram shown on Figure 174 was linearized and used to evaluate compatibility of the flutter suppression system. System compatibility is further discussed in Paragraph 6.8.

6.4 Load Alleviation Systems Analysis. Changes in the mathematical model discussed in Section 4 dictated a reevaluation of the load alleviation systems to determine if the changes affected the load reduction capability of the systems. The load alleviation systems defined during the previous design cycle were evaluated for the following performance objectives:

● To achieve the original goal of 15 percent reduction in critical wing root vertical bending

● To make the wing loads maneuver critical

● To achieve the design loads established by performance of the load alleviation during the previous design cycle

Incremental wing load reduction with the gust load alleviation was comparable to that predicted in the former analysis. However, steady state loads at the gust design condition were greater than previously predicted.

162

- MACH: 0.86
- ALTITUDE: 15,000 FEET
- UNSCALED EOM

MODE	OPEN LOOP		RSS, GLA, RCS	RSS, GLA, RCS CLOSED	RSS, GLA, RCS & FSS CLOSED	
	DAMPING (ζ)	FREQUENCY (HZ)	DAMPING (ζ)	FREQUENCY (HZ)	DAMPING (ζ)	FREQUENCY (HZ)
q_1 (FLUTTER MODE)	0.0105	14.235	0.0237	14.3610	0.0214	14.4207
q_2	-0.1190	20.137	-0.1191	20.1379	0.1794	18.4798
q_3	0.0024	21.715	0.0024	21.7151	0.0095	21.8347
q_4	0.4521	23.249	0.4520	23.3480	0.1899	22.8006
q_5	0.0084	33.241	0.0099	33.3191	0.0066	33.2614
q_6	0.0619	33.711	0.0618	33.7122	0.0479	33.8730
q_7	0.05265	49.051	0.0527	49.0388	0.0529	49.0566
q_8	0.0118	63.182	0.0120	63.2052	0.0120	63.2052
q_9	0.0238	67.556	0.0238	67.5629	0.0238	67.5629
q_{10}	0.0524	73.600	0.0524	73.5996	0.0524	73.5996
SERVOVALVE ACTUATOR			0.3997	49.9746	0.3997	49.9746
ACTUATOR NOTCH			0.2995	75.996	0.2398	75.996
FILTER			1.0000	101.859	1.0000	101.859
FILTER			1.0000	32.149	1.0000	32.149
FILTER			1.0000	23.873	0.9974	25.9728
FILTER			1.0000	0.3183	1.0000	0.2479
NOTCH 1			0.9089	15.760	0.8660	13.5282
NOTCH 2			0.3610	13.528	0.2811	8.5460

FIGURE 111

DAST ARW-2 SYMMETRIC SYSTEM COMPATIBILITY

The maneuver load alleviation system provided less incremental load reduction than the former prediction, but 1 g loads did not increase at the maneuver design condition. With load alleviation system active, total maneuver design loads were less than gust design loads; therefore, wing loads are not maneuver critical as desired.

The load alleviation system provides an 18 percent reduction in total critical wing root vertical bending moment. Although total wing loads with load alleviation system active are greater than the former prediction, positive margins of safety are maintained at critical stress points.

A method and supporting data are presented in Paragraph 6.4.4 to utilize pseudorandom excitation of the inboard aileron to evaluate wing load reduction capability of the gust load alleviation system.

6.4.1 Gust Load Alleviation System. The GLA system defined during the previous design cycle was evaluated for gust load reduction capability with the revised mathematical model.

The revised mathematical model produced larger wing root vertical bending moment (WRVBM) in the basic airplane as shown on Figure 112. The GLA system provided approximately the same incremental reduction in WRVBM as shown on Figure 112; however, because steady state (1g) airplane loads were increased, the design load values established in the previous design cycle were not achieved.

The stabilizer loop of the previously defined system produced excessive stabilizer rate requirements at high frequencies which were not contributing to the load reduction capability of the system. These rate requirements exceeded the capability of the stabilizer actuation hardware. During this design cycle, a first order filter of $90/(S + 90)$ was added to attenuate high frequency feedback signals. This filter did not affect the low frequency feedback response which provides the load reduction function of the system. PSD/RMS plots of stabilizer rate response to random gust of Figure 113 show the benefit of adding the stabilizer filter. The additional stabilizer filter reduces peak rate requirement for the design gust level from 188 degrees/second to 97 degrees/second.

The GLA system contains gain scheduling to reduce outboard aileron and stabilizer deflections at dynamic pressures greater than that at the GLA design condition. The previous system which attenuates the feedback signal inversely proportional to dynamic pressure did not have adequate phase margin in the stabilizer loop at the off design maximum dynamic pressure condition as shown on Figure 114(A). The gain schedule was revised to provide additional gain reduction in both the outboard aileron and stabilizer loops at high dynamic pressures. The gain reduction provided adequate phase margin at maximum dynamic pressure as shown on Figure 114(B).

164
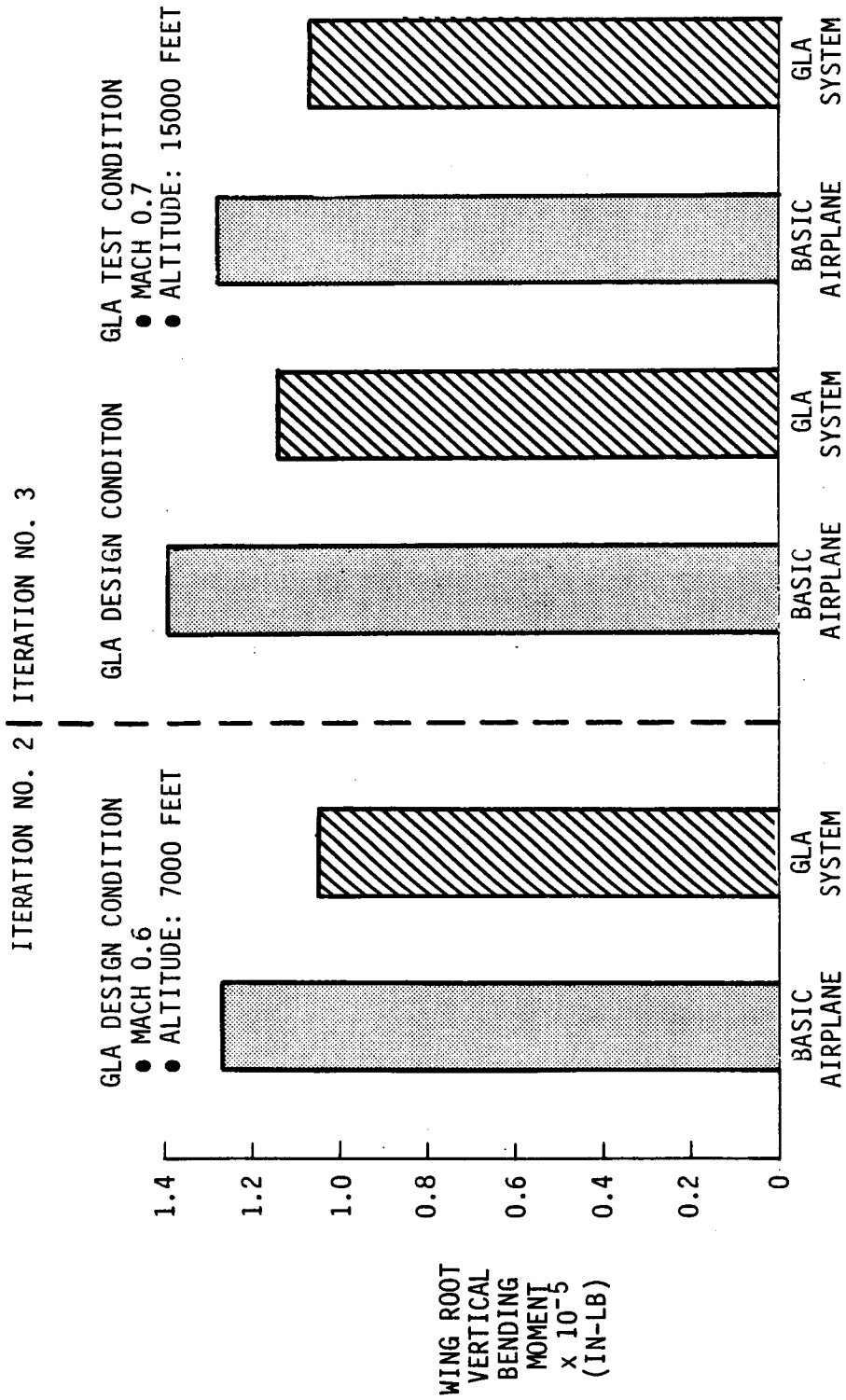
FIGURE 112

WING ROOT VERTICAL BENDING MOMENT FOR GLA SYSTEM

- MACH 0.60
- ALTITUDE: 7000 FEET
- GROSS WEIGHT: 2500 LBS.
- PRIMARY AFCS, RSS AND GLA SYSTEMS CLOSED
- VON KARMAN GUST SPECTRUM, L = 2500 FT
  PEAK AMPLITUDE = 62 FPS
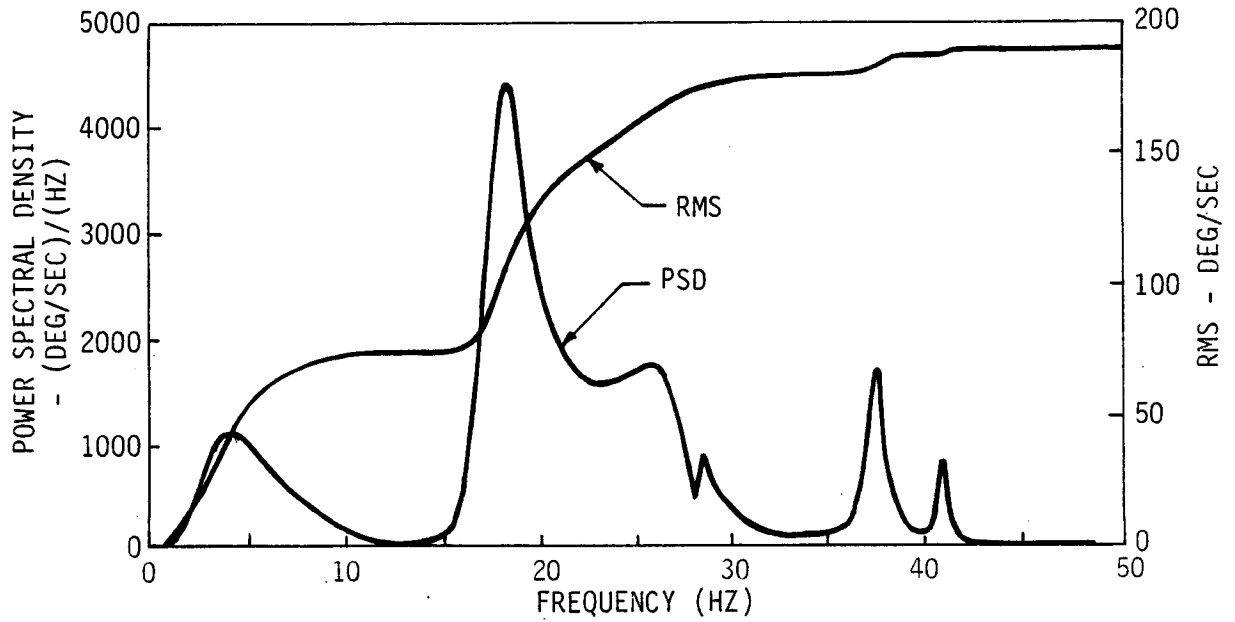
(A) PREVIOUS SYSTEM
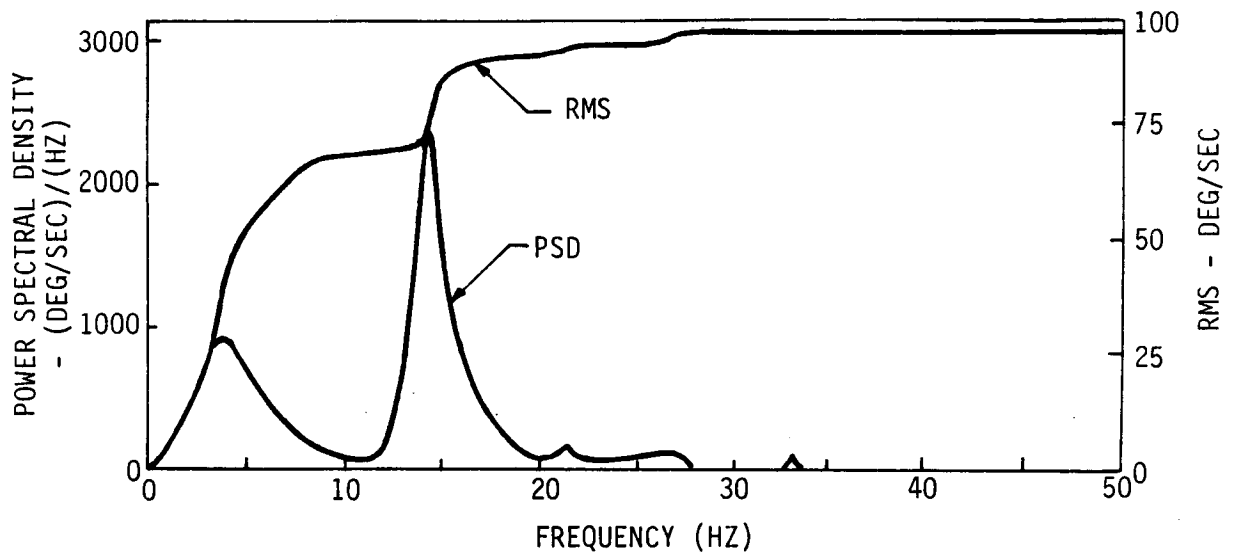
(B) REVISED SYSTEM

FIGURE 113

STABILIZER RATE REQUIREMENT COMPARISON

MACH 0.86
ALTITUDE: 15000 FEET
GROSS WEIGHT: 2350 LBS.
PRIMARY AFCS, RSS AND GLA OUTBOARD AILERON LOOPS CLOSED

□ OPERATING GAIN
○ +4.5 dB

+j30 (RAD/SEC)

-30° PHASE
(TYPICAL)

+j20

+j10

σ (RAD/SEC)

+30° PHASE
(TYPICAL)

10

-10

(A) PREVIOUS GAIN

+j30 (RAD/SEC)

+j20

+j10

σ (RAD/SEC)

10

-10

(B) REVISED GAIN
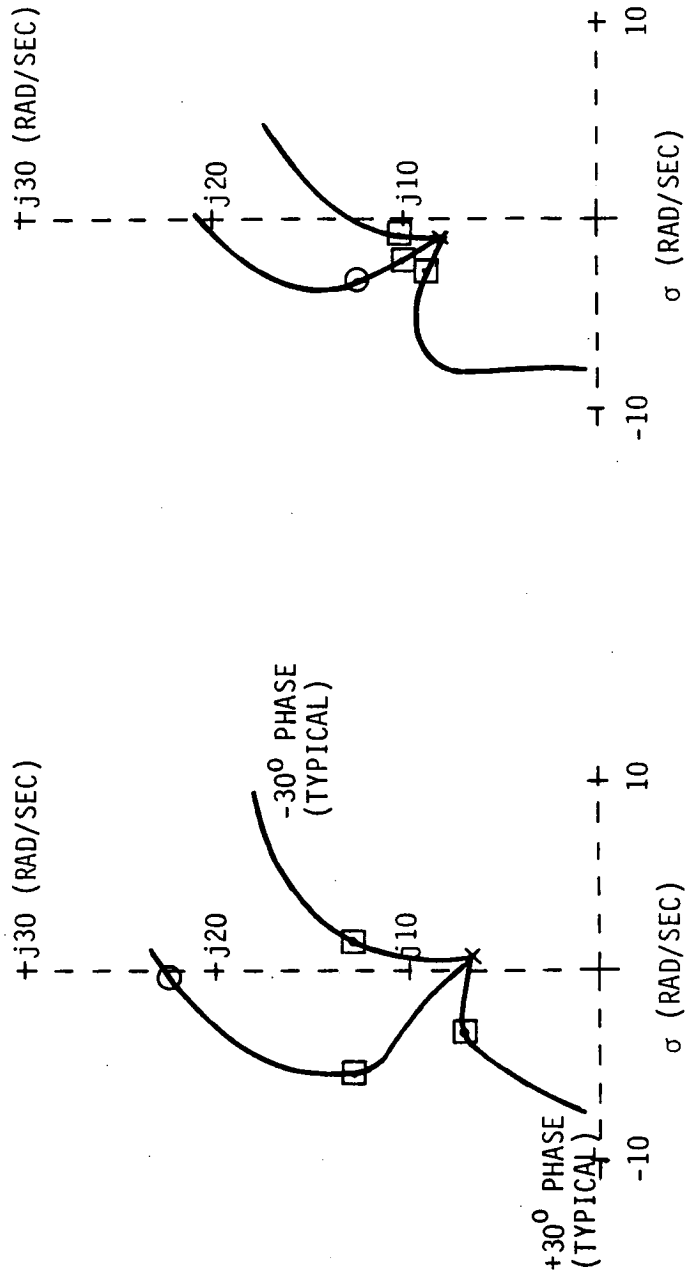
FIGURE 114

GLA STABILIZER ROOT LOCUS COMPARISON MAXIMUM DYNAMIC PRESSURE CONDITION

167

A block diagram of the revised GLA system is shown on Figure 115. Neither of the system changes above affect the load reduction capability of the GLA at the GLA design condition.

Power spectral density/root mean square plots of wing root vertical bending, fuselage vertical acceleration and GLA surface displacements and rate at the GLA design condition are shown on Figure 116. GLA system performance is based on the Von Karman gust spectrum with a scale length of 2,500 feet. The peak gust amplitude is 62 feet/second at the GLA condition.

The GLA design condition is on the V_c curve (350 KCAS) at 7,000 feet where the maximum gust occurs. Since flight tests are limited to altitudes above 10,000 feet, a test condition of 350 KCAS at 15,000 feet was selected. Airplane response to gust at the test condition should be very similar to that at the design condition as indicated by wing root vertical bending PSD/RMS plots shown on Figure 117.

6.4.2 Maneuver Load Alleviation System. The MLA system defined during the previous design cycle was evaluated for maneuver load reduction effectiveness with the revised mathematical model.

The MLA system consists of the GLA system and symmetric inboard aileron and an additional stabilizer signal. The inboard aileron and additional stabilizer signal are controlled by inputs from the longitudinal primary AFCS. With the revised mathematical model for this analysis, maneuver loads for steady state (1g) flight were approximately the same as before the revision. Wing control surfaces were less effective than the previous predictions; therefore, the MLA system did not provide as much maneuver load reduction. Figure 118 compares WRVBM to that of the previous design cycle. The MLA provides less incremental load reduction than previously predicted; however, basic airplane maneuver loads had not increased, and as a result, maneuver loads were less than gust loads. Changes in the model which affect MLA performance are explained in Section 4.

During this design cycle, two modifications were made to the MLA inboard aileron and stabilizer command system. Previously, the inboard aileron command was proportional to the load factor command input to the primary AFCS. The aileron command was revised to make the control surface proportional to actual load factor response for load factor commands greater than +0.5g incremental and equal to load factor command otherwise. This change was made to assure that the MLA system response corresponds to actual large load factors when, at some flight conditions and C.G. positions, airplane response may not exactly equal the command. The other modification changed the signal gain relating stabilizer to inboard aileron from 0.28 to 0.11 to adjust for different pitching moment effects of the inboard aileron in the revised model. The revised MLA inboard aileron and stabilizer control system is shown in the block diagram on Figure 119.
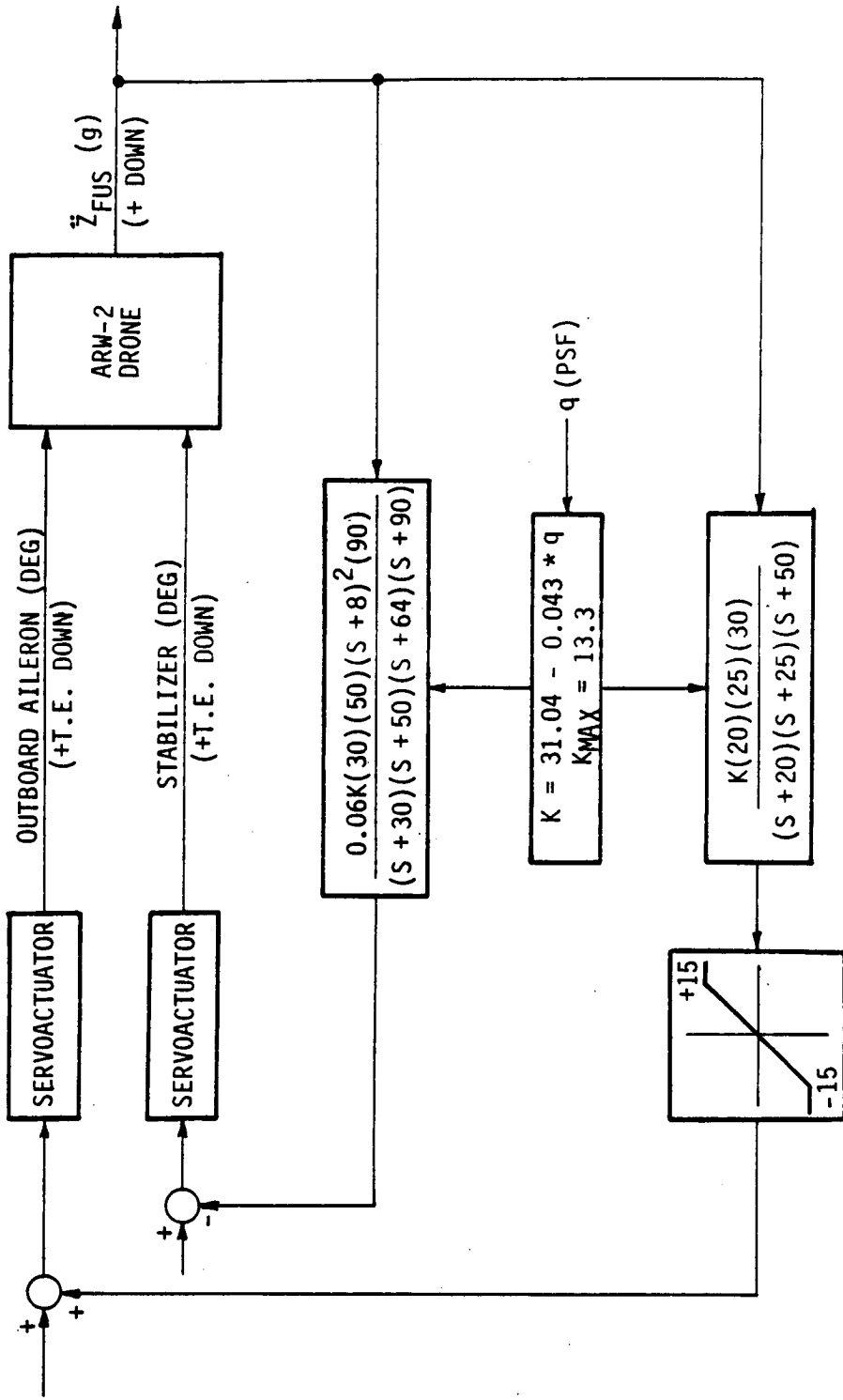
FIGURE 115

GUST LOAD ALLEVIATION SYSTEM BLOCK DIAGRAM

169

- MACH 0.60
- ALTITUDE: 7000 FEET
- GROSS WEIGHT: 2500 LBS.
- PRIMARY AFCS, RSS AND GLA SYSTEMS CLOSED
- VON KARMAN GUST SPECTRUM, L = 2500 FEET,
  PEAK AMPLITUDE = 62 FPS
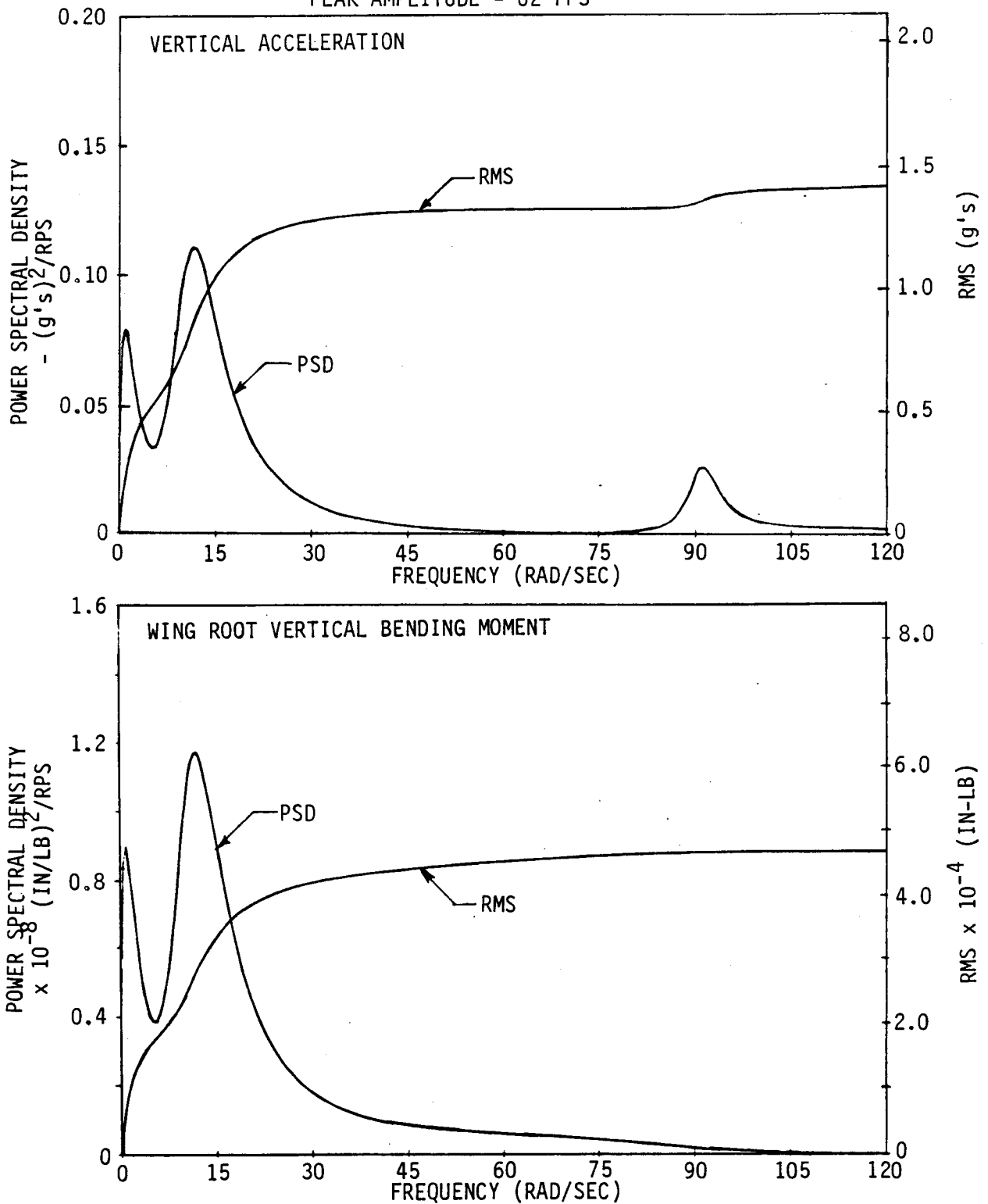
FIGURE 116

FUSELAGE VERTICAL ACCELERATION AND INCREMENTAL WING ROOT VERTICAL BENDING MOMENT
PSD/RMS WITH GLA SYSTEM

- MACH 0.60
- ALTITUDE: 7000 FEET
- GROSS WEIGHT: 2500 LBS.
- PRIMARY AFCS, RSS AND GLA SYSTEMS CLOSED
- VON KARMAN GUST SPECTRUM, L = 2500 FEET
  PEAK AMPLITUDE = 62 FPS
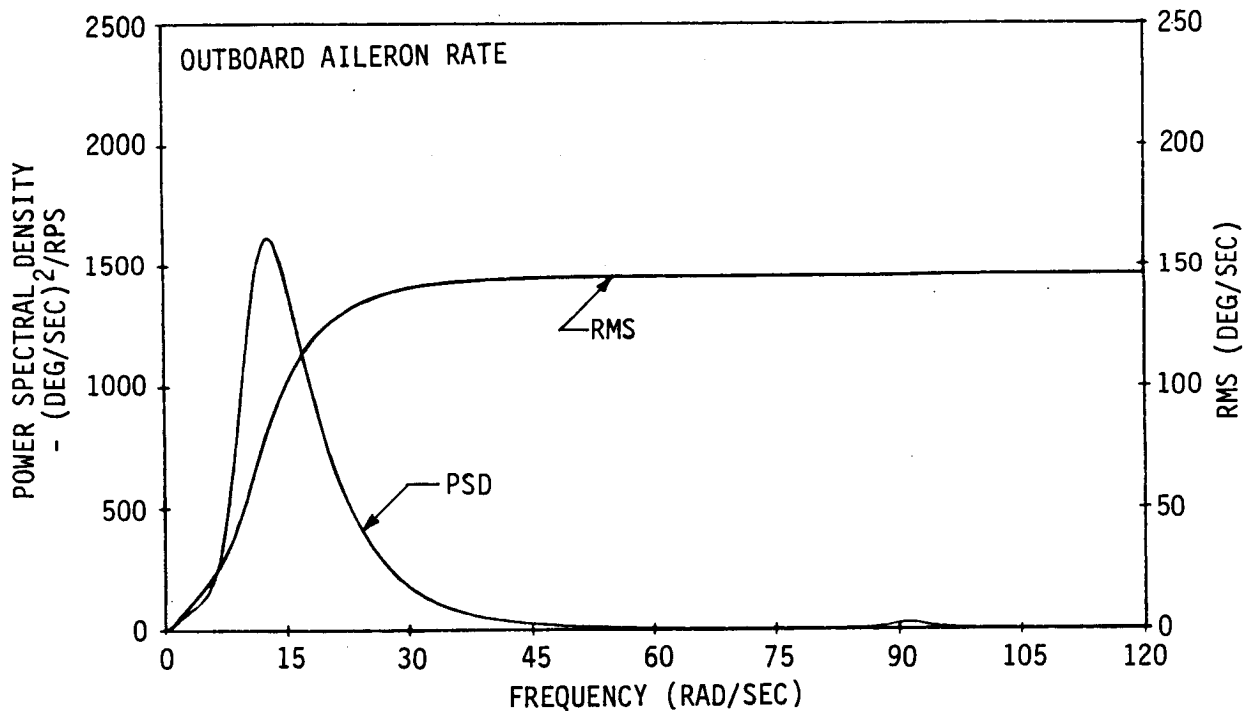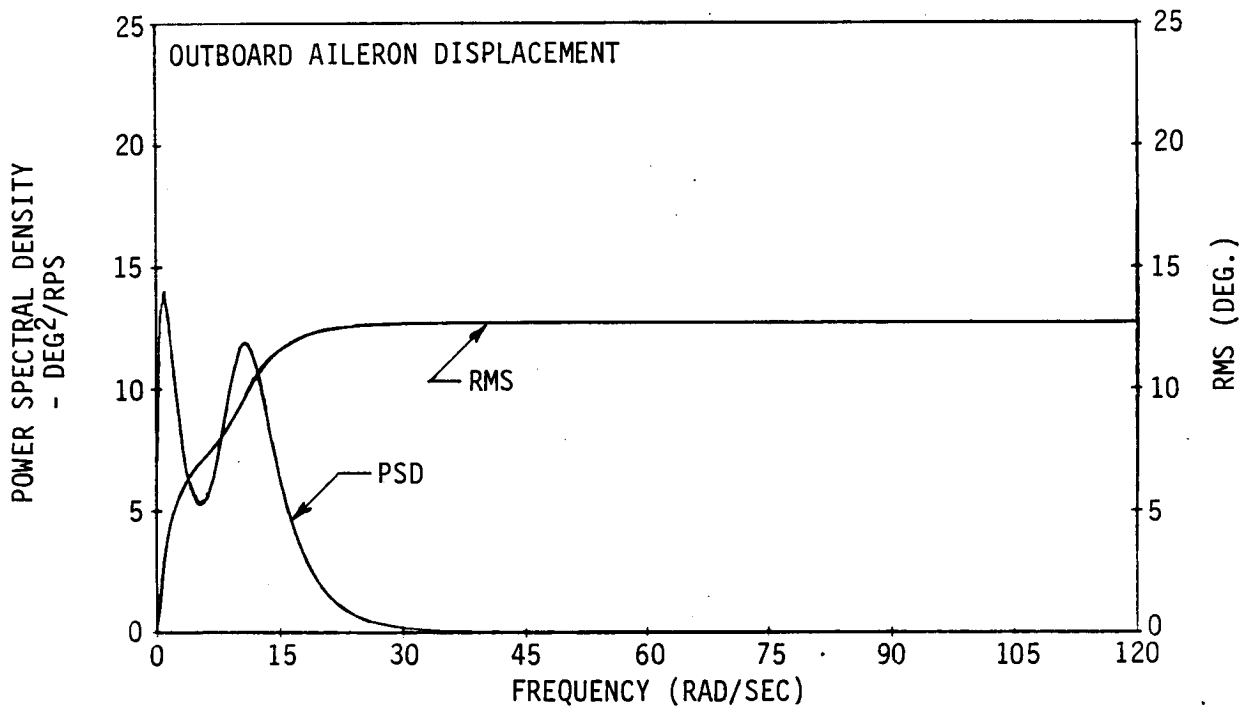
FIGURE 116 (CONTINUED)

OUTBOARD AILERON DISPLACEMENT AND RATE PSD/RMS FOR DESIGN GUST WITH GLA

- MACH 0.60
- ALTITUDE: 7000 FEET
- GROSS WEIGHT: 2500 LBS.
- PRIMARY AFCS, RSS AND GLA SYSTEMS CLOSED
- VON KARMAN GUST SPECTRUM, L = 2500 FEET
   PEAK AMPLITUDE = 62 FPS
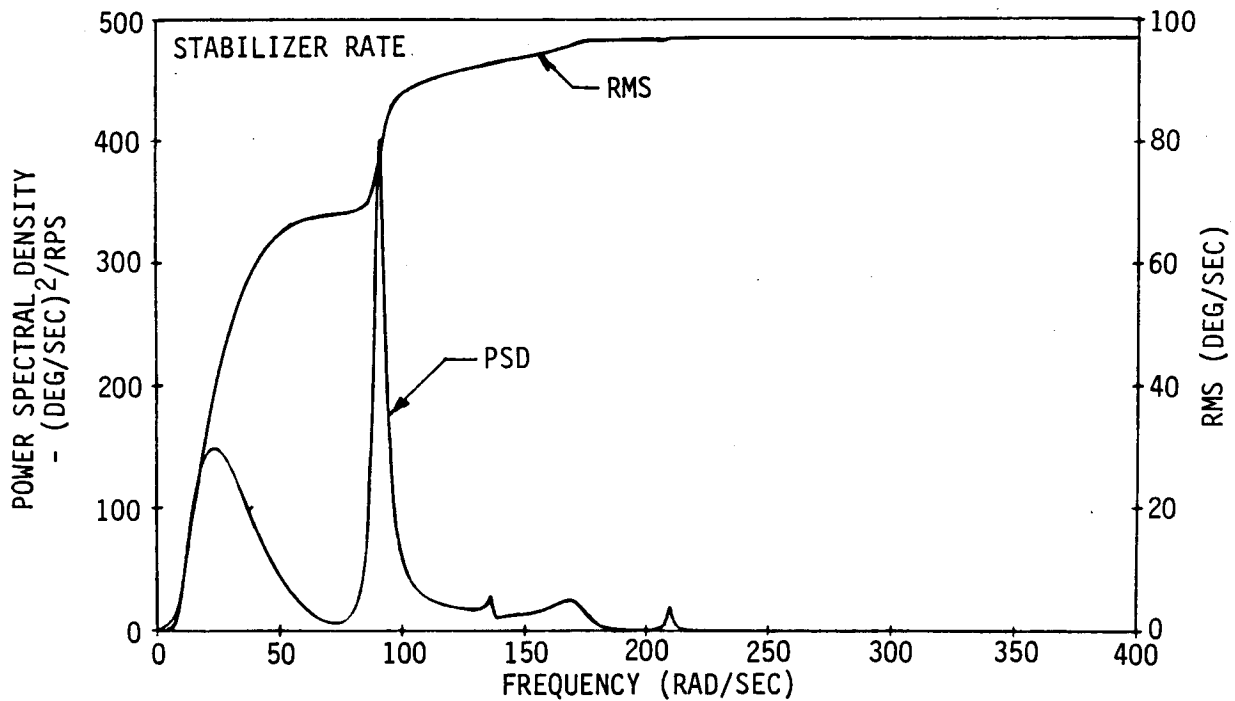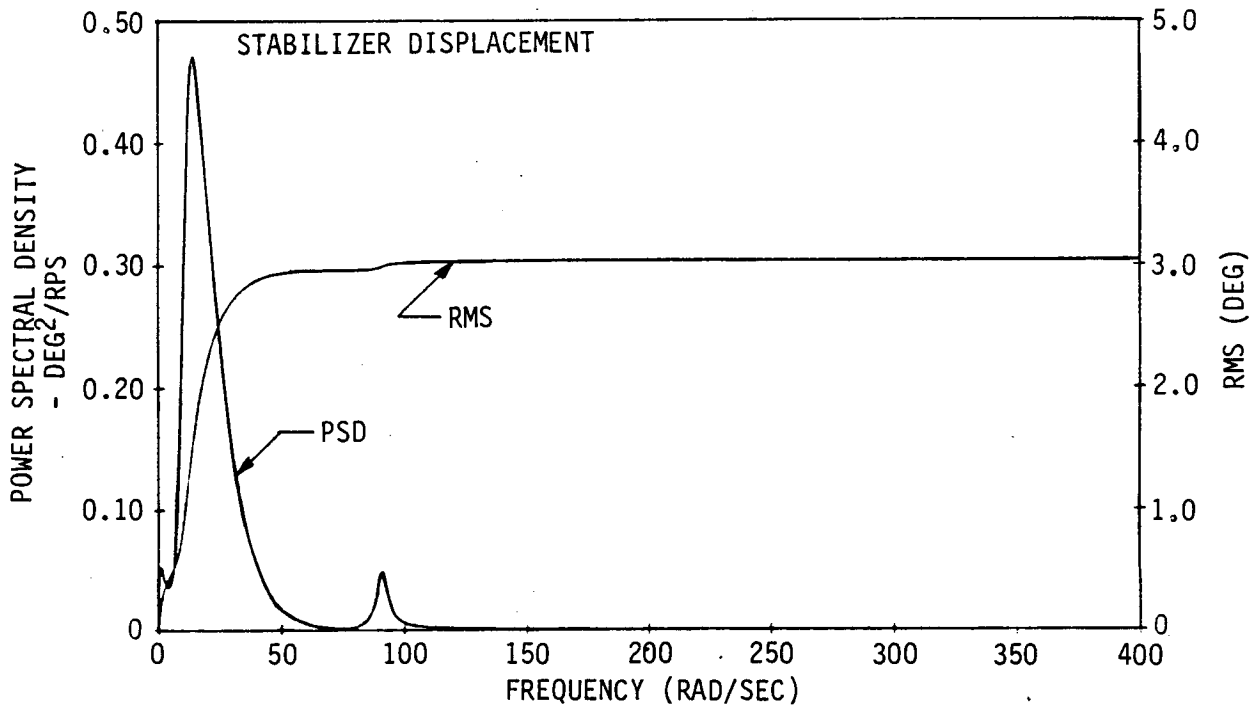
FIGURE 116 (CONCLUDED)

STABILIZER DISPLACEMENT AND RATE PSD/RMS FOR DESIGN GUST WITH GLA

PRIMARY AFCS, RSS AND GLA SYSTEMS CLOSED

——————— GLA TEST CONDITION: MACH: 0.70
ALTITUDE: 15000 FT.
GROSS WEIGHT: 2350 LBS.

— — — —GLA DESIGN CONDITION: MACH: 0.60
ALTITUDE: 7000 FT.
GROSS WEIGHT: 2500 LBS.
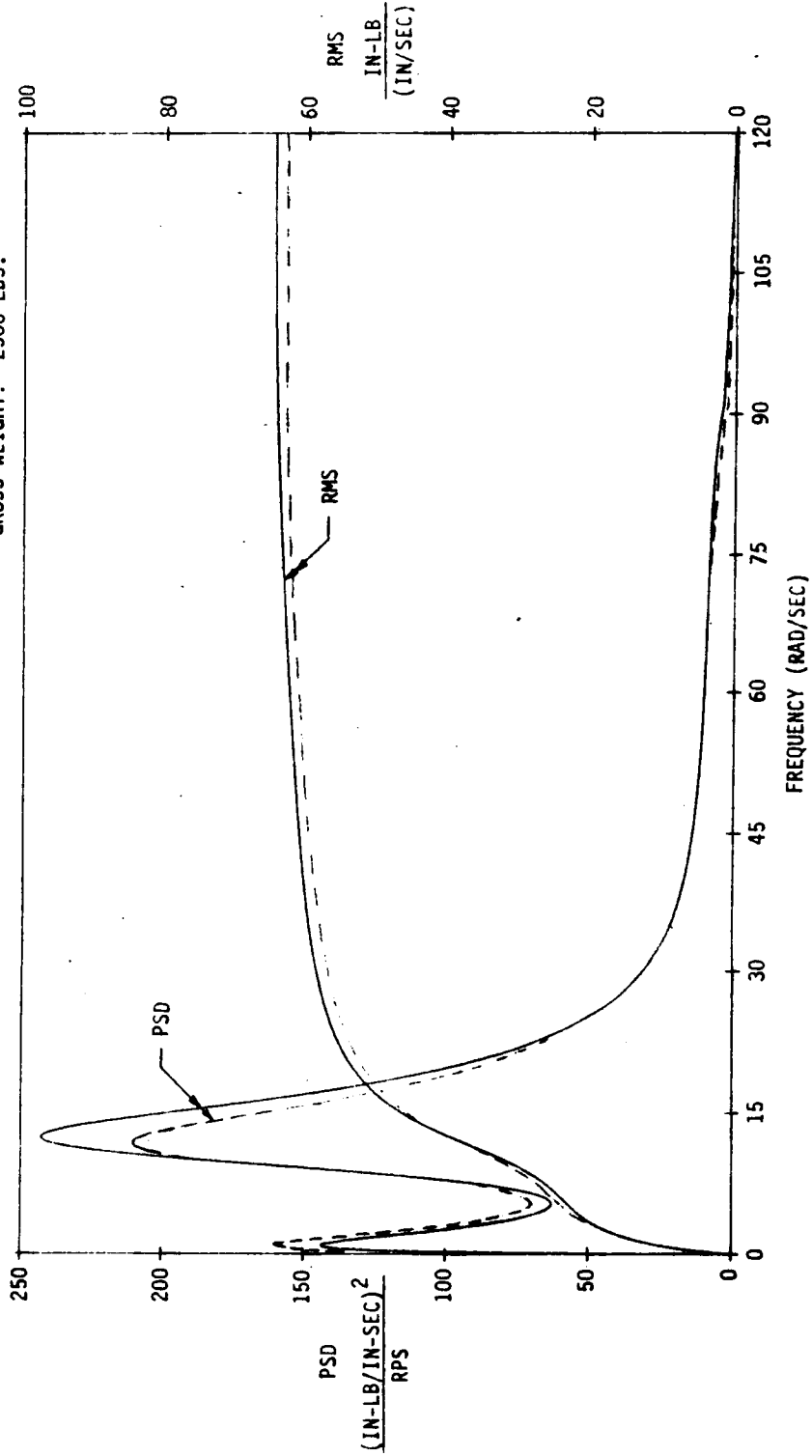
FIGURE 117

WING ROOT VERTICAL BENDING MOMENT/GUST COMPARISON AT GLA TEST AND DESIGN CONDITIONS

173

ITERATION NO. 2 | ITERATION NO. 3

MLA DESIGN CONDITION
● MACH: 0.35
● ALTITUDE: SEA LEVEL

MLA DESIGN CONDITION

MLA TEST CONDITION
● MACH: 0.42
● ALTITUDE: 10000 FEET

WING ROOT
VERTICAL
BENDING
MOMENT
x 10⁻⁵
(IN-LB)

BASIC AIRPLANE

MLA SYSTEM

BASIC AIRPLANE

MLA SYSTEM

BASIC AIRPLANE
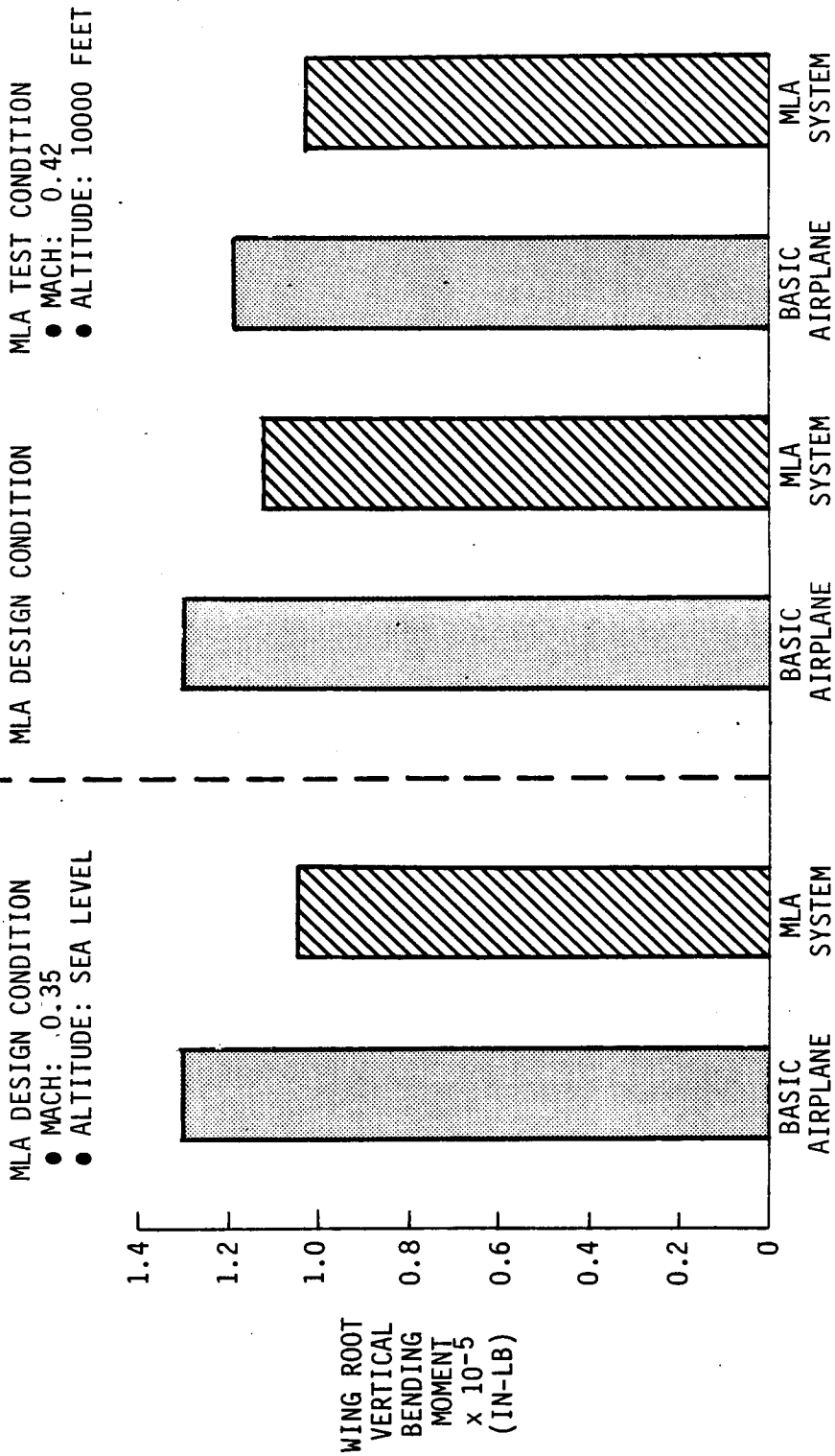
MLA SYSTEM

FIGURE 118

WING ROOT VERTICAL BENDING MOMENT FOR MLA SYSTEM
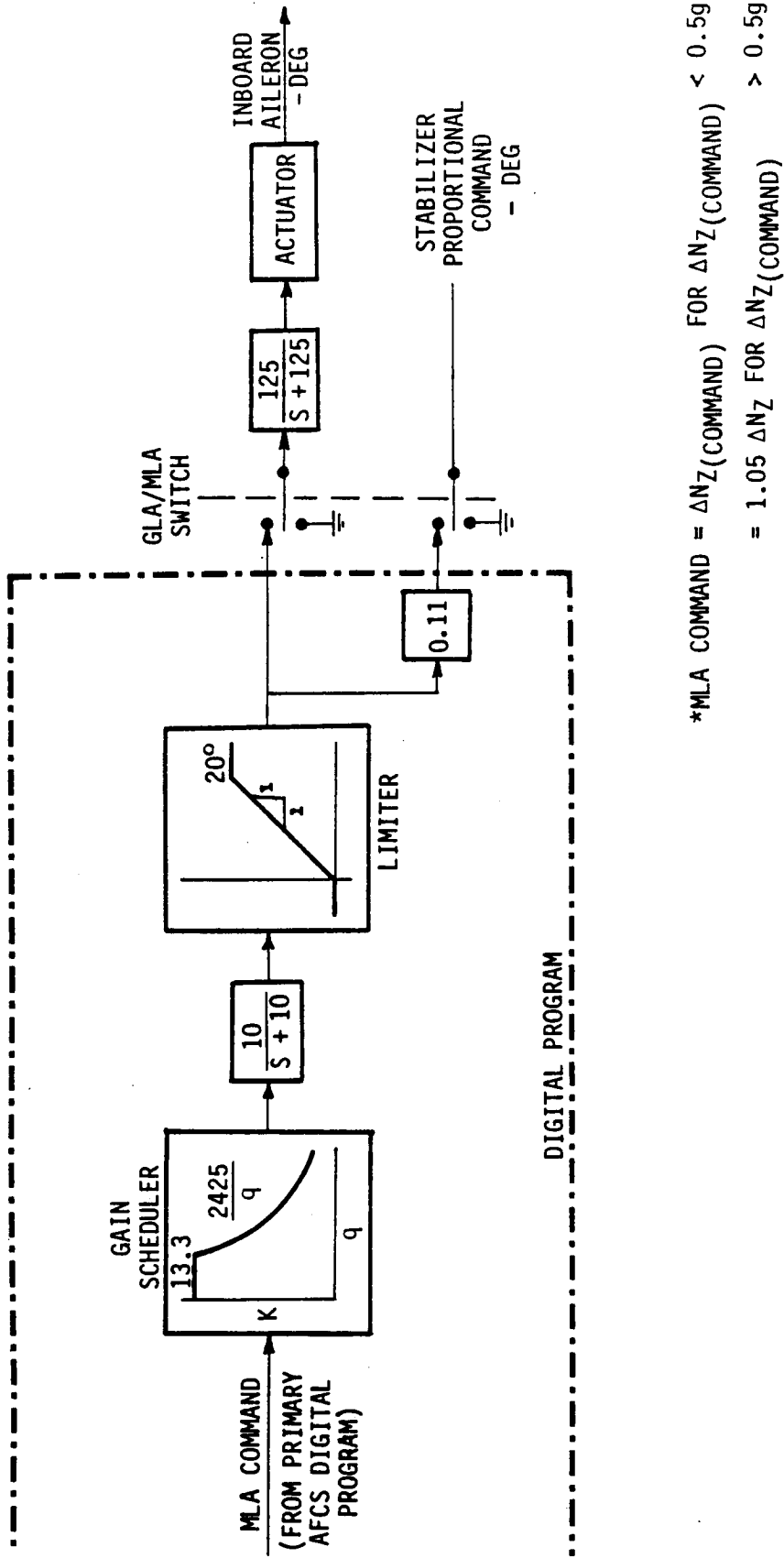
FIGURE 119

MLA INBOARD AILERON SYSTEM BLOCK DIAGRAM

Figure 118 also shows WRVBM for a selected flight test condition at 10,000 feet. The design condition occurs at the minimum speed and altitude that a 2.5g maneuver can be executed. The test condition for positive maneuvers was selected as the minimum speed that a 2.5g maneuver can be executed at 10,000 feet.

Maneuver time responses of load factor, WRVBM, and control surfaces with the MLA are shown on Figure 120.

6.4.3 Load Alleviation System Performance. Gust loading produced maximum WRVBM for both basic airplane and with load alleviation systems engaged. The reduction in critical WRVBM with the load alleviation systems closed is 18 percent; however, maximum loads with the systems engaged are greater than the design loads predicted in the previous design cycle.

Gust and maneuver loads along the wing span with load alleviation systems closed are shown on Figures 121 and 122. Vertical bending moment along the entire span is greater for gust; consequently, the wing is not maneuver critical as desired.

Since the design loads of the previous design cycle were not achieved, a structural resizing iteration was anticipated. A stress analysis exercise using the critical combination of wing loads from Figures 121 and 122 indicated that positive margins of safety could be obtained at· critical stress points by eliminating some conservatism in the ·previous stress analysis. The previous stress analysis did not include the load carrying capability of effective areas of the skin forward of the front spar. A comparison of minimum margins of safety of critical components for the previous and present stress analyses is shown on Figure 123.

6.4.4 Simulated Gust Analysis. The difficulty and time required to find large amplitude gust conditions and DAST flight time limitations make it desirable to have an alternate method of verifying the gust load reduction capability of the GLA system and verifying analytical modeling of the airplane and load dynamics.

Gust load reduction is provided by outboard aileron and stabilizer response. The inboard aileron can be used to generate airplane load responses similar to that produced by random gust. Random excitation of the inboard aileron produces WRVBM response having PSD characteristics similar to that due to random gust disturbances. Desired PSD characteristics are obtained by passing a signal from a shift register noise generator through a set of first order lag and washout filters selected to give the desired PSD shape.

Implementation of the inboard aileron random excitation generator is shown on Figure 124. The shift register noise generator provides a good representation of white noise out to approximately 10 percent of the clock frequency. The noise generator has a repetitive cycle time of approximately 174 minutes.

- MACH 0.35
- ALTITUDE: SEA LEVEL
- GROSS WEIGHT: 2500 LBS.
- 0.4 SECOND RAMP HOLD COLUMN INPUT
- RSS, PCS AND MLA/GLA ENGAGED
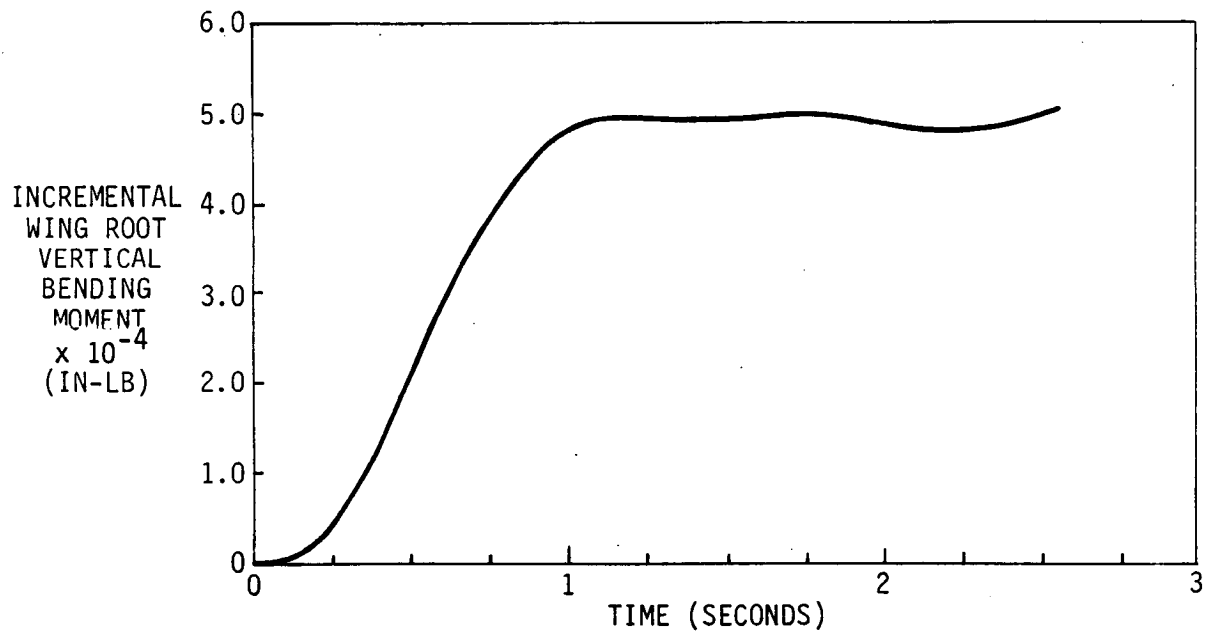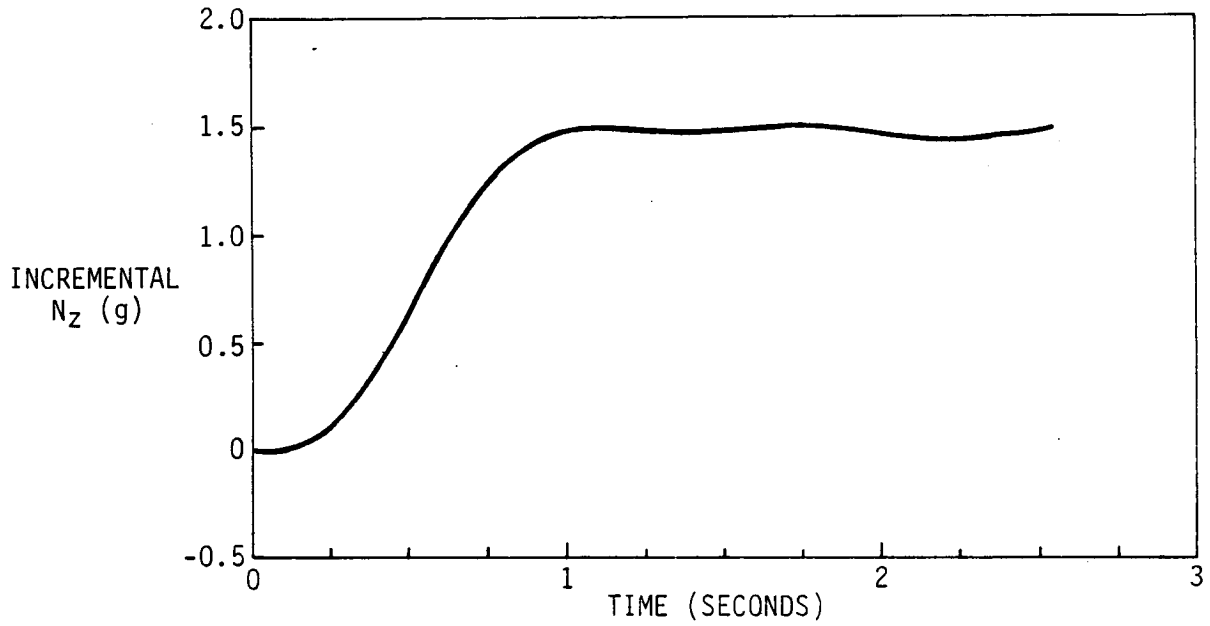
FIGURE 120

LOAD FACTOR AND WING ROOT VERTICAL BENDING MOMENT RESPONSES FOR DESIGN MANEUVER

- MACH 0.35
- ALTITUDE: SEA LEVEL
- GROSS WEIGHT: 2500 LBS.
- 0.4 SECOND RAMP HOLD COLUMN INPUT
- RSS, PCS AND MLA/GLA ENGAGED
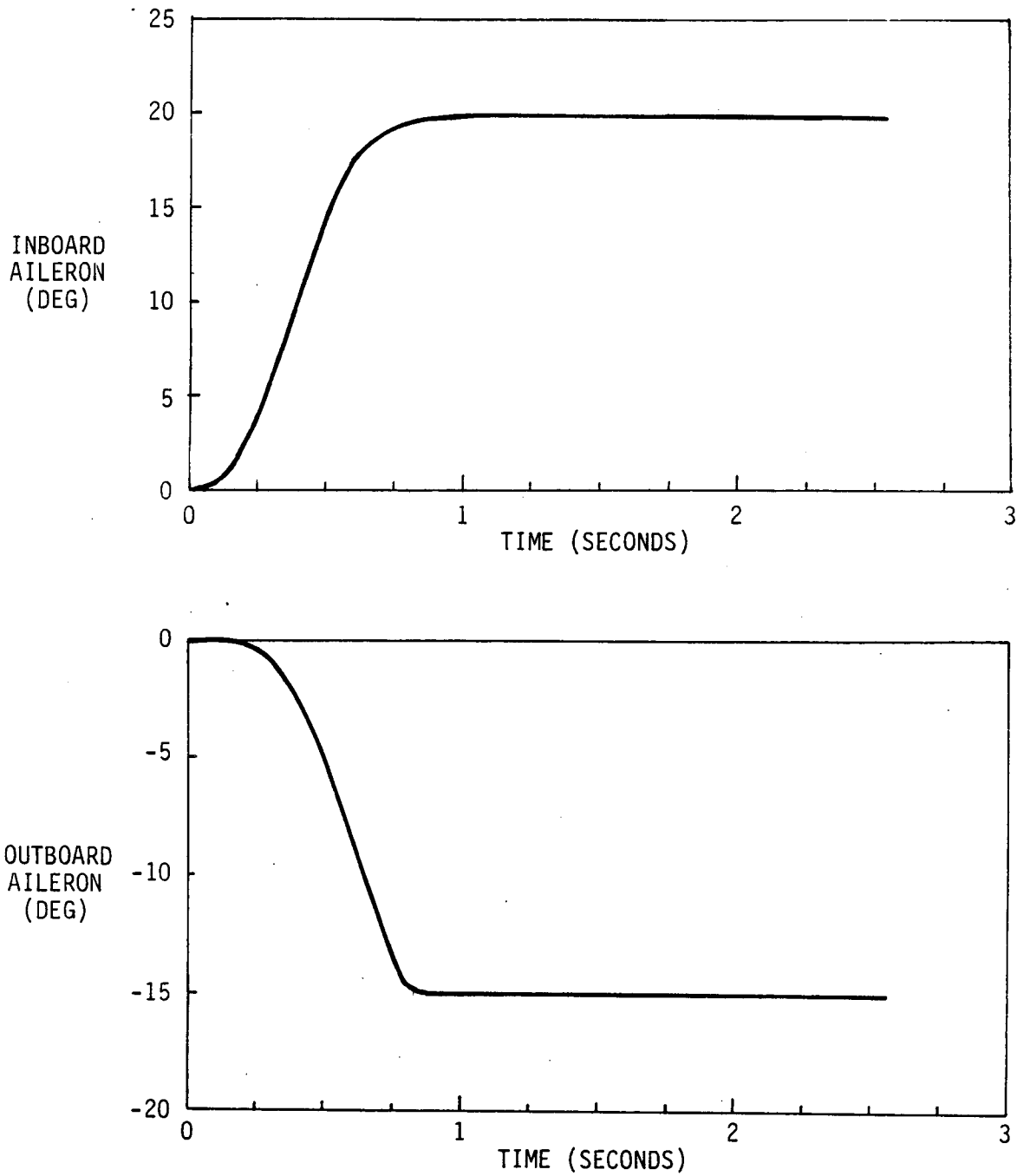
FIGURE 120 (CONTINUED)

INBOARD AILERON AND OUTBOARD AILERON RESPONSES FOR DESIGN MANEUVER

- MACH 0.35
- ALTITUDE: SEA LEVEL
- GROSS WEIGHT: 2500 LBS.
- 0.4 SECOND RAMP HOLD COLUMN INPUT
- RSS, PCS AND MLA/GLA ENGAGED
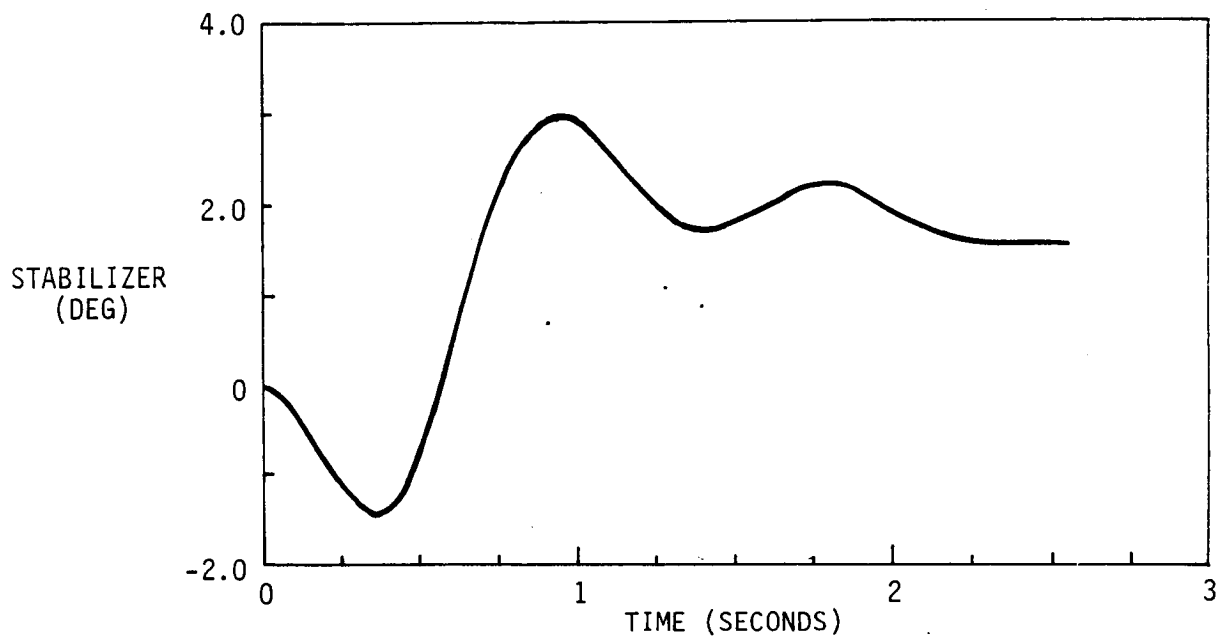
FIGURE 120 (CONCLUDED)

STABILIZER SURFACE RESPONSE FOR DESIGN MANEUVER
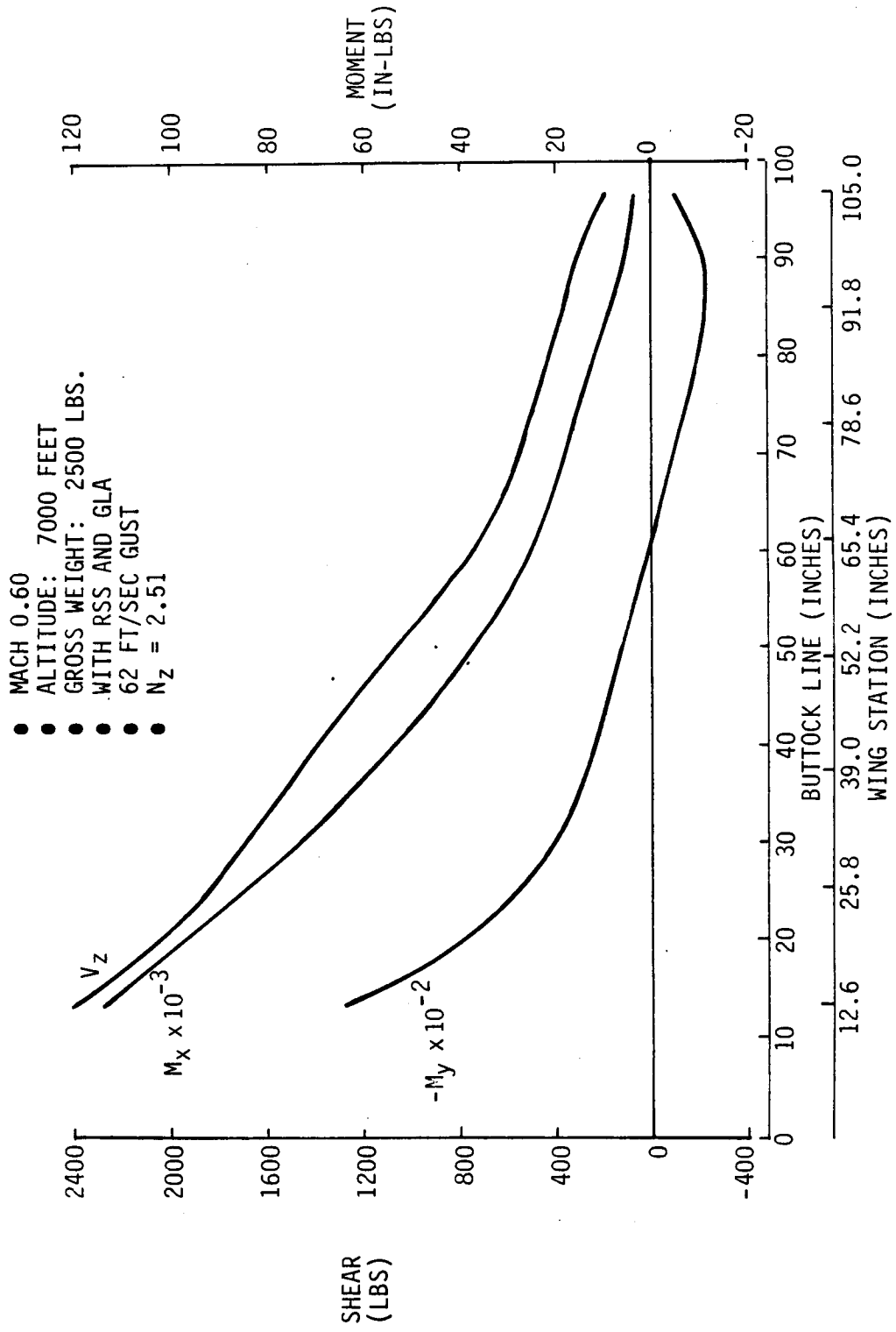
FIGURE 121

GUST DESIGN LIMIT WING SHEAR, VERTICAL BENDING MOMENT AND TORSION

- MACH 0.70
- ALTITUDE: 15,000 FEET
- GROSS WEIGHT: 2350 LBS.
- PRIMARY AFCS AND RSS CLOSED
- RMS INBOARD AILERON COMMAND
  = 1.38 DEG.

- — — GLA ON
- —— GLA OFF
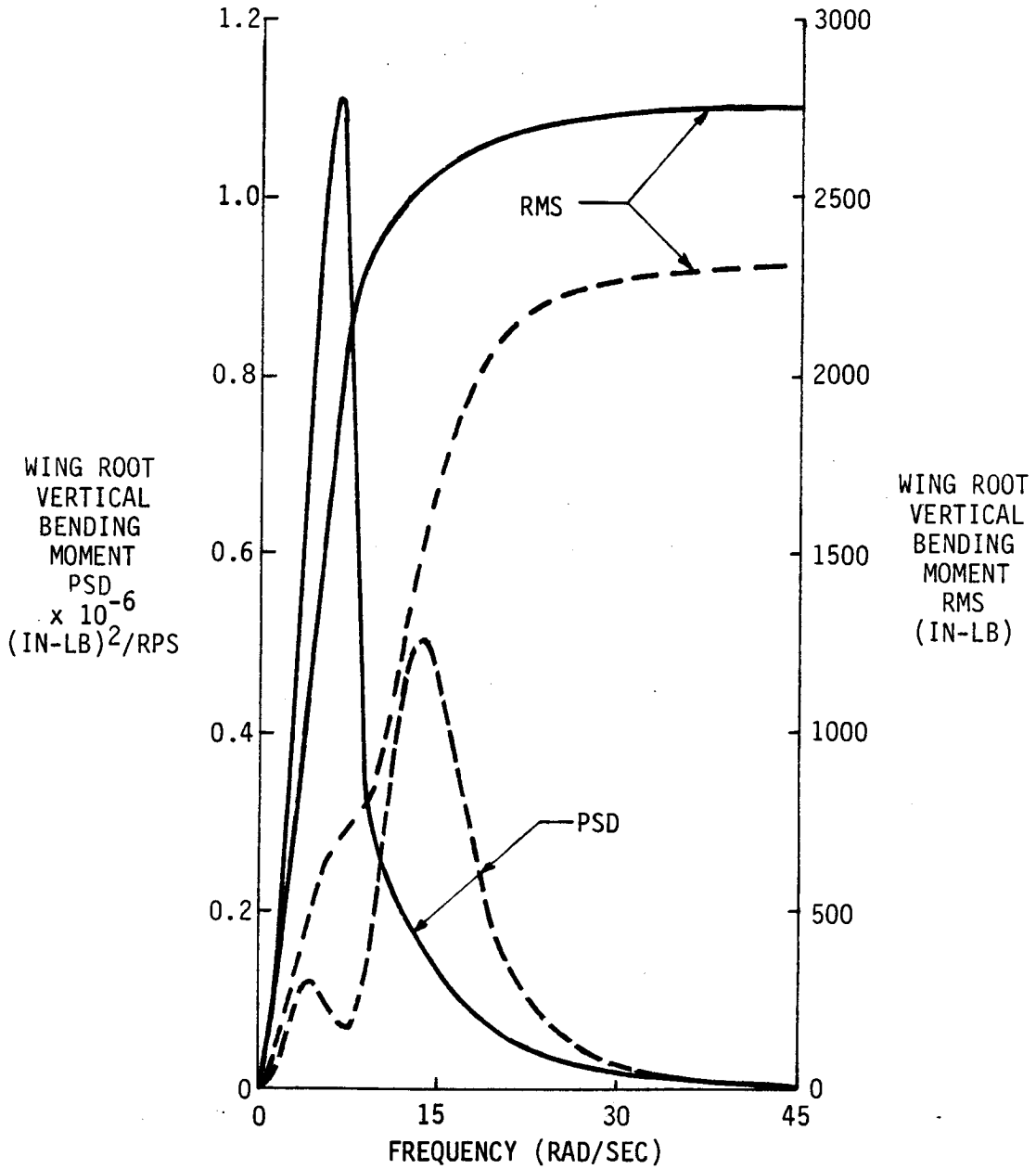
FIGURE 128

WING ROOT VERTICAL BENDING MOMENT PSD/RMS PLOTS FOR INBOARD
AILERON RANDOM EXCITATION

- MACH 0.70
- ALTITUDE: 15,000 FEET
- 10 DEGREE PEAK INBOARD
  AILERON RANDOM EXCITATION
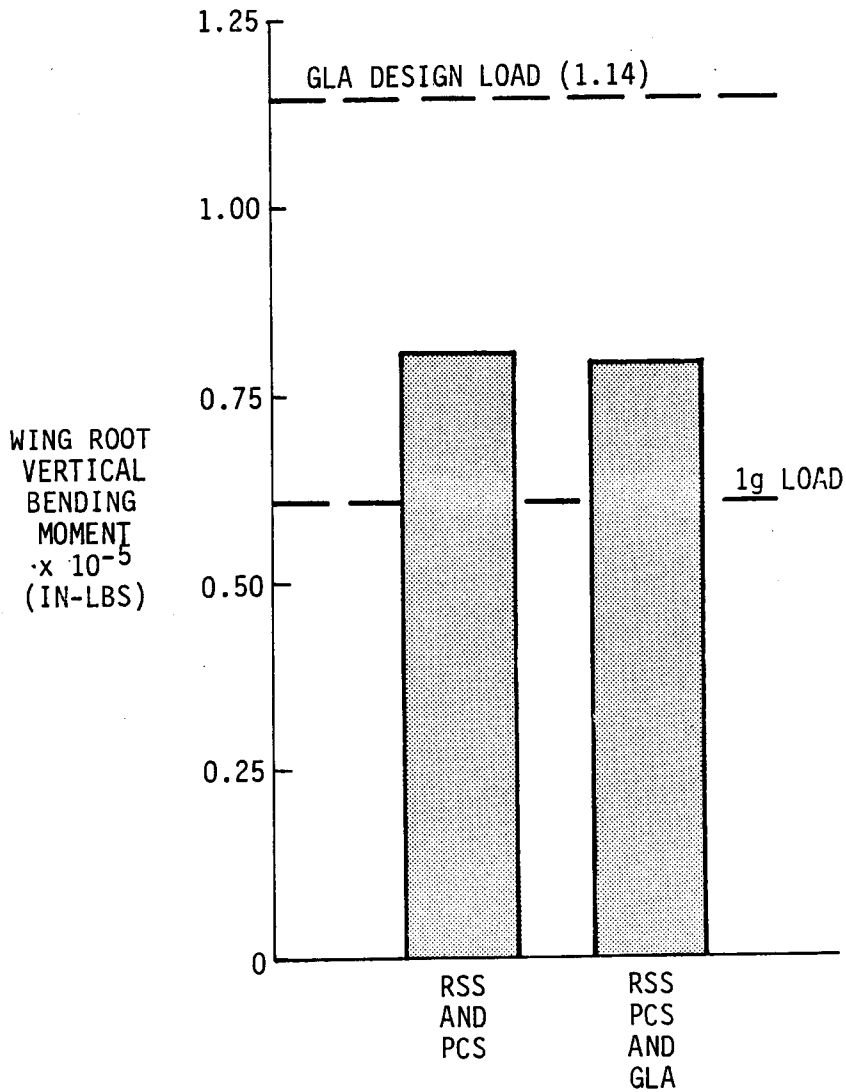
FIGURE 127

MAXIMUM PREDICTED TOTAL WING ROOT VERTICAL BENDING MOMENT
WITH INBOARD AILERON RANDOM EXCITATION

- MACH 0.70
- ALTITUDE: 15,000 FEET
- GROSS WEIGHT: 2350 LBS.
- PRIMARY AFCS AND RSS CLOSED
- RMS GUST = 1 INCH/SECOND

— — GLA ON

——— GLA OFF
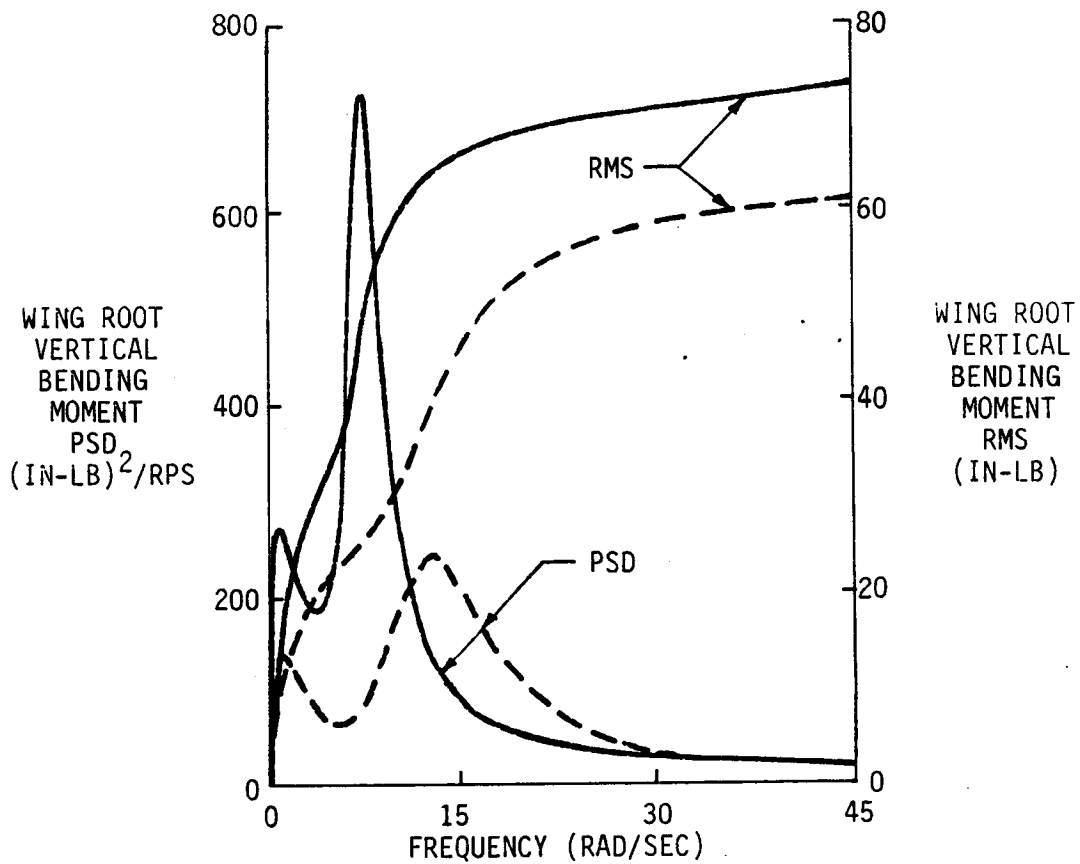
FIGURE 129

WING ROOT VERTICAL BENDING MOMENT PSD/RMS PLOTS FOR RANDOM GUST

		GLA TEST CONDITION		GLA DESIGN CONDITION	
		2350 LB		2500 LB	
		*GLA OFF	*GLA ON	*GLA OFF	*GLA ON
WING ROOT VERTICAL BENDING MOMENT	INCREMENTAL LOAD DUE TO GUST (IN-LB/FPS)	±906.84	±776.74	---	±782.26
	INCREMENTAL LOAD DUE TO INBOARD AILERON (IN-LB/DEG)	±2017.3	±1684.2	---	---
	1g LOADS (IN-LB)	.61300		65500	
VERTICAL ACCELERATION	INCREMENTAL ACCELERATION DUE TO GUST (FT/SEC^2/FPS)	.859	.790	---	.733
	INCREMENTAL ACCELERATION DUE TO INBOARD AILERON FT/SEC^2/DEG	2.44	2.28	---	---

*PRIMARY AFCS AND RSS ENGAGED

FIGURE 130

GLA TEST AND DESIGN CONDITIONS ANALYSIS PREDICTIONS

MACH 0.60
ALTITUDE: 7000 FEET
GROSS WEIGHT: 2500 LBS.
RSS, PCS AND ALTITUDE HOLD ON

5 SEC
(TYPICAL)

VERTICAL
GUST
- FT/SEC

σ = 4.98

GLA OFF

VERTICAL
ACCELERATION
- FT/SEC²

σ = 3.87

GLA ON

VERTICAL
ACCELERATION
-FT/SEC²

σ = 3.54
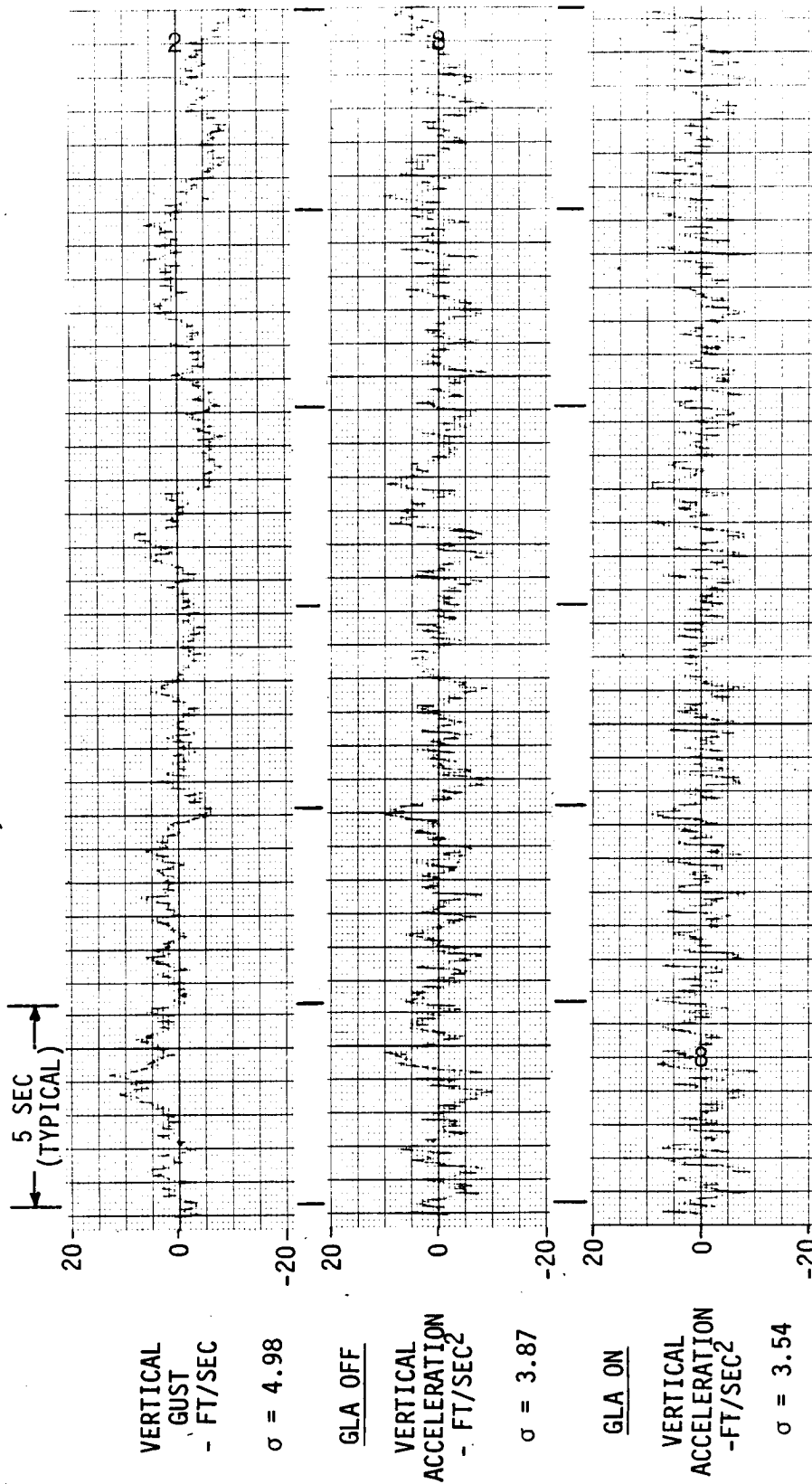
FIGURE 131

VERTICAL ACCELERATION RESPONSE TO RANDOM VERTICAL GUST

- MACH 0.60
- ALTITUDE: 7000 FEET
- GROSS WEIGHT: 2500 LBS.
- RSS, PCS AND ALTITUDE HOLD ON
- RMS AILERON RANDOM EXCITATION = 1 DEG.

5 SEC
(TYPICAL)

AILERON
RANDOM
EXCITIAION
- DEG
σ = 1 DEG.

GLA OFF

VERTICAL
ACCELERATION
- FT/SEC^2
σ = 2.71

GLA ON

VERTICAL
ACCELERATION
- FT/SEC^2
σ = 2.24
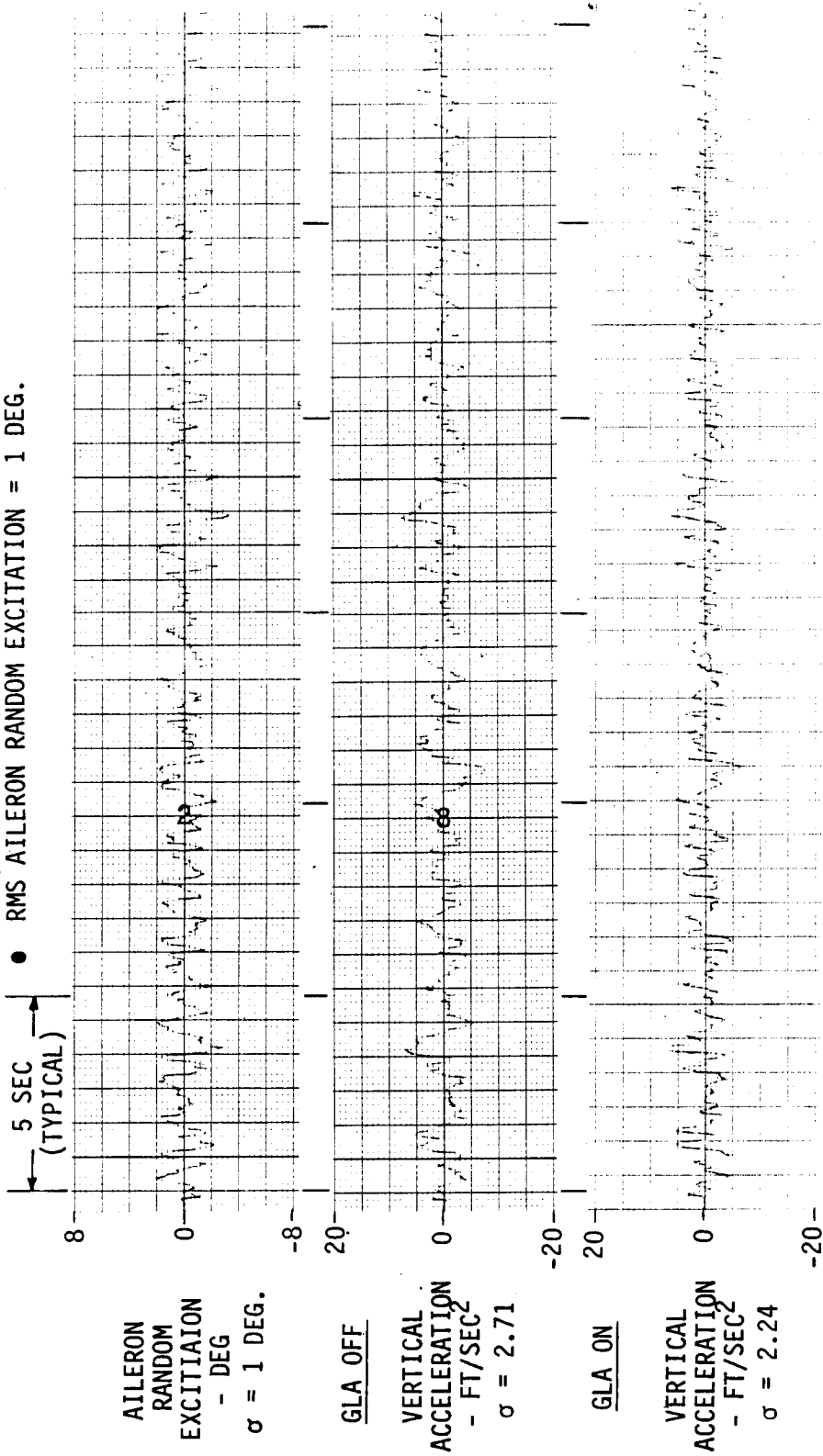
FIGURE 132

VERTICAL ACCELERATION RESPONSE TO INBOARD AILERON RANDOM EXCITATION

192

- MACH 0.70
- ALTITUDE: 15,000 FEET
- PRIMARY AFCS AND RSS CLOSED

INBOARD AILERON
RANDOM EXCITATION
- 3.33 DEG. RMS
  (10 DEG., 3σ PEAK)

VERTICAL GUST
- 7.42 FPS RMS
  (22.25 FPS, 3σ PEAK)

PEAK INCREMENTAL WING ROOT VERTICAL BENDING MOMENT x 10^{-4} (IN-LBS)

GLA OFF   GLA ON   GLA OFF   GLA ON
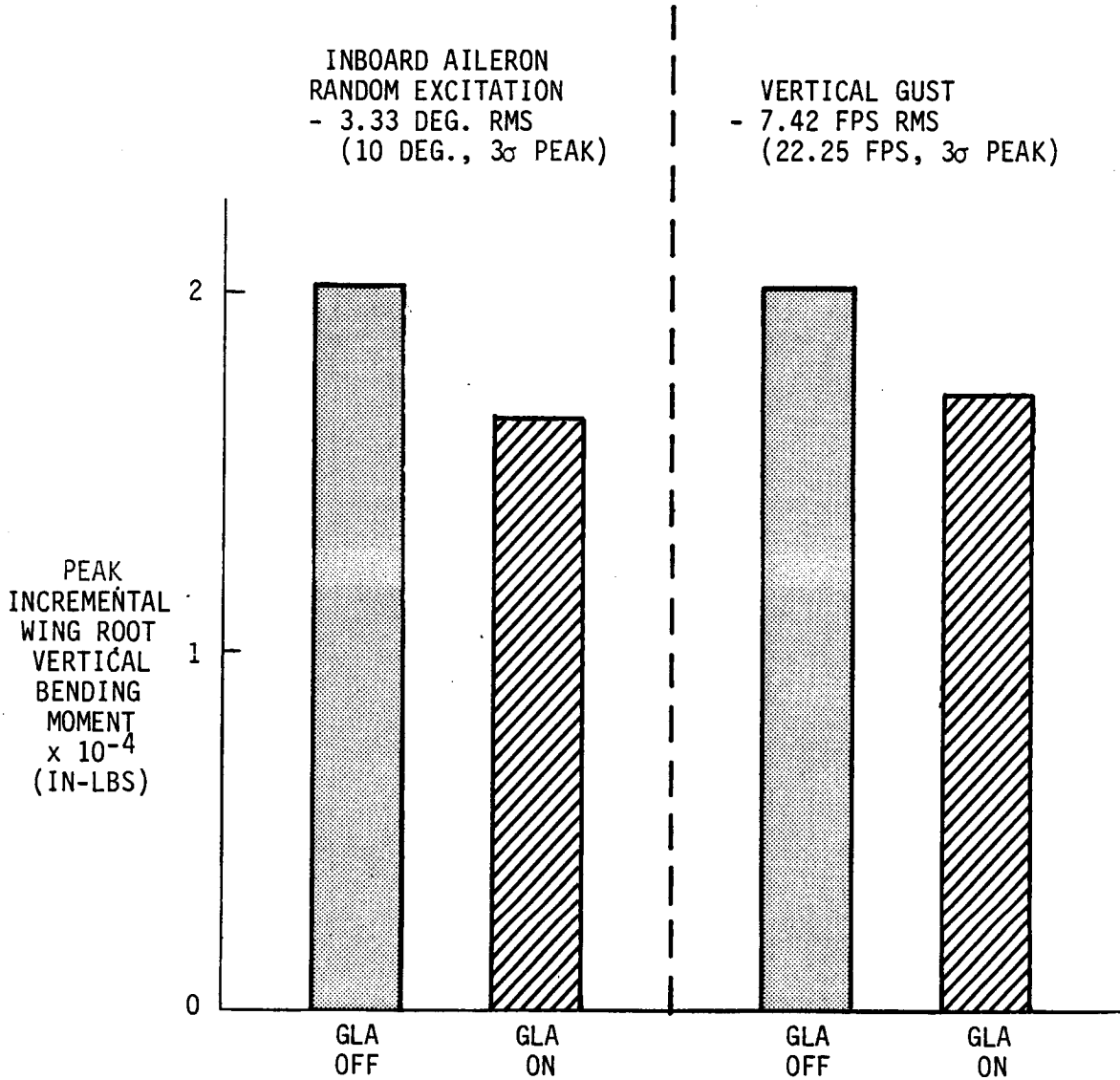
FIGURE 126

PREDICTED INCREMENTAL WING ROOT VERTICAL BENDING MOMENT REDUCTION WITH GLA FOR MAXIMUM AVAILABLE INBOARD AILERON AND EQUIVALENT GUST

186

MACH 0.70
ALTITUDE: 15,000 FEET
GROSS WEIGHT: 2350 LBS.
RANDOM EXCITATION SCALED FOR UNITY RMS AT 40 RPS
PRIMARY AFCS AND RSS CLOSED

——— VERTICAL GUST
——— INBOARD AILERON
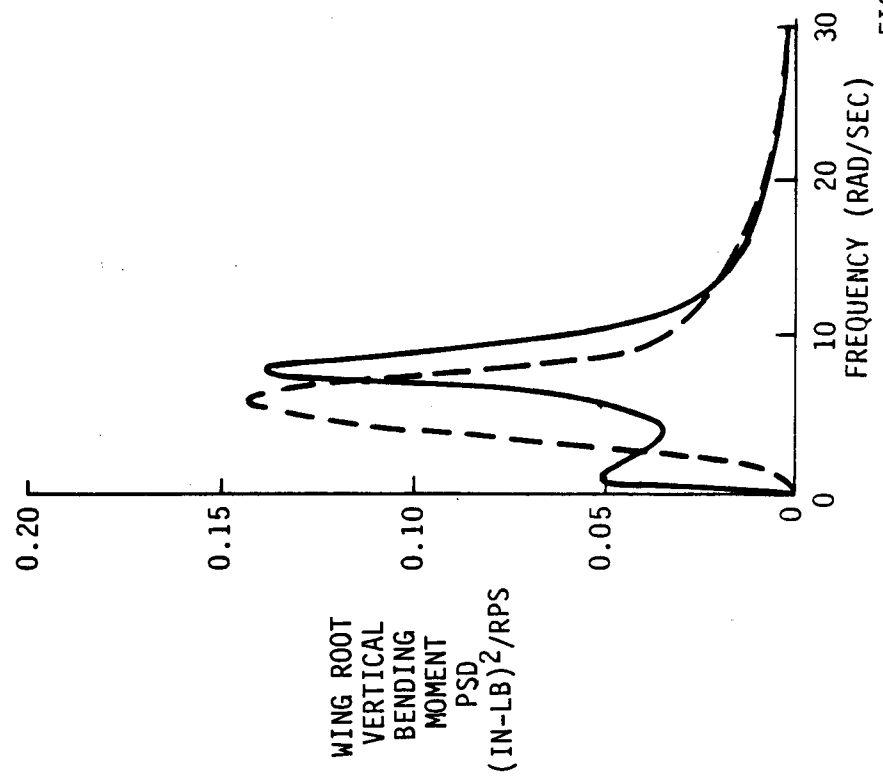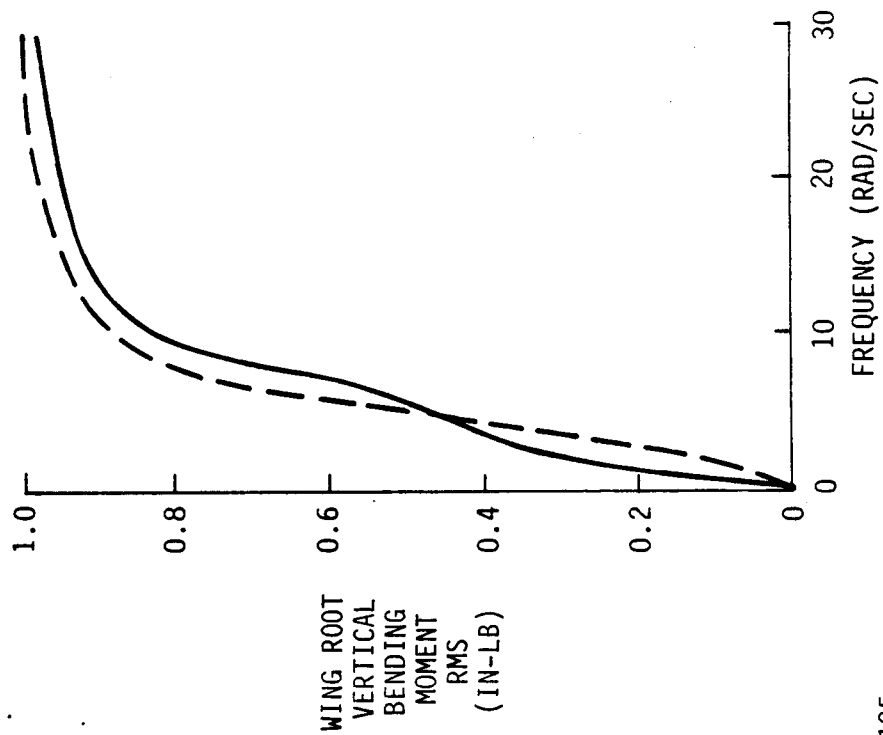
FIGURE 125

WING ROOT VERTICAL BENDING MOMENT FREQUENCY DISTRIBUTION COMPARISON OF RANDOM GUST AND
INBOARD AILERON RANDOM EXCITATION

185
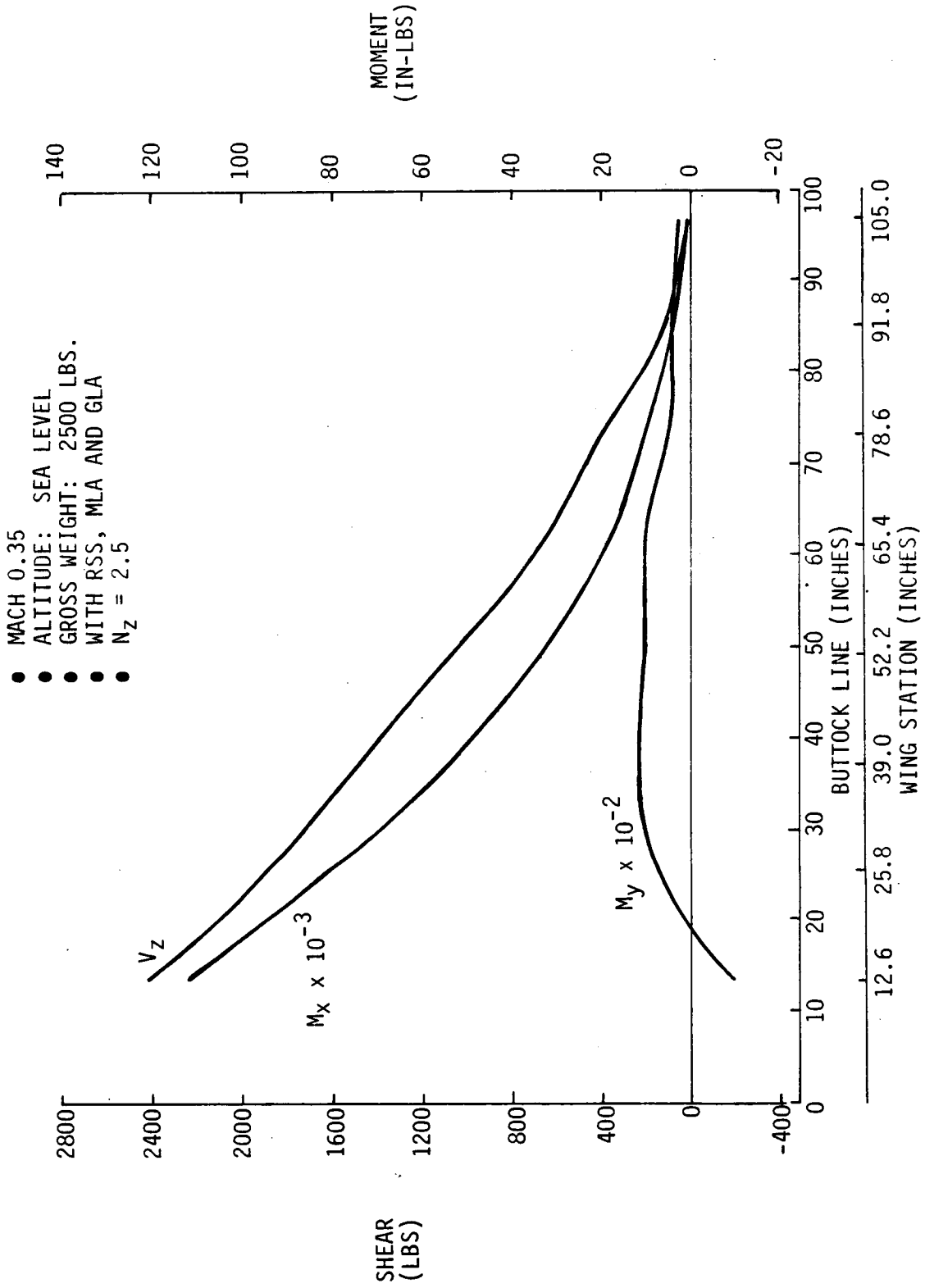
FIGURE 122

MANEUVER DESIGN LIMIT WING SHEAR, VERTICAL BENDING MOMENT AND TORSION

STRUCTURAL COMPONENT	ENGINEERING DRAWING	MINIMUM MARGIN OF SAFETY		LOAD/STRESS TYPE	WING STATION
		ITERATION 2	ITERATION 3		
FRONT SPAR	35-34620				
- UPPER CHORD		+0.21	+0.13	CRIPPLING	WS 25.8
- LOWER CHORD		+0.10	+0.06	TENSION	WS 25.8
- WEB		+0.09	+0.13	BUCKLING	WS 52.2 - 65.4
REAR SPAR	35-34620				
- UPPER CHORD		+0.05	+0.01	CRIPPLING	WS 25.8
- LOWER CHORD		+0.15	+0.25	TENSION	WS 25.8
- WEB		+0.13	+0.08	BUCKLING	WS 52.2 - 65.4
SKIN PANELS	35-34620				
- EDGE		+0.17	+0.13	TENSION	WS 25.8
- PANEL		+0.00	+0.46	BUCKLING	WS 25.8
- ATTACHMENT		+0.06	+0.57	BEARING	WS 12.6 - 25.8
TYPICAL RIB	35-34618	+HIGH	△1	- -	- -
CENTER SECTION	35-34619	+0.31	△1	TENSION	- -
WING ATTACHMENT	35-34619				
- SPAR FITTING		+0.02	+0.14	BENDING	- -
- BOLTS		+0.07	+0.19	TENSION & SHEAR	- -
CENTER SECTION TO DRONE ATTACH	35-34625	+0.01	△1	TENSION	- -
LEADING EDGE	35-34625	+2.85	△1	BENDING	- -
TRAILING EDGE	35-34625	+HIGH	△1	BENDING	- -
FAIRING	35-34621	+0.80	△1	TENSION	- -

△1 NONCRITICAL COMPONENTS ≥ ITERATION 2

FIGURE 123

MINIMUM MARGIN OF SAFETY FOR CRITICAL COMPONENTS
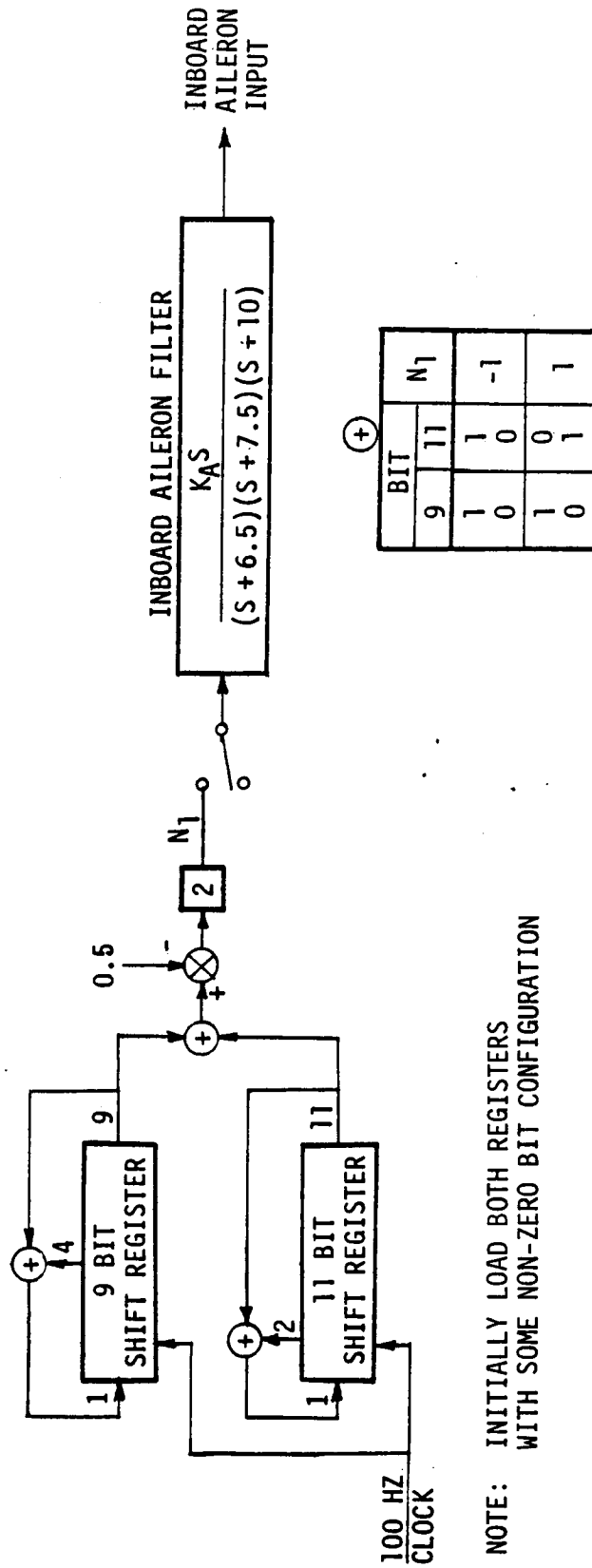
FIGURE 124

INBOARD AILERON RANDOM EXCITATION SYSTEM

183

The noise filter on Figure 124 shapes the generated white noise to roughly match the PSD of the WRVBM due to gust as shown on Figure 125. Limitations on the number of filters that could be incorporated in the hardware package determined how close a match that could be produced. The intent was to place a large percentage of the power of WRVBM due to inboard aileron in the same frequency range as that due to gust. As indicated on Figure 125, the system adequately accomplishes that intent.

Performance of the GLA system can be verified by relating test data with inboard aileron excitation to analysis data with inboard aileron excitation and gust. All baseline GLA testing should be conducted with the primary AFCS and RSS engaged. Performance of the GLA system can also be verified by comparing the incremental improvement beyond that obtained with these systems. The predicted reduction in WRVBM with the maximum available inboard aileron excitation and an equivalent level of random gust is indicated on Figure 126. The reduction in WRVBM with aileron excitation is 16.5 percent and 14.3 percent with random gust. With the similarity in predicted percent reduction and the similarity of load power as a function of excitation frequency, a close match of inboard aileron excitation test data to analysis data should substantiate that the gust load increment will be as predicted.

With maximum available inboard aileron excitation, peak loads are predicted to be well below the design load limit as shown on Figure 127.

PSD/RMS plots of WRVBM due to inboard aileron random excitation and gust are shown on Figures 128 and 129, respectively. Predicted steady-state (1g) values of WRVBM and incremental RMS (or peak) values per unit RMS (or peak) inboard aileron and gust excitation are shown on Figure 130. RMS (or peak) ratios of fuselage vertical acceleration are also shown on Figure 130.

Gain of the inboard aileron random excitation filter was initially scaled for required RMS values on the six DOF airplane dynamics simulation discussed in Reference 1 and later verified by hardware tests discussed in Section 9. Time responses and RMS data of random excitation and airplane motion were obtained from the simulation. Random gust in the six DOF simulation was also produced by the shift register pair on Figure 124 combined with a set of four first-order linear filters selected to closely approximate the frequency content of the Von Karman gust spectrum.

Typical time responses of input excitation and airplane vertical acceleration are shown on Figures 131 and 132. The ratio of vertical acceleration to input excitation agrees well with PSD/RMS analysis results shown on Figure 130.

The measured probability distribution function of the inboard aileron random excitation is compared to the Gaussian distribution on Figure 133. The inboard aileron random excitation provides a reasonable match to Gaussian characteristics as indicated on Figure 133.

184
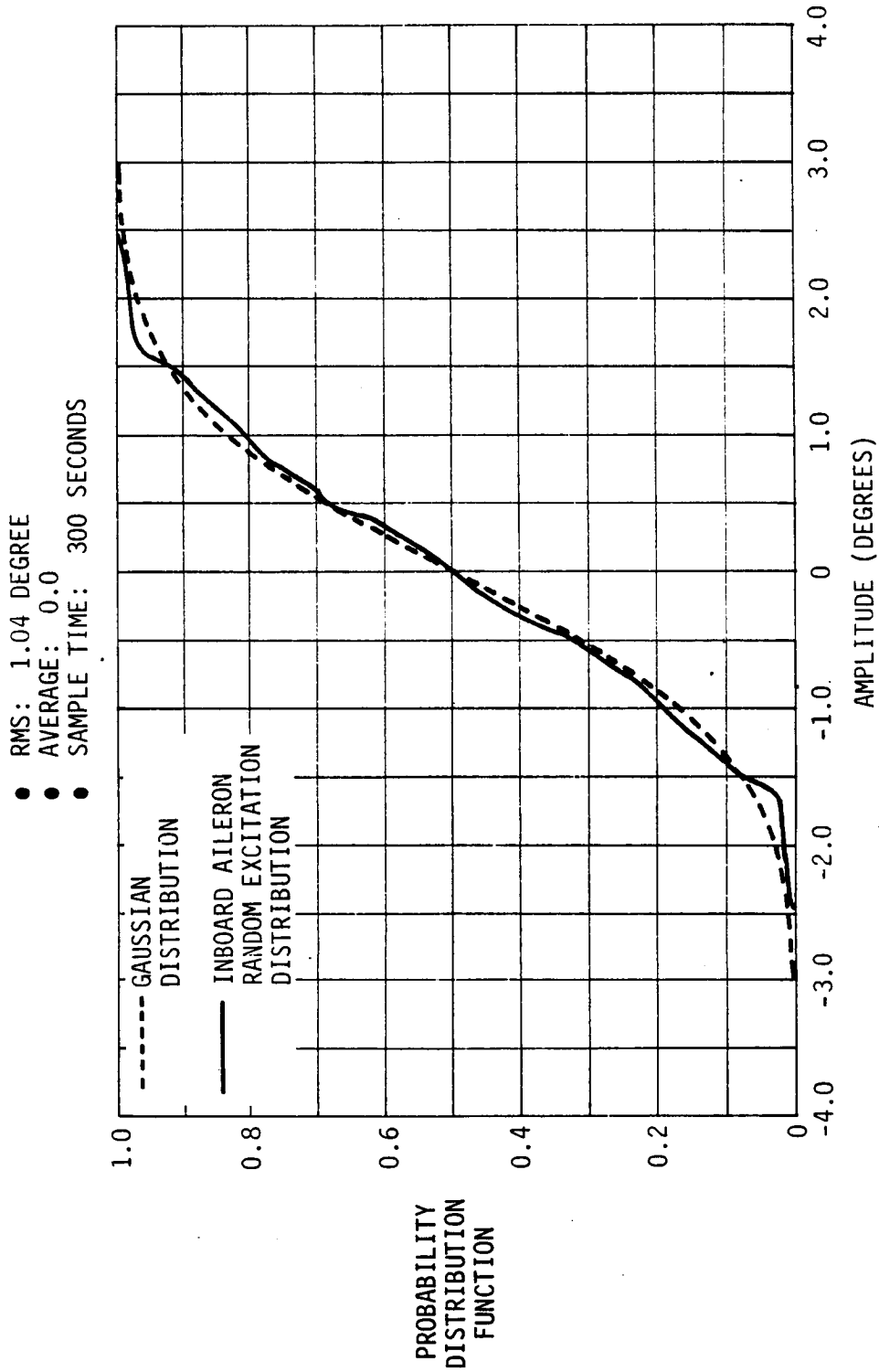
FIGURE 133

INBOARD AILERON RANDOM EXCITATION PROBABILITY DISTRIBUTION FACTOR

193

6.5 Relaxed Static Stability System Analysis. RSS System defined in the previous design iteration was evaluated for the capability to maintain stability at all flight conditions and C.G. variations with fuel burn.

The RSS system permits flight at aft, unstable C.G. positions to take advantage of reduced drag associated with reducing or eliminating down trim tail loads by placing the C.G. aft.

The RSS permits flight at an aft C.G. position of 33 percent MAC over the entire flight envelope. The neutral point of the trim cruise condition is 38.6 percent MAC as shown on Figure 37; however, a large forward shift in neutral point at other flight conditions limits the capability of the RSS to stabilize the aircraft at C.G. positions aft of 33 percent MAC. The largest static instability that the RSS stabilizes is -18.5 percent MAC at the maximum dynamic pressure condition.

At the DAST 2 launch condition, the static neutral point was determined to be 29.7 percent MAC. The launch C.G. was selected by NASA to be 20 percent MAC, providing a stable launch condition. The weight to C.G. relationship for the selected fuel burn sequence is shown on Figure 39. The cruise drag versus C.G. position shown on Figure 40 indicates that minimum trim drag is well back of the 33 percent aft C.G. limit.

The critical condition for static stability are indicated by the C_M versus α curves on Figure 134. At the maximum dynamic pressure condition the C_M curve has an unstable slope at trim angle of attack. At the cruise condition, an unstable C_M slope occurs during positive maneuvers. Neutral points for maximum dynamic pressure and a 1.2g maneuver at cruise are 14.5 and 16.7 percent MAC, respectively. These two conditions are the most critical for RSS performance.

A revision of the RSS was required to meet stability criteria at the critical conditions. Without the primary AFCS engaged, which provided some stability, a gain increase of 1.7 was required to meet minimum gain margin. The critical condition which dictated the 1.7 gain increase is maximum Q flight condition, 33 percent MAC C.G. position with the backup AFCS engaged. A root locus for this condition is shown on Figure 199 of Appendix E.

A low frequency lag-lead filter (S + .1)/(S + .05) was added to the RSS feedback loop to double the gain at zero frequency. At the aft C.G., 1.2g maneuver cruise condition with the primary AFCS and also the GLA system closed, the low frequency gain increased the stability of an unstable real characteristic root which approached a zero near the origin as shown on Figures 180 and 182 of Appendix E.

The revised RSS system is shown in the block diagram on Figure 135. Short period and phugoid damping and frequency from the evaluation of RSS and other appropriate systems with the structural dynamic equations of motion are shown on Figures 136 and 137. The weights of Figure 136 and 137 are the most typical weights for each test condition.

194
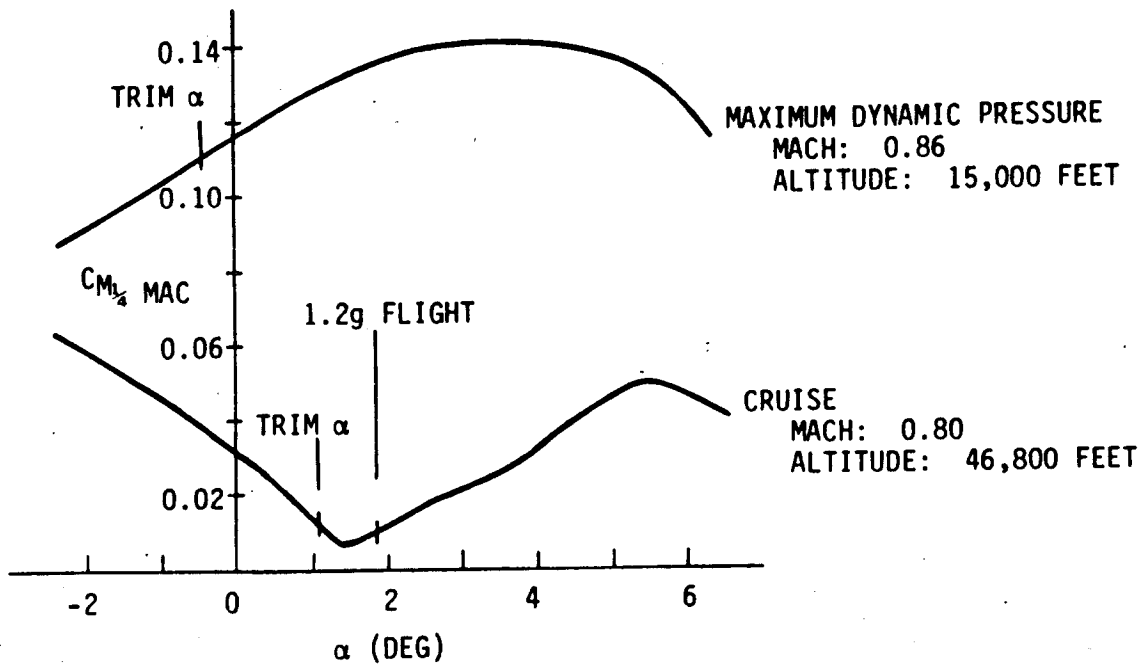
FIGURE 134

PITCHING MOMENT COEFFICIENT VS. ANGLE-OF-ATTACK AT CRITICAL STABILITY CONDITIONS

C-3
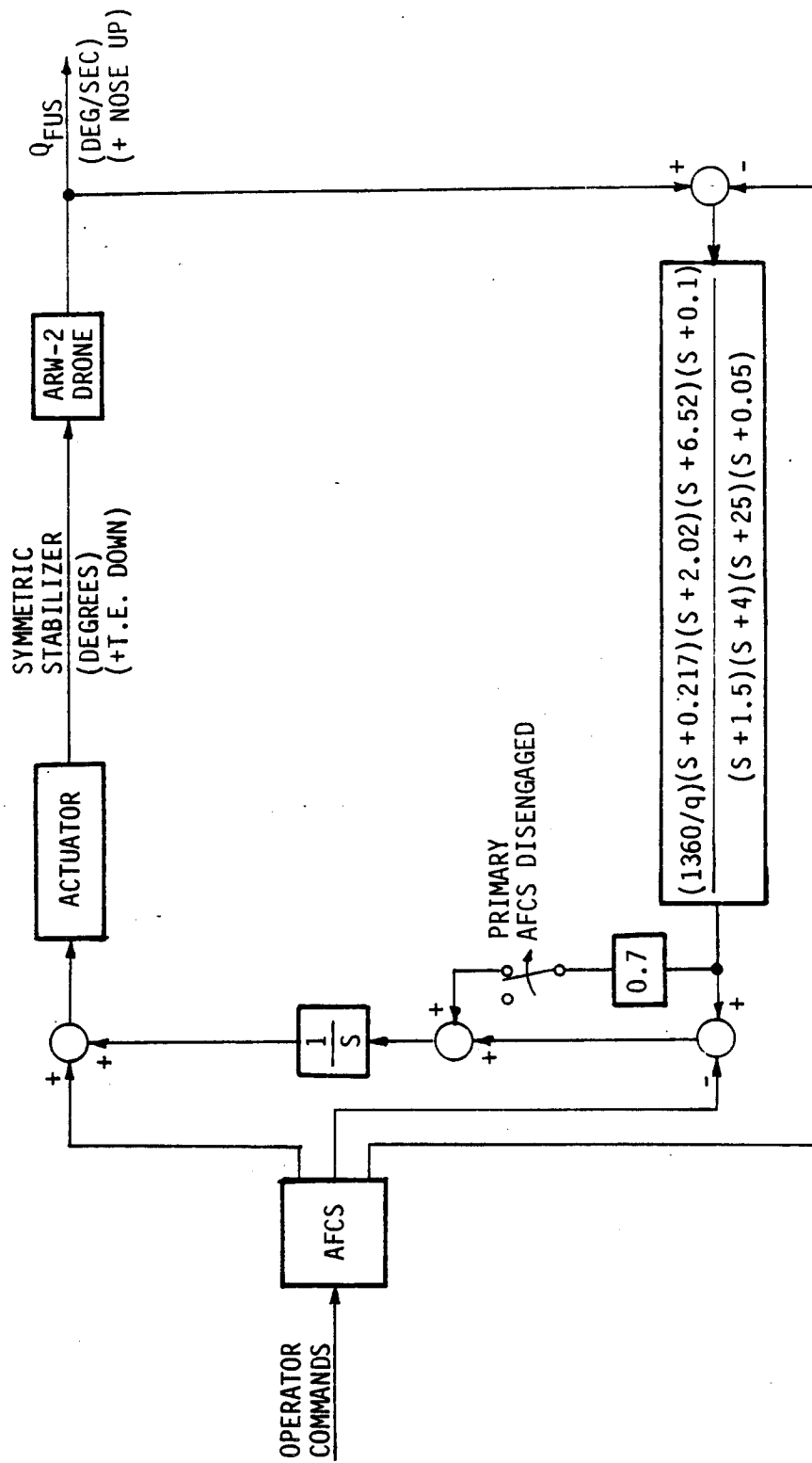
FIGURE 135

RSS SYSTEM BLOCK DIAGRAM

- STRUCTURAL DYNAMIC EQM
- SYSTEMS ON:
  - PRIMARY AFCS (EXCLUDING ALTITUDE HOLD)
  - GLA/MLA
  - RSS

FLIGHT CONDITION		CONFIGURATION		CHARACTERISTIC ROOTS $S = (\ ) \pm j(\ )$	DAMPING RATIO, ζ_{SP} [1]	FREQUENCY, ω_{NSP} (RAD/SEC)	
MACH	ALTITUDE (FEET)	WEIGHT (LBS)	C.G. (% MAC)			ANALYSIS	CRITERIA (MAXIMUM)
0.35	SEA LEVEL	2500	19.9	$-2.90\pm j6.37$	0.41	7.0	7.0
0.41	10,000	2350	27.4	$-2.95\pm j6.09$	0.44	6.8	7.2
0.60	7,000	2350	27.4	$-4.7\pm j10.04$	0.42	11.1	11.3
0.70	15,000	2350	27.4	$-4.33\pm j10.28$	0.39	11.2	11.3
0.40	15,000	2500	19.9	$-2.75\pm j6.04$	0.41	6.6	6.02
0.70	50,000	2350	27.4	$-3.07\pm j5.7$	0.47	6.5	5.1
0.80	46,800	2350	27.4	$-2.67\pm j7.57$	0.33	8.03	7.37
0.86	15,000	2350	27.4	$-2.15\pm j10.15$	0.21	10.4	14.7

[1] DAMPING CRITERIA LEVEL 1 $0.3 < \zeta_{SP} < 2.0$

FIGURE 136

CLOSED LOOP ACS AND AFCS SHORT PERIOD CHARACTERISTICS

197

- STRUCTURAL DYNAMIC EOM

- SYSTEMS ON:
  - PRIMARY AFCS (EXCLUDING ALTITUDE HOLD)
  - GLA/MLA
  - RSS

FLIGHT CONDITION		CONFIGURATION		CHARACTERISTIC ROOTS $S = (\ ) \pm j(\ )$	DAMPING RATIO, ζ_p △1	FREQUENCY, ω_{Np} (RAD/SEC)
MACH	ALTITUDE (FEET)	WEIGHT (LBS)	C.G. (% MAC)			
0.35	SEA LEVEL	2500	19.9	$-0.447 \pm j0.208$	0.21	0.212
0.41	10,000	2350	27.4	$-0.046 \pm j0.21$	0.21	0.216
0.60	7,000	2350	27.4	$(-0.0197)(-0.0705)$	>1.0	0.0373
0.70	15,000	2350	27.4	$-0.0317 \pm j0.167$	0.186	0.17
0.40	15,000	2500	19.9	$-0.0522 \pm j0.0327$	0.848	0.0616
0.70	50,000	2350	27.4	$(-0.0088)(-0.125)$	>1.0	0.0332
0.80	46,800	2350	27.4	$(-0.030)(-0.0407)$	>1.0	0.0349
0.86	15,000	2350	27.4	$(-0.0077)(0.0136)$	>1.0	0.0103

△1 DAMPING CRITERIA LEVEL 1 $\zeta_p > 0.04$

FIGURE 137

CLOSED LOOP ACS AND AFCS PHUGOID CHARACTERISTICS

Short period characteristics at the weight and C.G. extremes obtained with the QSE equations of motion are shown on Figures 166 and 167.

6.6 Automatic Flight Control Systems. The primary and backup AFCS systems defined during the previous study were re-evaluated using revised aerodynamic and physical properties.

The longitudinal primary AFCS was revised to be more compatible with larger variations in aerodynamic characteristics at different flight conditions. An altitude hold mode was added to the primary longitudinal AFCS. The altitude hold mode and other AFCS functions are compatible except during banked turns where an offset in altitude occurs as discussed in Paragraph 6.8.1.

Simulation time response evaluation still indicates a possibility of exceeding positive load factor limits if the backup system is engaged in a descent condition at high dynamic pressure conditions. To eliminate the possibility of exceeding limit load factor, a circuit which will ramp in the initial stabilizer step command change should be considered for the longitudinal backup AFCS.

The lateral-directional AFCS control laws required no change in the present design cycle. Signal synchronization of primary and backup lateral-directional AFCS modes was added.

6.6.1 Primary Longitudinal AFCS. The primary function of the system is to accept operator inputs in the form of a load factor command and process the input and load factor feedback to generate a stabilizer command to provide desirable airplane response. Additional functions of the system are to provide a MLA system command when that system is engaged and to provide a positive angle of attack limit. A block diagram of the revised system is shown on Figure 138. The changes to the system are discussed below.

With aerodynamic characteristics used in the previous design iteration, steady-state load factor response agreed closely with load factor command. The close agreement in response and command previously allowed a load factor limit feature to be implemented by limiting the command. Due to the wider variations in aerodynamic characteristics in the present iteration, the response did not always agree exactly with the command; and consequently, the limits on the command had to be removed to provide for limit maneuvers in the cases when the response was less than the command.

With the previous close agreement of response to command, a low gain load factor error signal was integrated and summed into the RSS integrator to provide further agreement of response to command. With the present differences in response and command, an input produced an initial response that for some conditions was significantly different

FIGURE 138

PRIMARY LONGITUDINAL AFCS BLOCK DIAGRAM

than the command and the integrator produced a sluggish ramp up to the input level. It also produced a sluggish decay after the input was removed.

The load factor error integrator was eliminated in the present iteration because a quick rising response that did not correspond exactly with the command was considered to be more desirable than one with a sluggish ramp response after an initial buildup.

A $1/\cos(\phi)$ load factor term which previously eliminated the operator having to apply a conventional column input for a steady-state turn was eliminated. With the difference in response and command in some cases, the column input with the $1/\cos(\phi)$ term, although small, might be opposite that of a conventional column command in a turn.

In the revised system, a third order filter duplicating the RSS filter was eliminated and the pseudo pitch rate command signal generated by the AFCS was summed into the RSS feedback loop upstream of the RSS filter instead of downstream. This change eliminated duplicating the complex filter but required one more uplink signal than the previously defined configuration.

A slight modification which simplified the angle of attack limiter reduced the amplitude of response transients when the angle of attack limit value was exceeded.

Another change to the primary longitudinal AFCS added an altitude hold mode option to the system as shown on Figure 138. Compatibility of the altitude hold mode is discussed in Section 6.8.1.

Typical airplane motion time responses for symmetric maneuvers with the primary AFCS and other appropriate systems at flight conditions spanning the flight range are shown on Figures 139 through 146. These responses illustrate the following characteristics:

● Variation of responses with center of gravity

● Variation of responses with use of the load alleviation systems

● Effects of the angle of attack limiter on responses

A flow diagram for the ground based primary AFCS digital program is included in Section 6.9.

6.6.2 Lateral-Directional Automatic Flight Control System. The lateral-directional AFCS defined in the previous design cycle was evaluated with the revised QSE mathematical model. Revisions to the QSE

- MACH: 0.40
- ALTITUDE: 15,000 FEET
- C.G.: 20% MAC
- PRIMARY AFCS AND RSS ON
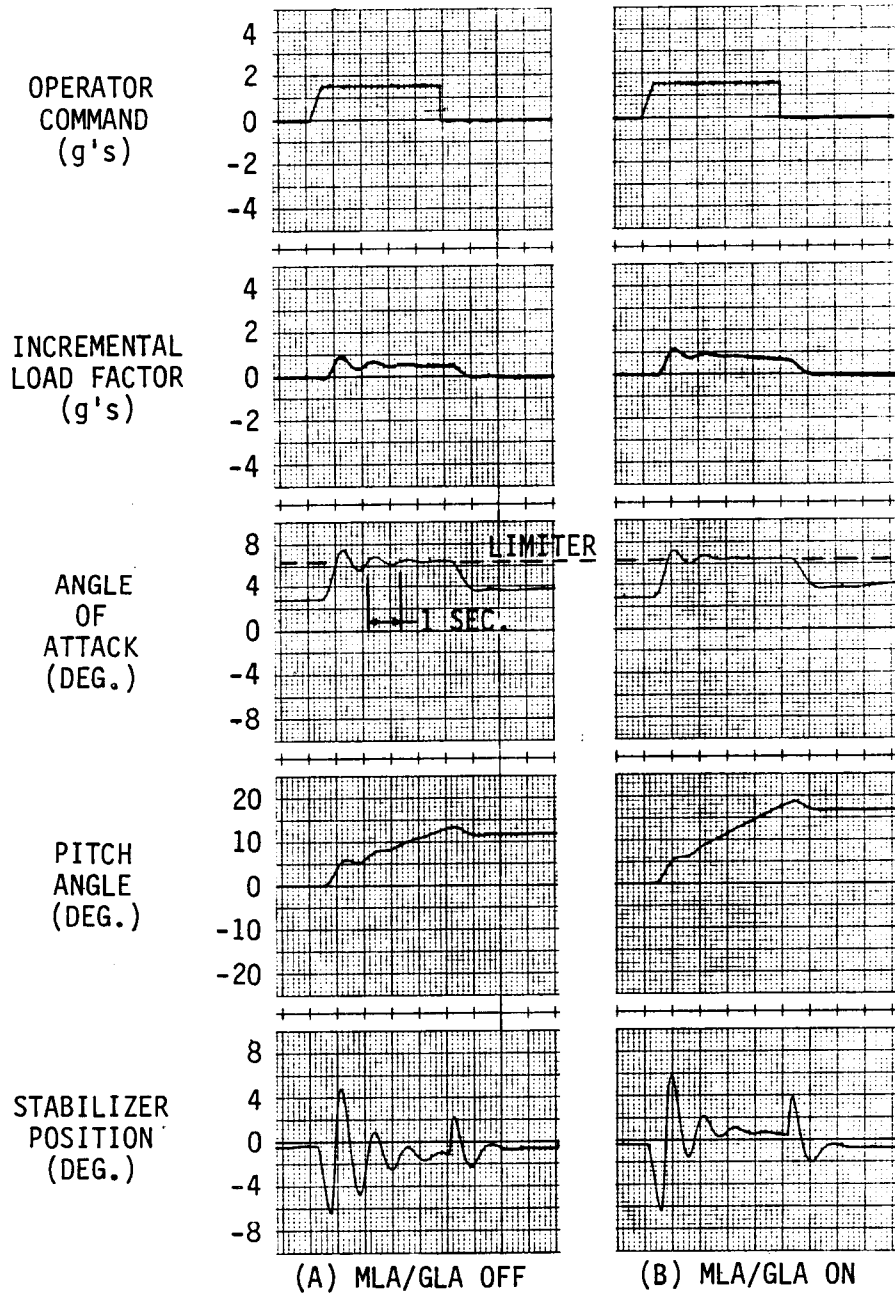
FIGURE 139

RESPONSE AT LAUNCH CONDITION FOR POSITIVE LOAD FACTOR COMMAND

- MACH: 0.40
- ALTITUDE: 15,000 FEET
- C.G.: 20% MAC
- PRIMARY AFCS AND RSS ON

OPERATOR COMMAND (g's)

INCREMENTAL LOAD FACTOR (g's)

ANGLE OF ATTACK (DEG.)

PITCH ANGLE (DEG.)

STABILIZER POSITION (DEG.)

(A) MLA/GLA OFF

(B) MLA/GLA ON
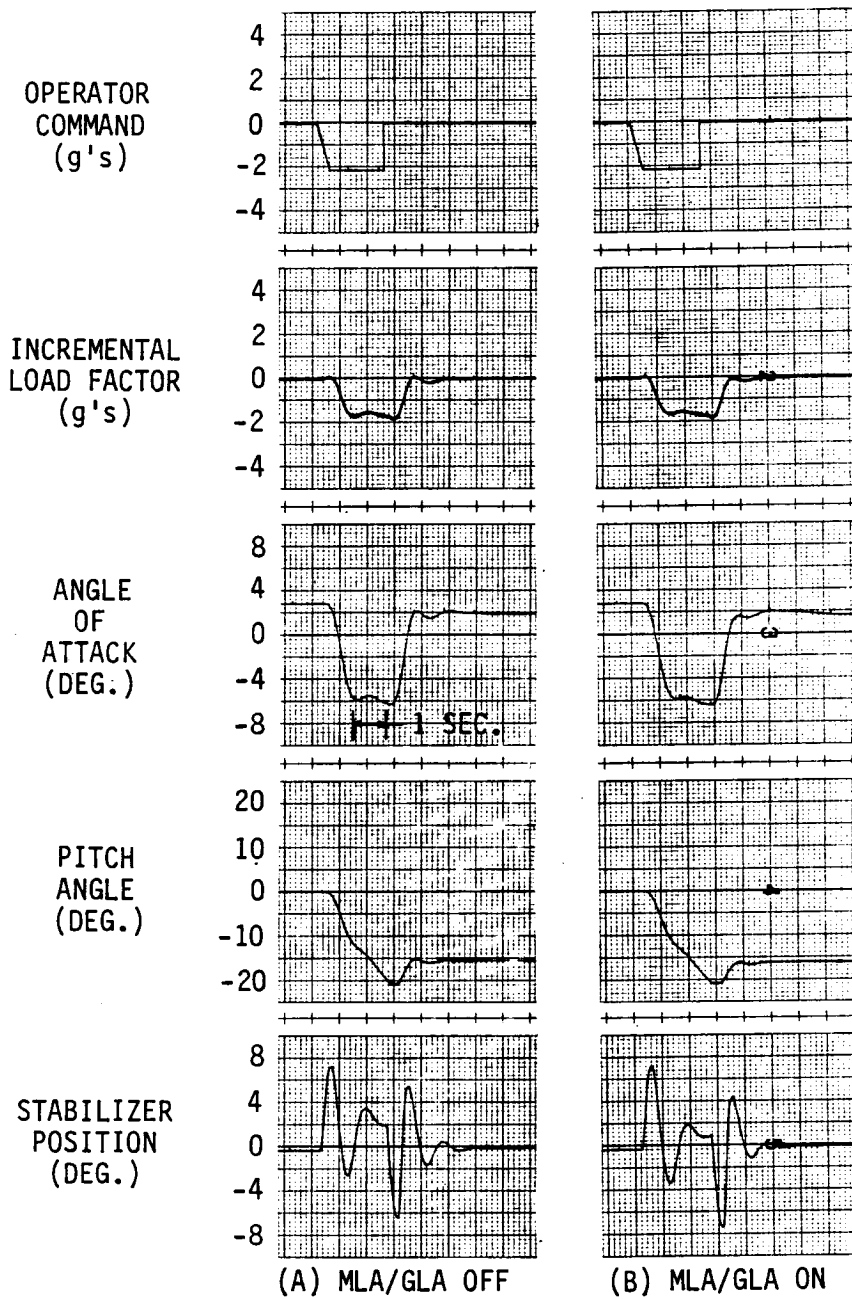
FIGURE 140

RESPONSE AT LAUNCH CONDITION FOR NEGATIVE LOAD FACTOR COMMAND

- MACH: 0.70
- ALTITUDE: 15,000 FEET
- C.G.: 27.5% MAC
- PRIMARY AFCS AND RSS ON

OPERATOR COMMAND (g's)

INCREMENTAL LOAD FACTOR (g's)

ANGLE OF ATTACK (DEG.)

1 SEC.

PITCH ANGLE (DEG.)

STABILIZER POSITION (DEG.)

(A) MLA/GLA OFF

(B) MLA/GLA ON
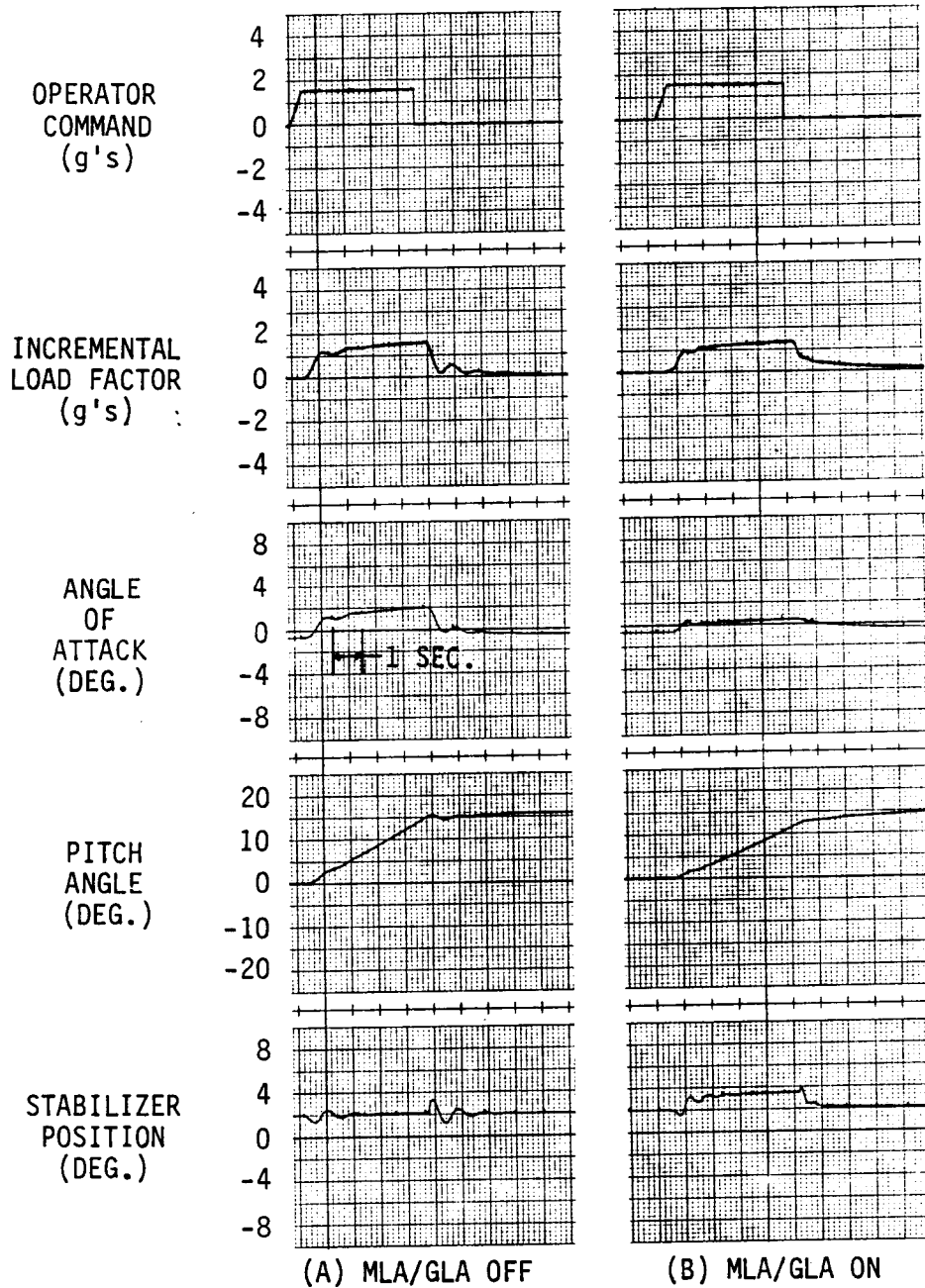
FIGURE 141

RESPONSE AT GLA TEST CONDITION FOR POSITIVE LOAD FACTOR COMMAND

- MACH: 0.70
- ALTITUDE: 15,000 FEET
- C.G.: 27.5% MAC
- PRIMARY AFCS AND RSS ON

OPERATOR COMMAND (g's)

INCREMENTAL LOAD FACTOR (g's)

ANGLE OF ATTACK (DEG.)

1 SEC.

PITCH ANGLE (DEG.)

STABILIZER POSITION (DEG.)

(A) MLA/GLA OFF
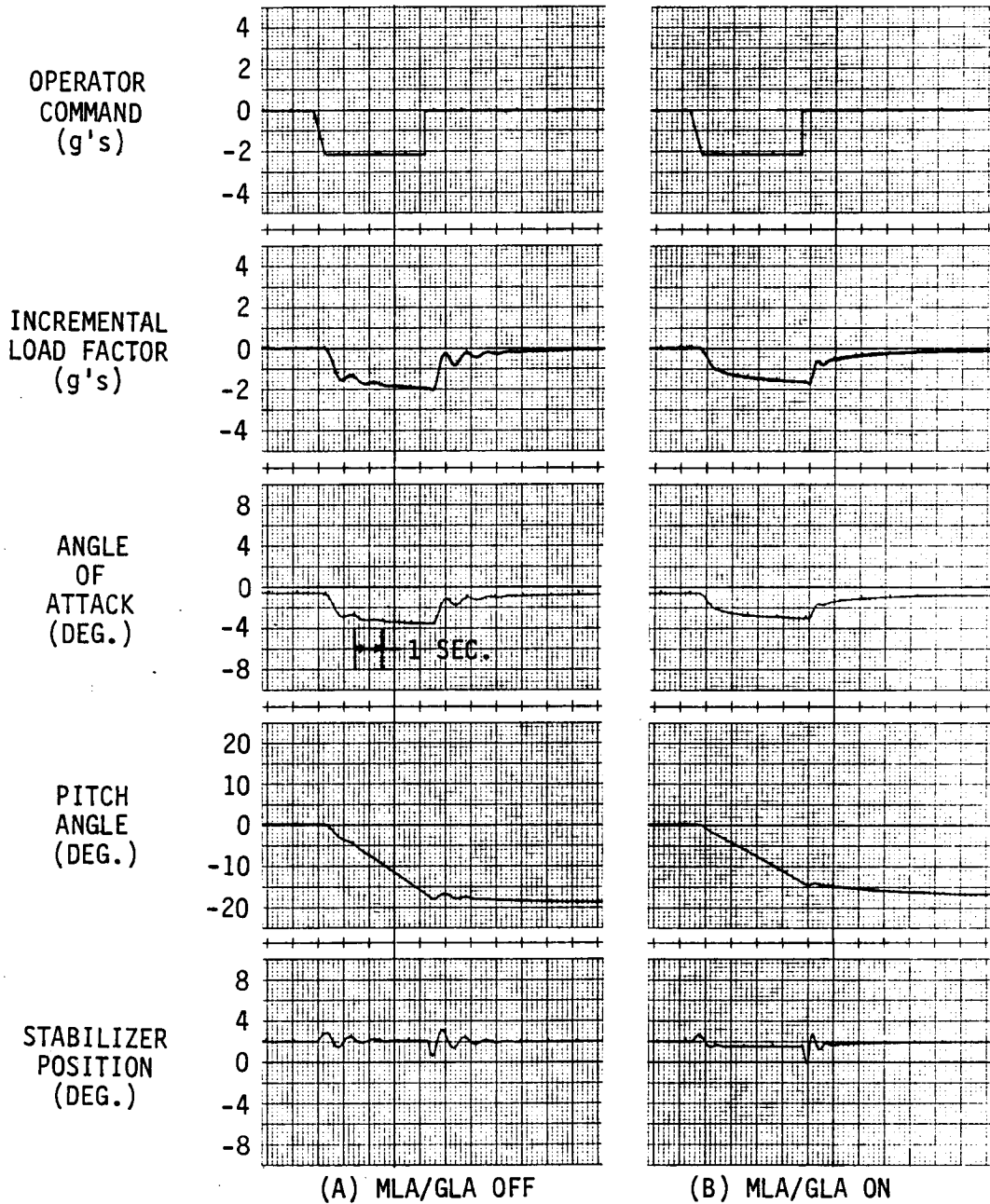
(B) MLA/GLA ON

FIGURE 142

RESPONSE AT GLA TEST CONDITION FOR NEGATIVE LOAD FACTOR COMMAND

- MACH: 0.42
- ALTITUDE: 10,000 FEET
- PRIMARY AFCS, RSS AND MLA/GLA ON
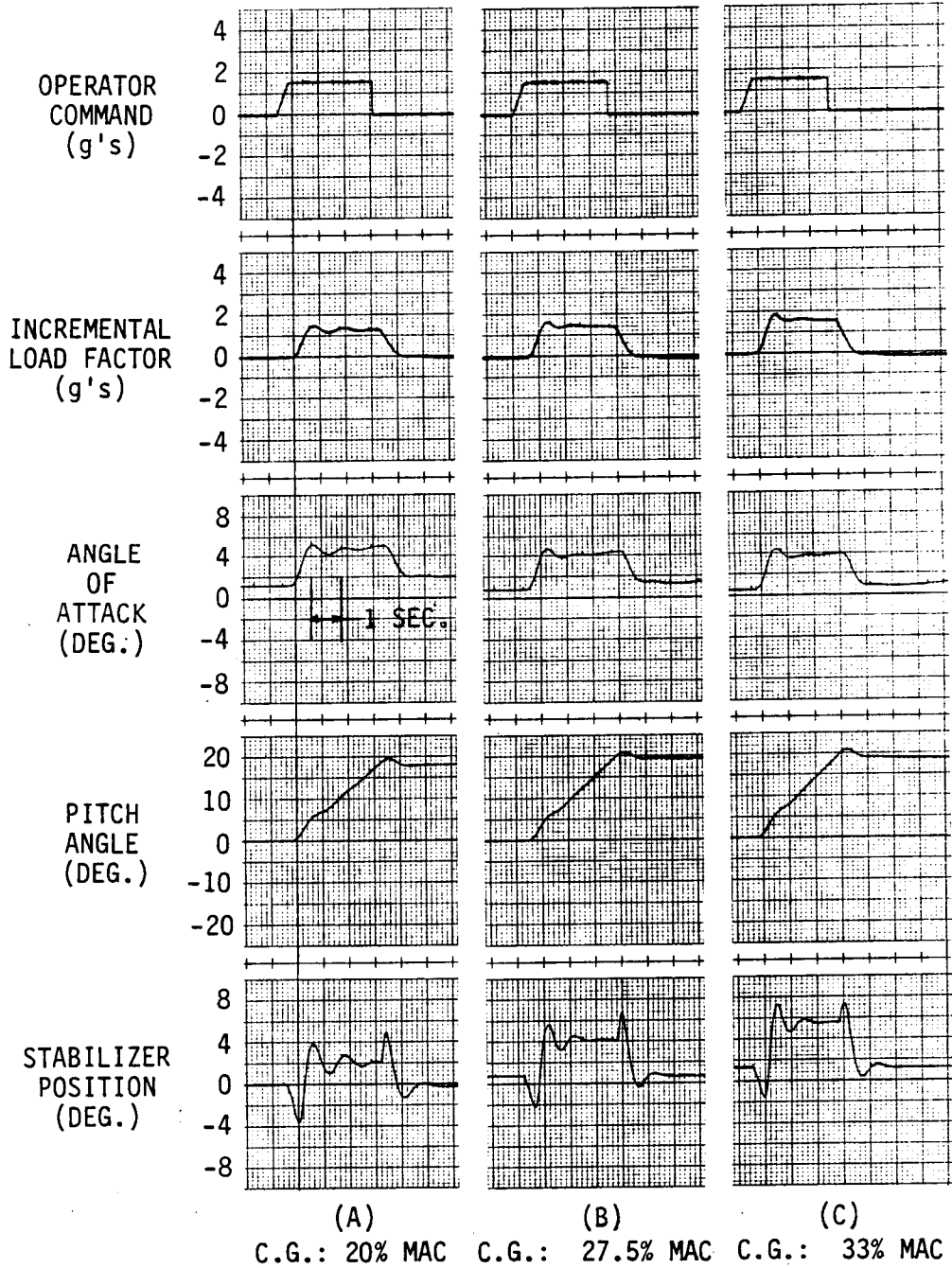
FIGURE 143

RESPONSE AT MLA TEST CONDITION FOR POSITIVE LOAD FACTOR COMMAND

- MACH: 0.80
- ALTITUDE: 46,800 FEET
- C.G.: 33% MAC
- PRIMARY AFCS AND RSS ON
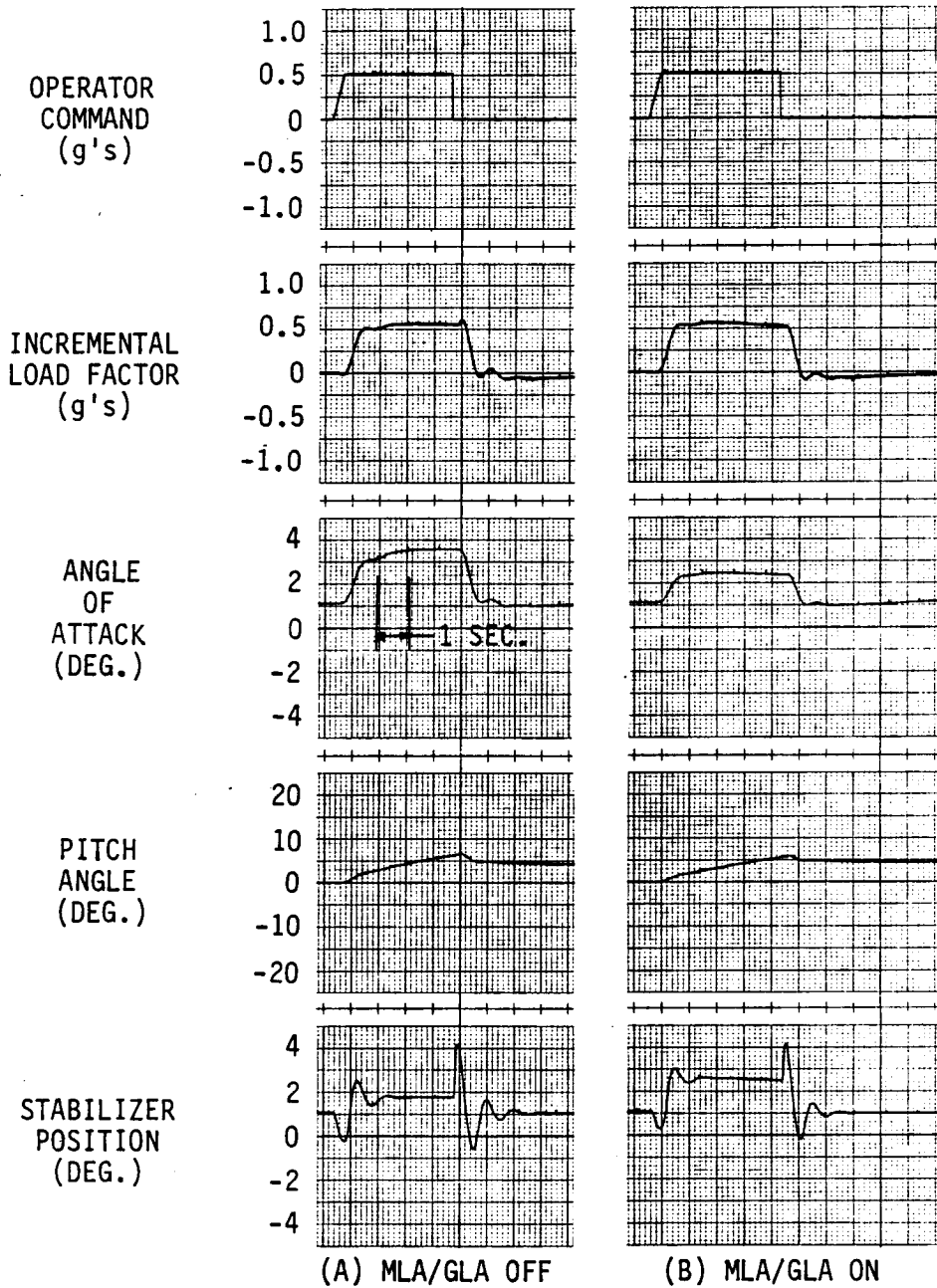
FIGURE 144

RESPONSE AT CRUISE FOR POSITIVE 0.5g LOAD FACTOR COMMAND

- MACH 0.80
- ALTITUDE: 46,800 FEET
- C.G.: 33% MAC
- PRIMARY AFCS AND RSS ON

(A) MLA/GLA OFF   (B) MLA/GLA ON
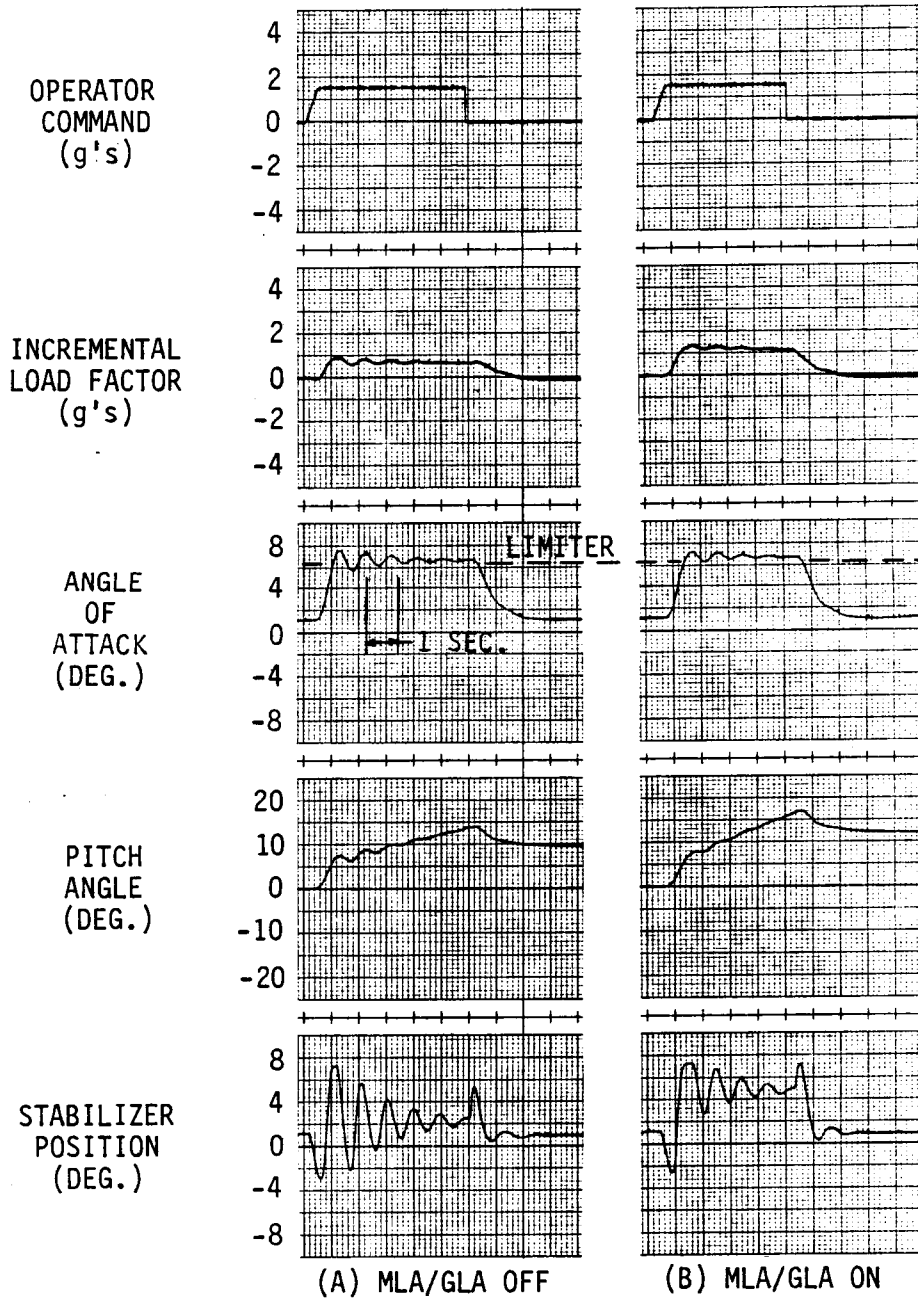
FIGURE 145

RESPONSE AT CRUISE FOR POSITIVE 1.5g LOAD FACTOR COMMAND

- MACH: 0.86
- ALTITUDE: 15,000 FEET
- C.G.: 33% MAC
- PRIMARY AFCS AND RSS ON
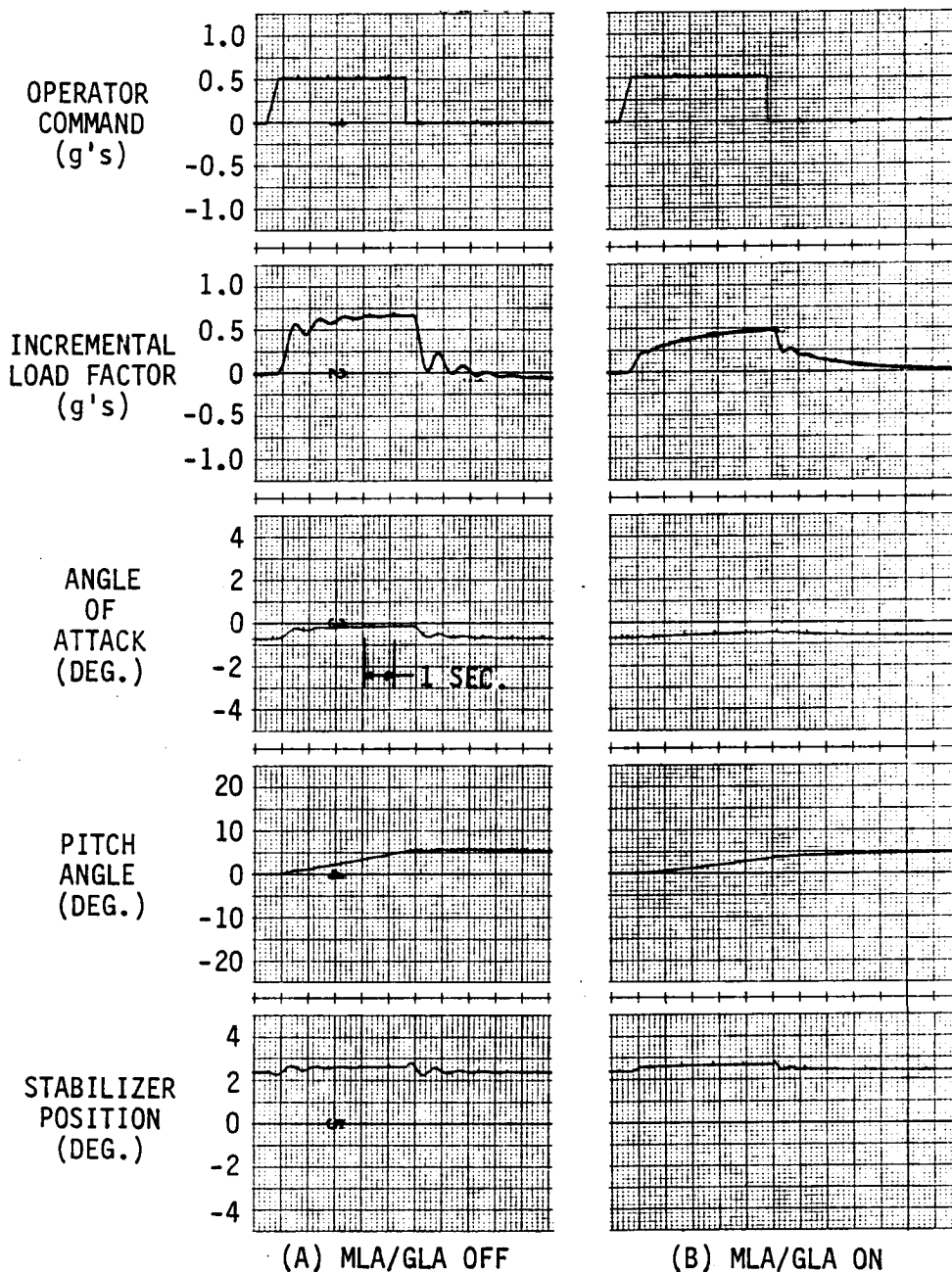
FIGURE 146

RESPONSE AT MAXIMUM DYNAMIC PRESSURE FOR POSITIVE LOAD FACTOR COMMAND

lateral-directional mathematical model consisted of a change to the yawing moment of inertia associated with the shift in center of gravity and correcting a sign error on the control derivative $C_{y\delta \text{ RUD}}$.

Figure 147 shows basic airplane lateral-directional characteristics at three flight conditions. The first two conditions which are low dynamic pressure cruise conditions have the most unstable Dutch roll characteristics and the third condition which is the maximum dynamic pressure condition has the largest Dutch roll frequency. With the present mathematical description, Dutch roll damping without the AFCS is not as unstable as previously indicated; however, it is still unstable at the cruise conditions and does not meet minimum damping criteria at any of the flight conditions.

Root loci of the individual rudder feedback loops, both of which provide Dutch roll stability, are shown on Figures 148 and 149 for the high altitude cruise condition. Lateral-directional airplane characteristics with the AFCS are shown on Figure 150 for the three flight conditions. Dutch roll damping with the AFCS is also greater than with the previous model.

The function characteristics of the lateral-directional AFCS required no change in the present design cycle; however, circuits were added to the roll axis feedback loops and command channels to synchronize the primary and backup mode signals. The revised system is shown in the block diagram on Figure 151. A flow diagram of the ground based primary AFCS digital program is included in Section 6.9.

6.6.3 Backup Longitudinal AFCS. The backup longitudinal AFCS is shown in the block diagram on Figure 152. No changes were made that affected the functional characteristics of the system during this design iteration. The block diagram has been revised to correct an error in gain distribution shown on Figure 7-72 of Reference 1. Also, the block diagram has been revised to show a signal going to the RSS integrator instead of a separate integrator as shown previously.

Time responses for flight subsequent to switching from primary mode to backup mode are shown on Figures 153 through 156 for various flight conditions. The responses are transitions from attitudes or maneuvers established in the primary mode to backup control with no backup operator commands. Figures 154 through 156 show responses for backup recovery from negative maneuvers at three flight conditions. Recovery from an initial pitch down attitude produces positive load factors that for certain combinations of pitch attitude and high values of dynamic pressure can exceed the wing design structural limit. Since the GLA/MLA system will not be engaged in the backup mode, limit load factor is approximately +2g (+1g incremental). Figure 154 shows responses for recovery from a pitch down attitude of 15 degrees at the launch condition. At this low dynamic pressure condition, the backup control

FLIGHT CONDITION		DUTCH ROLL			ROLL CONVERGENCE τ_R (SEC)	SPIRAL $T_{1/2}$ (SEC)
MACH NO.	ALTITUDE (FEET)	ζ	ω_n	$\zeta\omega_n$		
0.70	50000	-0.19	1.21	-0.23	0.28	13.8
0.80	46800	-0.08	1.36	-0.11	0.23	20.1
0.86	15000	0.07	3.75	0.26	0.10	29.3
MIL-F-8785 CRITERIA		≥ 0.08	≥ 0.4	≥ 0.15	≤ 1.4	$T_2 \geq 20$

FIGURE 147

BASIC AIRPLANE LATERAL-DIRECTIONAL MODE CHARACTERISTICS

- MACH: 0.70
- ALTITUDE: 5000 FT.
- RUDDER/ROLL RATE LOOP CLOSED
- DIFFERENTIAL STABILIZER/ROLL RATE LOOP CLOSED

NO.	GAIN	dB	
1	0.595	-4.5	
2	1.000	0.0	(OPERATING GAIN)
3	1.680	4.5	

PHASE ANGLE = 0°

PHASE ANGLE = -30°

PHASE ANGLE = 30°

jω (RAD/SEC)

σ (RAD/SEC)
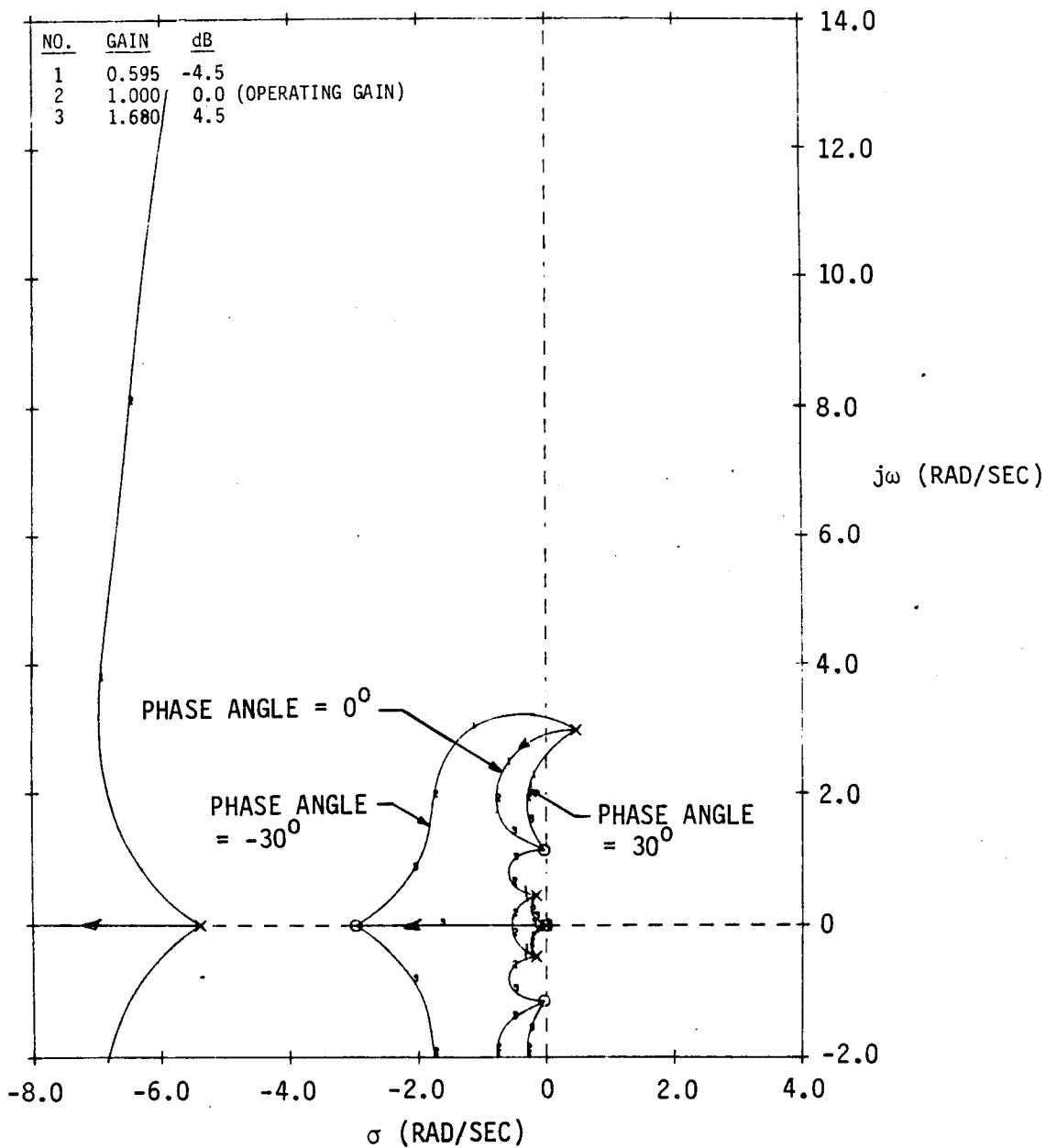
FIGURE 148

RUDDER/YAW RATE LOOP PHASE-GAIN ROOT LOCI

212
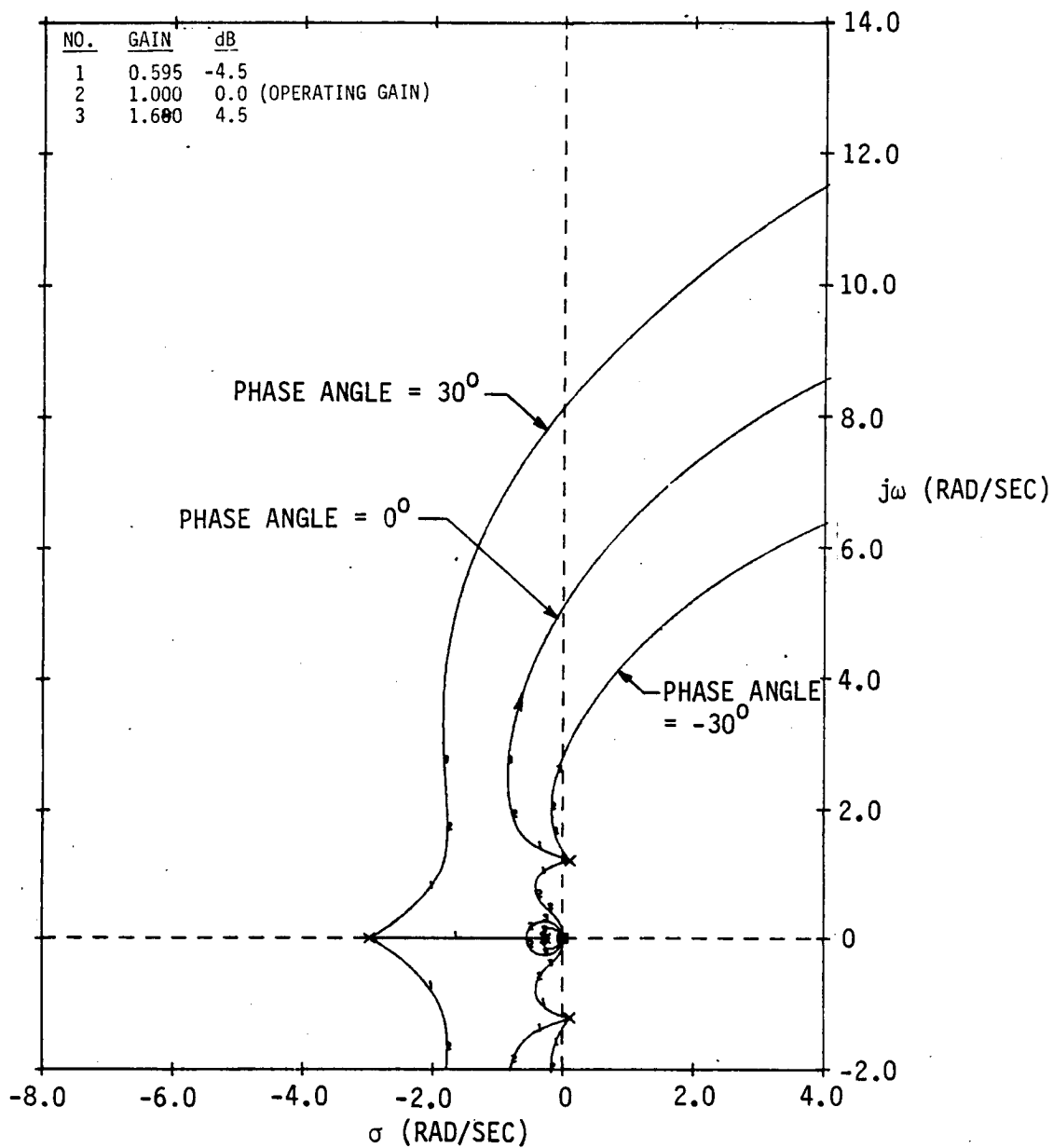
FIGURE 149

RUDDER/ROLL RATE LOOP PHASE-GAIN ROOT LOCI

FLIGHT CONDITION		DUTCH ROLL			ROLL CONVERGENCE τ_R (SEC)	SPIRAL $T_{\frac{1}{2}}$ (SEC)	ROLL-SPIRAL OSCILLATION $\zeta_{RS}\omega_{RS}$
MACH NO.	ALTITUDE (FEET)	ζ	ω_n	$\zeta\omega_n$			
0.70	50000	0.33	2.04	0.77	---	---	0.52
0.80	46800	0.67	1.78	1.19	0.50	∞	---
0.86	15000	0.76	4.59	3.47	0.63	2.32	---
MIL-F-8785 CRITERIA		≥ 0.08	≥ 0.40	≥ 0.15	≤ 1.4	$T_2 \geq 20$	≥ 0.50

FIGURE 150

LATERAL-DIRECTIONAL MODE CHARACTERISTICS WITH AFCS
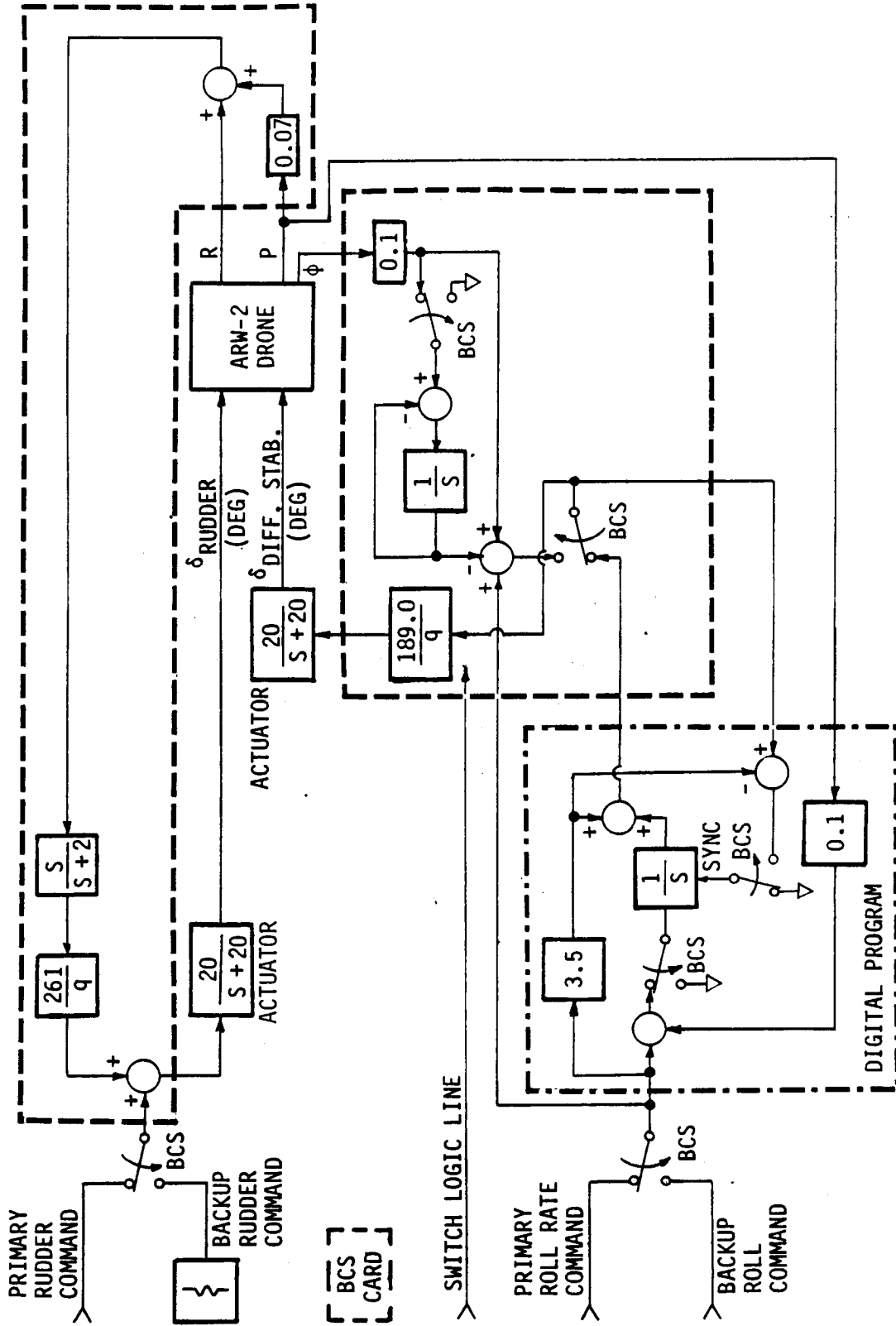
FIGURE 151

LATERAL-DIRECTIONAL AUTOMATIC FLIGHT CONTROL SYSTEM BLOCK DIAGRAM
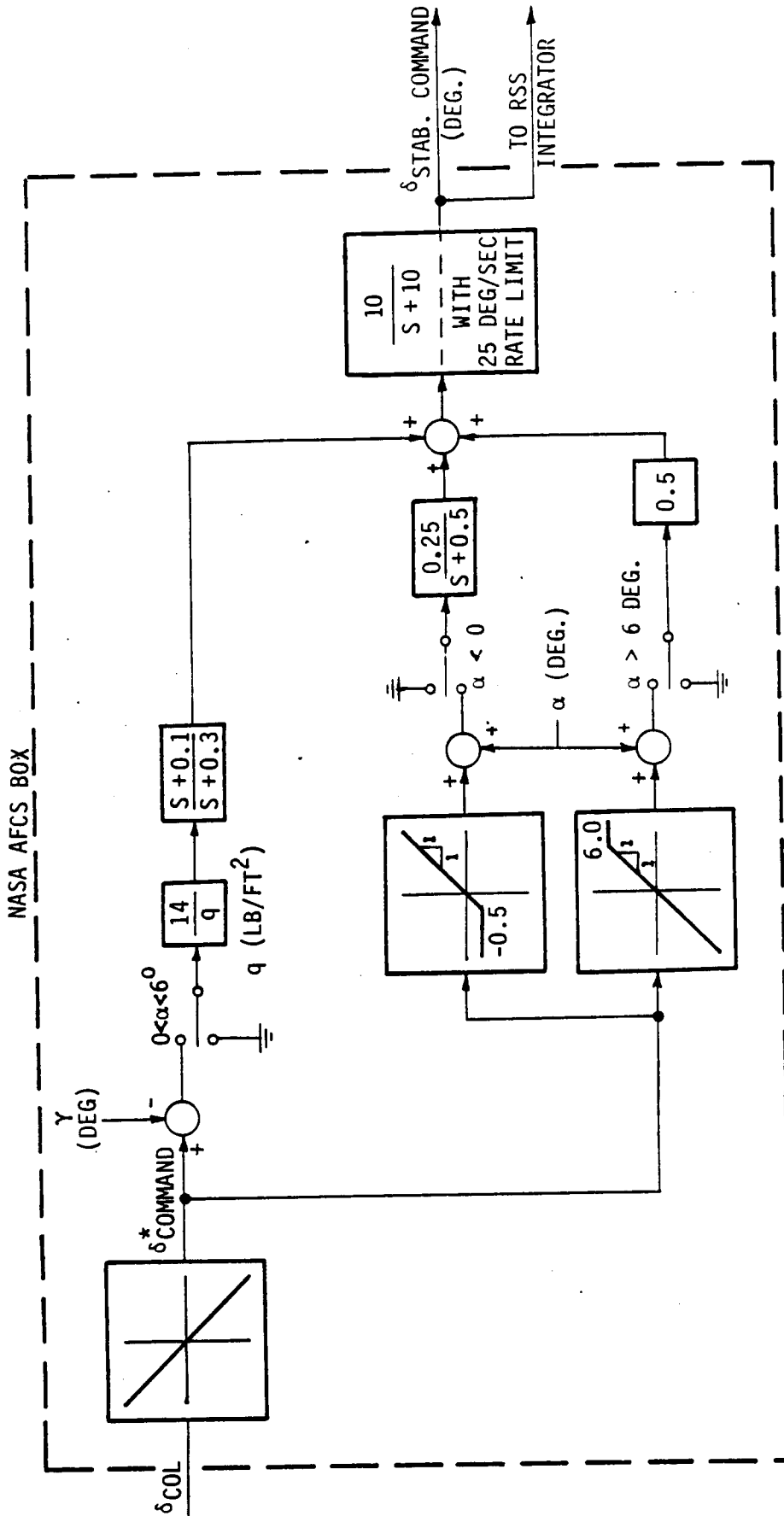
*SCALE FOR MAXIMUM GLIDE ANGLE

FIGURE 152

BACKUP LONGITUDINAL AFCS BLOCK DIAGRAM

- MACH: 0.40
- ALTITUDE: 15,000 FEET
- C.G.: 27.5% MAC

INCREMENTAL
LOAD FACTOR
(g's)

BACKUP
MODE
ENGAGED

STABILIZER
POSITION
(DEG.)

ANGLE
OF
ATTACK
(DEG.)

PITCH
ANGLE
(DEG.)

1 SEC.

GLIDE
ANGLE
(DEG.)
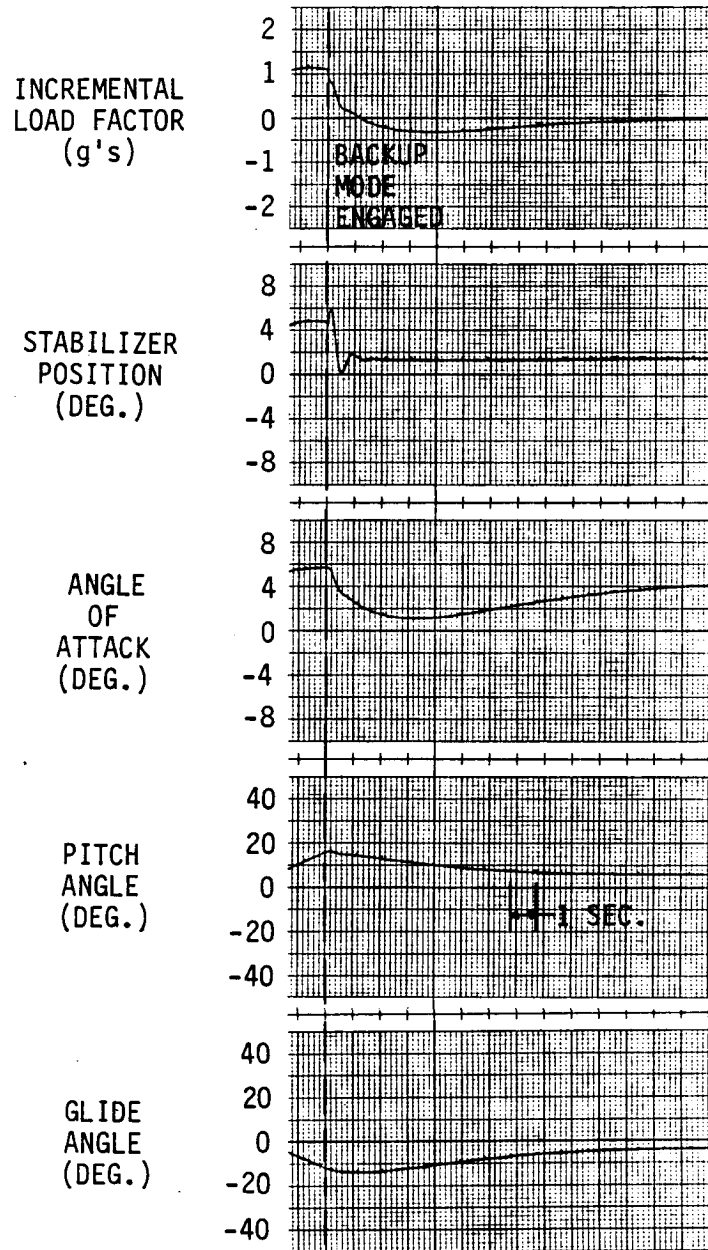
FIGURE 153

BACKUP MODE TRANSITION RESPONSE FROM PITCH UP MANEUVER AT LAUNCH CONDITION

- MACH: 0.40
- ALTITUDE: 15,000 FEET
- C.G.: 27.5% MAC
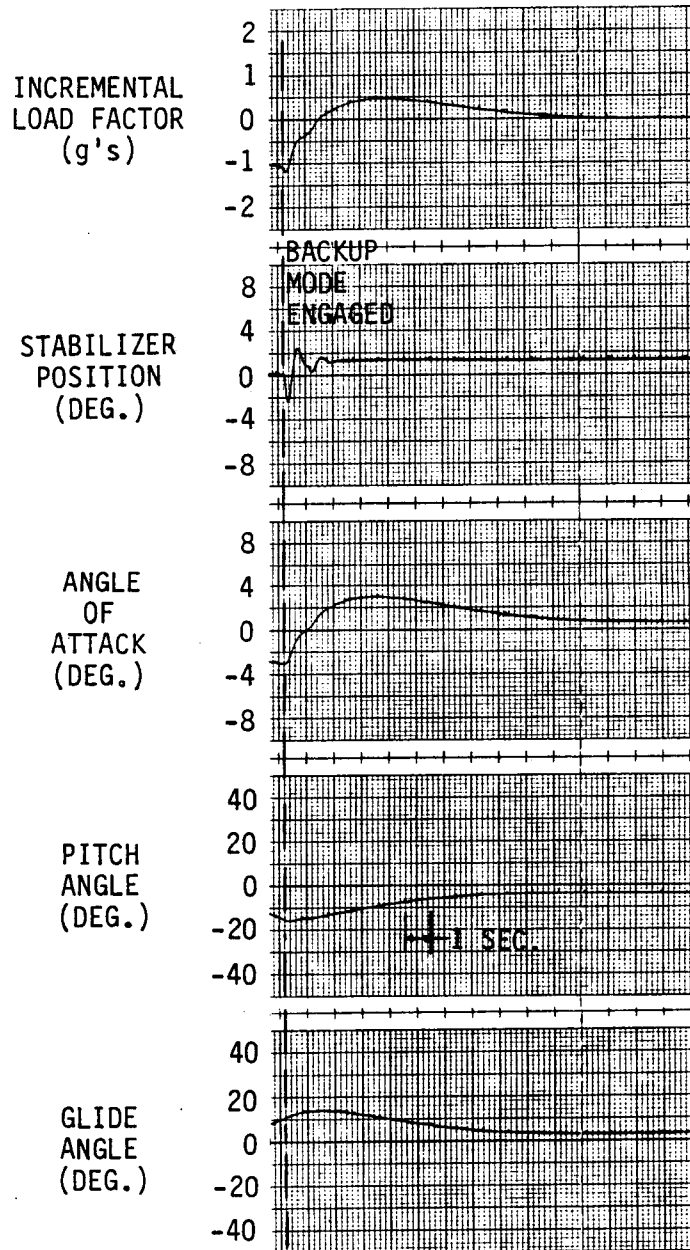
FIGURE 154

BACKUP MODE TRANSITION RESPONSE FROM PITCH DOWN MANEUVER AT LAUNCH CONDITION

- MACH: 0.70
- ALTITUDE: 15,000 FEET
- C.G.: 27.5% MAC
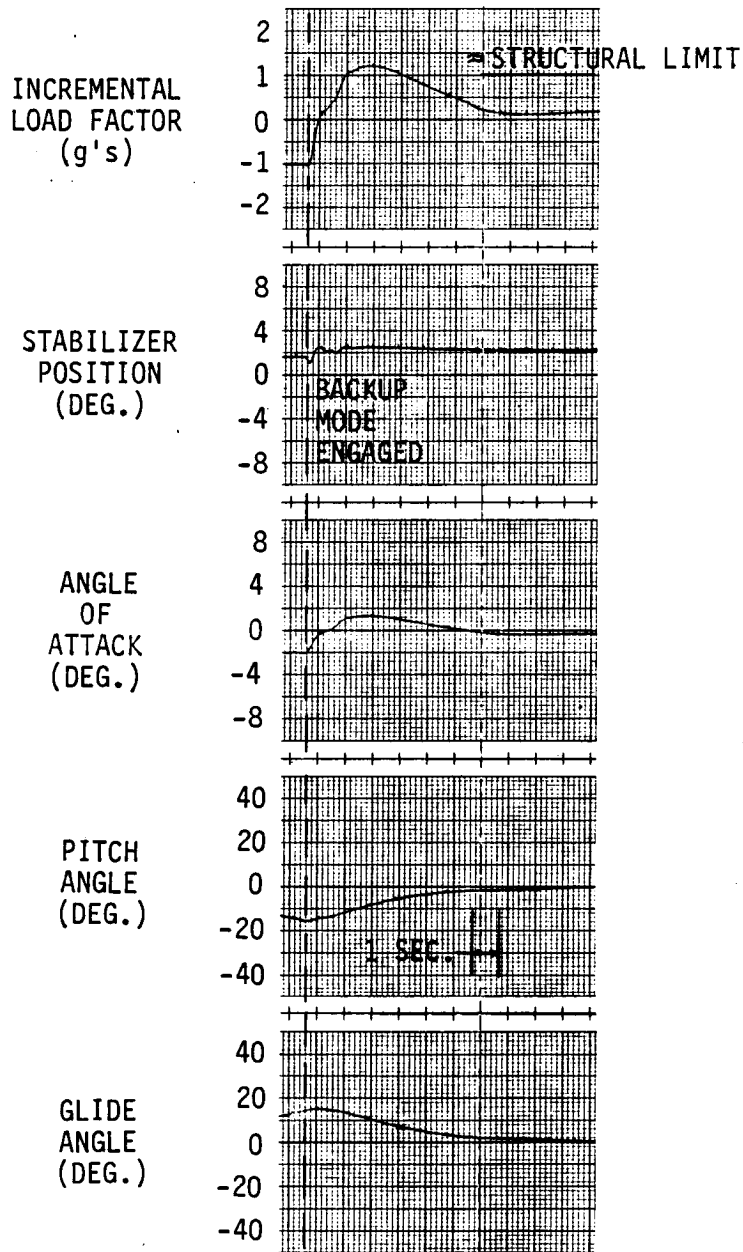
FIGURE 155

BACKUP MODE TRANSITION RESPONSE FROM PITCH DOWN MANEUVER AT GLA TEST CONDITION

- MACH: 0.86
- ALTITUDE: 15,000 FEET
- C.G.: 27.5% MAC

INCREMENTAL
LOAD FACTOR
(g's)

STRUCTURAL LIMIT

BACKUP
MODE
ENGAGED

STABILIZER
POSITION
(DEG.)

ANGLE
OF
ATTACK
(DEG.)

BACKUP α LIMITS
$0^{0}<\alpha<6^{0}$

PITCH
ANGLE
(DEG.)

1 SEC.

GLIDE
ANGLE
(DEG.)
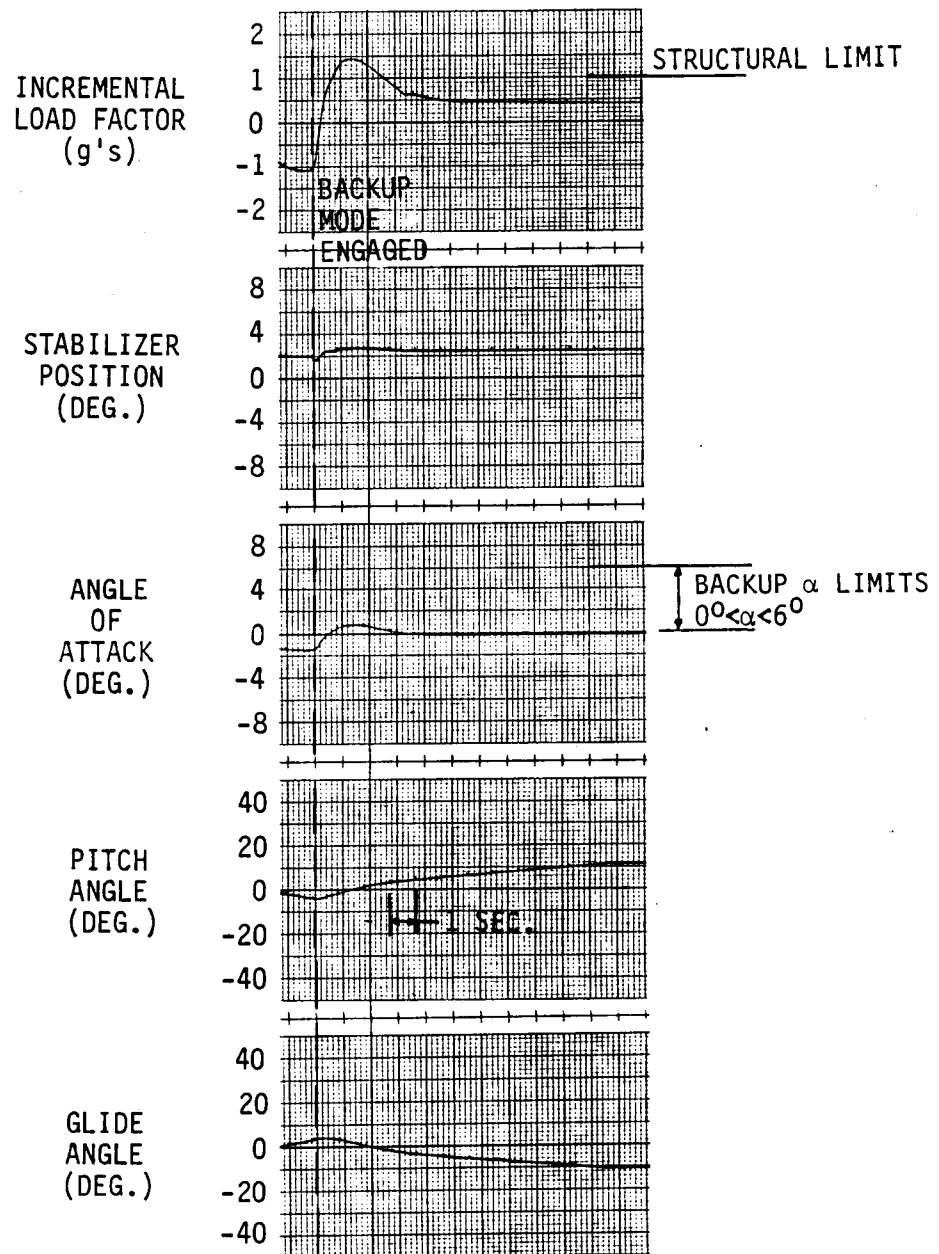
FIGURE 156

BACKUP MODE TRANSITION RESPONSE FROM PITCH DOWN MANEUVER
AT MAXIMUM DYNAMIC PRESSURE

system produced a +1.5g (+0.5g incremental) load factor. At the high dynamic pressure GLA test condition, recovery from 15 degrees pitch down produced a load factor of 2.2g as shown on Figure 155. At the maximum dynamic pressure condition, recovery from only 4 degrees initial pitch down produced a load factor of 2.4g as shown on Figure 156. These results are similar to those obtained with the previous mathematical model.

6.7 Horizontal Tail Authority Evaluation. The DAST stabilizer configuration provides +7 degrees (trailing edge down) and -12 degrees displacement of the individual stabilizer surfaces which are moved symmetrically for pitch control and antisymmetrically for roll control. Two features of the DAST II configuration increase the requirement for positive stabilizer. More positive stabilizer is required to trim out the positive pitching moment due to moving the center of gravity aft for minimum trim drag. Also, positive stabilizer instead of conventional negative stabilizer is required for positive maneuvers with the maneuver load alleviation system to counteract the pitching characteristics of the wing control surfaces. These stabilizer requirements are illustrated on Figure 157 which shows load factor and stabilizer responses for positive maneuvers with MLA as the C.G. is moved aft. At the aft C.G. limit, symmetric stabilizer is very near the positive limit. Any significant roll command at the 33 percent C.G. position will drive one stabilizer surface into the positive limit. Symmetric stabilizer is required for aircraft stability at aft C.G. conditions and saturating one surface essentially reduces the gain of the stabilizer feedback systems by one-half. This alters the load factor to operator command relationship which could possibly result in a response exceeding the design limit if operator corrective symmetric action does not accompany the antisymmetric commands as illustrated on Figures 158 and 159. Saturating one surface could also potentially create an instability since one-half gain is below the minimum gain margin designed into the systems.

Analysis results indicate that more positive stabilizer authority is desirable. Without increased positive authority, extreme caution should be used when applying antisymmetric commands during large positive maneuvers at low dynamic pressure conditions with aft C.G. positions and the load alleviation system engaged.

6.8 Control System Compatibility. Operational and stability requirements dictate that some of the ACS/AFCS systems operate together. Various analysis tasks were conducted to assure that systems operating together were compatible. The following four combinations of system are required to operate together during some phase of flight tests:

● RSS and PCS

● RSS, PCS and GLA/MLA

STABILIZER REQUIREMENT FOR LIMIT POSITIVE MANEUVER WITH C.G. POSITION VARIATIONS

FIGURE 157

FIGURE 158.

TIME RESPONSES TO ASYMMETRIC CONTROL INPUTS DURING LIMIT SYMMETRIC MANEUVER

MACH = 0.42
ALTITUDE = 10,000 FEET
GROSS WEIGHT = 2200 LBS.
C.G. = 32.75% MAC

NO SYMMETRIC
STABILIZER CORRECTION

WITH SYMMETRIC
STABILIZER CORRECTION

RIGHT STABILIZER - DEG

LEFT STABILIZER - DEG

LOAD FACTOR - g

ROLL ANGLE - DEG

≈ 1.0 SEC
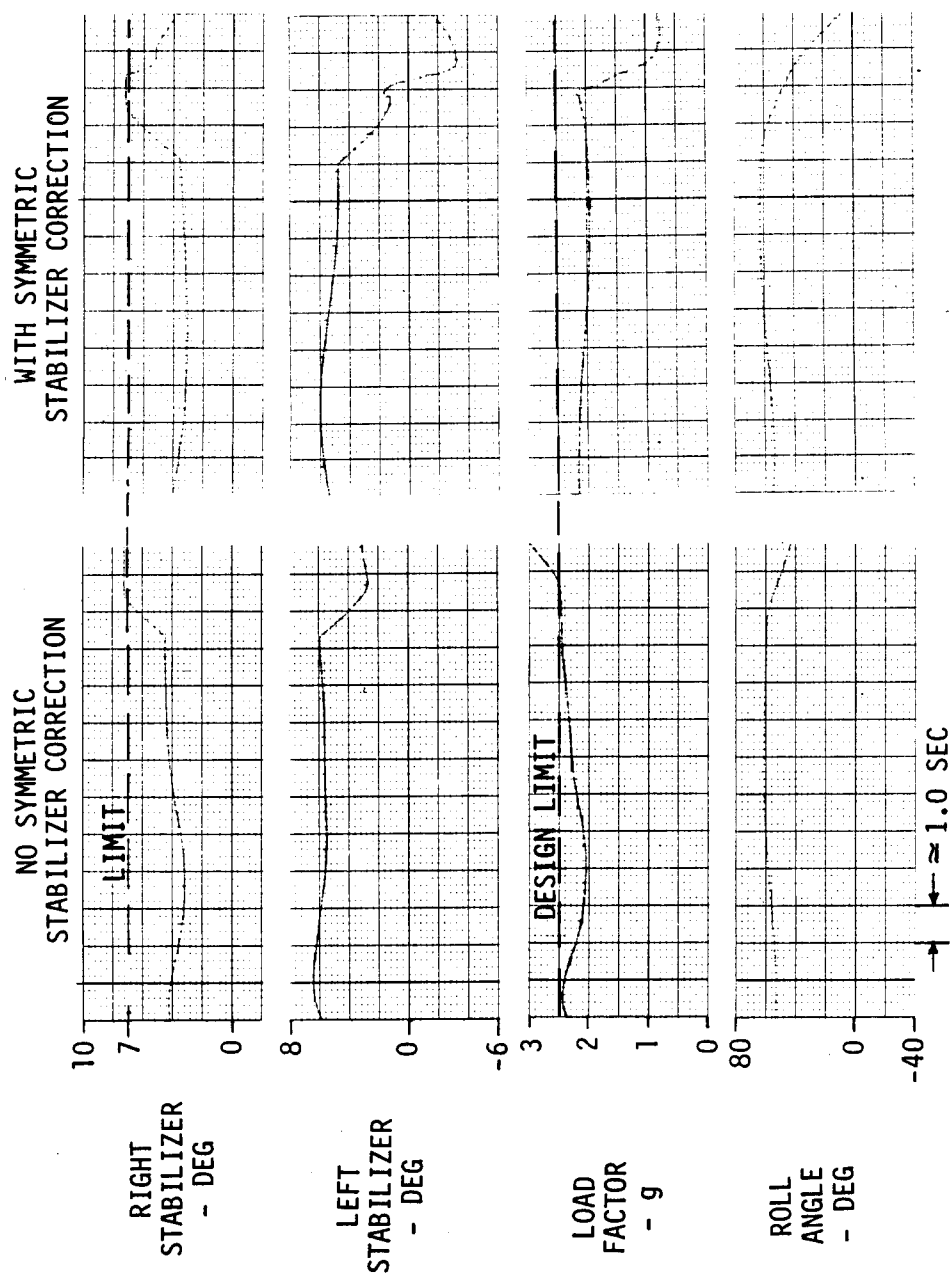
FIGURE 159

TIME RESPONSE TO ROLL COMMAND INPUT FROM LARGE BANK ANGLE

- RSS, PCS, GLA/MLA and FSS

- RSS and BCS

Operations of the PCS systems will at times include the altitude hold mode.

Tasks to verify system compatibility involved linear analysis and evaluation of the system combinations on the non-linear 6 DOF airplane simulation. The functional capability of each individual system was verified with other appropriate systems closed. These effects are included in the sections of this report which discuss the individual systems. Other tasks to determine tangible performance such as stability margins and handling qualities are discussed in the following subsections.

6.8.1 Altitude Hold System Compatibility. The Altitude Hold Control System shown on Figure 138 supplied by NASA was evaluated for control effectiveness and compatibility with the other control systems.

The altitude hold system is a very low gain system and does not significantly affect airplane characteristic roots as shown on Figure 160. Since the system had an insignificant effect on airplane characteristic roots, the effects of the system were not included in the evaluation of stability margins or frequency and damping discussed in the following sections.

Typical airplane vertical translation due to random gust with the altitude hold system is shown on Figure 161. Peak vertical displacement is on the order of 3 feet per feet/second RMS vertical gust at the GLA design condition. Figure 162 shows airplane response at cruise when the altitude hold system is engaged in an initial 10 degree dive. The airplane settles out at the altitude at the time the altitude hold was engaged in approximately 30 seconds.

The altitude hold system provides good control for straight flight but a steady-state altitude offset occurs in turns as shown on Figure 163. The altitude offset occurs because the altitude hold system must generate a steady-state error signal to compensate for a steady-state pitch rate feedback signal to the stabilizer through the RSS system. If it becomes desirable to eliminate the altitude offset in turns, it is suggested that the ground based digitally programmed altitude hold system provide an additional function to the signal transmitted to the RSS filter which, computed as a function of roll angle and airplane velocity, will compensate for steady-state turning pitch rate.

- MACH: 0.70
- ALTITUDE: 15,000 FEET
- GROSS WEIGHT: 2350 LBS.

CLOSED LOOP AIRPLANE CHARACTERISTIC ROOTS
(STRUCTURAL MODES NOT INCLUDED)

GLA, RSS AND PCS WITHOUT ALTITUDE HOLD	GLA, RSS AND PCS WITH ALTITUDE HOLD $\dot{H}$ AND $\ddot{H}$ FEEDBACK LOOPS	GLA, RSS AND PCS WITH ALTITUDE HOLD θ FEEDBACK LOOP
$(S+4.814\pm j10.928)$	$(S+4.814\pm j10.928)$	$(S+4.734\pm j10.959)$
$(S+3.408)$	$(S+3.408)$	$(S+3.414)$
$(S+1.538)$	$(S+1.538)$	$(S+1.538)$
$(S+.099)$	$(S+.099)$	$(S+.100)$
$(S+.059)$	$(S+.062)$	$(S+.088)$
$(S+.025)$	$(S+.023)$	$(S+.0213)$

FIGURE 160

EFFECTS OF ALTITUDE HOLD LOOPS ON AIRPLANE CHARACTERISTIC ROOTS

MACH: 0.60
ALTITUDE: 7000 FEET
GROSS WEIGHT: 2500 LBS.
RSS, GLA, PCS AND ALTITUDE HOLD ENGAGED
RMS VERTICAL GUST: 0.5 FPS

VERTICAL
GUST
(FPS)
(POSITIVE
UP)

VERTICAL
DISPLACEMENT
(FEET)
(POSITIVE
DOWN)

1 SEC.
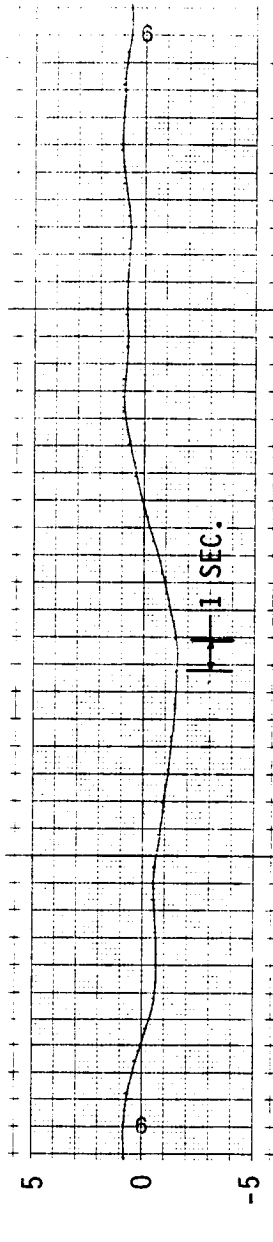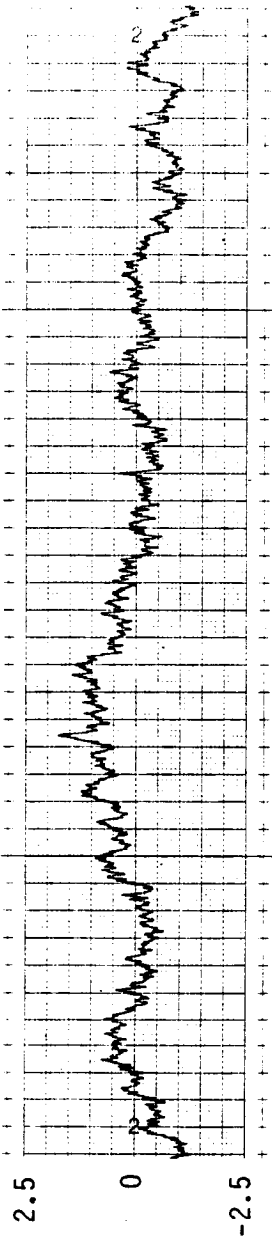
FIGURE 161

AIRPLANE VERTICAL RESPONSE DUE TO GUST WITH ALTITUDE HOLD ENGAGED

227

MACH: 0.80
ALTITUDE: 46800 FEET
GROSS WEIGHT: 2350 LBS.
RSS, PCS AND GLA SYSTEMS ENGAGED
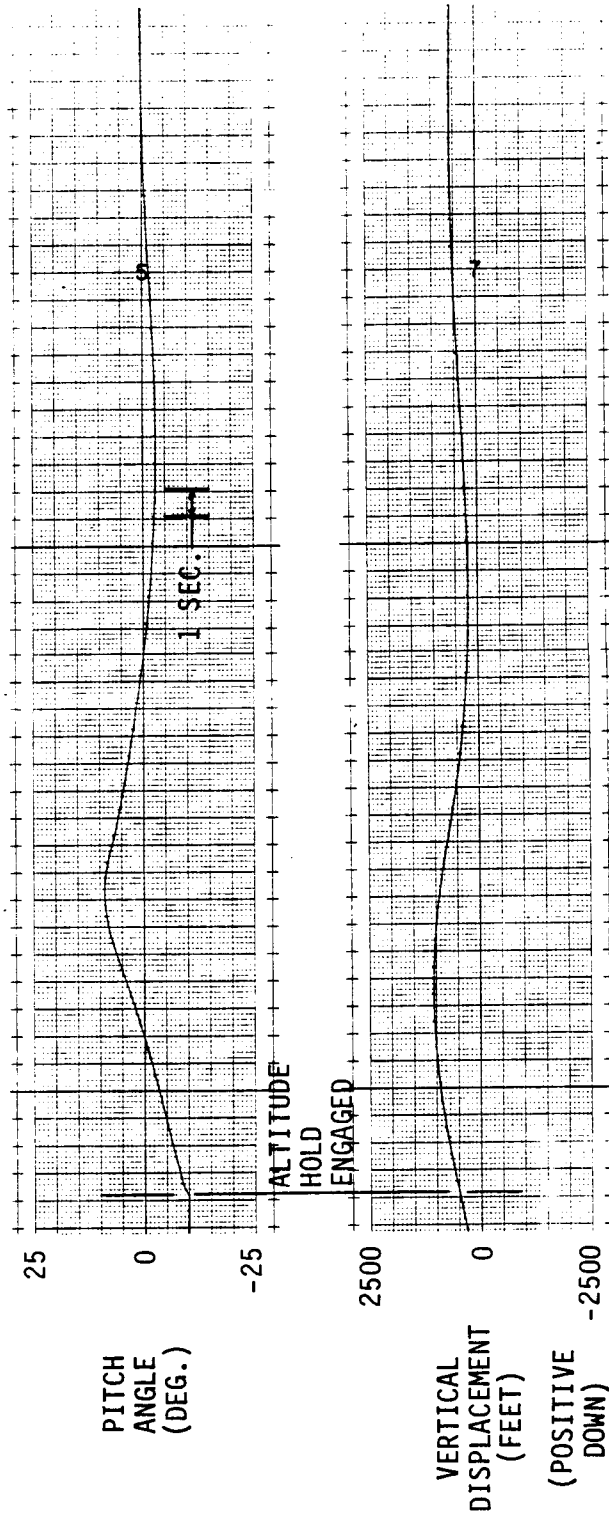
FIGURE 162

AIRPLANE RESPONSE WITH ALTITDUE HOLD ENGAGED IN A 10 DEGREE DIVE

PITCH ANGLE (DEG.)

VERTICAL DISPLACEMENT (FEET)

(POSITIVE DOWN)

ALTITUDE HOLD ENGAGED

1 SEC.

- C.G.: 27.5% MAC
- PRIMARY AFCS WITH ALTITUDE HOLD,
  RSS AND GLA/MLA ENGAGED

ROLL ANGLE (DEG.)

ALTITUDE ERROR (FEET)

(A) GLA TEST CONDITION, MACH: 0.70,
ALTITUDE: 15000 FEET

ROLL ANGLE (DEG.)

ALTITUDE ERROR (FEET)

(B) CRUISE CONDITION, MACH: 0.80, ALTITUDE: 46800 FEET
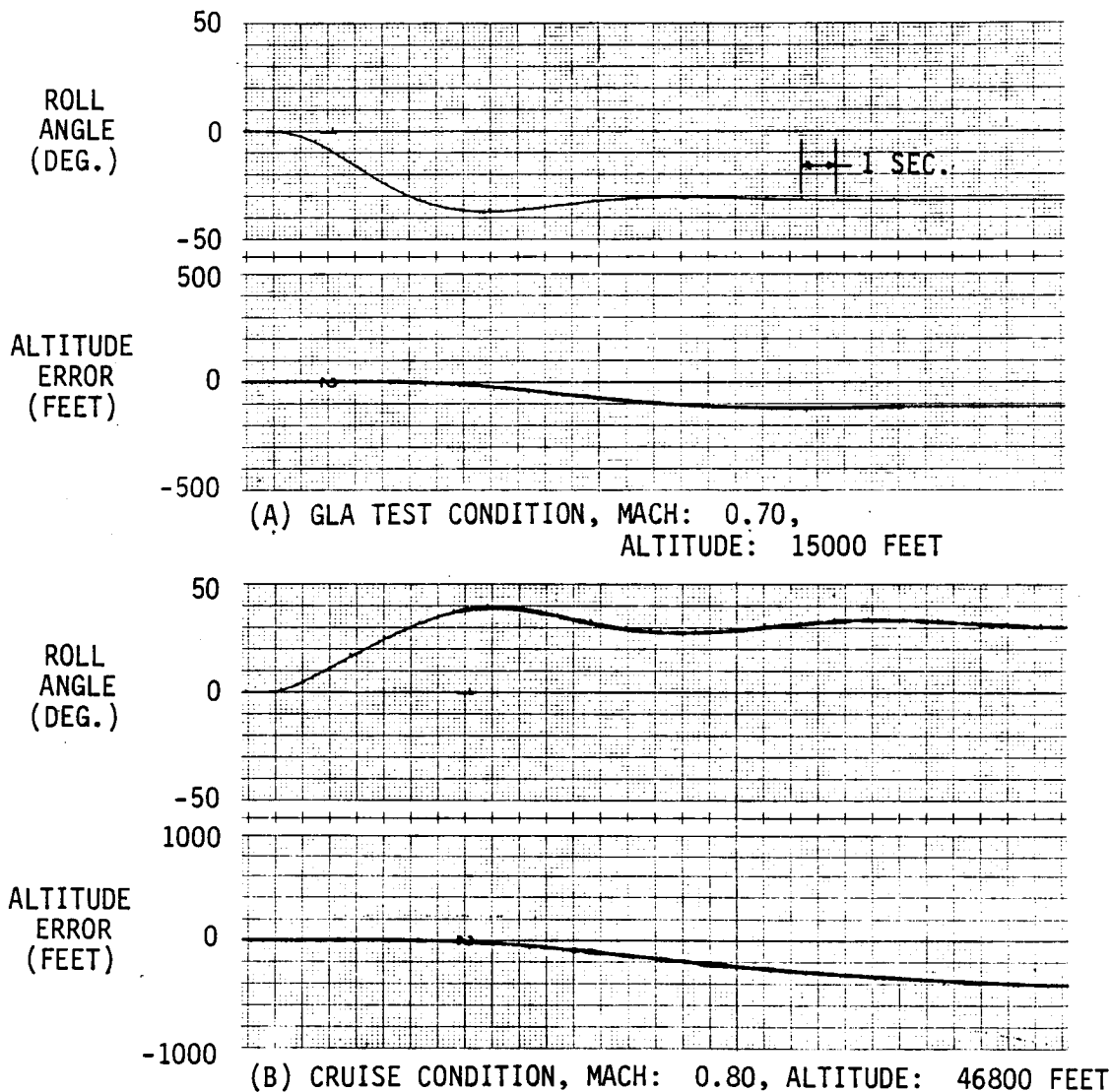
FIGURE 163

EFFECTS OF STEADY STATE BANK ANGLE ON ALTITUDE HOLD PERFORMANCE

6.8.2 System Gain and Phase Margins. Gain and phase stability margins of each individual loop of each system were determined for each combination of systems that will be closed during some phase of flight testing.

The FSS had an insignificant effect on the airplane basic translation and rotation modes as discussed in Section 6.3. The stability margins of the FSS on airplane structural dynamic modes are presented in Section 6.3.

All ACS/AFCS systems, excluding the FSS, did not significantly affect airplane structural modes as indicated on Figure 164; therefore, the stability margins of these systems were determined using QSE EOM. Those system combinations and the various flight conditions and C.G. extremes where stability margins were determined are shown on Figure 165.

Phase and gain root loci for each element on Figure 165 are shown in Appendix E.

All system loops meet gain criteria of ± 4.5 dB at all conditions. Except for the maximum dynamic pressure-aft C.G. condition, all loops meet the phase criteria of $\pm 30^{\circ}$. At the maximum dynamic pressure-aft C.G. condition, the RSS and PCS had only approximately 25 degrees phase lag when these two systems were the only symmetric systems engaged. These system phase margins characteristics are shown on Figures 196 and 197 of Appendix E. With the GLA/MLS system engaged, the RSS and PCS loops meet phase margin criteria. No tests at the maximum dynamic pressure condition without GLA/MLA engaged are anticipated.

6.8.3 Flying Qualities. Airplane dynamics were evaluated for flying quality characteristics with each combination of systems that may be closed.

The lightest damped closed loop system characteristic roots in the short period frequency range are compared to MIL-F-8785C Level 1 short period damping and frequency criteria on Figure 166. Time response evaluation on the 6 DOF simulation indicates that these characteristic roots are dominant during typical maneuvers. The closed loop systems produce high values of short period frequency, slightly exceeding the criteria in some cases and just below maximum criteria in the other cases. Short period frequency increases with increasing gain in the RSS and PCS feedback loops and are highest for forward C.G. positions. The gain values were selected to provide gain margins of the divergent real roots resulting from unstable pitching characteristics at aft C.G. positions.

Except for operation of the RSS and PCS only at the maximum dynamic pressure condition, the systems meet minimum damping ratio criteria. At this condition, the GLA provides criteria level damping ratios with some increase in short period frequency as indicated on Figure 166.

230

- GLA TEST CONDITION
- MACH: 0.70
- ALTITUDE: 15,000 FEET

MODE	BASIC AIRPLANE		RSS AND PCS CLOSED		RSS, PCS AND GLA CLOSED	
	FREQUENCY (HZ)	DAMPING RATIO (ζ)	FREQUENCY (HZ)	DAMPING RATIO (ζ)	FREQUENCY (HZ)	DAMPING RATIO (ζ)
SHORT PERIOD	.352	.449	1.248	.194	1.899	.402
q_1	14.238	.010	14.212	.015	14.474	.031
q_2	14.743	.273	14.768	.272	14.738	.274
q_3	21.762	.007	21.762	.007	21.761	.007
q_4	26.276	.059	26.275	.059	26.268	.059
q_5	33.275	.007	33.272	.008	33.316	.007
q_6	34.190	.044	34.189	.044	34.187	.044
q_7	48.146	.045	48.104	.046	48.181	.046
q_8	63.133	.011	63.166	.011	63.150	.011
q_9	67.221	.022	67.228	.022	67.225	.022
q_{10}	74.316	.024	74.316	.024	74.316	.024

FIGURE 164

EFFECTS OF CLOSED LOOP SYSTEMS ON AIRPLANE MODES FREQUENCY AND DAMPING

231

FLIGHT CONDITION	AIRPLANE CONFIGURATION	RSS	RSS WITH PCS CLOSED	RSS WITH PCS AND GLA CLOSED	RSS WITH BCS CLOSED	PCS WITH RSS CLOSED	PCS WITH RSS AND GLA CLOSED	GLA AILERON WITH RSS, PCS AND GLA STAB. CLOSED	GLA STAB. WITH RSS, PCS AND GLA AILERON CLOSED	BCS WITH RSS CLOSED
MLA TEST MACH: 0.42 ALT.: 10,000 FT.	G.W.: 2500 LBS. C.G.: 20% MAC	X	X	X	X	X	X			X
	G.W.: 2200 LBS. C.G.: 33% MAC	X	X	X	X	X	X	X	X	X
GLA TEST MACH: 0.70 ALT.: 15,000 FT.	G.W.: 2500 LBS. C.G.: 20% MAC	X	X	X	X	X	X	X	X	X
	G.W.: 2200 LBS. C.G.: 33% MAC	X	X	X	X	X	X	X	X	X
LAUNCH MACH: 0.40 ALT.: 15,000 FT.	G.W.: 2500 LBS. C.G.: 20% MAC	X	X	X	X	X	X			X
	G.W.: 2200 LBS. C.G.: 33% MAC	X	X	X	X	X	X	X	X	X
HIGH ALTITUDE MACH: 0.70 ALT.: 50,000 FT.	G.W.: 2500 LBS. C.G.: 20% MAC	X	X	X	X	X	X			X
	G.W.: 2200 LBS. C.G.: 33% MAC	X	X	X	X	X	X	X	X	X
CRUISE MACH: 0.80 ALT.: 46,800 FT.	G.W.: 2500 LBS. C.G.: 20% MAC 1.0g FLIGHT	X	X	X	X	X	X			X
	G.W.: 2200 LBS. C.G.: 33% MAC 1.2g FLIGHT	X	X	X	X	X	X	X	X	X
MAXIMUM q (V_d) MACH: 0.86 ALT.: 15,000 FT.	G.W.: 2500 LBS. C.G.: 20% MAC	X	X	X	X	X	X			X
	G.W.: 2200 LBS. C.G.: 33% MAC	X	X*	X	X	X*	X	X	X	X

*HAS ONLY APPROXIMATELY -25° PHASE MARGIN

FIGURE 165

FLIGHT CONDITION - LONGITUDINAL SYSTEM STABILITY ANALYSIS MATRIX

| FLIGHT CONDITION | CRITERIA - LEVEL 1 DAMPING RATIO $0.3<\delta_{SP}<2.0$ | | AIRPLANE CONFIGURATION | CLOSED LOOP DAMPING RATIO AND FREQUENCY | | | | | |
| | MINIMUM FREQUENCY (RAD/SEC) | MAXIMUM FREQUENCY (RAD/SEC) | | RSS ONLY | | RSS AND PCS | | RSS, PCS AND GLA | |
				DAMPING RATIO	FREQUENCY (RAD/SEC)	DAMPING RATIO	FREQUENCY (RAD/SEC)	DAMPING RATIO	FREQUENCY (RAD/SEC)
MLA TEST MACH: 0.42 ALT.: 10000 FT.	2.00	7.16	C.G.: 20% MAC	0.44	7.33	0.37	5.76	0.45	6.07
			C.G.: 33% MAC	0.43	8.43	0.37	6.50	0.46	7.08
GLA TEST MACH: 0.70 ALT.: 15000 FT.	3.24	11.63	C.G.: 20% MAC	0.41	8.16	0.24	7.21	0.51	9.66
			C.G.: 33% MAC	0.42	9.07	0.23	7.76	0.65	13.50
LAUNCH MACH: 0.40 ALT.: 15000 FT.	1.68	6.03	C.G.: 20% MAC	0.44	7.29	0.39	5.59	0.45	5.76
			C.G.: 33% MAC	0.42	8.42	0.38	6.38	0.45	6.73
HIGH ALTITUDE MACH: 0.70 ALT.: 50000 FT.	1.43	5.12	C.G.: 20% MAC	0.43	7.69	0.46	5.48	0.49	5.56
			C.G.: 33% MAC	0.39	8.93	0.45	6.38	0.48	6.55
CRUISE MACH: 0.80 ALT.: 46800 FT.	2.06	7.37	C.G.: 20% MAC 1.0g FLIGHT	0.37	8.49	0.31	6.57	0.36	6.85
			C.G.: 33% MAC 1.2g FLIGHT	0.37	9.49	0.36	7.05	0.41	7.60
MAXIMUM q (Vd) MACH: 0.86 ALT: 15000 FT.	4.10	14.7	C.G.: 20% MAC	0.49	8.41	0.21	7.69	0.34	9.54
			C.G.: 33% MAC	0.54	9.42	0.19	7.99	0.39	11.18

FIGURE 166

SHORT PERIOD DAMPING AND FREQUENCY WITH PRIMARY AFCS AND ACTIVE CONTROL SYSTEMS

Short period frequency and damping with the BCS engaged are compared to Level 3 criteria on Figure 167. With the relaxed criteria for backup mode of operation, the systems meet frequency and damping criteria at all flight conditions and C.G. extremes.

Each combination of closed loop systems meets phugoid damping criteria. No lightly damped or unstable roots occur in the low frequency (phugoid) frequency range as indicated in the root loci plots on Figures 189 through Figure 204 of Appendix E.

6.8.4 Airplane Stability Derivative Sensitivity. ACS and AFCS sensitivity to variations in longitudinal stability derivatives C_{M_α}, C_{L_α}, C_{M_Q}, C_{D_U} and C_{L_U} and lateral-directional derivatives C_{l_β}, C_{l_β},

C_{N_β} and C_{N_R} were evaluated on the 6 DOF simulation of airplane dynamics. During the last iteration, sensitivity to stability derivative variations was determined by computing airplane characteristic roots with ± 20 percent change in the derivatives. The stability derivatives were varied individually at each of six flight conditions listed on Figure 166. No unstable or even lightly damped characteristics were produced with stability derivative variations; and for step control surface inputs, changes in airplane responses with the stability derivative variations were minimal.

As indicated on Tables 7-IX and 7-XV of Reference 1, the most lightly damped Dutch roll response occurred with variations in C_{l_p}. Airplane response with variations in C_{l_p} at the most lightly damped condition indicated in Reference 1 is shown on Figure 168.

6.9 Computer Implementation of Ground Based Control Systems. The following control systems will be implemented on the ground based computer:

o   MLA Inboard Aileron and Stabilizer Functions

●   Primary Longitudinal AFCS

●   Differential Stabilizer/Roll Rate Loop of Primary Lateral-Directional AFCS.

With the restriction that the GLA/MLA systems should always be engaged at high dynamic pressure conditions, simulation and analysis results indicate satisfactory performance of the ground based systems using the expected iteration time increment of 0.025 second.

Difference equation constants which are to be computed using the final ground station/drone data transmittal iteration time increment (DT) are given on Figure 169. Flow diagrams for implementation of the ground based systems are shown on Figures 170 through 173.

FLIGHT CONDITION	CRITERIA - LEVEL 3 DAMPING $\zeta > 0.15$		AIRPLANE CONFIGURATION	CLOSED LOOP DAMPING RATIO AND FREQUENCY	
	MINIMUM FREQUENCY (RAD/SEC)	MAXIMUM FREQUENCY (RAD/SEC)		DAMPING RATIO	FREQUENCY (RAD/SEC)
MLA TEST MACH: 0.42 ALT.: 10000 FT.	1.51	11.93	C.G.: 20% MAC	0.45	7.33
			C.G.: 33% MAC	0.43	8.41
GLA TEST MACH: 0.70 ALT.: 15000 FT.	2.45	19.38	C.G.: 20% MAC	0.41	8.17
			C.G.: 33% MAC	0.42	9.08
LAUNCH MACH: 0.40 ALT.: 15000 FT.	1.27	10.05	C.G.: 20% MAC	0.44	7.28
			C.G.: 33% MAC	0.42	8.42
HIGH ALTITUDE MACH: 0.70 ALT.: 50000 FT.	1.08	8.53	C.G.: 20% MAC	0.43	7.70
			C.G.: 33% MAC	0.39	8.93
CRUISE MACH: 0.80 ALT.: 46800 FT.	1.55	12.28	C.G.: 20% MAC 1.0g FLIGHT	0.37	8.49
			C.G.: 33% MAC 1.2g FLIGHT	0.37	9.49
MAXIMUM q (V_d) MACH: 0.86 ALT.: 15000 FT.	3.10	24.50	C.G.: 20% MAC	0.49	8.40
			C.G.: 33% MAC	0.55	9.44

FIGURE 167

CLOSED LOOP SYSTEM SHORT PERIOD DAMPING AND FREQUENCY FOR BACKUP MODE OF OPERATION

- MACH: 0.80
- ALTITUDE: 46800 FEET
- GROSS WEIGHT: 2350 LBS.
- SYSTEM RSS, GLA, PCS AND ALTITUDE HOLD ENGAGED
- +1° STEP RUDDER FOR 1 SECOND

ROLL
ANGLE
(DEG.)

$C_{l_p} = 0.8$ NOMINAL

ROLL
ANGLE
(DEG.)

$C_{l_p} =$ NOMINAL

1 SEC.

ROLL
ANGLE
(DEG.)

$C_{l_p} = 1.2$ NOMINAL

FIGURE 168

ROLL RESPONSE FOR STEP RUDDER WITH C_{l_p} VARIATIONS

```
                    C  SHAPING FILTER CONSTANTS

                                            } INPUT DT [TIME INCREMENT]

    YAZ = EXP (-0.5 * DT)
    XAZ = (YAZ - 1.0 + 0.5 * DT)/(0.25 * DT)
    WAZ = (1.0 - YAZ-0.5 * YAZ * DT)/(0.25 * DT)
    Y10 = EXP(-10. * DT)
    X10 = (Y10 - 1.0 + 10. * DT)/10./DT
    W10 = (1.0 - Y10 - 10.* Y10 * DT)/10./DT
    GLL = 25.0 * DT
```
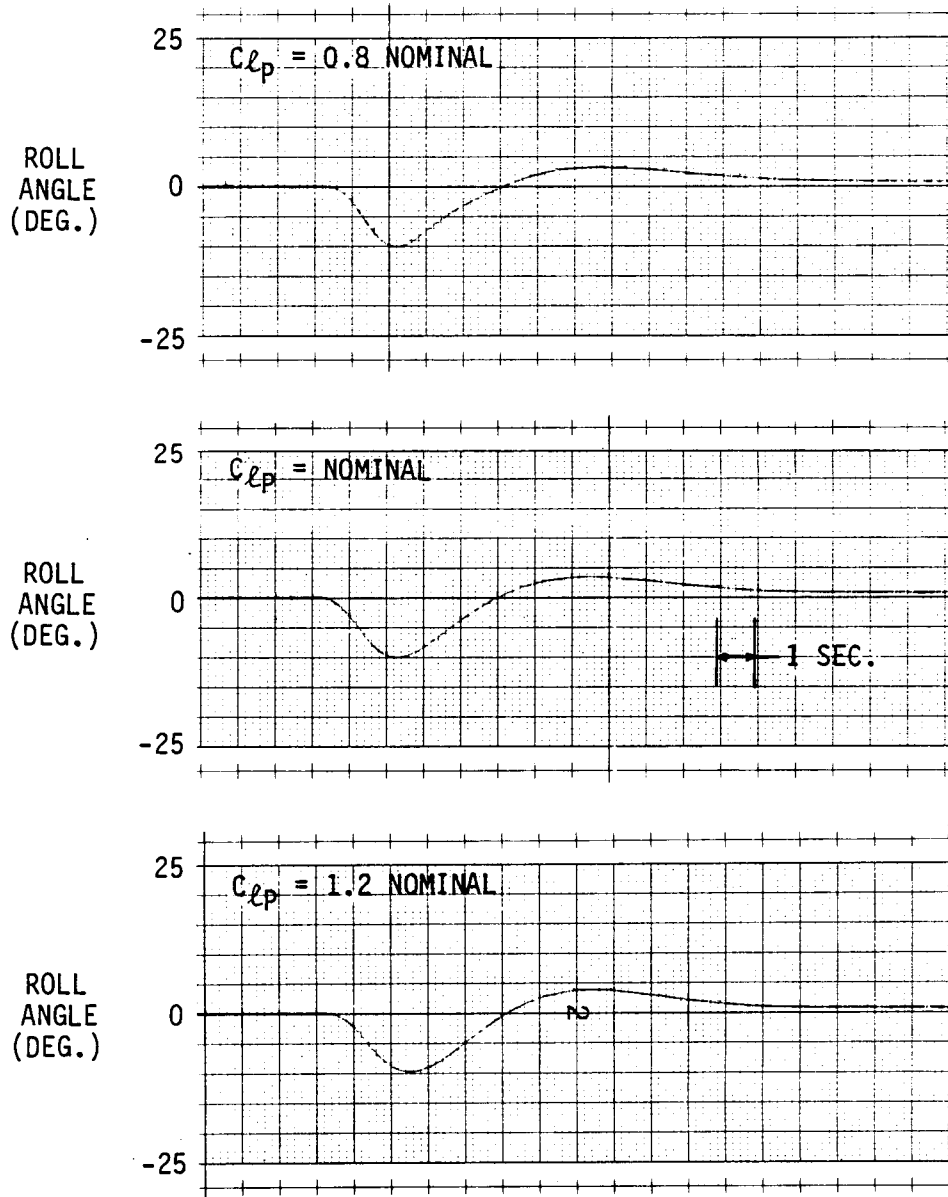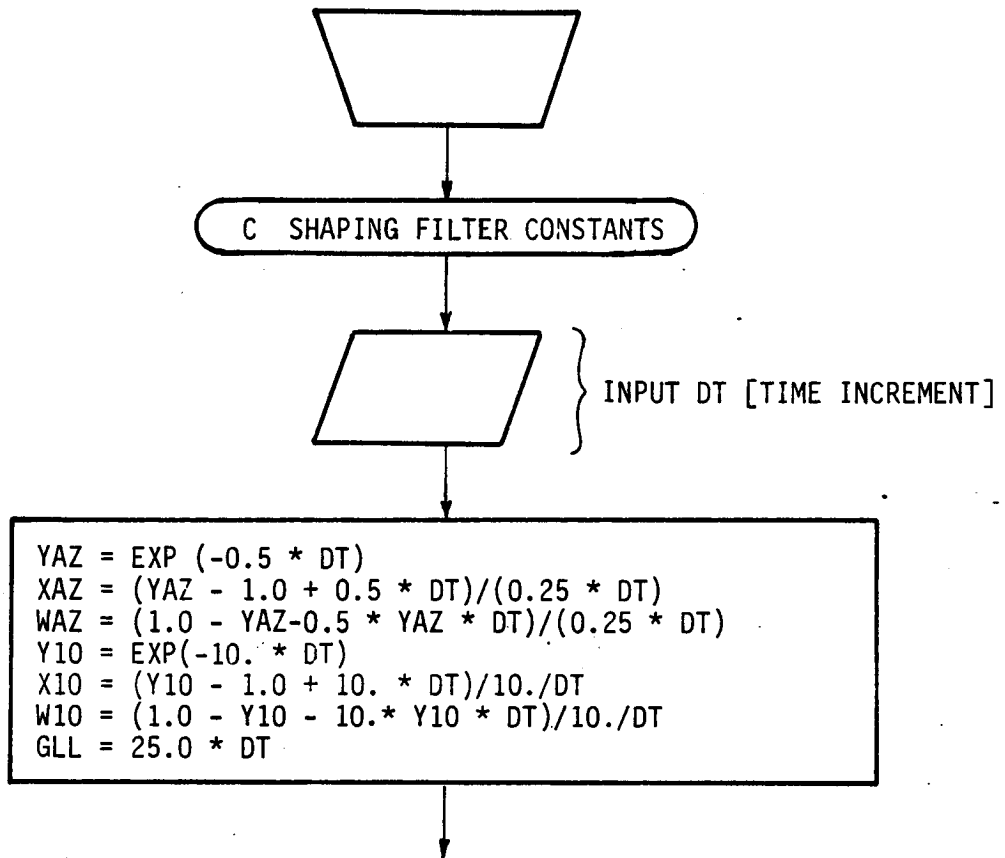
FIGURE 169

AFCS AND MLA DIGITAL PROGRAM CONSTANTS

237

```
C  LONGITUDINAL PRIMARY AFCS
C   INPUT DATA
C    AI (OPERATOR COLUMN COMMAND - INCREMENTAL G'S)
C    DP (DYNAMIC PRESSURE - PSF)
C    ALFDG (ANGLE OF ATTACK - DEG)
C    AZ1 (INCREMENTAL NORMAL ACCELERATION - G'S)
C    U (TRUE VELOCITY - FPS)
C    ISH (ALTITUDE HOLD ENGAGE SIGNAL -
C      ISH = 1, ALT. HOLD ON; ISH = 0, ALT. HOLD OFF
C    ZH (ALTITUDE - FT)
C    ZHD (ALTITUDE RATE - FT/SEC)
C    THTDG (PITCH ANGLE - DEG)
```

READ INPUT
DATA

```
AZSC = AI
AZM = 0.0015 * DP * (6.5 - ALFDG) + AZ1
```

IF(AZSC.GT.AZM) — T

```
AM = AZM +AZSC *(AZM - AZ1)
CALL LIMIT(AM, AZSC, 0.0)
AZSC = AM
```

(A)

FIGURE 170
PRIMARY LONGITUDINAL AFCS FLOW DIAGRAM

238
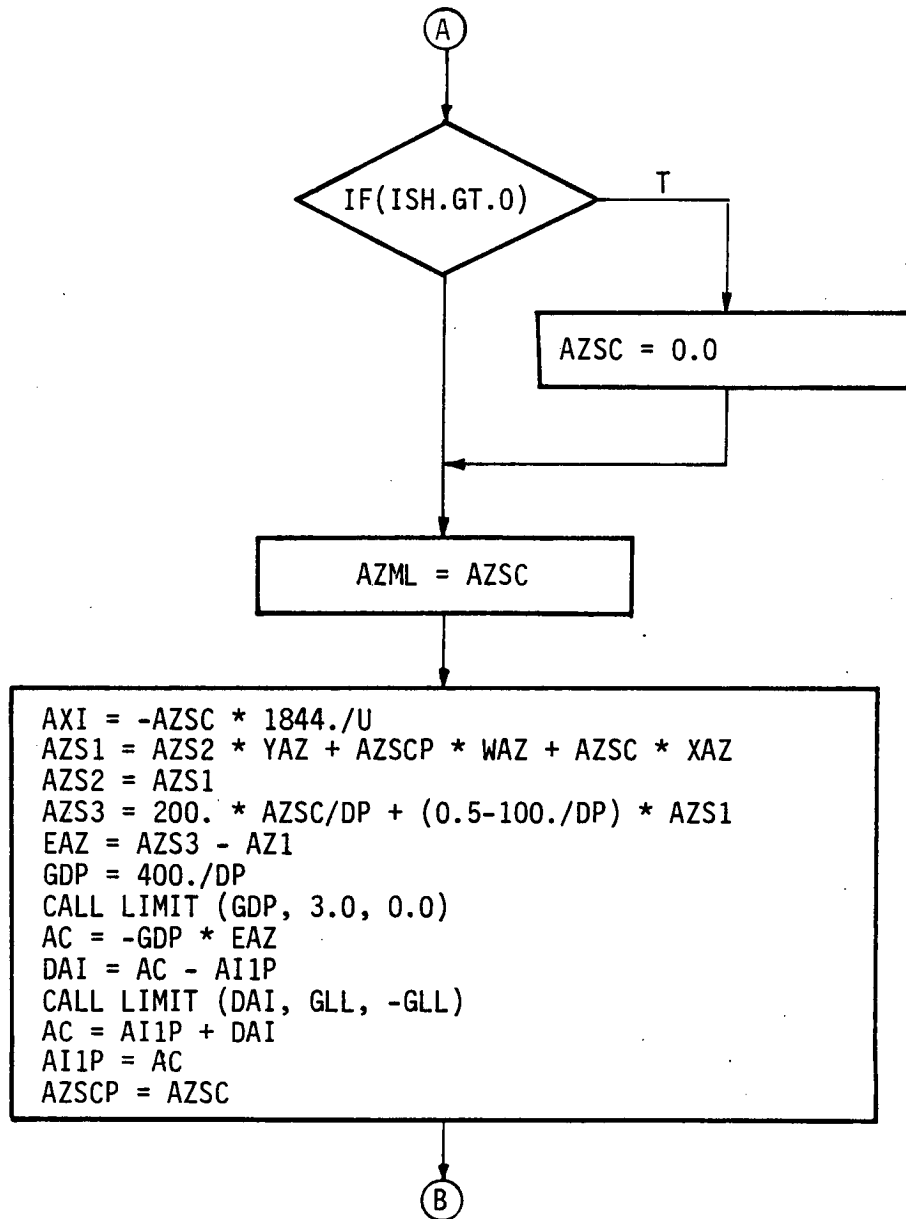
FIGURE 170 (CONTINUED)

PRIMARY LONGITUDINAL AFCS FLOW DIAGRAM

(B)

IF(ISH.LT.1) ──T──>

```
AIH = 0.025*(THTDG-THTP)+0.024 *
      (ZHD-ZDP)+0.006*(ZH-RH)
CALL LIMIT (AIH, 2.0, -2.0)
AHX = 0.001 * (ZH - RH)
AC = AC + AIH
```

```
AIH = 0.0
AHX = 0.0
RH = ZH
THTP = THTDG
ZDP = ZHD
```

```
C   OUTPUT VARIABLES
C   AC (STABILIZER PROPORTIONAL COMMAND - DEG.)
C   AXI (INPUT TO RSS FILTER CIRCUIT - DEG/SEC)
C   AHX (INPUT TO RSS INTEGRATOR - DEG/SEC)
C   AZML (INPUT TO MLA INBOARD AILERON SYSTEM - G'S)
```
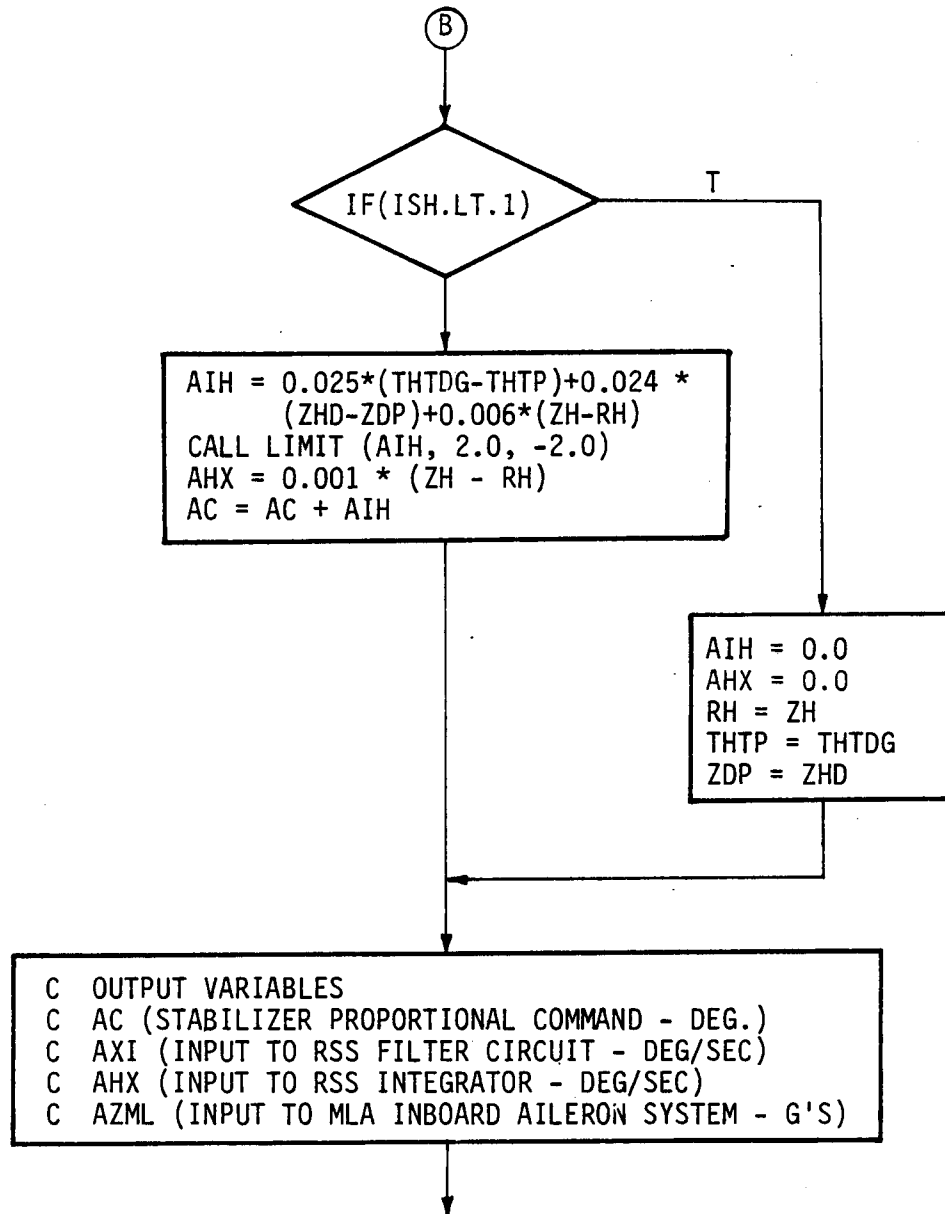
FIGURE 170 (CONCLUDED)

PRIMARY LONGITUDINAL AFCS FLOW DIAGRAM

```
C  LATERAL-DIRECTIONAL PRIMARY AFCS DIGITAL PROGRAM
C   INPUT DATA
C    DSTI (OPERATOR DIFFERENTIAL STAB. COMMAND - DEG)
C    P (ROLL RATE - DEG/SEC)
C    DSS (DIFFERENTIAL STABILIZER COMMAND
C     SYNCHRONIZATION SIGNAL - DEG)
C    ISP (PRIMARY AFCS ENGAGE SIGNAL -
C     ISP = 1, PCS ON; ISP = 0, PCS OFF)
```

SL = DSTI - 0.1 * P

IF(ISP.LT.1) — T

SLI = DSS - 3.5 * DSTI

SLI = SLI + (SL + SLP) *DT/2.0

SLP = SL
DSTO = SLI + 3.5 * DSTI

```
C  OUTPUT VARIABLE
C  DSTO (DIFFERENTIAL STABILIZER COMMAND - DEG)
```

FIGURE 171

PRIMARY LATERAL-DIRECTIONAL AFCS DIGITAL PROGRAM

241

NOTE:
Place downstream of longitudinal primary AFCS program.

C   MLA SYSTEM INBOARD AILERON SYSTEM
C   INPUT DATA (GENERATED OR USED PREVIOUSLY IN
C   LONGITUDINAL PRIMARY AFCS PROGRAM)
C   AZML (COLUMN COMMAND - INCREMENTAL G'S)
C   DP (DYNAMIC PRESSURE - PSF)
C   AZ1 (INCREMENTAL NORMAL ACCELERATION - G'S)
C   AC (STABILIZER PROPORTIONAL COMMAND - DEG)

IF(AZML.GT.0.5)   T

AZIA = AZML

AZIA = 1.05 * AZ1

ASL = 2425./DP
CALL LIMIT (ASL, 13.33, 0.0)
AZIA = AZIA * ASL
GMS = GMSP * Y10 + AZIAP * W10 + AZIA * X10
GMSP = GMS
AZIAP = AZIA
CALL LIMIT (GSM, 20.0, 0.0)
AC = AC + 0.11 * GMS

C   OUTPUT VARIABLES
C   GMS (INBOARD AILERON COMMAND - DEG)
C   AC (STABILIZER PROPORTIONAL COMMAND - DEG)

FIGURE 172
MLA INBOARD AILERON FUNCTION FLOW DIAGRAM

FIGURE 173

LIMITER FOR PRIMARY AFCS AND MLA

(This page intentionally left blank)

7. ELECTRICAL/ELECTRONIC DESIGN AND MODIFICATION

This section details design requirements and the methods used to comply with these requirements for the DAST ARW-2 Active Control System (ACS) electrical and electronic components.

The ACS electronics include motion feedback sensors, uplink and downlink telemetry signal conditioning, mechanization of the flutter suppression, gust load alleviation and relaxed static stability filters and a function generator for inputing commands to the outboard aileron servoactuators for flutter suppression system testing, a random noise generator to apply commands to the inboard aileron servoactuator feedback loops and servovalve drive amplifiers. Figure 174 shows the "as-delivered" functional block diagram of the ACS, however, modifications were made after delivery to NASA Langley. The changes made to the ACS were a result of a "hardware-in-the-loop" (HITL) simulation at NASA Langley which produced airplane responses different from the responses obtained in the ACS simulation performed at Boeing. The changes are covered in detail in Paragraph 7.5 of this document. Excitation voltages required by the ACS accelerometers and servoactuator position and pressure feedback transducers were furnished by DC to DC converters. Figure 175 defines symbols used on the block diagram shown on Figure 174.

7.1 Design Philosophy. The basic philosophy was to provide as much flexibility as possible to ease maintenance and to provide required performance within the constraints of reasonable cost, minimum physical size and the expected drone flight environment.

The number of circuit cards and components was kept to a minimum. The components are military grade mounted on two-sided mica ply etched circuit cards with plated through holes. Card edge connectors are not used in order to decrease the possibility of receiving intermittent signals during vibration.

Filter networks were isolated to allow critical break frequencies to be Selected At Test (SAT). A built-in test generator with selectable mode and signal amplitude telemetry triggering was provided. Parameter changes are implemented by SAT component provisions for infrequent changes, variable gain controls for rapid changes between flights and inflight logic-controlled gain changes and parameter time constant scheduling.

The sensors and output signals are analog and are compatible with the existing telemetry system.

FSS GAIN #1 TM J5-15 >—1J2-22—> →◁— ⊐ —1J2-56— 7J1-60 —[-K]— + Σ —7J1-29— J5-36
7J1-58 —> J7-111 (TP108)
OFFSET ADJ.

FSS GAIN #2 TM J5-17 >—1J2-21—> →◁— ⊐ —1J2-54— 7J2-34 —[-K]— + Σ —7J1-30— J5-37
7J1-59 —> J7-113 (TP109)
OFFSET ADJ.

GLA GAIN #1 TM J5-19 >—1J2-50—> →◁— ⊐ —1J2-53— 7J2-31 —[-K]— + Σ —7J2-3— J5-38
7J2-33 —> J7-107 (TP106)
OFFSET ADJ.

GLA GAIN #2 TM J5-21 >—1J2-20—> →◁— ⊐ —1J2-51— 7J2-2 —[-K]— + Σ —7J2-5— J5-39
7J2-35 —> J7-109 (TP107)
OFFSET ADJ.

RSS GAIN #1 TM J5-23 >—1J1-28—> →◁— ⊐ —1J2-33— 7J2-6 —[-K]— + Σ —7J2-7— J5-40
7J2-37 —> J7-103 (TP104)
OFFSET ADJ.

RSS GAIN #2 TM J5-25 >—1J1-57—> →◁— ⊐ —1J2-31— 7J2-10 —[-K]— + Σ —7J2-9— J5-41
7J2-39 —> J7-105 (TP105)
OFFSET ADJ.

LAUNCH TM J5-1 >—1J1-27—> →◁— ⊐ —1J1-60— 7J2-17 —[-K]— + Σ —7J2-18— J5-29
7J2-47 —> J7-115 (TP110)
OFFSET ADJ.

FSS EXC. AMP TM J5-7 >—1J1-56—> →◁— ⊐ —1J1-58— 7J2-13 —[-K]— + Σ —7J2-19— J5-32
7J2-49 —> J7-119 (TP112)
OFFSET ADJ.

FSS EXC. SYM/TM J5-9 >—1J2-39—> →◁— ⊐ —1J2-42— 7J2-16 —[-K]— + Σ —7J2-20— J5-33
7J2-50 —> J7-117 (TP111)
OFFSET ADJ.

GUST EXC. AMP #1 J5-11 >—1J2-9—> →◁— ⊐ —1J2-44— 7J2-23 —[-K]— + Σ —7J2-22— J5-34
7J2-52 —> J7-125 (TP115)
OFFSET ADJ.

GUST EXC. AMP #2 J5-13 >—1J2-38—> →◁— ⊐ —1J2-41— 7J2-25 —[-K]— + Σ —7J2-24— J5-35
7J2-54 —> J7-127 (TP116)
OFFSET ADJ.

START SWEEP J5-5 >—2J2-20—> →◁— ⊐ —2J2-19— 7J2-28 —[-K]— + Σ —7J2-57— J5-31
7J2-56 —> J7-123 (TP114)
OFFSET ADJ.

START DOUBLET J5-3 >—2J2-24—> →◁— ⊐ —2J2-18— 8J1-4 —[-K]— + Σ —8J1-6— J5-30
8J1-36 —> J7-121 (TP113)
OFFSET ADJ.

BCSCMD J3-19 >—1J2-8—> →◁— ⊐
J7-101 >—>
—1J2-11—
(TP103)

FIGURE 174

DACE BLOCK DIAGRAM (UPLINK CONTROL SIGNALS)
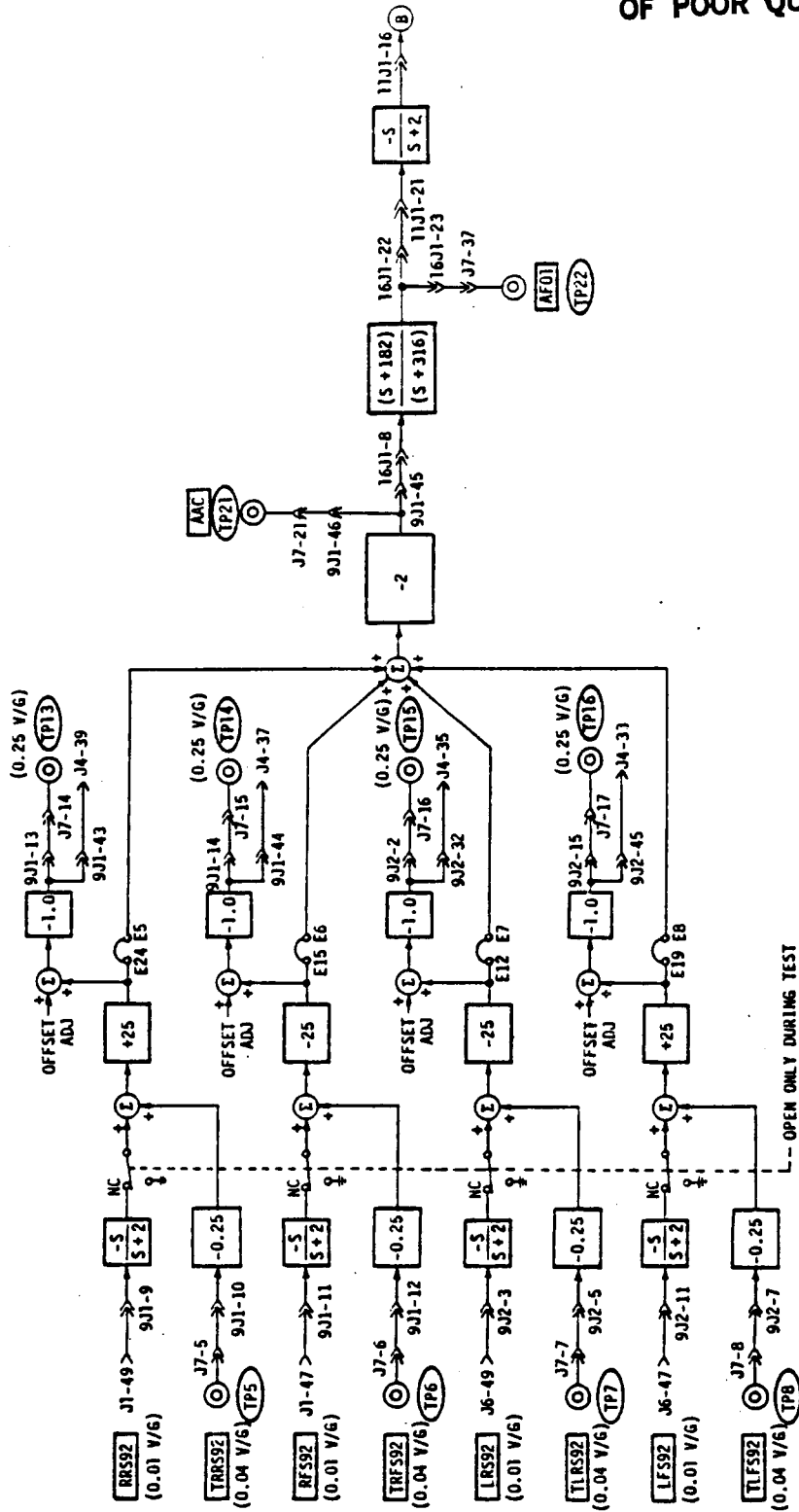
246

FIGURE 174 (CONTINUED)

DACE BLOCK DIAGRAM (FSS SYSTEM)

247

FIGURE 174 (CONTINUED)

DACE BLOCK DIAGRAM (FSS SYSTEM)

SYMMETRIC CHANNEL

12J2-58 → FL1 $(4.15)(s^2+251s+314^2)$ / $(s+640)^2$ → E1 E4 → FL2 $0.647(s^2+232s+123^2)$ / $(s^2+180s+99^2)$ → E5 E6 → FL3 $(0.901)(s^2+63.25+158^2)$ / $(s+150)^2$ → E7 E8 → FL4 $(s^2+147.25+85^2)$ / $(s^2+61.375+85^2)$ → E9 E12 → FL5 $(13.9)(s^2+30s+470^2)$ / $(s+1750)^2$ → 12J1-40 → -1.0 → 12J1-60 → C

A

ANTISYMMETRIC CHANNEL

11J2-58 → FL1 $(0.694)(s^2+84s+180^2)$ / $(s+150)^2$ → E1 E4 → FL2 $(0.647)(s^2+232s+123^2)$ / $(s^2+180s+99^2)$ → E5 E6 → FL3 $(4.15)(s^2+251s+314^2)$ / $(s+640)^2$ → E7 E8 → FL4 $(s^2+190.5s+110^2)$ / $(s^2+79.4s+110^2)$ → E9 E12 → FL-5 $(7.41)(s^2+20s+455^2)$ / $(s+1750)^2$ → 11J1-40 → -1.0 → 11J1-60 → D

B

FIGURE 174 (CONTINUED)

DACE BLOCK DIAGRAM (FSS SYSTEM)

249
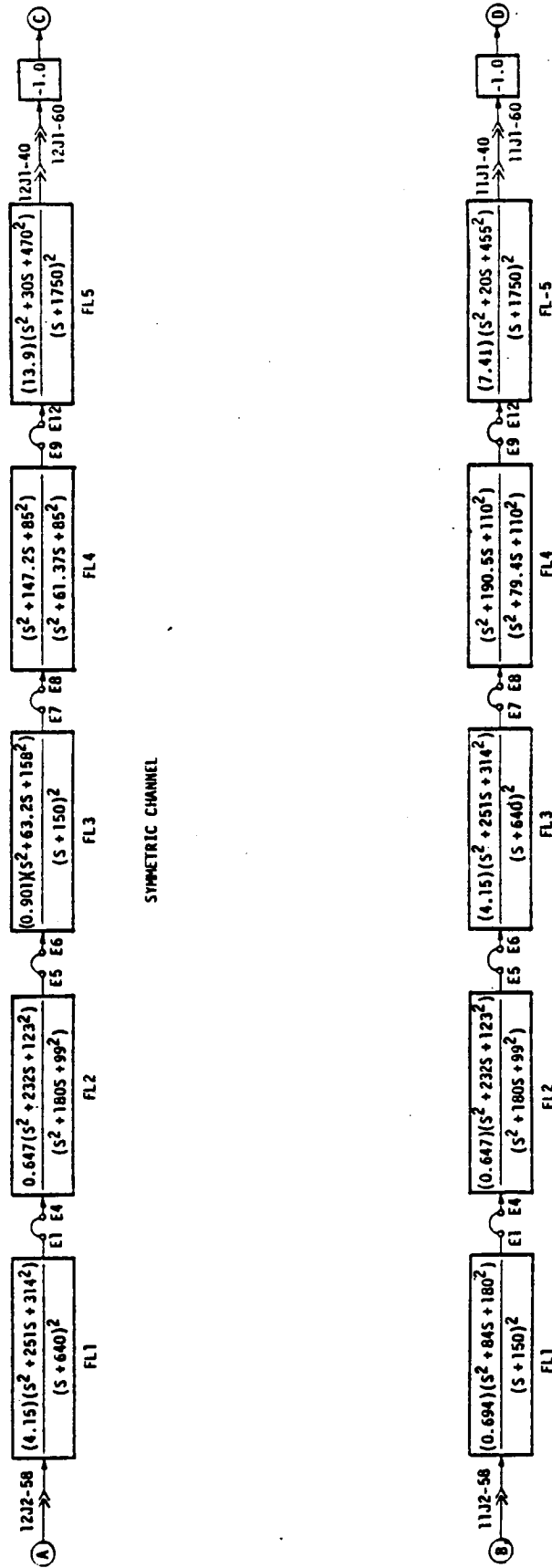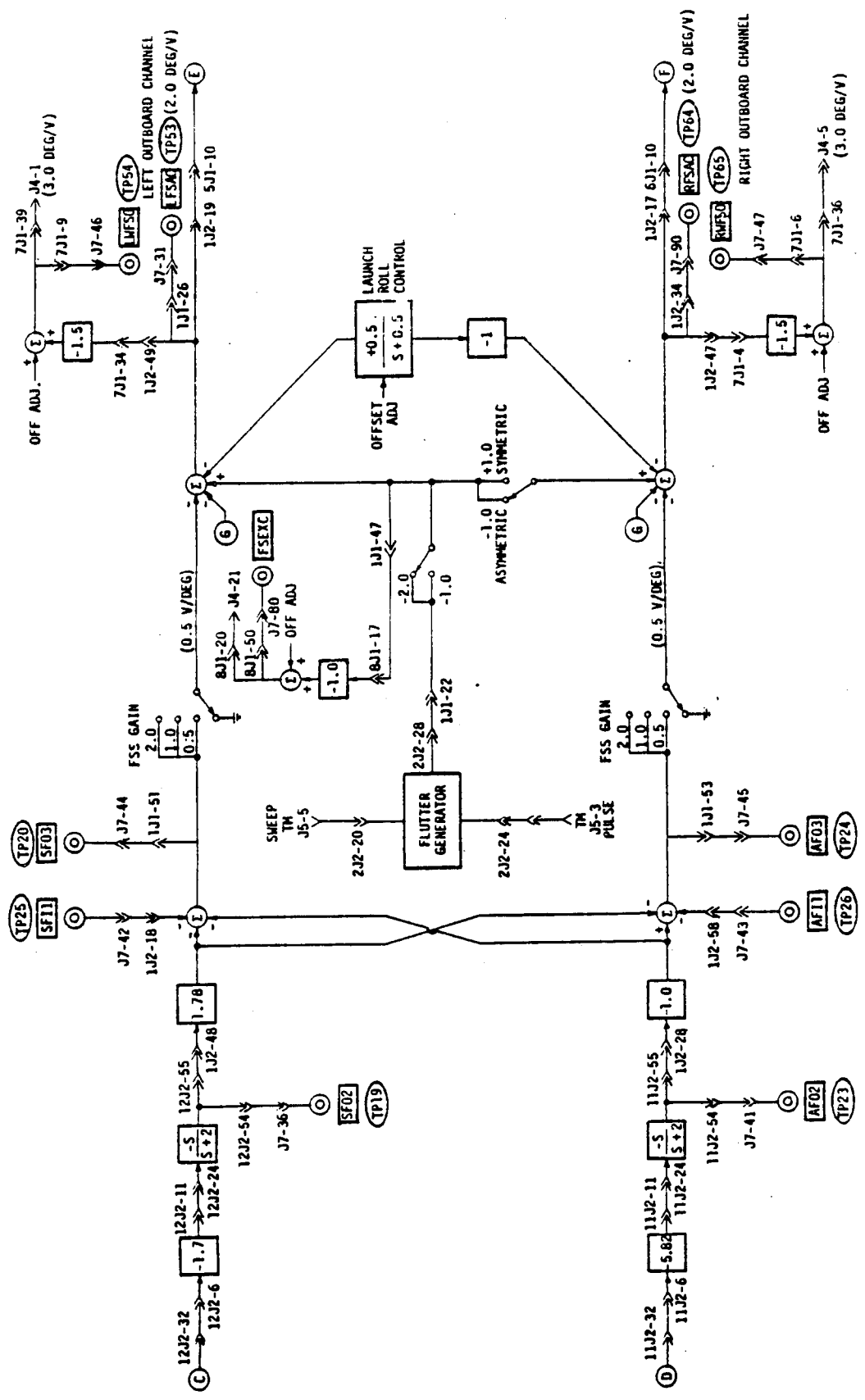
FIGURE 174 (CONTINUED)

DACE BLOCK DIAGRAM (OUTBOARD AILERON SUMMING)

FIGURE 174 (CONTINUED)

DACE BLOCK DIAGRAM (RSS AND GLA SYSTEMS)

251

FIGURE 174 (CONTINUED)

DACE BLOCK DIAGRAM (RSS AND GLA SYSTEMS)
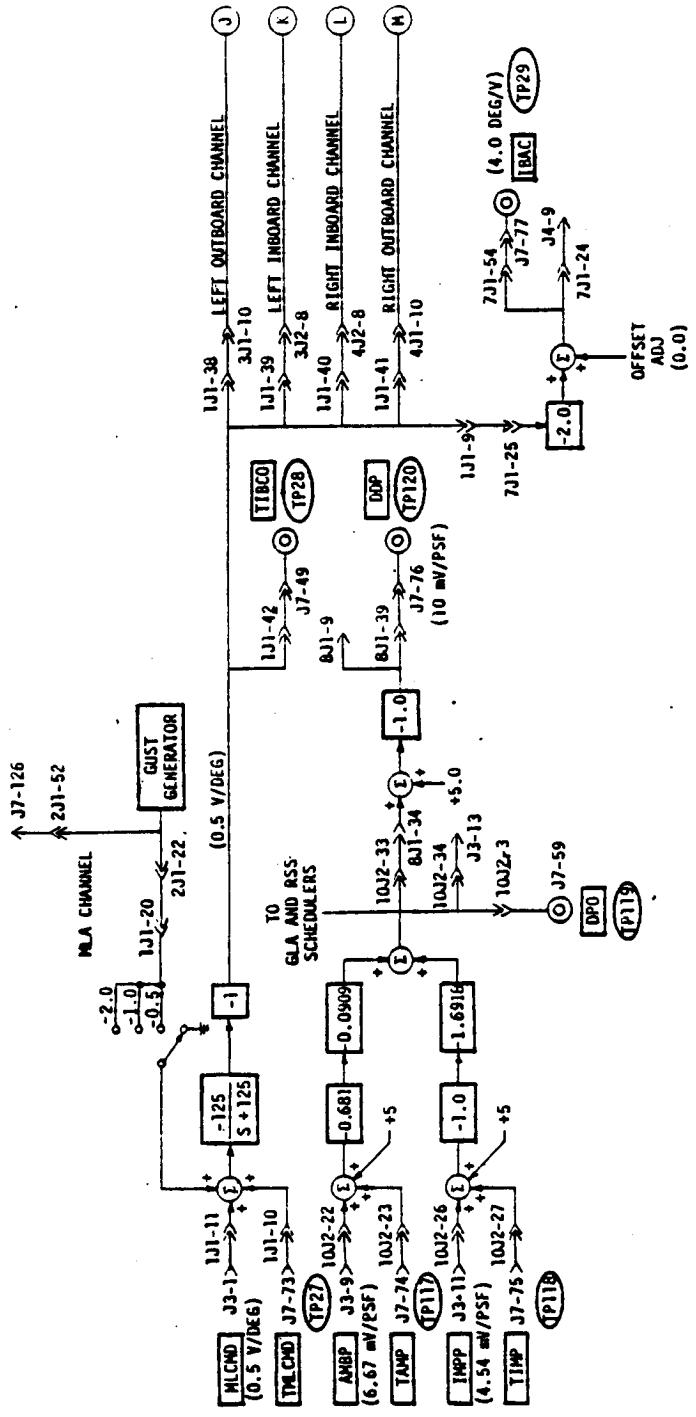
FIGURE 174 (CONTINUED)

DACE BLOCK DIAGRAM (MLA SYSTEM)

253

FIGURE 174 (CONTINUED)

DACE BLOCK DIAGRAM (LOBS)

254

FIGURE 174 (CONTINUED)
DACE BLOCK DIAGRAM (ROBS)

255

FIGURE 174 (CONTINUED)

DACE BLOCK DIAGRAM (LIBIBS)

256
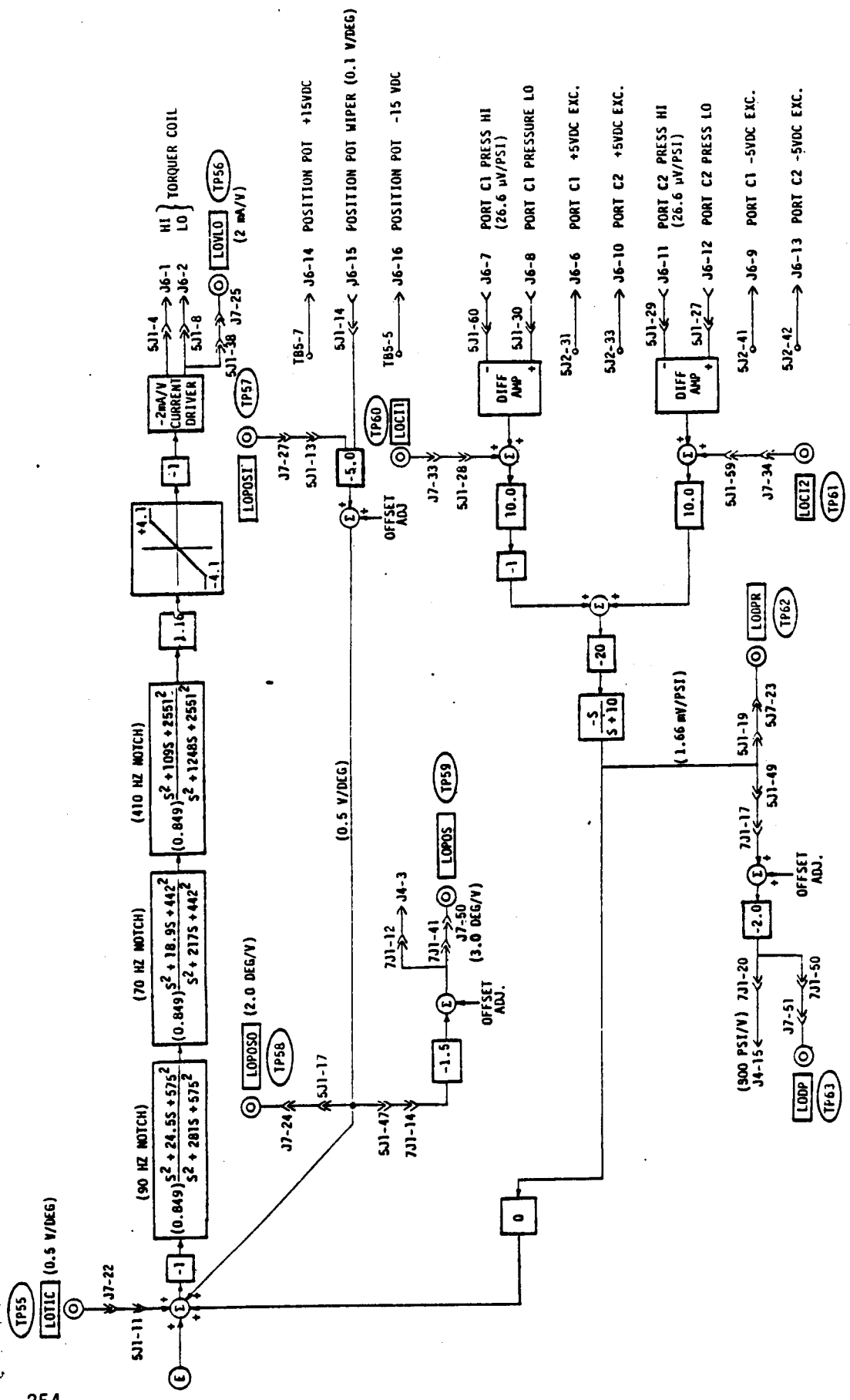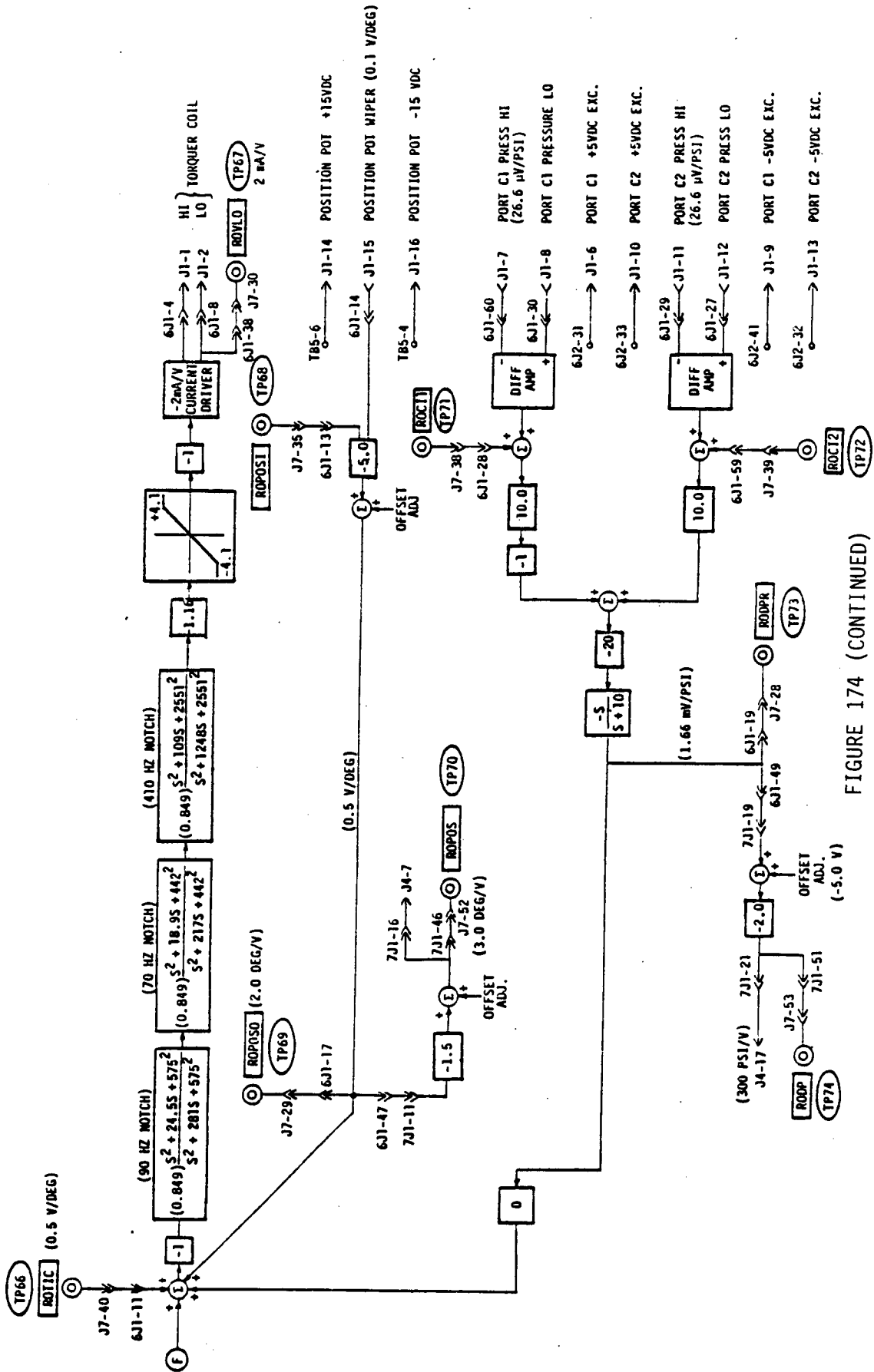
FIGURE 174 (CONTINUED)

DACE BLOCK DIAGRAM (LIBOBS)

FIGURE 174 (CONTINUED)

DACE BLOCK DIAGRAM (RIBIBS)
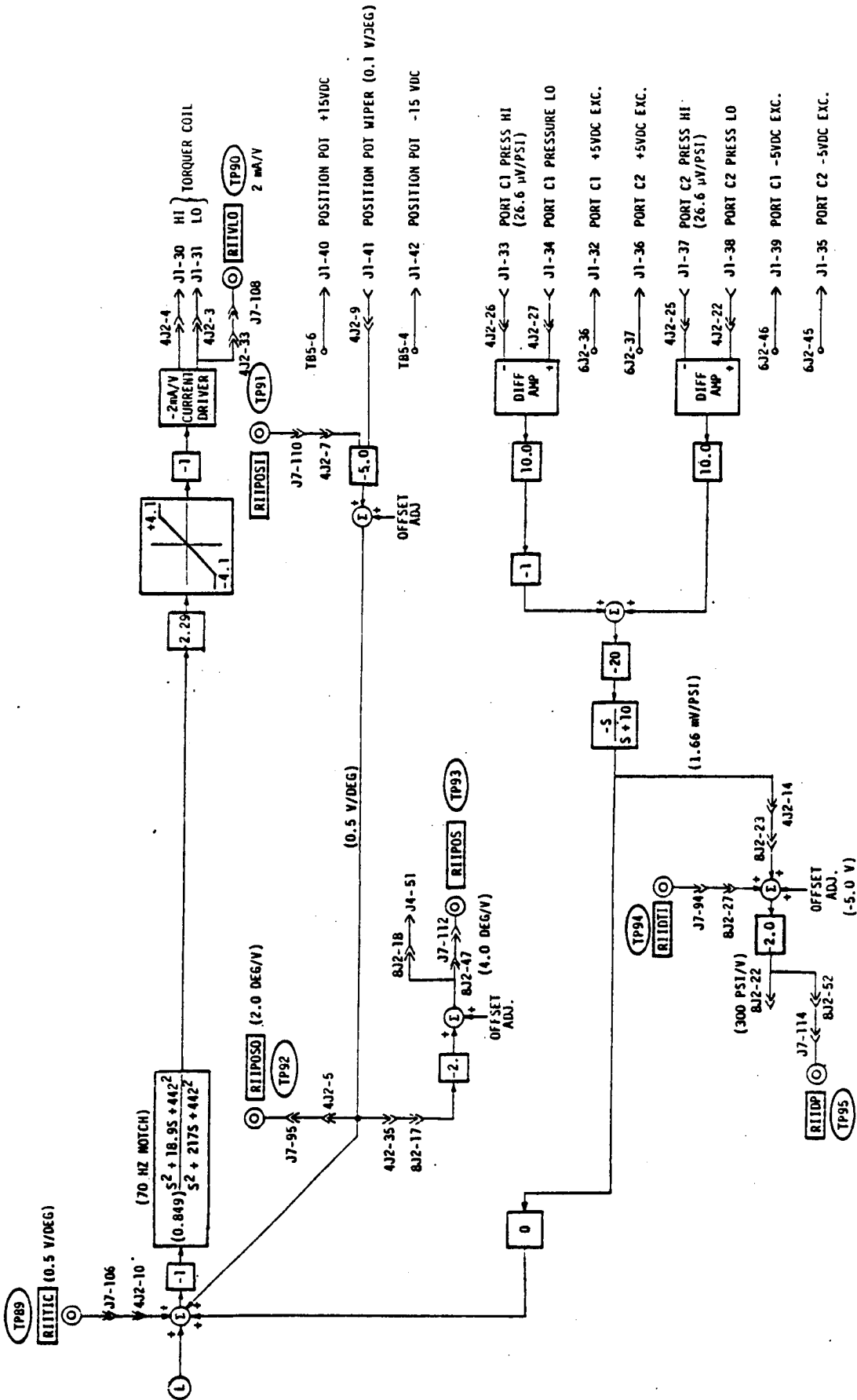
FIGURE 174 (CONCLUDED)

DACE BLOCK DIAGRAM (RIBOBS)

INPUT/OUTPUT MNEMONICS

AAC	Antisymmetric Acceleration Command
AFI1	Antisymmetric Filter Test Input 1
AFO1	Antisymmetric Filter Test Output 1
AFO2	Antisymmetric Filter Test Output 2
AFO3	Antisymmetric Filter Test Output 3
ALT HOLD	Altitude Hold Input
AMBP	Ambient Pressure Input
BS250	Body Station 250 Acceleration Input
BUSS	Backup Symmetric Stabilizer Input
DBS250	Body Station 250 Acceleration Downlink
DPP	Dynamic Pressure Downlink
DLRSI	RSS Integrator Output Downlink
DLTSS	Total Symmetric Stabilizer Downlink
DPO	Dynamic Pressure Output
DKGLA	Scheduled GLA Gain Downlink
FSEXC	Flutter Suppression Excitation Command
GAO1	GLA Aileron Loop Test Output 1
GLO1	GLA Test Output 1
GLO2	GLA Test Output 2
GSO1	GLA Stabilizer Loop Test Output 1
GSO2	GLA Stabilizer Loop Test Output 2
IBAC	Inboard Aileron Command Downlink
IMPP	Impact Pressure Input
KBLA	Scheduled GLA Gain
LFSXX	Left Front Spar (WBLXX)
LRSXX	Left Rear Spar (WBLXX)
LWFSAC	Left Wing Flutter Suppression Actuator Command
LWFSO	Left Wing Flutter Suppression Output (Downlink)
MLCMD	MLA Command Input
PPR	Pseudo Pitch Rate
PPRO1	Pseudo Pitch Rate Test Output 1
RFO1	Relaxed Static Stability Filter Test Output
RFSXX	Right Front Spar (WBLXX)
RRSXX	Right Rear Spar (WBLXX)
RSEO	Relaxed Static Stability Error Output
RWFSAC	Right Wing Flutter Suppression Actuator Command
RWFSO	Right Wing Flutter Suppression Output (Downlink)
SAC	Symmetric Acceleration Command
SFI1	Symmetric Filter Test Input 1
SFO2	Symmetric Filter Test Output 1
SFO2	Symmetric Filter Test Output 2
SFO3	Symmetric Filter Test Output 3
SPR	Sensor Pitch Rate Input
SPRO1	Sensor Pitch Rate Test Output 1

INPUT/OUTPUT MNEMONICS

TALT HOLD	Altitude Hold Test Input
TAMP	Ambient Pressure Test Input
TBUSS	Backup Symmetric Stabilizer Test Input
TIMP	Impact Pressure Test Input
TIBCO	Inboard Aileron Command Test Output
TMLCMD	MLA Command Test Input
TBS250	Body Station 250 Acceleration Input
TLFSXX	Test Input Left Front Spar (WBLXX)
TLRSXX	Test Input Left Rear Spar (WBLXX)
TRFSXX	Test Input Right Front Spar (WBLXX)
TRRSXX	Test Input Right Rear Spar (WBLXX)
TRSID	RSS Integrator Test Output
TPPR	Pseudo Pitch Rate Test Input
TSPR	Sensor Pitch Rate Test Input
TSS	Total Symmetric Stabilizer Output

INBOARD AILERON MNEMONICS

LIBIBS (L11)	Left Inboard Aileron, Inboard Segment
LIBOBS (L10)	Left Inboard Aileron, Outboard Segment
RIBIBS (R11)	Right Inboard Aileron, Inboard Segment
RIBOBS (R10)	Right Inboard Aileron, Outboard Segment
XXXDP	Differential Pressure, Downlink
XXXDTI	Differential Pressure, Downlink Test Input
XXXPOS1	Position Test Input
XXXPOSO	Position Test Output
XXXTIC	Test Input Command
XXXVLO	Valve, Low Side

OUTBOARD AILERON MNEMONICS

LOBS (LO)	Left Outboard Segment
ROBS (RO)	Right Outboard Segment
XXCI1	Port C1 Test Input
XXCI2	Port C2 Test Input
XXDP	Differential Pressure Downlink
XXDPR	Differential Pressure Test Output
XXPOS	Position Downlink
XXPOSI	Position Test Input
XXPOSO	Position Test Output
XXTIC	Test Input Command
XXVLO	Valve Low Side

FIGURE 175

LIST OF SYMBOLS FOR THE ACS BLOCK DIAGRAM

7.2 ACS Electronics Box Design. The box is required to house the ACS electronics and mate with an existing BQM-34E/F mounting tray. All connectors are required to be mounted on the front of the box for accessibility. Space is available beneath the mounting tray for mounting of the ACS electronics power supplies.

The electronics box is a Boeing designed and fabricated aluminum box (Drawing Number 35-35100-1) that mates with an existing mounting tray in the drone fuselage at Body Station 212.8. Electronic components used are military qualified or commercial grade meeting military environmental specifications. The electronics box is 17.75 inches long, 9.4 inches wide and 6.3 inches high with extending mounting flanges making an overall length of 22.5 inches. The box weight is 24 pounds.

The circuit card sizes are 4.475 inches high and 9.05 inches wide, and 3.3 inches wide and 4.55 inches high. The box includes provisions for 18 circuit cards and all interface connectors are mounted on the front. Figures showing the box design size are presented in Paragraph 8.1. All power is supplied by externally mounted DC to DC converters. EMI filters are included on all power lines. All cable connectors include EMI backshells to ensure electromagnetic compatibility. Boeing Document D3-12115-2, EMC Qualification Report for the Active Control System DAST (ARW-2), 12 January 1983 verifies FSS electronics compliance with MIL-STD-461A.

7.3 Flutter Suppression Systems Sensors. The DAST ARW-2 flutter suppression system requires wing accelerometers as the aircraft motion sensors for feedback signals. The gust load alleviation system requires a fuselage accelerometer as the aircraft motion sensor for feedback sensors and pressure transducers are required for actuator load telemetry data. The following paragraphs outline performance and installation requirements of these sensors as well as the design philosophy and approach.

7.3.1 Sensor Performance Requirements. The ACS requires nine motion sensors with type, orientation and location as defined on Figure 176.

The vertical accelerometers in the wings should have their sensitive axes vertical when the wing is in 1g flight at Mach 0.86, 15,000 feet.

The accelerometers shall have the following characteristics:

Sensors	Amplitude Range	Frequency Range	Accuracy (% of Applied Accel.)
1,2,3,4, 5,6,7,8	±10g	0.5 - 1000 Hz	3
9	± 5g	0.5 - 200 Hz	4

SENSOR	TYPE	LOCATION	ORIENTATION	BS	WBL	WL
1	Accelerometer	Left Wing	Vertical (±1 Deg)	Rear Spar	84	Center of Rear Spar
2	Accelerometer	Left Wing	Vertical (±1 Deg)	Rear Spar	92	Center of Rear Spar
3	Accelerometer	Left Wing	Vertical (±1 Deg)	Front Spar	82	Center of Front Spar
4	Accelerometer	Left Wing	Vertical (±1 Deg)	Front Spar	92	Center of Front Spar
5	Accelerometer	Right Wing	Vertical (±1 Deg)	Rear Spar	84	Center of Rear Spar
6	Accelerometer	Right Wing	Vertical (±1 Deg)	Rear Spar	92	Center of Rear Spar
7	Accelerometer	Right Wing	Vertical (±1 Deg)	Front Spar	82	Center of Front Spar
8	Accelerometer	Right Wing	Vertical (±1 Deg)	Front Spar	92	Center of Front Spar
9	Accelerometer	Fuselage (Center Line)	Vertical (±1 Deg)	250		

FIGURE 176

MOTION SENSOR DEFINITION

The sensors are required to be flightworthy. All sensors are required to meet these requirements while operating in the BQM-34E/F drone environment defined by NASA - DFRC Process Specification 21-1 and 21-2. Figure 177 contains the accelerometers performance requirements.

PARAMETER	REQUIREMENT	
	WING	FUSELAGE
Range	±10g	±5g
Natural Frequency	1000 Hz	200 Hz
Size	0.3 x 0.5 Inches	1.25 x 1.75 Inches
Damping Ratio	0.6 Minimum	
Resolution	0.02g Minimum	
Hysteresis	0.001g Minimum	
Threshold	0.001g Minimum	
Cross-Axis Sensitivity	0.05g/g Maximum	
Temperature Range	-40°F to 200°F	

FIGURE 177

COMPOSITE ACCELEROMETER PERFORMANCE REQUIREMENTS

The potentiometer performance requirements are presented on Figure 178. The potentiometers are mounted on the rotary servoactuator shafts for inboard ailerons as shown on NASA Drawing LD-316091. The potentiometers are mounted on a potentiometer mounting extension for outboard ailerons as shown on Boeing Drawing 35-34617. Size and resolution were the primary requirements.

Case Diameter	0.5 Inch
TYpe Resistive Element	Conductive Plastic
Usable Angle of Rotation	±20 Degrees Minimum
Output Gradient	±1.0 Volt for 10 Degree Rotations, Minimum
Center Tap Required	No

FIGURE 178

POTENTIOMETER PERFORMANCE REQUIREMENTS

The pressure transducer performance requirements are presented on Figure 179. Twelve transducers are required, two for each servoactuator to measure C1 and C2 port pressures.

Pressure Range	0 to 1500 psi
Rated Exciation	10 VDC
Input Impedance	350 OHM Nominal
Sensitivity	40 MV ±5% (Open Circuit at Rated Excitation)
Frequency Responses	>1000 Hz

FIGURE 179
PRESSURE TRANSDUCER PERFORMANCE REQUIREMENTS

7.3.2 Sensor Selection. A sketch of the wing accelerometer selected is shown on Figure 180. The manufacturer specifications are listed on Figure 181. Performance requirements of the ARW-2 were met by the sensors used on ARW-1.

More space was available for mounting transducers in the fuselage, allowing the use of a servo type accelerometer for measuring fuselage acceleration. Manufacturer's specifications, availability and NASA's recommendations from ARW-1 led to the selection of the Sundstrand Model QA-1100-AA01-12 accelerometer. Figure 182 shows a sketch of the accelerometer and the manufacturer's specifications are listed on Figure 183.

The potentiometers selected are the New England Instrument Company Model 55 FL1-134. These potentiometers are single turn 300° precision conductive plastic type presenting nearly infinite resolution. The ½ inch diameter was selected to be compatible with the space available. The manufacturer specifications are listed on Figure 184.

The pressure transducers selected are the Bell & Howell Type 4-326-0001. These transducers are a four-arm active strain gage Wheatstone design with rugged construction offering highly reliable service. Figure 185 shows the outline dimensions for the Type 4-326-001 pressure transducer and the manufacturer's specifications are listed on Figure 186.

7.4 Circuit Design. The electronics provide signal conditioning for the analog signals from the sensors, accepts uplink discrete telemetry commands and provides downlink analog and discrete signals to be compatible with the existing telemetry system. The primary function of the electronics is signal shaping. The filter network required flexibility to allow critical break points to be selected by resistor changes at designated places in the circuitry. A built-in sweep and doublet generator is required to provide FSS test signals to assist in

264
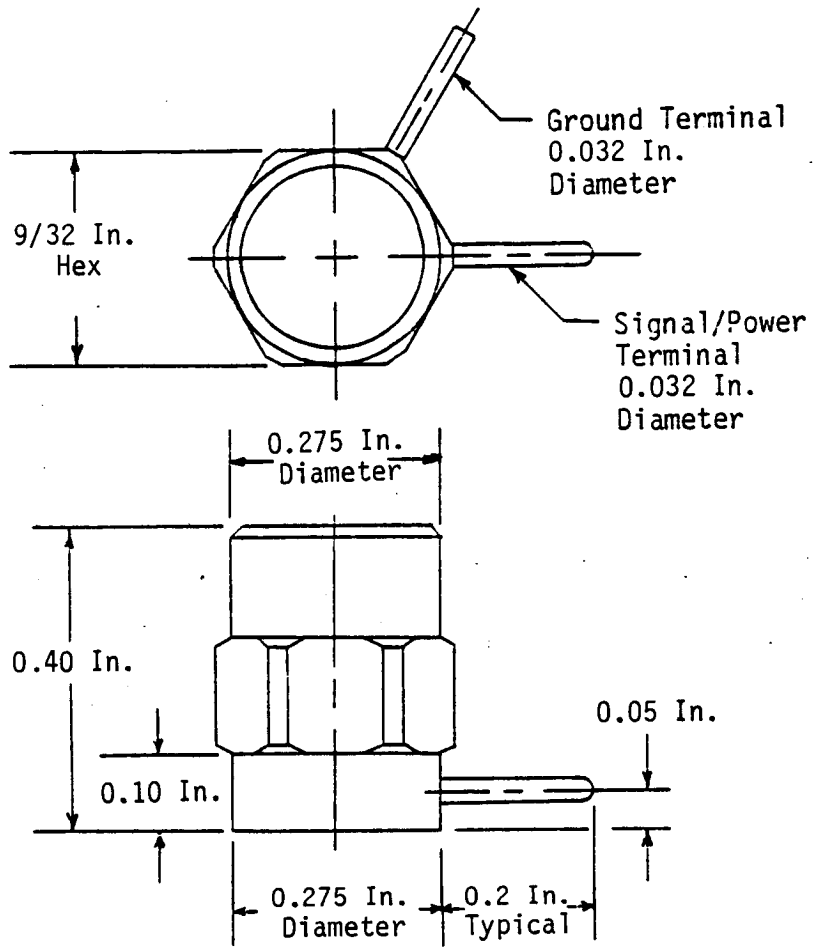
FIGURE 180 - SKETCH OF PCB PIEZOTRONICS MODEL 303A03 MINIATURE
ACCELEROMETER

Sensitivity, Nominal	10 mV/g
Resolution	0.2g
Resonant Frequency, MTD.	70 KHz
Frequency Range, $\pm$5%	1 to 10 000 Hz
Overload Recovery	10 uSec
Discharge Time Constant	1 Sec
Amplitude Linearity	1% FS
Range for $\pm$5V	$\pm$500g
Output Impedance	100 Ohms
Output Bias	11 Volts
Transverse Sensitivity	5%
Strain Sensitivity	.05 g/μ in/in
Temperature Sensitivity	-40°F to 200°F
Vibration Maximum	$\pm$1000g
Shock, Maximum	$\pm$2000g
Structure	Iso-Compression, Upright
Size, Hex x Height	9/32 x .42 inch
Connections	Solder Pins
Case Material	Aluminum/Titanium
Power Supply Voltage	+18 to +24 Volts
Power Supply Current	2 to 20mA thru Current Regulation Diode

FIGURE 181

PCB 303A03 ACCELEROMETER PEFORMANCE SPECIFICATION
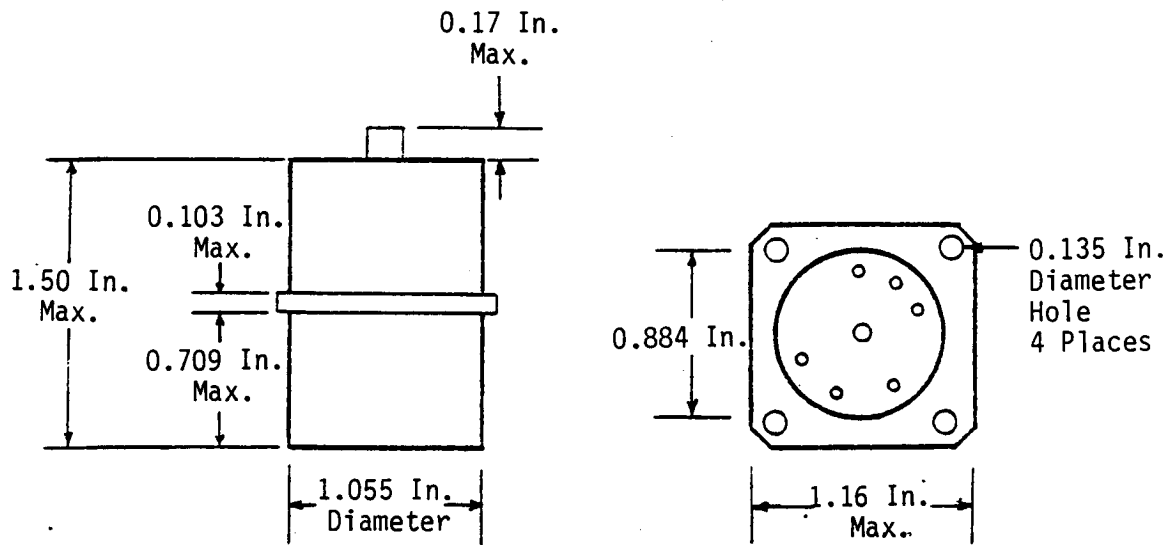
FIGURE 182   SUNDSTRAND MODEL QA1100-AA01-12 ACCELEROMETER

Parameter	Accuracy/Range
Range, Maximum Full Scale	±g
Scale Factor/Sensitivity	250mV/g±10%
Frequency Response (±5%)	300 Hz
Natural Frequency	Greater Than 800 Hz
Damping Ratio	0.3 to 0.7
Noise 0-10 Hz / 0-50 Hz / 500-10 K Hz	<10 Nanoamps RMS / <100 Nanoamps RMS / <1 Microamp RMS
Excitation/Power Supply Voltage	±13 VDC to ±28 VDC
Excitation/Power Supply Quiescent Current	15 mA per Supply
Scale Factor/Sensitivity Shift with Supply Voltage	.002%/V
Bias/Zero Shift with Supply Voltage	10 Micro-g/V
Resolution (DC)	0.000001 g
Threshold (DC)	0.000001 g
Linearity (DC) QA-1000, 1100, 1200	20 μg/g^2
Hysteresis	0.001% of Full Scale
Repeatability	0.003% of Full Scale
Bias/Zero Unbalance	±3 Milli-g Typical / ±10 Milli-g Max

Parameter	Accuracy/Range
Scale Factor Temperature Coefficient/Thermal Sensitivity Shift	180 ppm/°C (maximum)
Axis Alignment/Transverse Sensitivity	0.002 g/g
Vibration Rectification Coefficient (Discrete Point)	75 μg/g^2 RMS Uncompensated
Constant g Random Spectrum 50 to 2 K Hz	40 μg/g^2 RMS
Grounding	Electronics are Isolated from Case 50 Megohms of 50 VDC. Shield is Common to Case.
Case Material	Stainless Steel
Temperature Operating Range / Specified Performance Range / Storage Range	-55 C° to 115 C° / -18 C° to 100 C° / -65 C° to 125 C°
Static Overload	100g
Shock Environmental / Heavy Duty	250g, 11 milliseconds, Half Sine, All Axes / 1000g, 0.5 milliseconds, Half Sine, All Axes
Vibration	50g Pk. Sine All Axes (20 Hz to 2 K Hz)
Humidity	Epoxy Sealed (Weld Seal on QA 1100 if Required)

FIGURE 183

SUNSTRAND QA1100-AA01-12 ACCELEROMETER PERFORMANCE SPECIFICATION

Electrical Specifications

Typical Absolute Linearity	$\pm$0.35%
Theoretical Electrical Angle	300^0
Resistance	5000 Ohms
Resistance Tolerance	$\pm$10%
Output Smoothness	$\pm$0.2% Maximum
Dielectric Withstanding Voltage	750V rms
Insulation Resistance	1000 Megohms Minimum

Mechanical Specifications

Starting Torque, Single Cup	0.2 oz-in Maximum
Mechanical Angle	360^0 Continuous Rotation
Weight, Single Cup	0.25 oz Maximum
Shaft Runout	.002 in/in of Shaft Length
Pilot Runout	.001 in T.1.R. Maximum
Lateral Runout	.001 in T.1.R. Maximum
Shaft Radial Play	.001 in T.1.R. Maximum
Shaft End Play	.005 in T.1.R. Maximum

Figure 184

NE1 55FL-134 POTENTIOMETER PERFORMANCE SPECIFICATIONS

269

PIN FUNCTION

A - Input
B - Output
C + Output
D + Input
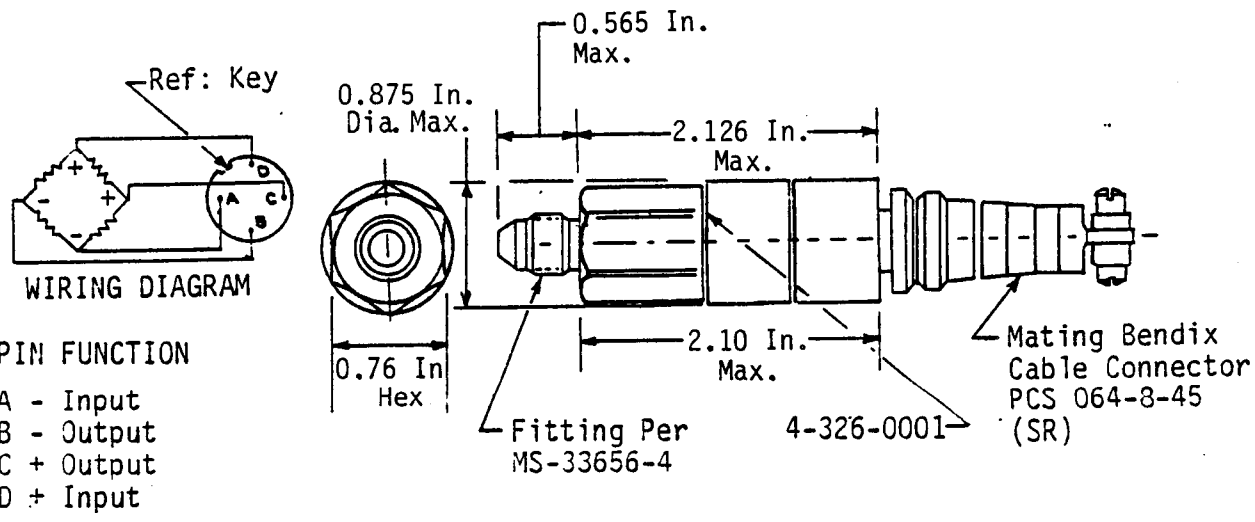
FIGURE 185 - BELL & HOWELL TYPE 4-326-0001 PRESSURE TRANSDUCER OUTLINE
DIMENSIONS

270

Parameter	Specification
Pressure Range	0 to 1500 psi
Pressure Limits	2.5 x rated pressure for 100 psi to 2 x for 3 minutes at room temperature with maximum zero set at 0.5% FR
Rated Excitation	10V DC
Maximum Excitation	12V DC or AC rms without damage
Input Impedance	350 ohms nominal, 330 ohms minimum at 77°F
Sensitivity	40 mV +20% -10% open circuit at rated excitation and 77°F
Residual Unbalance	Within +5% FR at zero pressure, rated excitation and 77°F
Combined Linearity and Hysteresis (Best straight line through calibration points)	Within ±0.5% FR
Natural Frequency	50000 Hz for 5000 psi units decreasing logarithmically with range of 10000 Hz for 25 psi units and below
Output Impedance	350 ohms +10% at 77°F
Resolution	Infinite
Temperature Range, Compensated	-65°F to +250°F
Temperature Range, Operable	-320°F to +300°F
Thermal Zero Shift	Within 0.010% FR/°F over compensated temperature range
Thermal Sensitivity Shift	Within 0.101% FR/°F over compensated temperature range
Static Acceleration (100 g)	0.005% FR/g for 5000 psi units increasing logarithmically with range of 0.05% FR/g for 10 psi
Linear Vibration (35g peak, 5 to 2000 Hz, .5 in D.A. maximum)	0.02% FR/g maximum for 100 psi units and above, increasing logarithmically with range to 0.08% FR/g for 10 psi units
Humidity	Meets MIL-F-5272C Proc 1
Shock	1000 g half-sine-wave pulse for 1 msec without damage
Insulation Resistance	500 megohms minimum at 45V DC over compensated temperature range
Weight (Excluding Mating Connector)	4 ounces maximum
Pressure Media	Compatible with 17-4PH and silver plated 321 SS O-ring
Mating Connector	Furnished, B&H P/N 84479-0004

FIGURE 186

BELL & HOWELL TYPE 4-326-001 PRESSURE TRANSDUCER PERFORMANCE SPECIFICATION

determining proper FSS operation during flight. A random noise generator has been provided to simulate vertical gusts and eliminate the need to search for actual gust inputs. Parameter changes are to be implemented by designated resistor changes for infrequent changes, variable gain controls for rapid changes between flights and in-flight logic-controlled gain changes and parameter gain scheduling.

The ACS electronics are designed with all circuitry on cards. When the cards are removed from the box, no electronics are left in the box except for EMI filters and wire harness.

7.4.1 Signal Conditioning. The uplink commands and downlink signals to be received and transmitted by telemetry are conditioned in the electronics to be compatible with the drone primary telemetry system.

The uplink commands are required to be compatible with the existing telemetry system. The telemetry commands are discrete 0 to 5 VDC Schottky TTL open-collector outputs.

The uplink commands consist of discrete signals and are defined on Figure 187. Figure 188 presents a typical uplink signal conditioning circuit. The circuitry will accept 0 to 5 VDC Schottky TTL open-collector telemetry outputs. The pull-up resistors are provided in the ACS box as shown on Figure 188 to improve noise immunity.

Static and impact pressure signals are included in the electronics and are required for gain scheduling. Access to these signals is through the AFCS interface cable.

The downlink signal requirement is to be compatible with an existing telemetry system. The telemetry system accepts ± 5 VDC analog signals and 0 to 5 VDC discrete signals.

The downlink signals consist of 13 discrete signals defined on Figure 187 and 25 analog signals defined on Figure 189. Figure 190 presents a typical downlink signal conditioning circuit. Additional inverting and noninverting circuits are provided on the downlink circuit cards for use as required. Provisions are provided to allow adjustment of offset and gain for the downlink signals. Multiple inputs are included for versatility.

A single card is used for signal conditioning outputs of the eight-wing accelerometers, PCB 303A03, and the single fuselage accelerometer, Sundstrand QA1100-AA01-12. The card provides the constant current sources required by the PCB accelerometers and the acceleration mixing circuit to provide the necessary vertical motion signals required by the ACS. A two radian washout is provided in each of the wing circuits to block the DC offset of the PCB accelerometer drive power electronics.

272

Launch	On/Off	5 VDC/0 VDC
Start Doublet	On/Off	5 VDC/0 VDC
Start Sweep	On/Off	5 VDC/0 VDC
FSS Excitation Amplifier	Hi/Low	5 VDC/0 VDC
FSS Excitation	Symmetric/Antisymmetric	5 VDC/0 VDC
Gust Excitation 1	On/Off	5 VDC/0 VDC
Gust Excitation 2	On/Off	5 VDC/0 VDC
GLA Gain 1	On/Off	5 VDC/0 VDC
GLA Gain 2	On/Off	5 VDC/0 VDC
RSS Gain 1	On/Off	5 VDC/0 VDC
RSS Gain 2	On/Off	5 VDC/0 VDC
FSS Gain 1	On/Off	5 VDC/0 VDC
FSS Gain 2	On/Off	5 VDC/0 VDC

Figure 187

UPLINK TELEMETRY COMMANDS
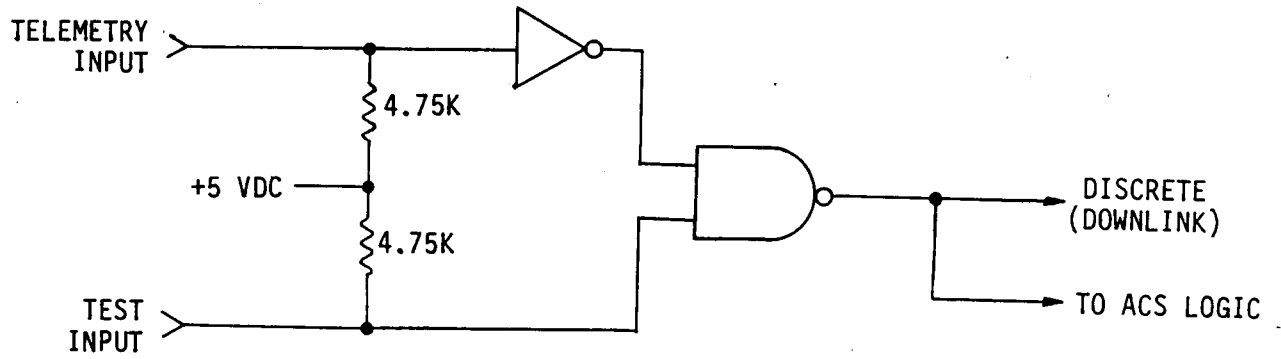
FIGURE 188

UPLINK SIGNAL CONDITIONING CIRCUIT

274

Measurement	Parameter Identi- fication	Range	Signal Level	Factor
Left Outboard Aileron Command	LWFSO	±15 Deg	±5 VDC	3.0 Deg/V
Right Outboard Aileron Command	RWFSO	±15 Deg	±5 VDC	3.0 Deg/V
Inboard Aileron Command	IBAC	+20 Deg -20 Deg	±5 VDC	4.0 Deg/V
Left Outboard Aileron Position	LOPOS	±15 Deg	±5 VDC	3.0 Deg/V
Right Outboard Aileron Position	ROPOS	±15 Deg	±5 VDC	3.0 Deg/V
Left Inboard Aileron Outboard Segment Position	LIOPOS	+20 Deg -10 Deg	+5 VDC -2.5 VDC	4.0 Deg/V
Right Inboard Aileron Outboard Segment Position	RIOPOS	+20 Deg -10 Deg	+5 VDC -2.5 VDC	4.0 Deg/V
Right Inboard Aileron Inboard Segment	RIIPOS	+20 Deg -20 Deg	+5 VDC -2.5 VDC	4.0 Deg/V
Left Outboard Differential Pressure	LODP	±1500 PSI	±5 VDC	300 PSI/V
Right Outboard Differential Pressure	RODP	±1500 PSI	±5 VDC	300 PSI/V
FSS Excitation	FSEXC	±2 Deg	±1 VDC	2 Deg/V
Symmetric Stabilizer SUM	DLTSS	±13 Deg	±5 VDC	2.6 Deg/V
Symmetric Stabilizer RSS	DLRSI	±13 Deg	±5 VDC	2.6 Deg/V
Symmetric Stabilizer GLA	DLGS	±13 Deg	±5 VDC	2.6 Deg/V
$\dot{\theta}_{act} - \dot{\theta}_{pseudo}$	TPMTS	+60 Deg/Sec	+5 VDC	12 Deg/Sec/V
$\ddot{z}_{BS\ 250}$	DBS250	±2 g	±5 VDC	0.4 g/V
Left Wing WBL 82 Front Spar	DLFS82	±20 g	±5 VDC	4 g/V
Left Wing WBL 84 Rear Spar	DLRS84	±20 g	±5 VDC	4 g/V
Right Wing WBL 82 Front Spar	DRFS82	±20 g	±5 VDC	4 g/V
Right Wing WBL 84 Rear Spar	DRRS84	±20 g	±5 VDC	4 g/V
Left Wing WBL 92 Front Spar	DLFS92	±20 g	±5 VDC	4 g/V
Left Wing WBL 92 Rear Spar	DLRS92	±20 g	±5 VDC	4 g/V
Right Wing WBL 92 Front Spar	DRFS92	±20 g	±5 VDC	4 g/V
Right Wing WBL 92 Rear Spar	DRRS92	±20 g	±5 VDC	4 g/V

FIGURE 189

DOWNLINK TELEMETRY SIGNALS
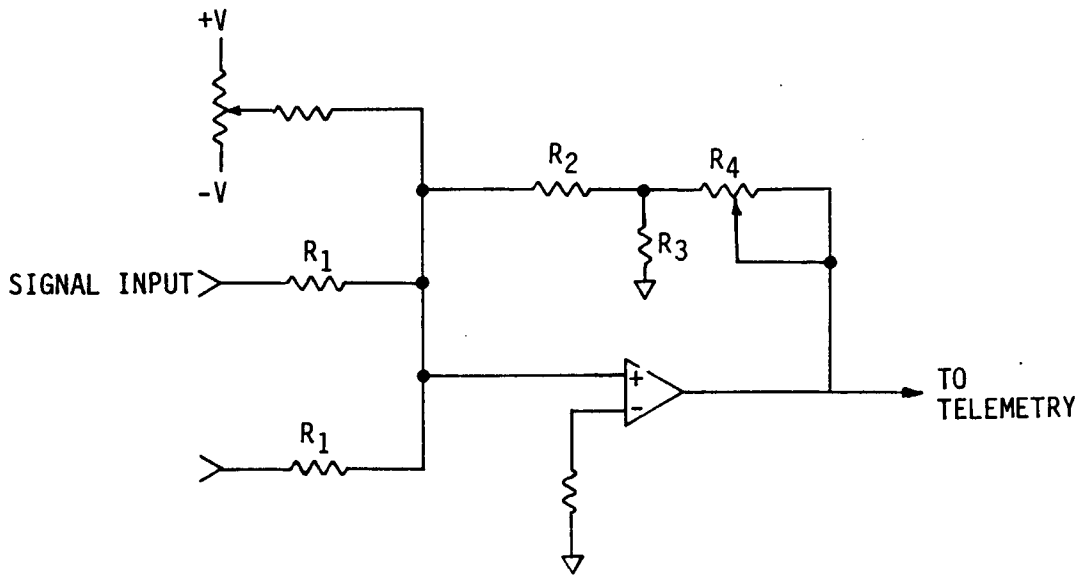
$$\text{GAIN} = \frac{R_2R_3 + R_2R_4 + R_3R_4}{R_1R_3}$$

FIGURE 190

DOWNLINK SIGNAL CONDITIONING CIRCUIT

7.4.2 FSS Signal Shaping. The requirements are summarized below. A functional block diagram of the ARW-2 flutter suppression system is presented on Figure 174. The tolerances on gain and phase as a function of frequency are presented on Figure 191.

Provisions for three discrete inflight gain changes are required. The gains required are nominal, half nominal and twice nominal.

The symmetric FSS sensor-to-surface sinusoidal steady-state phasing is as follows:.

WING MOTION (↑up, ↓down)				Aileron Trailing Edge
Left Wing	Rear Spar	84↓	92↓	
	Front Spar	82↑	92↑	TED
Right Wing	Rear Spar	84↓	92↓	
	Front Spar	82↑	92↑	TED

The antisymmetric FSS sensor-to-surface steady-state sinusoidal phasing is as follows:

WING MOTION (↑up, ↓down)				Aileron Trailing Edge
Left Wing	Rear Spar	84↓	92↓	
	Front Spar	82↑	92↑	TED .
Right Wing	Rear Spar	84↓	92↓	
	Front Spar	82↑	92↑	TEU

The flutter suppression system consists of wing accelerometers driving the ailerons through appropriate symmetric and antisymmetric shaping filters.

The primary function of the FSS electronics is signal shaping. Each shaping filter input and output is brought out to the circuit card connector to facilitate adding a filter if required anywhere in the electronic circuitry. The filters are mechanized by a second order over a second order with the general transfer function:

$$\frac{Eo}{Ei}(S) = \frac{K(S^2 + 2\delta\omega_{n_1} S + \omega_{n_1}^2)}{(S^2 + 2\delta_2\omega_{n_2} S + \omega_{n_2}^2)} \text{ volts/volt}$$

The second order blocks are implemented in state variable form with voltage out of operational amplifiers being proportional to first or second derivatives of the output, or proportional to the output itself. The state variable design approach facilitates relatively easy gain and

277
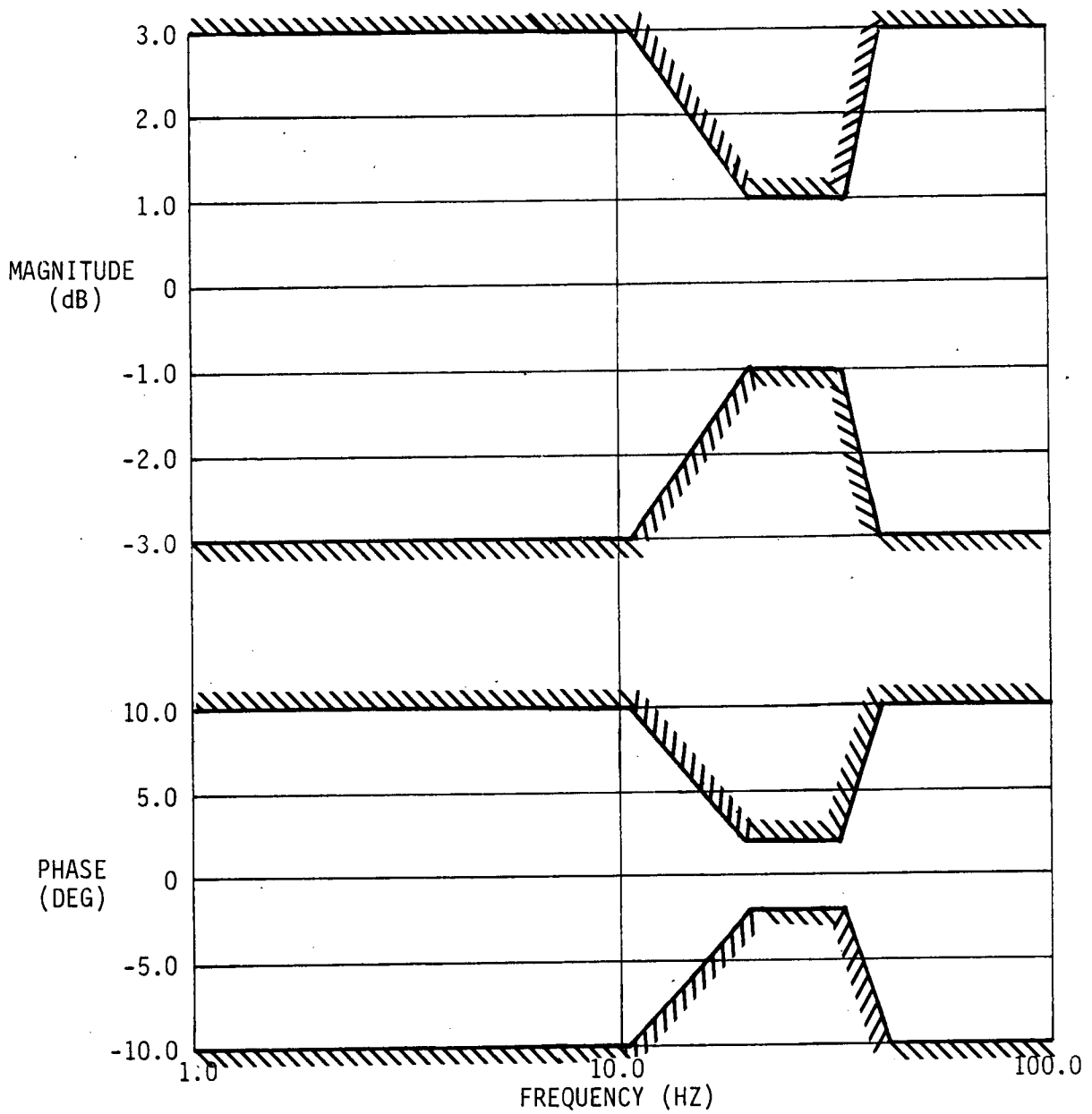
FIGURE 191

ALLOWABLE TOLERANCES FOR FLUTTER SUPPRESSION SYSTEM FILTERS

break point changes throughout the filters. Figure 192 presents a typical filter circuit as implemented in the electronics. The resistor values are calculated as shown on the figure.

The symmetric and antisymmetric filters are mechanized using the same basic circuit described above and shown on Figure 192. The same circuit boards are used for all filters. The transfer functions are given on Figure 174.

The uplink and summing card provides final gains for the FSS system. The inflight gain select and the FSS engage functions are mechanized on this circuit card and receive commands from the uplink logic. The gains on the symmetric and antisymmetric circuit card are adjustable and are shown by the symmetric gains between connections 11J2-6/11J2-11 and 12J2-6/12J2-11 on Figure 174.

7.4.3 FSS Parameter Scheduling. Analyses stipulate that parameter scheduling as a function of Mach number is not required within the flight envelope due to thrust limit actions. Antisymmetric gain scheduling is required to achieve FSS stability to $1.2V_d$, which lies outside the flight envelope. The gain schedule required is shown on Figure 193 with block diagram and proposed schematic of the scheduler shown on Figures 194 and 195, respectively.

7.4.4 GLA Signal Shaping. The requirements are summarized below. A functional block diagram of the ARW-2 gust load alleviation system is presented on Figure 115. The tolerances on gain and phase as a function of frequency are presented on Figure 196.

Provisions for three discrete inflight gain changes are required. The gains required are nominal, half nominal and twice nominal.

The sensor-to-control steady-state phasing is as follows:

BS250	Aileron Trailing Edge	Stabilizer Trailing Edge
UP	TEU	TED

The gust load alleviation system consists of a single servo-type accelerometer located at fuselage BS 250 (wing center section) driving the outboard ailerons and stabilizer through appropriate shaping filters.

The shaping filters are mechanized using the state variable filters identical in form to those used in the flutter suppression system. The transfer functions are given on Figure 174.

The uplink and summing card provides final gains for the GLA system. The inflight gain select and GLA engage functions are mechanized on this circuit card and receive their command from the uplink logic.

279
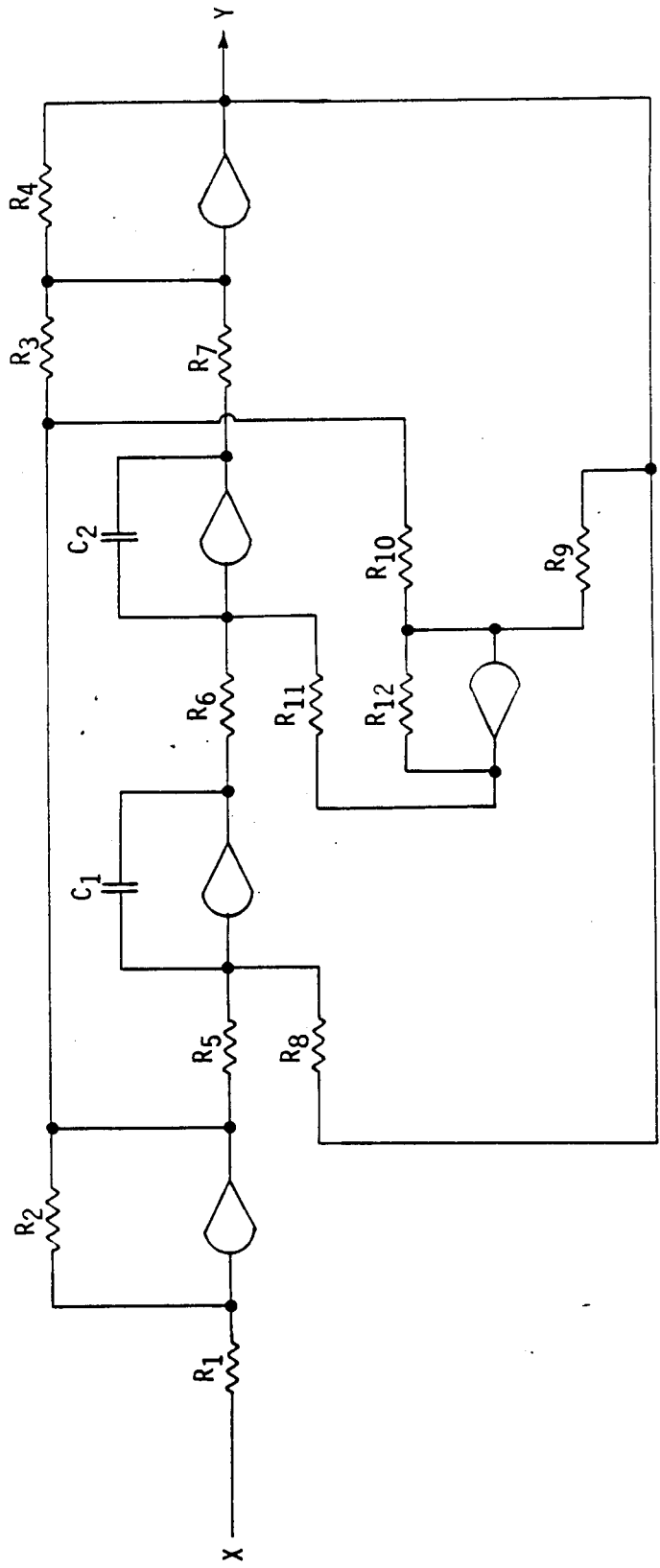
$$\frac{R_4 R_2}{R_3 R_1}\left(s^2 + \frac{R_{12}R_3}{R_{10}R_7}\ \frac{1}{R_{11}C_2}\ s + \frac{R_3}{R_7}\ \frac{1}{R_6C_2}\ \frac{1}{R_5C_1}\right)$$

$$s^2 + \frac{R_4 R_{12}}{R_7 R_9}\ \frac{1}{R_{11}C_2}\ s + \frac{R_4}{R_7}\ \frac{1}{R_8C_1}\ \frac{1}{R_6C_2}$$

FIGURE 192

ANALOG FILTER MECHANIZATION
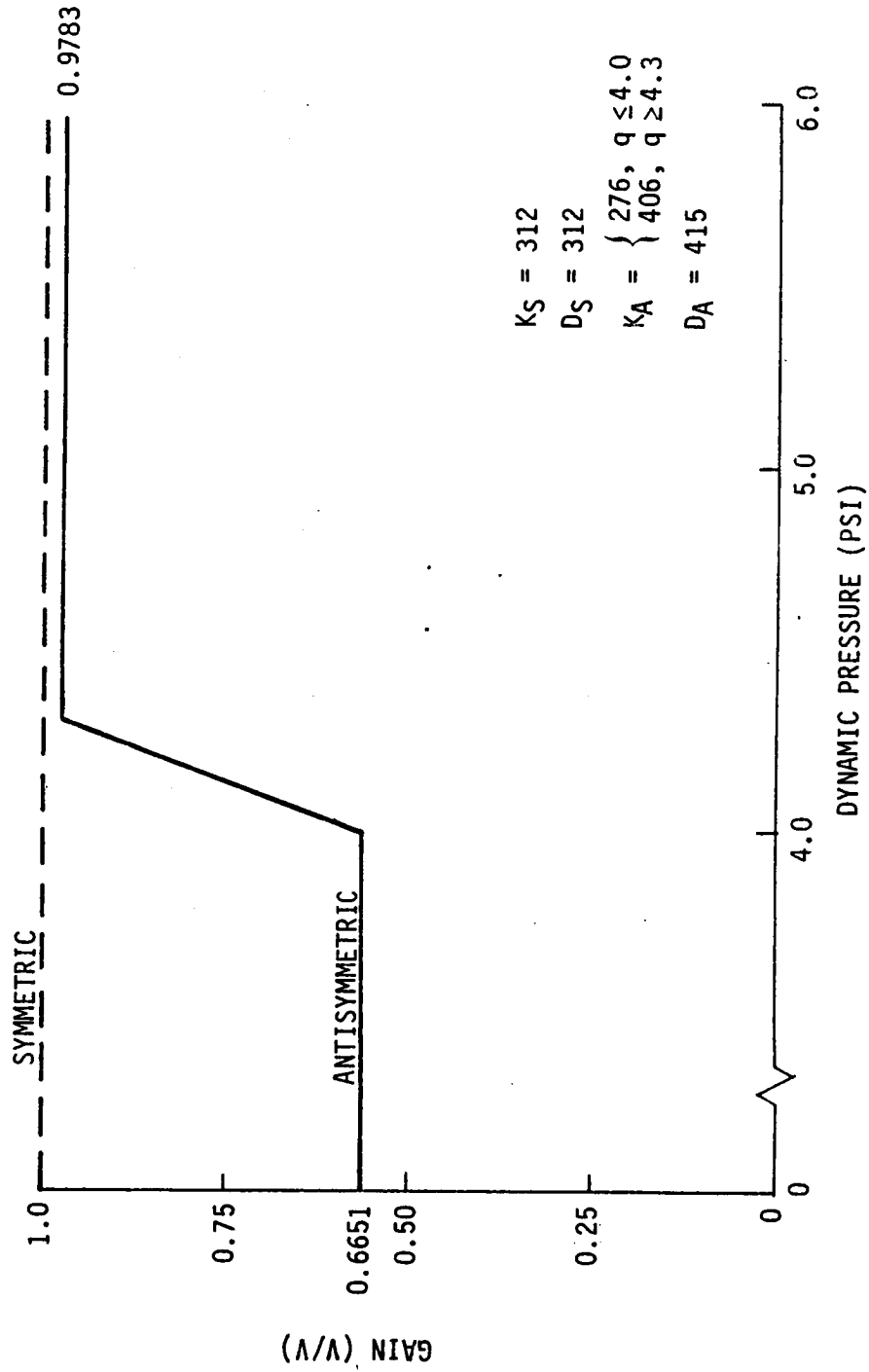
FIGURE 193

PARAMETER SCHEDULING FOR ALL MACH NUMBERS (NOT IMPLEMENTED)
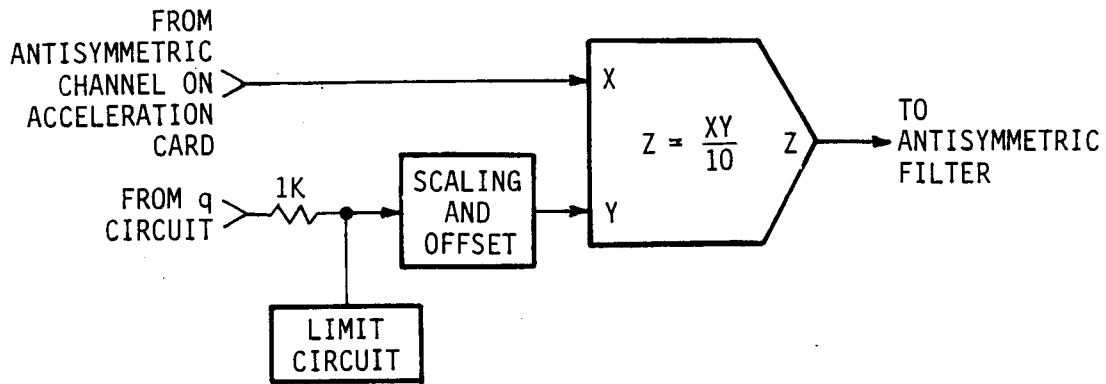
FIGURE 194

BLOCK DIAGRAM OF ANTISYMMETRIC GAIN SCHEDULER

FIGURE 195

PROPOSED SCHEMATIC OF ANTISYMMETRIC GAIN SCHEDULER

283
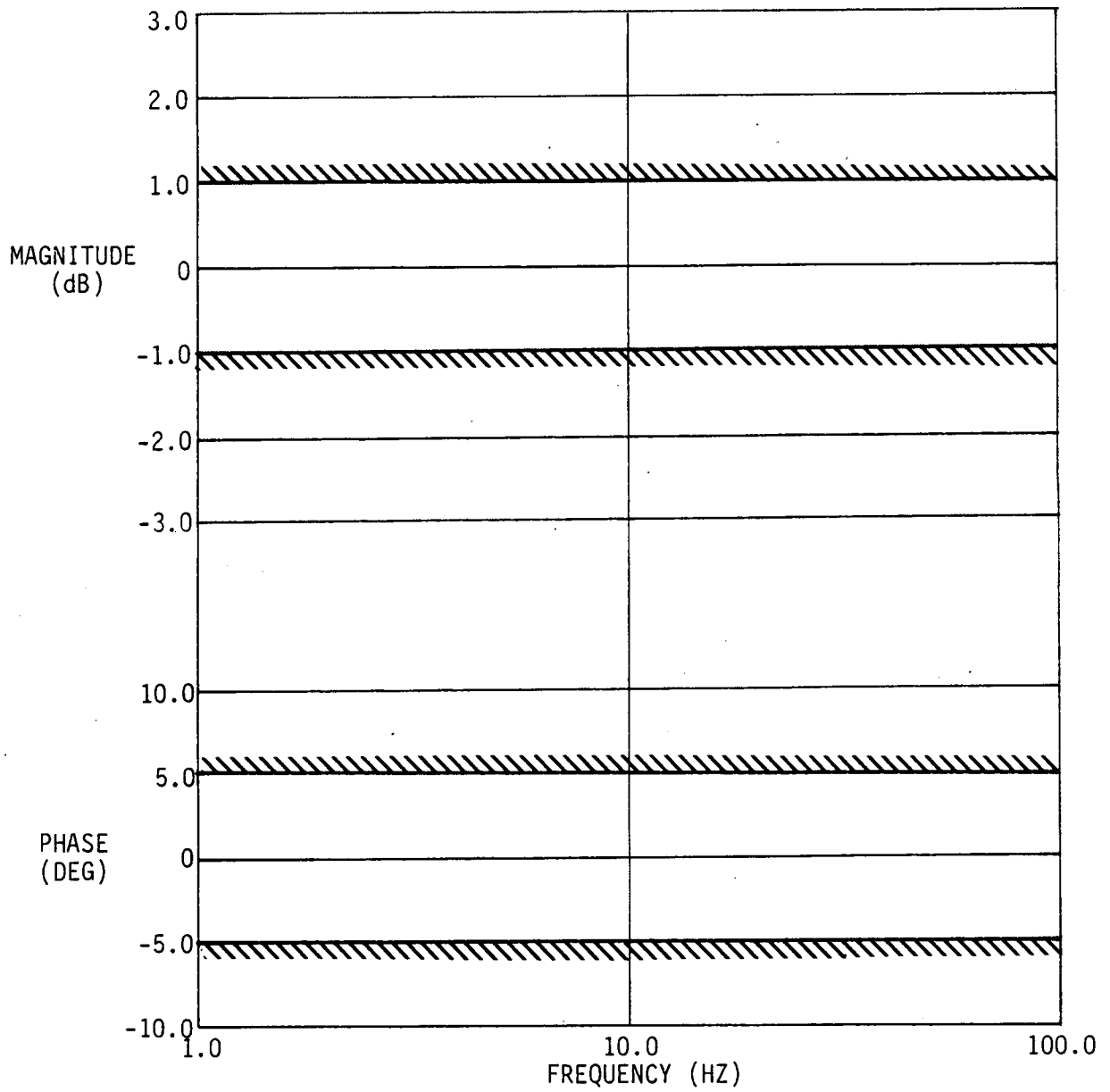
FIGURE 196

ALLOWABLE TOLERANCES FOR GUST LOAD ALLEVIATION SYSTEM FILTERS

7.4.5 GLA Gain Scheduling. The GLA gain scheduler is implemented on the scheduler circuit card. The accelerometer signal is multiplied by the gain schedule derived from the dynamic pressure computing circuit located on the scheduler card. After being scheduled, the signal is split for individual processing in the aileron and stabilizer filters. The maximum on-card scheduled gain is 10.0 as compared to the analytical gain of 13.3. The additional 1.33 factor is picked up downstream of the scheduler.

7.4.6 RSS Signal Shaping. The requirements are summarized below. A functional block diagram of the ARW-2 relaxed static stability system is presented on Figure 135. The gain and phase tolerances as a function of frequency are presented on Figure 197.

Provision for three discrete inflight gain changes is required. The gains required are nominal, half nominal and twice nominal.

The sensor-to-control surface steady-state phasing is as follows:

Pseudo Pitch Rate	Sensor Pitch Rate	Stabilizer Trailing Edge
+(nose up)	-(nose down)	TEU

The relaxed static stability system consists of a pseudo pitch rate command and sensor pitch rate feedback signals driving the stabilizer through appropriate shaping filters.

The shaping filters are mechanized using the state variable filters identical in form to those used in the flutter suppression system. The transfer functions are given on Figure 174. The uplink and summing card provides final gains for the RSS system. The inflight gain select and RSS engage functions are mechanized on this circuit card and receive their commands from the uplink logic.

7.4.7 RSS Gain Scheduling. The RSS gain scheduler is implemented on the Scheduler Circuit Card. The pitch rate error signal is divided by the dynamic pressure signal (derived on the scheduler card). After being scheduled, the signal is passed to the stabilizer filter.

7.4.8 Function Generator. The requirements are summarized below. An aileron square wave doublet and sine wave sweep excitation is required in the onboard ACS electronics box. The design requirements are as follows:

- Sinusoidal Sweep

    - Frequency Range   10 to 40 Hz
    - Duration   10 Seconds
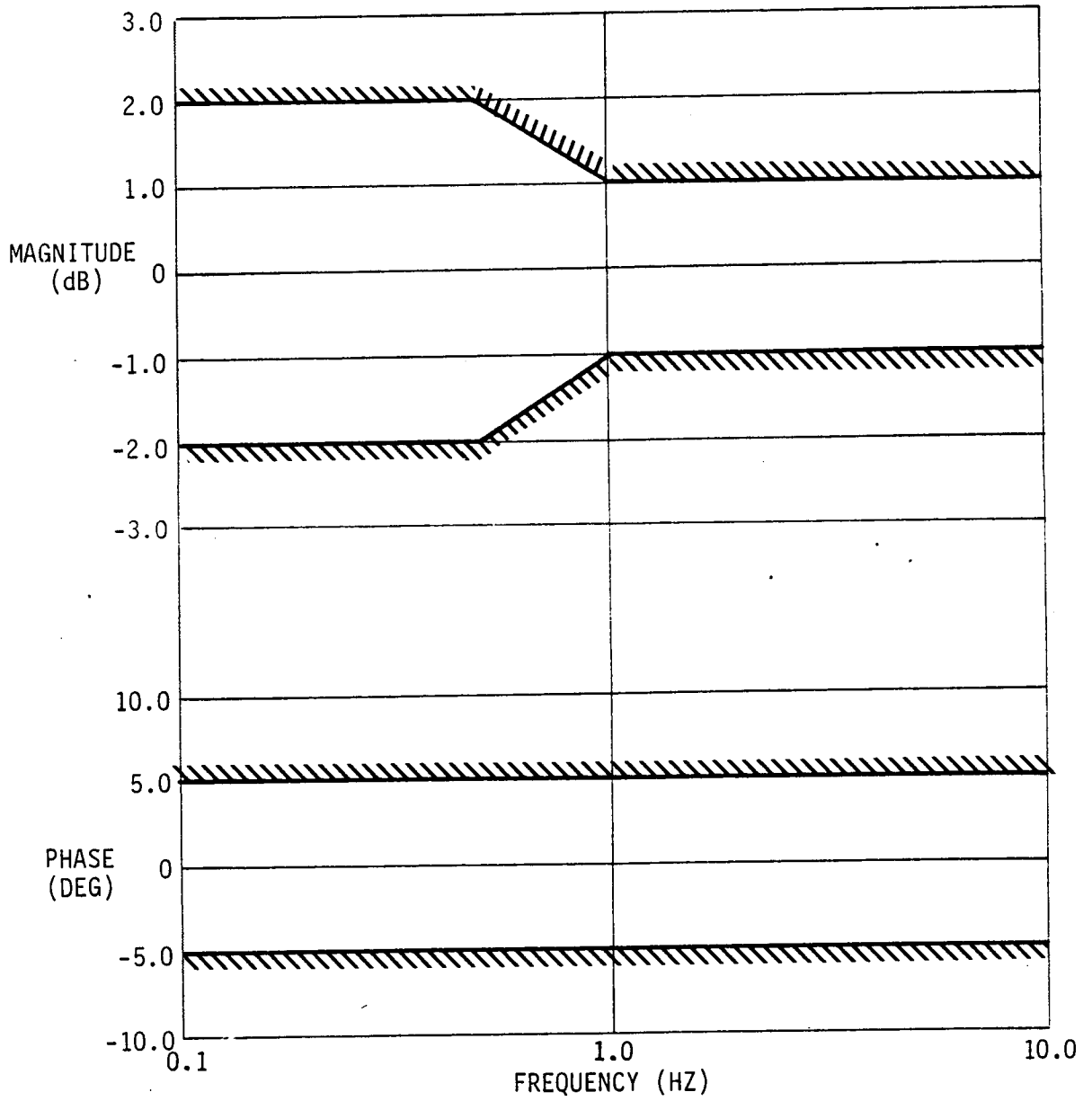
FIGURE 197

ALLOWABLE TOLERANCES FOR RELAXED STATIC STABILITY SYSTEM FILTERS

- Type of Sweep	Antilog
- Amplitudes	2 and 4 Degrees Aileron

●   Square Wave Doublet

- Frequency	25 Hz
- Duration	1 Cycle
- Amplitudes	2 and 4 Degrees Aileron

Provisions are required to allow the sweep and doublet amplitudes to be changed by circuit modification. One uplink command is used to select a "high" or "low" gain for both sweep and doublet.

The excitation generator is required to have capability to select symmetric or antisymmetric inputs to the control surfaces. Automatic reset capability is required when the excitation is disengaged.

The function generator is included in the ACS electronics to provide inputs to the aileron for testing the flutter suppression system. The functional block diagram shown on Figure 198 indicates the theory of operation of the function generator.

The Voltage Controlled Oscillator (VCO) is free running at the start frequency initially set. The output of the multiplier is approximately zero and the analog switch output is zero. The "start logic" will enable the log sweep generator. At the same time, the analog switch is opened and the integrator begins to ramp up and limits at 10 VDC in 0.15 seconds. The sweep function causes the VCO frequency to increase until the stop frequency is reached. At that time, the reset logic is enabled and sweep logic is inhibited causing the integrator to ramp down and the sweep is reset to zero and the analog switch is closed. The frequency is swept according to:

$$f = \frac{af_0}{a - t} = \dot{\Delta}$$

$$a = \frac{f_1 T}{f_1 - f_0}$$

$$\delta = \delta_0 \sin$$

where:

f_0 = start frequency

f_1 = end frequency
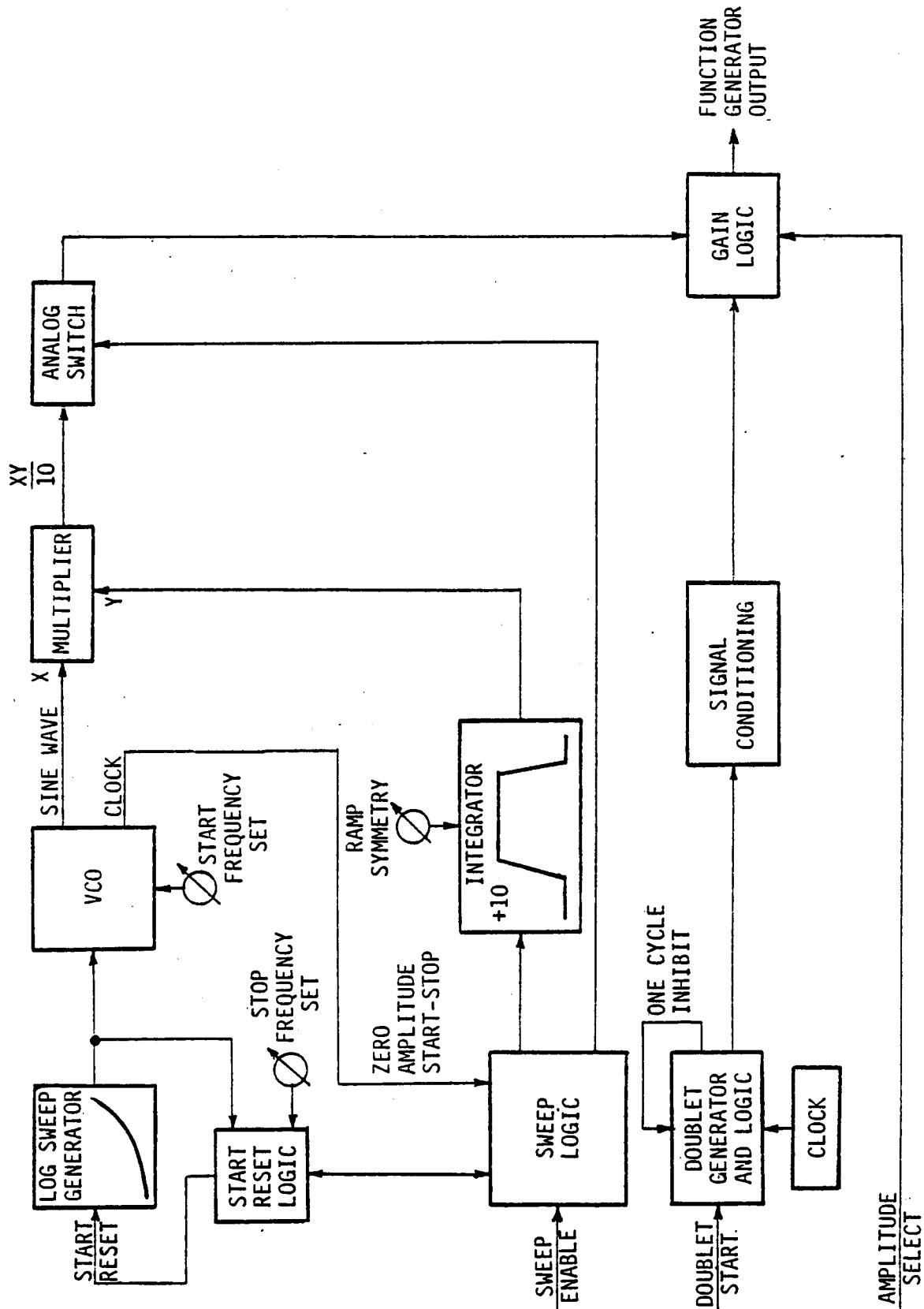
FIGURE 198 FUNCTION GENERATOR BLOCK DIAGRAM

f = output frequency

T = sweep time

δ = control surface angle

δ_0 = maximum control surface angle

Δ = phase angle

The sweep enable signal must be present to allow a complete sweep. Only one sweep can occur for each time the sweep enable signal is applied. The sweep will immediately stop after the amplitude ramps down when the sweep enable signal is removed.

A square wave doublet is generated when the doublet start signal is applied. The period of the doublet is determined by the clock. Only one doublet can occur for each time the doublet start signal is applied. The doublet cannot be terminated before completion once it has been initiated.

An amplitude select signal will cause the amplitude of either the sine wave or the doublet to be increased by a factor of two. Both the sine wave and doublet can be initiated at the same time. A logical "one" (+5 VDC) enables all function generator commands. The sine wave sweep start and stop frequencies may be varied +5.0 Hz. The sweep duration is variable from five to 20 seconds. The soft start and stop provided by the nominal integration ramp time of 0.5 seconds, which can be adjusted over the range 0.7 seconds up and 0.3 seconds down to 0.3 seconds up and 0.7 seconds down. The square doublet is not variable and can be changed only by circuit modification.

The function generator provides a method to input commands to the FSS during flight testing. The function generator when used in conjunction with the FSS gain commands can provide open loop (gain off) or closed loop (gain on) modes of operation.

7.4.9 Pseudo Random Noise Generator. The random noise generator is implemented to provide a method of flight test verification of the gust load alleviation system. The random noise generator is shown on Figure 124. The output of the noise generator is passed through a shaping filter and applied to the inboard aileron servoactuator. The motion of the inboard aileron surfaces produces wing root bending moment power spectral densities similar to those produced by actual vertical gusts. The power spectral densities are compared in Paragraph 6.4.4.

The random noise generator is mechanized with two finite length shift registers whose output sequences are combined to produce a sequence of length equal to the product of the length of each individual shift

register. The random noise generator is capable of producing 174 minutes of uncorrelated noise with the existing 100 hertz clock.

To begin the sequence, each shift register is loaded with a non-zero initial value. The initial value is loaded when the doublet command is depressed. The initial value is constant, therefore the sequence always begins at the same point each time the shift register is loaded.

The digital sequence is passed through a shaping filter mechanized as a state-variable filter. The random-noise then passes through a variable gain amplifier to scale the magnitude of the noise which is then applied to the inboard aileron input.

7.4.10 Servo Electronics. The requirements are summarized below. The final gains were set experimentally. The servoactuator loops are essentially the same for all surfaces. Variance in loop gains and notch filter location is the only difference between the servoactuators.

Six wing control surfaces are powered by hydraulic servoactuators. Each of the servoactuators utilize position feedback. The position feedback signal comes from a potentiometer mounted to measure actuator shaft angular position. The position signal is fed back through gain only.

A load pressure signal is formed from the outputs of the strain gage bridge and pressure transducers plumbed into the hydraulic lines between the servovalve control ports and actuator. The load pressure signal is sent to the drone telemetry system for inflight monitoring.

Notch filters were added to reduce the effects of actuator and fluid modes on the servoactuator stability. The outboard valve driver required three notches located at 402 Hz, 90 Hz and 72 Hz. The outboard segment of the inboard aileron required two notches located at 285 Hz and 72 Hz. The inboard segment required a single notch at 72 Hz.

The servoamplifier is required to accept two input commands, one from the Drone Active Control Electronics (DACE) and one from the ground support equipment. The outboard aileron command from the DACE includes FSS symmetric and antisymmetric filter outputs, closed loop GLA/MLA filter output and function generator output.

The inboard aileron command from the DACE includes the open-loop MLA output and the random noise generator output. The feedback signals to the servoamplifier are provided by the surface position potentiometers. Provision for surface position nulling, feedback gain adjustment and forward path gain adjustment are included.

Pressure feedback is not required for servoactuator stabilization. Pressure feedback is provided for control surface load monitoring via the drone telemetry system. The pressure feedback signal processing electronics is located on the valve driver circuit card.

7.5 ACS Modifications

7.5.1 Pre-Delivery Modifications. Washouts are added in front of and behind the FSS shaping filters eliminating the propagation of DC offsets through the shaping filters and servoactuators.

Addition of the altitude hold input to the RSS integrator to the Primary Control System (PCS) was made after the circuit boards had been populated.

The 0.7 gain increase in the RSS system when the Backup Control System (BCS) is engaged was made after the circuit boards had been populated.

7.5.2 Post-Delivery Modifications. During hardware-in-the-loop simulation at NASA-Langley, a number of changes were made. These changes are not reflected in the data package sent with the DACE. Changes were made in RSS and GLA stabilizer feedback loops. The changes made were as follows:

a. GLA stabilizer gain was incorrect. Investigation yielded two items:

(1) GLA Filter #3 had a gain 2.8 V/V more than that indicated by the block diagram in the operations manual. R101 on the 39-28047 circuit card was changed from 280K to 100K to reduce the excess gain. This change brought the implementation in line with the block diagram of the operations manual.

(2) The block diagram of the operations manual showed the stabilizer deflection to a 1g input to be 0.874^{o}. The deflection to a 1g input called out by the analysis should be 0.798^{o}. R46 on the 39-28031 circuit card was changed from 1.21 Meg to 1.10 Meg to reduce the excess gain. This change brought the implementation in line with the analysis block diagram of the Preliminary Design Review (PDR).

b. RSS Gain Scheduler was found to limit at the MLA condition (0.42M at 10,000 feet, approximately 127 psf).

(1) R53 on the 39-28043 scheduler circuit card was changed from 20K to 4.99K. This change reduces the signal amplitude going into the divider by a factor of 4.

(2) R95 on the 39-28051 RSS filter circuit card was changed from 115K to 459K. This change increased the filter gain by 4, which results in no net gain change in the RSS path.

7.6 Active Control System Power. The power required for the ACS is obtained from Crestronics, Inc., DC to DC converters utilizing the 28 VDC power onboard the drone. The power levels required and converter part numbers are:

Voltage	Current	Part Number
+15 VDC	600 mA	PS 333-24-30-BCT
+ 5 VDC	800 mA	PS 333-24-10-BCT
+24 VDC	130 mA	PS 333-24-26-FW

The external DC to DC converters were selected to furnish the excitation power to the ACS electronics to eliminate as much wasted power within the electronics box as possible. The manufacturer's specifications are as listed on Figure 199.

The converters are rated for one ampere continuous and the currents listed above are the actual requirements. The three converters are mounted side by side on to 6.0 x 10.0 x 1.0 inch aluminum extrusion. Dow Corning PC 340 white silicone grease was used for mounting to reduce the temperature coefficient. The assembled unit has a weight of 5 pounds and is to be mounted beneath the ACS electronics box. A 6.7 microfarad 35 VDC capacitor was installed at the 28 VDC input and one at each power output.

7.7 Active Control System Electrical Wiring. All drone wiring was done by NASA with Boeing furnishing the wing wire. Figure 200 shows the DAST ARW-2 ACS wiring. All wire furnished for the wiring bundles except the power cable which is described below was either two, three, or four wire shielded 22 AWG M27500 MIL specification wire, except the servo valve wire which was unshielded.

Six primary cable harnesses are required for interfacing the ACS electronics with the drone. One cable interfaces to the DC to DC converter power unit, one cable will interface with the drone AFCS box, one connects to the uplink receiver, one interfaces with the downlink transmitter, two connects the ACS electronics box to each wing semispan cable harness through the pressure bulkhead. Provisions are also included for a ground test cable to permit day-to-day preflight checkout of the ACS.

Figures 201 through 207 list the connector pin assignments. The power cable power wire size is 18 AWG and includes one each for each voltage level. The power returns are wire size 16 AWG and includes one each for the +26 VDC and five for the +5 VDC and +15 VDC. This power cable attaches to the terminal strip provided on the converter power unit. The 28 VDC main ships power also attaches to the designated terminals on this terminal strip.

```
Model Number:  PS 333

      Case Units:              1.5 x 3.0 inch Extruded Aluminum
      $I_{IN\ MAX}$:            2.00 Amps
      Case Depth:              3.80 inch
      Mounting Dimension:      2.50 x 1.20 inch

Rectifier System

      FW  - Full Wave
      BCT - Bridge Center Tap

Regulated Units
  Input

      $E_{IN\ MAX}$ - Voltage:  Customer may specify any input voltage
                                between 11 and 28 volts DC.  $E_{IN\ MIN}$ is
                                the lowest input voltage applied.  This
                                should include the lowest excursion of
                                ripple.

      $\Delta E_{IN}$  - Input Voltage Differential:  The normal $\Delta E_{IN}$ is
                                4 volts.  For $\Delta E_{IN}$ greater than 4 volts
                                derate the input current to

                                $$I\ Derate = \frac{(6)I_{IN\ MAX}}{\Delta E_{IN} + 2}$$

      $I_{IN\ MAX}$ - Input Current:  2.0 amps
                      $I_{IN\ MAX}$ shall be derated for $\Delta E_{IN}$ greater than 4 volts.
                      $I_{IN\ MAX}$ shall be derated for $70^{0}C$ operation
                      (Derate input $I_{IN\ MAX}$ 1%/$^{0}C$)

  Output

      $E_{0}$ - Voltage:  The output voltage is screwdriver adjustable
                          from -20% to +5% of nominal.

      $P_{0}$ - Power:    The output power is expressed as:

                          $(0.7E_{IN\ MAX}I_{IN}) - I_{0}$

  Regulation

      Line:          0.01%/$\Delta$input volt
      Temperature:   (0.02%/$^{0}C$) -2mV/$^{0}C$
      Load:          100% to 10%
                     For 30 VDC and over:  3% Regulation
                     For 29 VDC and under:

                          % Regulation = $(0.02E_{0} + 0.3)/(E_{0} \times 10^{-2})$

Efficiency:  $\dfrac{(0.75E_{IN}I_{IN}) - I_{0}}{E_{IN}I_{IN} \times 10^{-2}}$
```

FIGURE 199

CRESTRONICS MODEL PS 333 DC TO DC CONVERTS PERFORMANCE SPECIFICATIONS

C - 4
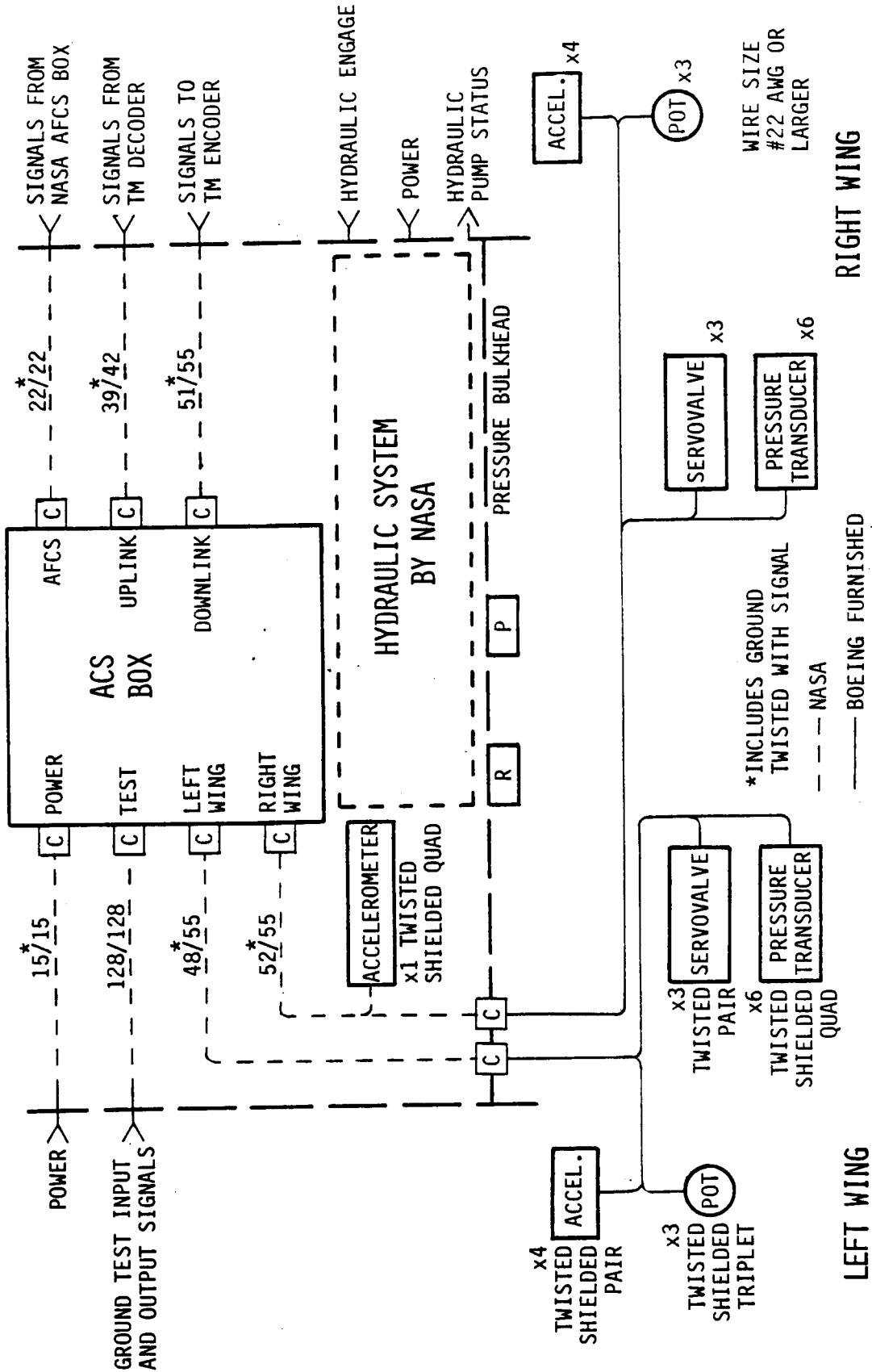
FIGURE 200

DAST ARW-2 ACS WIRING

Box Mount Receptacle JTP02RE-14-15P
Cable Connector JT06RE-14-15S

Connector and Pin	Signal Name and Type	Wiring Format	Signal Range	Scale Factor	Adjustment Offset	Gain
J2-A	+26 VDC HI		N/A	N/A		
-B	Power Return		N/A	N/A		
-C	+15 VDC HI		N/A	N/A		
-D	+15 VDC HI		N/A	N/A		
-E	-15 VDC HI		N/A	N/A		
-F	-15 VDC HI		N/A	N/A		
-G	+5 VDC HI		N/A	N/A		
-H	+5 VDC HI		N/A	N/A		
-J	-5 VDC HI		N/A	N/A		
-K	-5 VDC HI		N/A	N/A		
-L	Power Return		N/A	N/A		
-M	Power Return		N/A	N/A		
-N	Power Return		N/A	N/A		
-P	Power Return		N/A	N/A		
-R	Power Return		N/A	N/A		

FIGURE 201

POWER INPUT CONNECTOR (J2)

295

Box Mount Receptacle JTP02RE-16-42P   Cable Connector JT06RT-16-42S

Connector and Pin	Signal Name and Type	Wiring Format	Signal Range	Scale Factor	Adjustment Offset	Gain
J5-1	Launch	Twisted Shielded Pair	TTL	Active HI		
-2	Ground					
-3	Start Doublet	Twisted Shielded Pair	TTL	Active HI		
-4	Ground					
-5	Start Sweep	Twisted Shielded Pair	TTL	Active HI		
-6	Ground					
-7	FSS Excitation Amplitude	Twisted Shielded Pair	TTL	Active HI		
-8	Ground					
-9	FSS Excitation Symmetric/Asymmetric	Twisted Shielded Pair	TTL	Active HI		
-10	Ground					
-11	Gust Excitation 1	Twisted Shielded Pair	TTL	Active HI		
-12	Ground					
-13	Gust Excitation 2	Twisted Shielded Pair	TTL	Active HI		
-14	Ground					
-15	FSS Gain 1	Twisted Shielded Pair	TTL	Active HI		
-16	Pair					
-17	FSS Gain 2	Twisted Shielded Pair	TTL	Active HI		
-18	Ground					
-19	GLA Gain 1	Twisted Shielded Pair	TTL	Active HI		
-20	Ground					
-21	GLA Gain 2	Twisted Shielded Pair	TTL	Active HI		
-22	Ground					
-23	RSS Gain 1	Twisted Shielded Pair	TTL	Active HI		
-24	Ground					
-25	RSS Gain 2	Twisted Shielded Pair	TTL	Active HI		
-26	Ground					
-27	Spare		N/A	N/A		
-28	Spare		N/A	N/A		
-29	Launch Confirm	Shielded Single	TTL	Active LO		
-30	Doublet Confirm	Shielded Single	TTL	Active LO		

FIGURE 202

UPLINK CONNECTOR (J5)

296

Connector and Pin	Signal Name and Type	Wiring Format	Signal Range	Scale Factor	Adjustment Offset	Gain
J5-31	Sweep Confirm		TTL	Active LO		
-32	FSS Amplitude Confirm		TTL	Active LO		
-33	FSS SYM/ASYM Confirm		TTL	Active LO		
-34	Gust Excitation #1 Confirm		TTL	Active LO		
-35	Gust Excitation #2 Confirm		TTL	Active LO		
-36	FSS Gain #1 Confirm		TTL	Active LO		
-37	FSS Gain #2 Confirm		TTL	Active LO		
-38	GLA Gain #1 Confirm		TTL	Active LO		
-39	GLA Gain #2 Confirm		TTL	Active LO		
-40	RSS Gain #1 Confirm		TTL	Active LO		
-41	RSS Gain #2 Confirm		TTL	Active LO		
-42	Spare					

FIGURE 202 (CONCLUDED)

UPLINK CONNECTOR (J5)

Box Mount Receptacle JTP02RE-16-35SD   Cable Connector JT06RT-16-35PD

Connector and Pin	Signal Name and Type	Wiring Format	Signal Range	Scale Factor	Adjustment Offset Gain
J1-1	Outboard Torquer Coil Hi	Twisted Pair	±10mA	0.338 in^3/sec/mA	Used only with MOOG Series 31 Servovalve
-2	Outboard Torquer Coil Lo				
-3	+5 VDC S.G. Excitation	Twisted Shielded Triplet	0-5V		
-4	Strain Gage Output				
-5	Ground				
-6	+5 VDC Outboard C1 P.T. Excitation	Twisted Shielded Quad	40mV	26.67 µV/psi	
-7	Outboard C1 Pressure Hi				
-8	Outboard C1 Pressure Lo				
-9	-5 VDC Outboard C1 P.T. Excitation				
-10	+5 VDC Outboard C1 P.T. Excitation	Twisted Shielded Quad	40mV	26.67 µV/psi	
-11	Outboard C2 Pressure Hi				
-12	Outboard C2 Pressure Lo				
-13	-5 VDC Outboard C2 P.T. Excitation				
-14	+15 VDC Outboard Pot Excitation	Twisted Shielded Triplet	2.0V	0.1 V/deg	
-15	Outboard Position				
-16	-15 VDC Outboard Pot Excitation				
-17	Outbd Seg.Inbd.Ail. Torquer Coil Hi	Twisted Pair	±10mA	0.110 in^3/sec/mA	
-18	Outbd Seg.Inbd.Ail. Torquer Coil Lo				
-19	+5 VDC Outbd Seg.Inbd.Ail.C1 P.T.Exc	Twisted Shielded Quad	40mV	26.67 µV/psi	
-20	Outbd Seg.Inbd.Ail. C1 Pressure Hi				
-21	Outbd Seg.Inbd.Ail. C1 Pressure Lo				
-22	-5 VDC Outbd Seg. Inbd.Ail.C1 P.T.Exc				
-23	+5 VDC Outbd Seg. Inbd.Ail.C2 P.T.Exc	Twisted Shielded Quad	40mV	26.67 µV/psi	
-24	Outbd Seg.Inbd.Ail.C2 Pressure Hi				
-25	Outbd Seg.Inbd.Ail.C2 Pressure Lo				
-26	-5 VDC Outbd Seg.Inbd.Ail.C2 P.T.Exc				
-27	+15 VDC Outbd Seg.Inbd.All. Pot Excit	Twisted Shielded Triplet	2.0V	0.1 V/deg	
-28	Outbd Seg. Inbd. Ail. Position				
-29	-15 VDC Outbd Seg.Inbd.Ail.Pot Excit				
-30	Inbd Seg.Inbd.Ail. Torquer Coil Hi	Twisted Pair	±10mA	0.110 in^3/sec/mA	

FIGURE 203

RIGHT WING CONNECTOR (J1)

Connector and Pin	Signal Name and Type	Wiring Format	Signal Range	Scale Factor	Adjustment Offset	Gain
J1-31	Inbd Seq.Inbd.Ail. Torquer Coil Lo	Twisted Pair				
-32	+5 VDC Inbd Seq.Inbd.Ail.Cl P.T. Exc					
-33	Inbd Seq.Inbd.Ail. Cl Pressure Hi	Twisted Shielded Quad	40mV	26.67 μV/psi		
-34	Inbd Seq.Inbd.Ail. Cl Pressure Lo					
-35	-5 VDC Inbd Seq.Inbd.Ail.Cl P.T.Exci					
-36	+5 VDC Inbd Seq.Inbd.Ail.C2 P.T.Exci					
-37	Inbd Seq.Inbd.Ail.C2 Pressure Hi	Twisted Shielded Quad	40mV	26.67 μV/psi		
-38	Inbd Seq.Inbd.Ail.C2 Pressure Lo					
-39	-5 VDC Inbd Seq.Inbd.Ail.C2 P.T.Exci					
-40	+15 VDC Inbd Seq.Inbd.Ail.Pot Excit	Twisted Shielded Triplet	2.0V	0.1 V/deg		
-41	Inbd Seq. Inbd. Ail. Position					
-42	-15 VDC Inbd Seq.Inbd.Ail.Pot Excit					
-43	ZWBL 82 Front Spar	Twisted Shielded Pair		10 mV/g		
-44	Ground					
-45	ZWBL 84 Rear Spar	Twisted Shielded Pair		10 mV/g		
-46	Ground					
-47	ZWBL 92 Front Spar	Twisted Shielded Pair		10 mV/g		
-48	Ground					
-49	ZWBL 92 Rear Spar	Twisted Sheidled Pair		10 mV/g		
-50	Ground					
-51	ZBS250 (From Sensor)			0.25 V/g		
-52	Ground					
-53	+15 VDC (Sensor Excitation)					
-54	-15 VDC (Sensor Excitation)					
-55	Spare					

FIGURE 203 (CONCLUDED)

RIGHT WING CONNECTOR (J1)

299

Box Mount Receptacle JTP02RE-16-35SA   Cable Connector JT06RT-16-35PA

Connector and Pin	Signal Name and Type	Wiring Format	Signal Range	Scale Factor	Adjustment Offset	Gain
J6-1	Outboard Torquer Coil Hi (A)	Twisted Pair	±10mA	0.338 in³/sec/mA		
-2	Outboard Torquer Coil Lo (A)					
-3	+5 VDC S.G. Excitation	Twisted Shielded Triplet	0-5V		Used Only With MOOG Series 31 Servovalve	
-4	Strain Gage Output (A)					
-5	Ground					
-6	+5 VDC Outboard C1 P.T. Excitation	Twisted Shielded Quad	±40mV	26.67 µV/psi		
-7	Outboard C1 Pressure Hi (A)					
-8	Outboard C1 Pressure Lo (A)					
-9	-5 VDC Outboard C1 P.T. Excitation					
-10	+5 VDC Outboard C2 P.T. Excitation	Twisted Shielded Quad	±40mV	26.67 µV/psi		
-11	Outboard C2 Pressure Hi (A)					
-12	Outboard C2 Pressure Lo (A)					
-13	-5 VDC Outboard C2 P.T. Excitation					
-14	+15 VDC Outboard Pot Excitation	Twisted Shielded Triplet	±2.0V	0.1 V/deg		
-15	Outboard Position (A)					
-16	-15 VDC Outboard Pot Excitation					
-17	Outbd Seq.Inbd.Ail. Torquer Coil Hi (A)	Twisted Pair	±10mA	0.11 in³/sec/mA		
-18	Outbd Seq.Inbd.Ail. Torquer Coil Lo (A)					
-19	+5 VDC Outbd Seq.Inbd.Ail.C1 P.T.Excit (A)	Twisted Shielded Quad	±40mV	26.67 µV/psi		
-20	Outbd Seq.Inbd.Ail.C1 Pressure Hi (A)					
-21	Outbd Seq.Inbd.Ail.C1 Pressure Lo (A)					
-22	-5 VDC Outbd Seq.Inbd.Ail.C1 P.T.Excit (A)					
-23	+5 VDC Outbd Seq.Inbd.Ail.C2 P.T.Excit (A)	Twisted Shielded Quad	±40mV	26.67 µV/psi		
-24	Outbd Seq.Inbd.Ail.C2 Pressure Hi (A)					
-25	Outbd Seq.Inbd.Ail.C2 Pressure Lo (A)					
-26	-5 VDC Outbd Seq.Inbd.Ail.C2 P.T.Excit (A)					
-27	+15 VDC Outbd Seq.Inbd.Ail.Pot Excit	Twisted Shielded Triplet	±2.0V	0.1 V/deg		
-28	Outbd Seq.Inbd.Ail. Position (A)					
-29	-15 VDC Outbd Seq.Inbd.Ail.Pot Excit					
-30	Inbd.Seq.Inbd.Ail. Torquer Coil Hi (A)	Twisted Pair	±10mA	0.11 in³/sec/mA		

FIGURE 204

LEFT WING CONNECTOR (J6)

Connector and Pin	Signal Name and Type	Wiring Format	Signal Range	Scale Factor	Adjustment Offset	Gain
J6-31	Inbd Seg.Inbd.Ail. Torquer Coil Lo (A)	Twisted Pair				
-32	+5 VDC Inbd Seq.Inbd.Ail.C1 P.I. Exci					
-33	Inbd Seq.Inbd.Ail.C1 Pressure Hi (A)	Twisted Shielded Quad	±40mV	26.67 µV/psi		
-34	Inbd Seq.Inbd.Ail.C1 Pressure Lo (A)					
-35	-5 VDC Inbd Seq.Inbd.Ail.C1 P.I. Exci					
-36	+5 VDC Inbd Seq.Inbd.Ail.C2 P.I. Exci					
-37	Inbd Seq.Inbd.Ail.C2 Pressure Hi (A)	Twisted Shielded Quad	±40mV	26.67 µV/psi		
-38	Inbd Seq.Inbd.Ail.C2 Pressure Lo (A)					
-39	-5 VDC Inbd Seq.Inbd.Ail.C2 P.I. Exci					
-40	+15 VDC Inbd Seq.Inbd.Ail.Pot Excit	Twisted Shielded Triplet				
-41	Inbd Seq. Inbd. Ail. Position (A)		±2.0V	0.1 V/deg		
-42	-15 VDC Inbd Seq.Inbd.Ail. Pot Excit					
-43	ZWBL 82 Front Spar	Twisted Shielded Pair		10 mV/g		
-44	Ground					
-45	ZWBL 84 Rear Spar	Twisted Shielded Pair		10 mV/g		
-46	Ground					
-47	ZWBL 92 Front Spar	Twisted Shielded Pair		10 mV/g		
-48	Ground					
-49	ZWBL 92 Rear Spar	Twisted Shielded Pair		10 mV/g		
-50	Ground					
-51	Spare					
-52	Spare					
-53	Spare					
-54	Spare					
-55	Spare					

FIGURE 204 (CONCLUDED)

LEFT WING CONNECTOR (J6)

Box Mount Receptacle JTP02RE-16-35S | | | | Cable Connector JT06RT-16-35P
| | | | | Adjustment |

Connector and Pin	Signal Name and Type	Wiring Format	Signal Range	Scale Factor	Offset	Gain
J4-1	Left Outboard Aileron Command	Twisted Shielded Pair	±5V	3.0 deg/V		
-2	Ground					
-3	Left Outboard Aileron Position	Twisted Shielded Pair	±5V	3.0 deg/V		
-4	Ground					
-5	Right Outboard Aileron Command	Twisted Shielded Pair	±5V	3.0 deg/V		
-6	Ground					
-7	Right Outboard Aileron Position	Twisted Shielded Pair	±5V	3.0 deg/V		
-8	Ground					
-9	Inboard Aileron Command	Twisted Shielded Pair	±5V	4.0 deg/V		
-10	Ground					
-11	LIBOBS Position	Twisted Shielded Pair	±5V	4.0 deg/V		
-12	Ground					
-13	LIBIB Position	Twisted Shielded Pair	±5V	4.0 deg/V		
-14	Ground					
-15	Left Outboard Diff. Pressure	Twisted Shielded Pair	±5V	300 psi/V		
-16	Ground					
-17	Right Outboard Diff. Pressure	Twisted Shielded Pair	±5V	300 psi/V		
-18	Ground					
-19	B.S. 250 Acceleration	Twisted Shielded Pair	±5V	0.4 g/V		
-20	Ground					
-21	FSS Excitation	Twisted Shielded Pair	±5V	2.0 deg/V		
-22	Ground					
-23	Spare					
-24	Ground					
-25	Left Wing Z̈WBL 82 Front Spar	Twisted Shielded Pair	±5V	2.0 g/V		
-26	Common					
-27	Left Wing Z̈WBL 84 Rear Spar	Twisted Shielded Pair	±5V	2.0 g/V		
-28	Common					
-29	Right Wing Z̈WBL 82 Front Spar	Twisted Shielded Pair	±5V	2.0 g/V		
-30	Common					

FIGURE 205

DOWNLINK CONNECTOR (J4)

Connector and Pin	Signal Name and Type	Wiring Format	Signal Range	Scale Factor	Adjustment Offset	Gain
J4-31	Right Wing ZWBL 84 Rear Spar	Twisted Shielded Pair	±5V	2.0 g/V		
-32	Common					
-33	Left Wing ZWBL 92 Front Spar	Twisted Shielded Pair	±5V	2.0 g/V		
-34	Ground					
-35	Left Wing ZWBL 92 Rear Spar	Twisted Shielded Pair	±5V	2.0 g/V		
-36	Ground					
-37	Right Wing ZWBL 92 Front Spar	Twisted Shielded Pair	±5V	2.0 g/V		
-38	Ground					
-39	Right Wing ZWBL 92 Rear Spar	Twisted Shielded Pair	±5V	2.0 g/V		
-40	Ground					
-41	Symmetric Stabilizer Sum	Twisted Shielded Pair	±5V	0.25 V/deg		
-42	Ground					
-43	Symmetric Stabilizer RSS (RSS)	Twisted Shielded Pair	±5V	0.25 V/deg		
-44	Ground					
-45	Symmetric Stabilizer GLA	Twisted Shielded Pair	±5V	0.25 V/deg/sec		
-46	Ground					
-47	Qs-Ap	Twisted Shielded Pair	±5V	0.25 V/deg		
-48	Ground					
-49	RIBOBS Position		±5V	4.0 deg/V		
-50	Ground					
-51	RIBIBS Position		±5V	4.0 deg/V		
-52	Ground					
-53	Spare		±5V	0.25 V/deg		
-54	Spare (GND)		N/A	N/A		
-55	Spare (GND)					

FIGURE 205 (CONCLUDED)

DOWNLINK CONNECTOR (J4)

Box Mounted Receptacle JTP02RE-12-35P · Cable Connector JT06RT-12-35S

Connector and Pin	Signal Name and Type	Wiring Format	Signal Range	Scale Factor	Adjustment Offset	Gain
J3-1	NLA Inboard Ail. Command (Primary)	Twisted Shielded Pair	±10V	0.5V/degrees		
-2	Ground					
-3	Pseudo Pitch Rate Command (Primary)	Twisted Shielded Pair				
-4	Ground					
-5	RSS Integrator Input (Backup)	Twisted Shielded Pair	±10V	N/A		
-6	Ground					
-7	Sensor Pitch Rate	Twisted Shielded Pair				
-8	Ground					
-9	Sensor Ambient Pressure	Twisted Shielded Pair	±5V	4.54 mV/psf		
-10	Ground					
-11	Sensor Impact Pressure	Twisted Shielded Pair	±5V	6.67 mV/psf		
-12	Ground					
-13	Dynamic Pressure (ACS)	Twisted Shielded Pair	±10V	10 mV/psf		
-14	Ground					
-15	Symmetric Stabilizer (ACS)	Twisted Shielded Pair				
-16	Ground					
-17	Altitude Hold Integrator Input		±10V	N/A		
-18	Ground					
-19	Backup AFCS CMD		TTL	Active III		
-20	Ground					
-21	ZBS250			2.5 V/g		
-22	Ground					

FIGURE 206

NASA AFCS CONNECTOR (J3)

Connector and Pin	Signal Name and Type		Wiring Format	Signal Range	Scale Factor	Adjustment Offset	Gain
J7-1	RRS84	Test In	All Wires Unshielded Singles	±40mV	40 mV/g		
-2	RFS82	Test In		±40mV	40 mV/g		
-3	LRS84	Test In		±40mV	40 mV/g		
-4	LFS82	Test In		±40mV	40 mV/g		
-5	RRS92	Test In		±40mV	40 mV/g		
-6	RFS92	Test In		±40mV	40 mV/g		
-7	LRS92	Test In		±40mV	40 mV/g		
-8	LFS92	Test In		±40mV	40 mV/g		
-9	TBS250	Test In		±1.0V	.25 V/g		
-10	RRS84	Downlink		±5.0V	2 g/V	9R17	9R16
-11	RFS82	Downlink		±5.0V	2 g/V	9R14	9R15
-12	LRS84	Downlink		±5.0V	2 g/V	9R4	9R3
-13	LFS82	Downlink		±5.0V	2 g/V	9R1	9R2
-14	RRS92	Downlink		±5.0V	2 g/V	9R21	9R20
-15	RFS92	Downlink		±5.0V	2 g/V	9R18	9R19
-16	LRS92	Downlink		±5.0V	2 g/V	9R8	9R7
-17	LFS92	Downlink		±5.0V	2 g/V	9R5	9R6
-18	PPRO1	Test Out		±5.0V	0.333 deg/sec/V	8R29	8R9
-19	DBS250	Downlink		±5.0V	0.8 g/V	9R12	9R13
-20	SAC	Test Out		N/A	N/A		
-21	AAC	Test Out		N/A	N/A		
-22	LOTIC	Test In		±7.5V	0.5 V/deg	----	5R8
-23	LODPR	Test Out		±1.5V	0.967 mV/psi	5R10	5R11
-24	LOPOSO	Test Out		±7.5V	2.0 deg/V		
-25	LOVLO	Test Out		±5.0V	2 mA/V		
-26	FSS Test Relay	Test In		0,+24	+24V Enable		
-27	LOPOSI	Test In		±1.5	0.1 V/deg		
-28	RODPR	Test Out		±1.5V	0.967 mV/psi	----	6R8
-29	ROPOSO	Test Out		±7.5	2.0 deg/V	6R10	6R11
-30	ROVLO	Test Out		±5.0	2 mA/V		
-31	LFSAC	Test Out		±7.5	2 deg/V		
-32	SFO1	Test Out		N/A	N/A		
-33	LOCI1	Test In		±0.04	26.7 µV/psi		
-34	LOCI2	Test In		±0.04	26.7 µV/psi		
-35	ROPOSI	Test In		±1.5	0.1 V/deg		

FIGURE 207

TEST CONNECTOR (J7)

Connector and Pin	Signal Name	Type	Wiring Format	Signal Range	Scale Factor	Adjustment Offset	Adjustment Gain
J7-36	SF02	Test Out		N/A	N/A	----	12RB
-37	AF01	Test Out		N/A	N/A		
-38	ROCI1	Test In		±0.04	26.7 µV/psi		
-39	ROCI2	Test In		±0.04	26.7 µV/psi		
-40	ROTIC	Test In		±7.5	0.5 V/deg	---	12RB
-41	AF02	Test Out		N/A	N/A		
-42	SFI1	Test In		±7.5	0.5 V/deg		
-43	AFI1	Test In		±7.5	0.5 V/deg		
-44	SF03	Test Out		N/A	N/A		
-45	AF03	Test Out		N/A	N/A		
-46	LWFSO	Downlink		±5.0	3 deg/V	7R39	7R19
-47	RWFSO	Downlink		±5.0	3 deg/V	7R40	7R20
-48	GLO1	Test Out		±10.0	0.4 g/V	9R10	9R11
-49	TIBCO	Test In		-10,+5	0.5 V/deg	7R38	7R18
-50	LOBPOS	Downlink		±5.0	3 deg/V	7R36	7R16
-51	LODP	Downlink		±5.0	300 psi/V	7R37	7R17
-52	ROBPOS	Downlink		±5.0	32 deg/V	7R35	7R15
-53	RODP	Downlink		±5.0	300 psi/V	8R35	8R15
-54	DKGLA	Downlink		±5.0	1 Unit/V		
-55	GSO2	Test Out		N/A	N/A		
-56	TSS	Test Out		±10.0	1.3 deg/V		
-57	LIIVLO	Test Out		±5.0	2 mA/V		
-58	GAO1	Test Out		N/A	N/A		
-59	TDPO	Test Out		0,+10	100 psf/V		
-60	GSO1	Test Out		N/A	N/A		
-61	DLGS	Downlink		±5.0	1.3 deg/V	8R33	8R13
-62	TPPR	Test In		±10.0	0.6 deg/sec/V		
-63	SPRO1	Test Out			1.2 deg/sec/V	8R28	8R8
-64	LIIPOSI	Test In		±1.5	0.1 V/deg		
-65	RSEO	Test Out		N/A	N/A		
-66	TRSID	Downlink		±5.0	2.6 deg/V		
-67	TSPR	Test In		±10.0	0.8333 V/deg/sec		
-68	RF01	Test Out		N/A	N/A		
-69	DLRSI	Downlink		±5.0	2.6 deg/V	8R31	8R11
-70	DLTSS	Downlink		±5.0	2.6 deg/V	8R32	8R12

FIGURE 207 (CONTINUED)

TEST CONNECTOR (J7)

Connector and Pin	Signal Name and Type		Wiring Format	Signal Range	Scale Factor	Adjustment Offset	Gain
J7-71	LTTPOS	Downlink		±5.0	4.0 deg/V	8R27	8R7
-72	LIIDP	Downlink		±5.0	300 psi/V	8R24	8R4
-73	TMLCMD	Test In		+5,-10	0.5 V/deg		
-74	TAMP	Test In		±5.0	4.54 mV/psf		
-75	TIMP	Test In		±5.0	6.67 mV/psf		
-76	DDP	Downlink		±5.0	100 psf/V	8R39	8R19
-77	IBAC	Downlink		±5.0	4.0 deg/V	7R34	7R14
-78	LIOPOS	Downlink		±5.0	4.0 deg/V	7R33	7R13
-79	RIOPOS	Downlink		±5.0	4.0 deg/V	8R30	8R10
-80	FSEXC	Downlink		±5.0	2.0 deg/V	8R36	8R16
-81	LIOTIC	Test In		±7.5	0.5 V/deg		
-82	Return Pwr	Test Out		N/A	N/A		
-83	+26 VDC Pwr	Test Out		N/A	N/A		
-84	+15 VDC Pwr	Test Out		N/A	N/A		
-85	-15 VDC Pwr	Test Out		N/A	N/A		
-86	+5 VDC Pwr	Test Out		N/A	N/A		
-87	-5 VDC Pwr	Test Out		N/A	N/A		
-88	GLO2	Test Out		N/A	N/A		
-89	RGLA	Test Out		0,+10	1 V/Unit		
-90	RFSAC	Test Out		±7.5	2 deg/V		
-91	IBUSS	Test In		N/A	N/A		
-92	RIODTI	Test In		±2.87	5.8 mV/psi	4R16	4R18
-93	RIOPOSO	Test Out		±7.5	2 deg/V	4R7	4R6
-94	RIIDTI	Test In		±2.87	5.8 mV/psi		
-95	RIIPOSO	Test Out		±7.5	2.0 deg/V		
-96	LIODTI	Test In		±2.87	5.8 mV/psi	3R16	3R18
-97	LIOPOSO	Test Out		±7.5	2 deg/V		
-98	LIIDTI	Test In		±2.87	5.8 mV/psi	3R7	3R6
-99	LIIPOSO	Test Out		±7.5	2 deg/V		
-100	LIOVLO	Test Out		±5.0	2 mA/V		
-101	Backup AFCS CMD	Test In		TTL	Active 10		
-102	LIOPOSI	Test In		±1.5	0.1 V/deg		
-103	RSS1	Downlink		TTL	Active 10	7R28	7R8
-104	LIODP	Downlink		±5.0	300 psi/V	8R25	8R5
-105	RSS2	Downlink		TTL	Active 10	7R27	7R7

FIGURE 207 (CONTINUED)

TEST CONNECTOR (J7)

Connector and Pin	Signal Name and Type		Wiring Format	Signal Range	Scale Factor	Adjustment Offset	Gain
J7-106	RIITIC	Test In		±7.5	0.5 V/deg	7R30	7R10
-107	GLA1	Downlink		TTL	Active LO		
-108	RIIVLO	Test Out		±5.0	2 mA/V	7R29	7R9
-109	GLA2	Downlink		TTL	Active LO		
-110	RIIPOSI	Test In		±1.5	0.1 V/deg	7R32	7R12
-111	FSS1	Downlink		TTL	Active LO	8R26	8R6
-112	RIIPOS	Downlink		-10,+5	4.0 deg/V	7R31	7R11
-113	FSS2	Downlink		TTL	Active LO	8R23	8R3
-114	RIIDP	Downlink		±5.0	300 psi/V	7R26	7R6
-115	Launch	Downlink		TTL	Active LO		
-116	RIOTIC	Test In		±7.5	0.5 V/deg	7R24	7R4
-117	ESS_SYM	Downlink		TTL	Active LO		
-118	RIOVLO	Test Out		±5.0	2 mA/V	7R25	7R5
-119	FSS AMP (HI)	Downlink		TTL	Active LO		
-120	RIOPOSI	Test In		±1.5	0.1 V/deg	7R40	7R20
-121	Doublet	Downlink		TTL	Active LO	8R22	8R2
-122	RIODP	Downlink		±5.0	300 psi/V	7R21	7R1
-123	Sweep	Downlink		TTL	Active LO		
-124	Talt Hold	Test In		±10V	N/A		
-125	GUST1	Downlink		TTL	Active LO	7R23	7R3
-126	Noise Gen	Test Out		N/A	μ=0 σ²=1		
-127	GUST2	Downlink		TTL	Active LO	7R22	7R2
-128	LIITIC	Test In		±7.5V	0.5 V/deg		

FIGURE 207 (CONCLUDED)

TEST CONNECTOR (J7)

7.8 Special Test Equipment.

7.8.1 ACS Tester. The ACS tester is used for conducting quick look
functional tests during preflight and troubleshooting to the card level.
Figure 208 shows a front view of this tester.

When a malfunction in the ACS electronics is identified the ACS tester
will be used to isolate the problem down to the card level. This tester
can be used with the electronics installed in the drone as well as for
bench tests. The ACS tester was also used during initial checkout and
later to check out the electronics at NASA Langley. ACS tester includes
all uplink commands, provisions for externally monitoring of downlink
signals, filter and function generator inputs and wing control surface
positions. Also provisions for external inputs to the system shaping
filters and servo valve drivers are included for open and closed loop
preflight testing.

7.8.2 Electronics Card Tester. The electronics card tester will be
used to isolate faults to individual components on the circuit cards.
This tester was required during electronics checkout and will be
required on site during the integration of the ACS into the drone
vehicle and during electronics checkout and will be required on site
during the integration of the ACS into the drone vehicle and during the
flight tests. The electronics card tester includes all necessary test
points and input capability to test all card types. External power must
be provided. Figure 209 shows the front view of this tester.

7.8.3 Additional Ground Support Equipment. In addition to the two
testers described above, other ground support equipment will be
required. This miscellaneous equipment is tabulated:

● 28 VDC Ground Power

● Hydraulic System Service Cart

● Strip Chart Recorder

● Transfer Function Analyzer

● Function Generator

● Variable $\pm$10 VDC Input

● Digital Voltmeter

● Oscilloscope
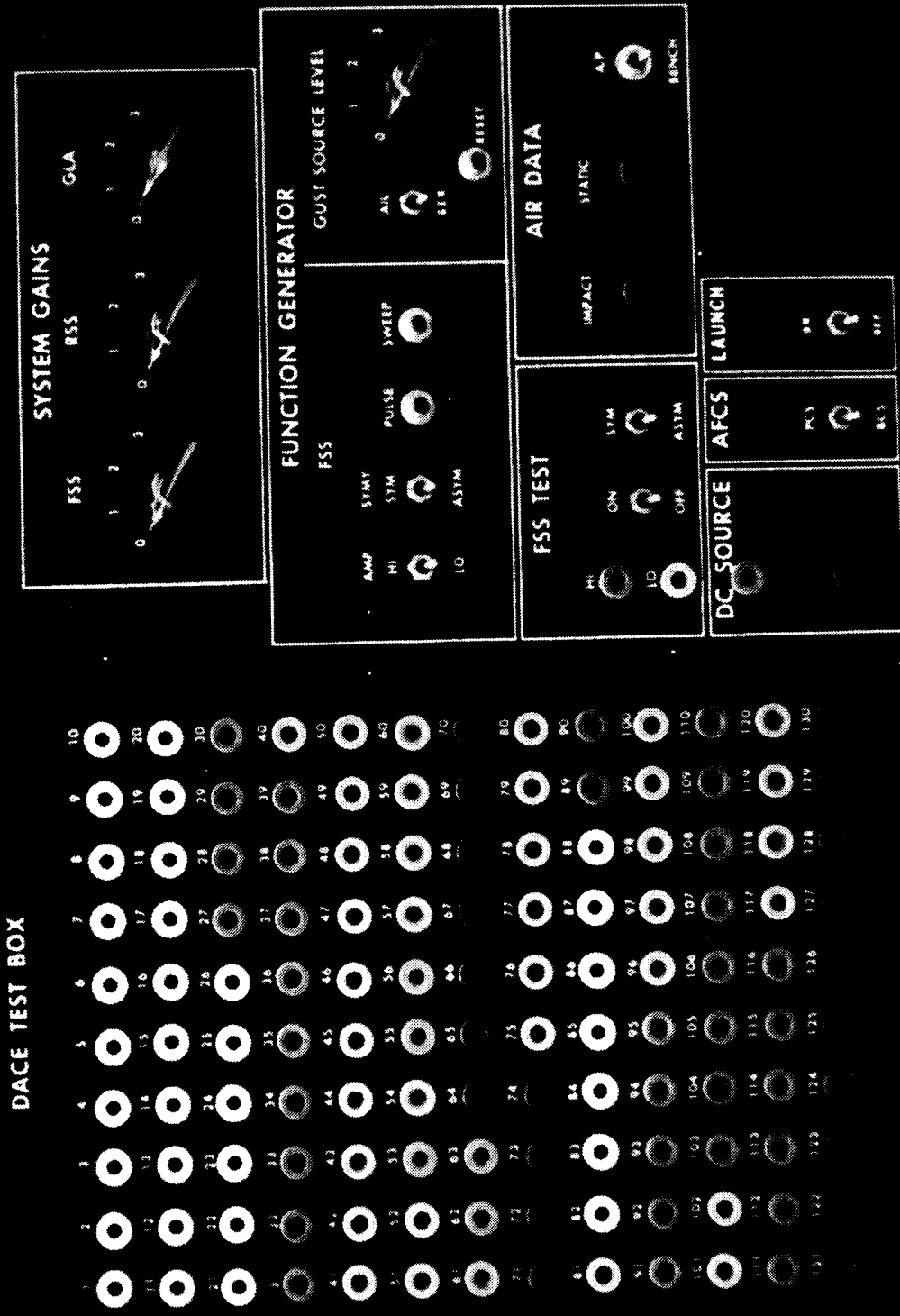
FIGURE 208   ACS TESTER

310
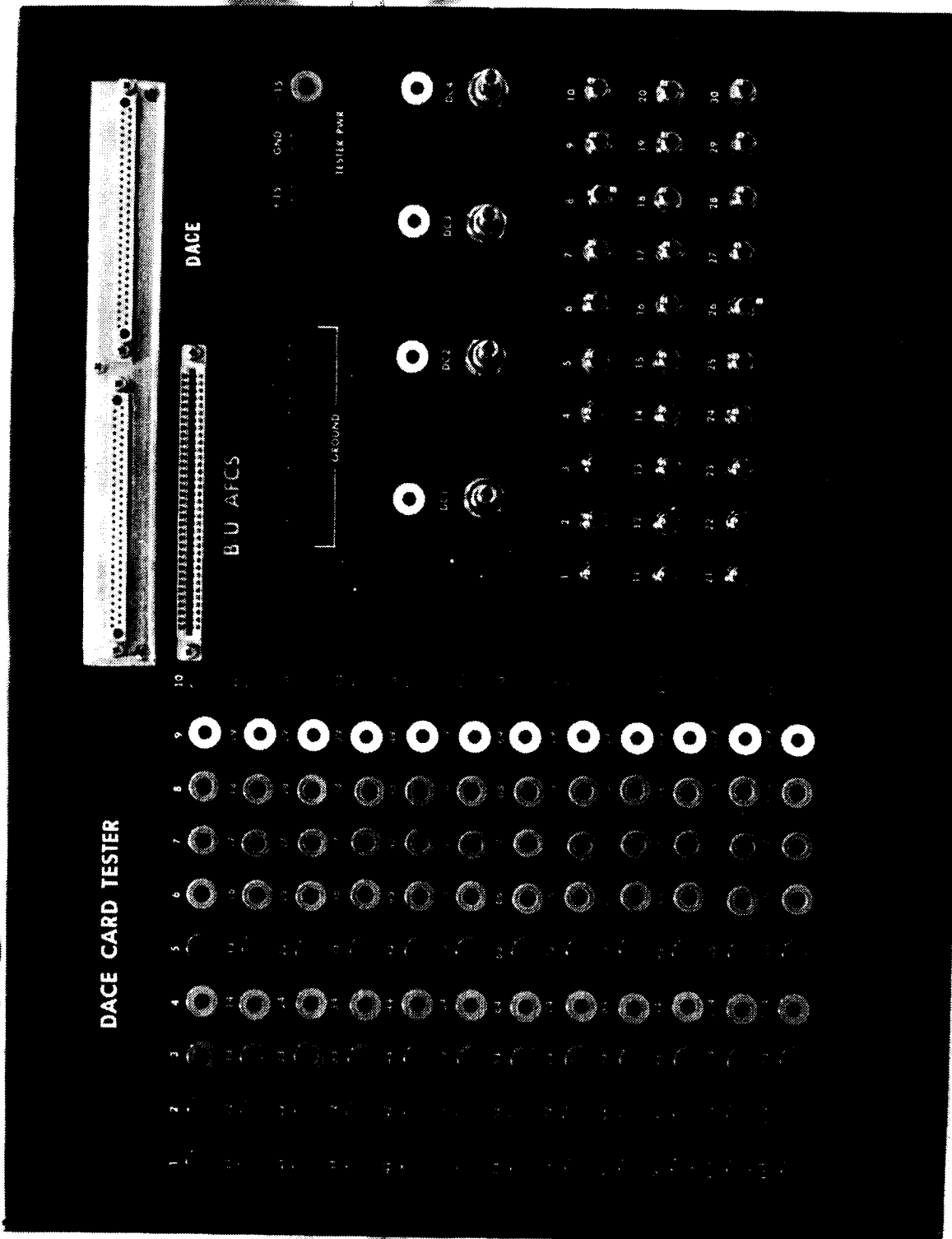
382-766

FIGURE 209   ELECTRONICS CARD TESTER

(This page intentionally left blank)

312

8. COMPONENT FABRICATION

All components required for installation of the flutter suppression system in the drone test vehicle except for the hydraulic power supply, actuators and filter were either fabricated or procured and shipped to NASA. The active control system electronics were fabricated by Boeing engineering staff laboratory personnel following drawings prepared by electronic design personnel.

Components purchased for installation in the drone were selected to operate within an aircraft environment and, in general, are of the quality normally utilized in military equipment. Some components were obtained in plant from Boeing stocks to minimize expenditures for components that had to be procured.

The following paragraphs discuss fabrication and assembly of the electronic components required for the DAST ARW-2 active control system installation.

8.1 Electronic Components. The electronics box is a Boeing designed and fabricated aluminum box 18.1 inches long, 4.85 inches wide and 4.58 inches high with extending mounting flanges making an overall length of 22.5 inches and an overall width of 5.4 inches. The box weighs 13.75 pounds. The box internal wiring is type AWG-22. Figures 210 through 213 present photographs of the fabricated electronics box. The box includes provisions for 18 circuit cards. Figure 213 shows 18 cards installed. Assembly drawings were included with the hardware delivery.

8.2 Spares. Spare components provided to NASA as backup to the DAST ARW-2 active control system components are shown in Figure 214. The spare components listed were specified by NASA.
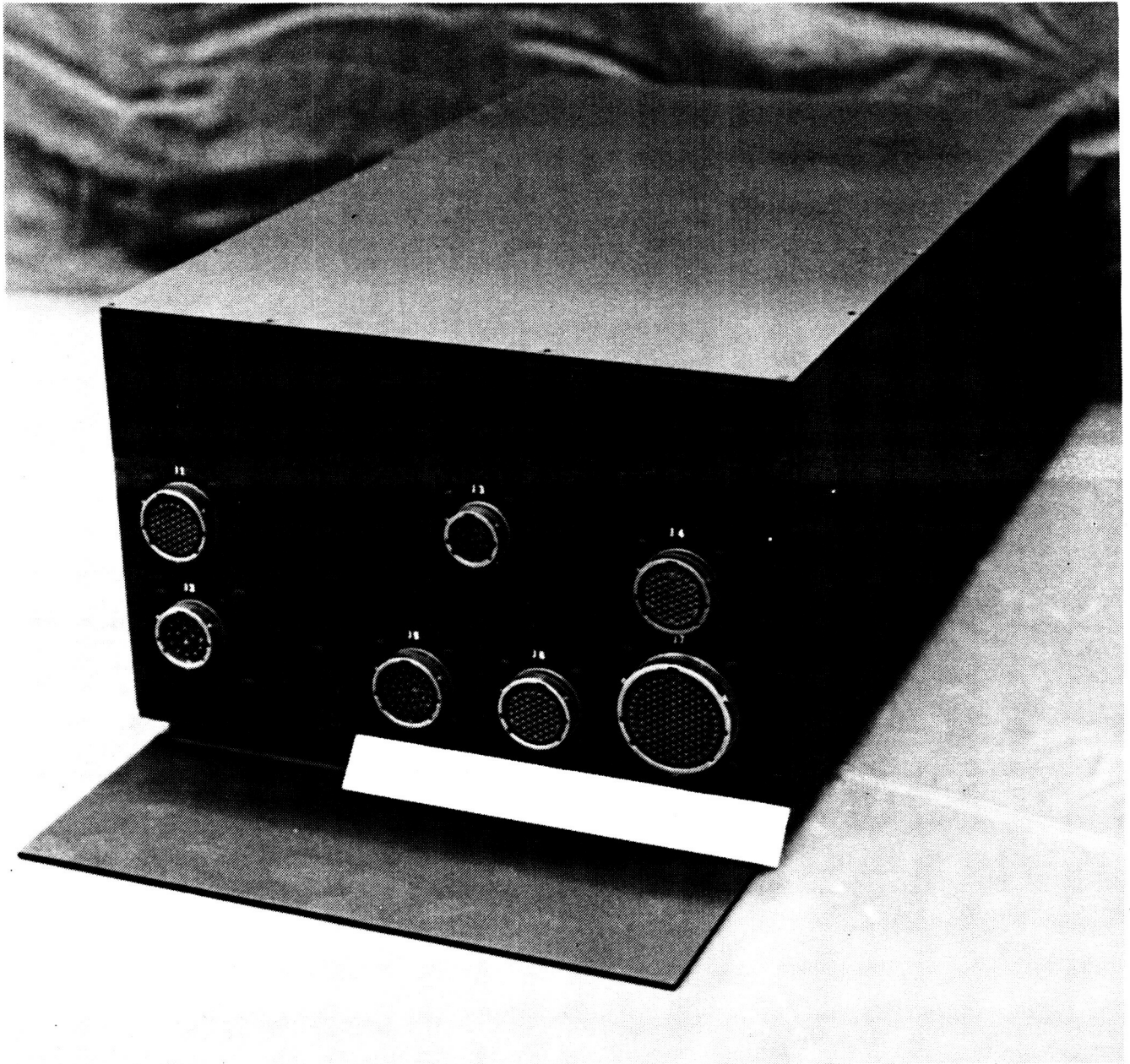
FIGURE 210

AFCS ELECTRONICS BOX, FRONT VIEW

382-763

FIGURE 211

ACS ELECTRONICS BOX, LEFT SIDE - REAR VIEW
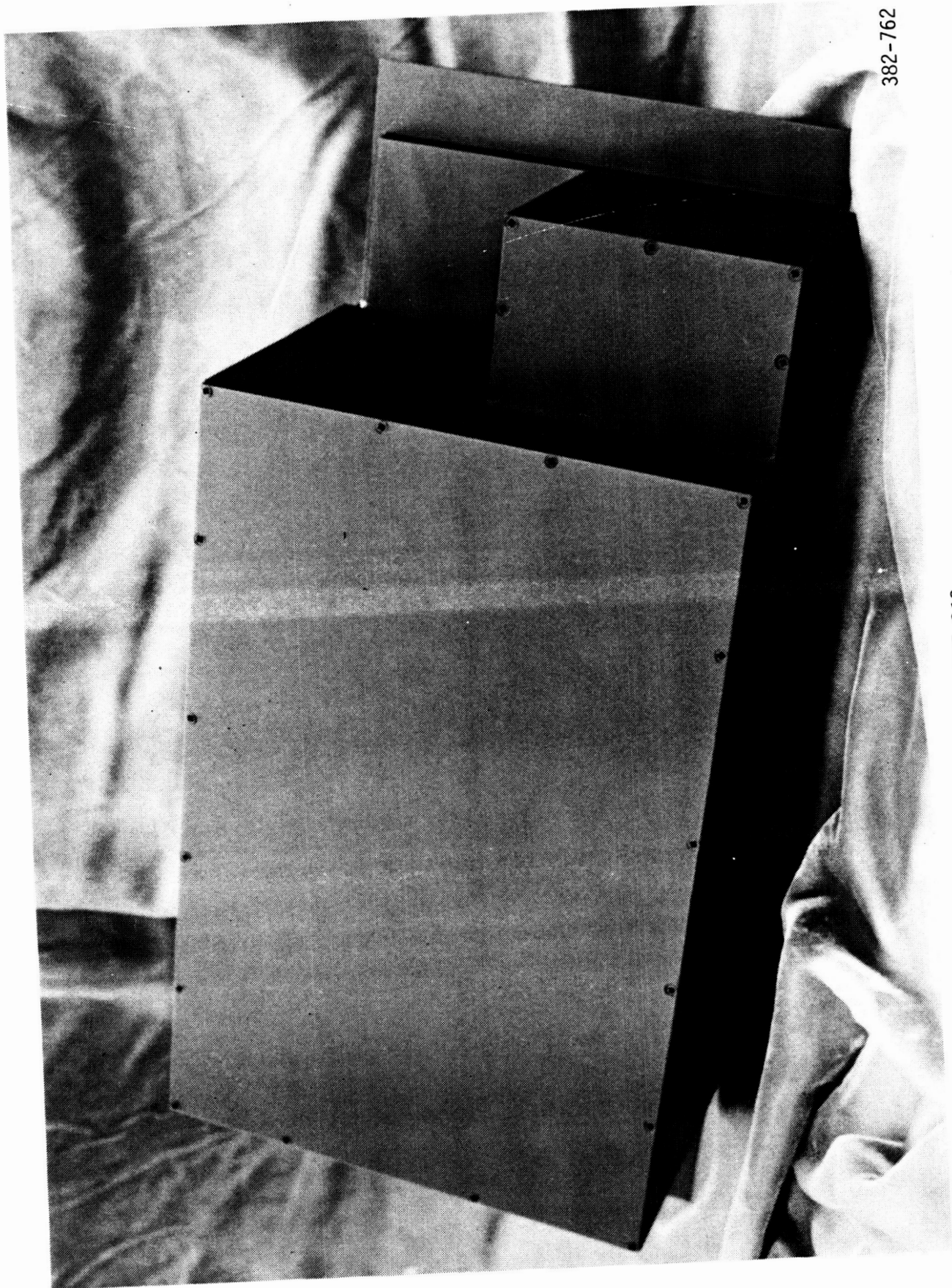
382-751

FIGURE 212

ACS ELECTRONICS BOX - TOP VIEW

382-762

FIGURE 213

ACS ELECTRONICS BOX - TOP COVER REMOVED

382-750

Component	Manufacturer	Part Number	Spares
Accelerometer	Sundstrand Data Control, Inc.	QA-1100-AA01-03	1
Accelerometer	PCB Piezotronics, Inc.	Model 303A03	3
Power Supplies	Crestronics	PS333-24-26-FW	1
		PS333-24-30-BCT	1
		PS333-24-10-BCT	1
		Various	1 of each card type

FIGURE 214

DAST ARW-2 FLUTTER SUPPRESSION SYSTEM SPARE COMPONENTS

9. FLIGHTWORTHINESS TESTING

The active control system electronics box was tested to demonstrate flightworthiness prior to delivery of the components to NASA. The tests conducted included component functional tests, interface tests of the electronics and servoactuators, vibration tests, temperature/altitude tests and electromagnetic compatibility tests.

Component functional tests are discussed in Paragraph 9.1. Flight assurance tests, including initial performance, integration, vibration, temperature/altitude, electromagnetic capability and final performance tests are summarized in Paragraph 9.2.

The temperature/altitude and vibration tests were conducted per NASA-DFRC Process Specification No. 21-2. Electromagnetic compatibility tests were conducted per required portions of MIL-STD-461A as discussed in Paragraph 9.2.5.

9.1 Component Functional Tests.

Functional tests of the active control system electronics and aileron actuation system components were conducted to assure satisfactory performance. The servoactuator functional test results showed two hydraulic fluid modes present in the system and that changes to the servoactuator compensation and/or the electronics would be required to give satisfactory performance. All populated cards in the electronics, including the spare cards, were tested for proper operation, the filters were tuned and required gains established.

9.1.1 Servoactuator System.

Functional tests were conducted on the DAST ARW-2 aileron servoactuators before the interface of the servoactuators with the active control system electronics was accomplished. The functional test was conducted to determine the dynamic performance that could be attained with the hardware as a verification of the linear stability analysis discussed in Paragraph 6.2. Results of the testing accomplished showed good agreement with the linear analysis having included the two hydraulic fluid modes in the analysis. The fluid modes are caused by the separation between the servovalve and actuator which would not be necessary on a full scale aircraft because sufficient space would exist to install the servovalve on the control surface actuator.

9.1.1.1 Test Setup.

Three complete servoactuators were set up for the functional tests using a steel bar (dummy load) rotary inertia, as described in the linear analysis of Paragraph 6.2, and ACS-type valve driver circuit card to close the feedback loops. An LM148 operational amplifier with current feedback was used as the servovalve drive amplifier. Fabrication of the DAST ARW-2 aileron control surfaces and active control system electronics was not finished when the servoactuator functional tests began.

Geometry of the hydraulic lines between the servovalve and actuator was set up similar to the installation required in the ARW-2 wing, except the line to the outboard actuator was given an additional 180° bend to minimize the size of the layout. Each servoactuator was rotated 90° to prevent interference between the dummy load inertia and the hydraulic tubing. The hydraulic lines were set up over a full-size installation drawing, hence the breadboard length did not differ appreciably from the wing installation. The pressure transducers were plumbed into the servovalve control ports with line length between the transducers and tee fittings in the manifold block about the same as was estimated for the installation in the drone wing.

Hydraulic power was provided by a laboratory hydraulic power unit with about 5 gal/min flow capability at 1500 psi. A 5 micron nominal, 15 micron absolute filter and an MS 28797-1 25 in^3 accumulator were plumbed into the pressure line between the pump and servovalve pressure ports. Pressure could be adjusted manually up to the desired 1500 psi supply pressure.

9.1.2 Electronic Components. All electronic components used were military qualified or commercial grade meeting military environmental specifications. Initially, all populated cards were tested for proper operation. The filters were tuned and required gains established. The box wiring was verified and all dimensions checked. The cards were installed function by function to verify operation. A complete operational check was then performed on the electronic box.

9.2 Flight Assurance Test Results. The Boeing test facilities were rescheduled twice because DACE functional checkout required more time than anticipated. A long term conflict of facilities would have occurred. DACE gain and phase tuning was halted until after temperature-altitude, EMC and vibration testing had occurred to avoid the conflict. Prior to final performance testing, DACE gain and phase tuning was completed. Direct comparison of final and initial test results is therefore extremely difficult. Test result comparison between similar tests (e.g. GLA aileron response, etc.) is valid and shows good agreement. The DACE was inspected for workmanship and then verification was made that the unit envelope would meet the required interface dimensions to the BQM-34E/F drone aircraft. The testing consisted of initial performance, temperature/altitude, vibration, interface and final performance. The results of these tests are presented by the following paragraphs. Data sheets may be found in Boeing Document D3-12115-1, Flight Assurance Report for the Active Control System DAST (ARW-2), 19 August 1983.

9.2.1 Initial Performance. The DACE only was tested during the initial performance test. Compatibility between the DACE and the hydraulic system was verified during the interface test.

9.2.1.1 Power Supply Performance. The input power was varied from 24.0 VDC to 32.0 VDC while providing the total load current required by the DACE. The operating currents for each power supply voltage level were measured. The results are recorded on Data Sheet 4.1.2.1. The power supplies successfully passed all tests.

9.2.1.2 FSS. The procedures of Test 4.1.3.1 were used to check the FSS. Filter gains and phases together with uplink and downlink functions associated with the FSS were within required tolerances and are recorded on Data Sheet 4.1.3.1.

9.2.1.3 Function Generator. The procedures of Test 4.1.3.2 were used to verify operation of the function generator. Results are recorded on Data Sheet 4.1.3.2. The function generator successfully passed all requirements.

9.2.1.4 MLA. The procedures of Test 4.1.3.3 were used to determine proper operation of the MLA. Results are recorded on Data Sheet 4.1.3.3. The MLA successfully passed all requirements.

9.2.1.5 GLA. The procedures of Test 4.1.3.4 were used to determine proper operation of the GLA. Included in these procedures were checkout of the GLA scheduler, filter gains and phases together with uplink and downlink functions. Results are recorded on Data Sheet 4.1.3.4. The GLA successfully passed all requirements.

9.2.1.6 RSS. The procedures of Test 4.1.3.5 were used to verify the RSS. The RSS scheduler, filters, uplink and downlink functions were checked out. Results are recorded on Data Sheet 4.1.3.5. The RSS successfully passed all requirements.

9.2.1.7 Valve Drivers. The procedures of Tests 4.1.3.6 were used to check out the left and right outboard valve drivers. Data are recorded on Data Sheets 4.1.3.6.

The procedures of Tests 4.1.3.7 were used to check out the left and right inboard and outboard segments of the inboard valve drivers. Data are recorded on Data Sheets 4.1.3.7. All valve drivers successfully passed all requirements.

9.2.1.8 Uplink Confirmation. The procedures of Tests 4.1.3.8 were used to check out the uplink confirmation (downlink) signals. All signals were within the required tolerances and are recorded on Data Sheet 4.1.3.8.

9.2.2 Electromagnetic Compatibility. The EMC tests were satisfactorily completed as discussed in Boeing Document D3-12115-2. A copy of the Pass-Fail Summary is given on Figure 215.

TEST		MIL-STD-461A TEST REQUIREMENTS
CEO3 BB	By Similarity	PASS
CEO3 NB		PASS
CEO4 BB		PASS
CEO4 NB		PASS
CS01		PASS
CO02	By Similarity	PASS
CS06		PASS
REO2 BB		PASS
REO2 NB		PASS
RSO3		PASS

FIGURE 215

EMC PASS-FAIL SUMMARY

9.2.3 Temperature/Altitude. This test was performed per the requirements and procedures of Boeing Document D3-12114-1, Flight Assurance Test Procedures for the Active Control System DAST (ARW-2), 7 May 1981. Figure 4.5.2 of Boeing Document D3-12114-1 presents the test plan that was followed during testing. The test was conducted in the BMAC Temperature/Altitude Facility on 9-13 July 1982. Figure 4.5.2 of Boeing Document D3-12114-1 shows the test instrumentation and Figure 11 of Boeing Document D3-12115-1 shows the DACE and power supplies installed in the test chamber.

9.2.3.1 Pretest Performance. The DACE was operated in standard ambient conditions. Performance data were recorded after temperature stabilization had occurred. The system met all requirements and the data are recorded on Data Sheet 4.5.3.1.

9.2.3.2 Startup and Operation at -65°F. After completion of the cold soak at -65°F, the system was turned on. The +15 VDC power supply was not immediately functional. Turn on voltage was +4.7 VDC. When the supply temperature reached -46°F, the output voltage suddenly came into tolerance. The dynamic pressure circuit was out of tolerance by 0.13 VDC (13 psf, equivalent), however, this was not deemed consequential since the GLA and RSS responses, whose schedules are a function of dynamic pressure, were well within the gain (+0.5 dB) and phase (+5.0 deg) to tolerances set. Performance results are recorded on Data Sheets 4.5.3.2.

9.2.3.3 Operation at -65°F, 60,000 Feet Altitude. After temperature stabilization, the DACE was turned on and the chamber altitude adjusted to 60,000 feet. Again, the dynamic pressure circuit was out of tolerance. No deviations were noted due to changes in altitude. The performance results are recorded on Data Sheets 4.5.3.3.

9.2.3.4 Performance at -40°F, 40,000 Feet Altitude. The chamber temperature was increased to -40°F and the altitude adjusted to 40,000 feet. The DACE successfully passed all requirements except the dynamic pressure circuit which has been previously discussed. The results are recorded on Data Sheets 4.5.3.4.

9.2.3.5 Operation at Standard Conditions. The chamber temperature and altitude were returned to laboratory ambient levels and the performance tests were repeated. The DACE successfully passed all requirements, except: (1) the sine wave sweep generator did not sweep in frequency and (2) the FSS symmetric channel phase exhibited an 8 degree phase lag. Inspection revealed a large amount of condensation on the circuit cards. When the condensation had been removed from the foil side of the function generator circuit card, the sine wave sweep resumed normal operation. When the condensation had been removed from the foil side of the symmetric filter card, the 8 degree phase lag was eliminated. Use of a heat blanket or conformal coating is recommended to prevent the accumulation of condensation on the circuit cards. The results are recorded on Data Sheets 4.5.3.5.

9.2.3.6 Performance at 160°F, 30,000 Feet. Following a 16 hour temperature soak at 160°F with power off, the altitude was adjusted to 30,000 feet. Upon reaching the specified altitude, the DACE was soaked for another 4 hours with power on. Following the 4 hour, power on, hot soak a performance test was conducted. The DACE successfully passed all tests, except the GLA scheduler was found to be out of tolerance by 0.24 VDC. The effect on GLA system performance was negligible as all responses were well within the tolerances set, +0.5 dB for gain and +5.0 deg for phase. Test results are recorded on Data Sheets 4.5.3.6.

9.2.3.7 Operation at 160°F, 60,000 Feet. The altitude was adjusted to 60,000 feet. The DACE successfully passed all tests, except for the GLA scheduler which was out of tolerance but had negligible effect on the GLA system performance. Test results are recorded on Data Sheets 4.5.3.7.

9.2.3.8 Operation at Standard Conditions. The chamber was returned to laboratory ambient conditions and the performance tests repeated. All functions operated properly and values returned close to those of the pretest. Inspection showed no physical damage had occurred. Operation was satisfactory. Results are contained on Data Sheets 4.5.3.8.

9.2.4 Vibration Tests. This test was performed per the requirements and procedures of Boeing Document D3-12114-1. Figures are to be found in Boeing Document D3-12115-1. Figure 12 presents the requirement and Figure 13 gives the test input equivalent of this requirement. The test was conducted in the BMAC Vibration Facility located in Building 342J on 16-19 July 1982.

Three axes sinusoidal excitation was applied to the DACE at laboratory ambient temperatures. The DACE was powered and operating during all testing. No gain or phase distortion was observed during the sweep or dwell periods. No signal distortion was observed on the oscilloscope during these periods.

Figures 14, 15, and 16 show the locations of accelerometer placement on the DACE.

Figures 17, 18, 19, and 20 show the response of the box to the vibration inputs. Test data is recorded on Data Sheets 4.3.5.

9.2.5 Interface Test. The purpose of the interface test was to verify electrical compatibility between the DACE and the hydraulic breadboard. Additional data on the actuators were taken and are presented on Figure 216.

9.2.5.1 Interface Performance Tests. These tests were performed to verify operation of the DACE after being connected to the hydraulic breadboard. The results of the tests showed agreement with the data taken during the initial performance test when the breadboard was

324

ACTUATOR	BANDWIDTH (HZ)	HYSTERESIS (DEGREES)	MAXIMUM RATE (DEG/SEC)
OUTBOARD AILERON	49.2	0.3	955
INBOARD AILERON OUTBOARD SEGMENT	22.0	0.1	129
INBOARD AILERON INBOARD SEGMENT	25.5	0.0	129

FIGURE 216

SERVOACTUATOR PERFORMANCE SUMMARY

disconnected from the DACE. One exception is notable but not significant. A deviation between initial and interface performance tests exists in the MLA response. In the initial performance test, the filter implemented was (20)/(S+20). This filter was determined to be in error and was subsequently corrected to (125)/(S+125).

9.2.5.2 Actuator Performance Tests. These tests were performed to verify operation of the hydraulic actuators. Figure 216 summarizes the results of these tests. During the testing, no crosstalk was observed nor were any hydraulic leaks observed.

9.2.5.3 Interface System Performance Tests. These tests were performed to obtain end-to-end data on the systems which utilized the actuators on the hydraulic breadboard. The data were expected to be the composite of the appropriate sections in paragraph 4.2.2 and the frequency responses in Paragraph 4.2.3.1 of Boeing Document D3-12114-1. The data taken met the expected results.

9.2.6 Final Performance. The DACE only was tested during the final performance test. Compatibility between the DACE and the hydraulic system was verified during the interface test. Data Sheets are to be found in Boeing Document D3-12115-1.

9.2.6.1 Test Setup. The test setup was performed per Paragraph 4.6.1.

9.2.6.2 Power Supply Voltage Check. The procedures of Test 4.6.2 were used to verify voltage levels of the power supply. The results are recorded on Data Sheet 4.6. The power supplies successfully passed all tests.

9.2.6.3 FSS. The procedures of Tests 4.6.3.1 and 4.6.3.2 were used to check the FSS. The final filter gains and phases were within the required tolerances and are recorded on Data Sheet 4.6.

9.2.6.4 GLA. The procedures of Tests 4.6.3.5 through 4.6.3.7 were used to determine proper operation of the GLA. Included in the procedures were checkout of the GLA scheduler, filter gains and phases together with the downlink signals. Results are recorded on Data Sheet 4.6. The GLA successfully passed all requirements.

9.2.6.5 RSS. The procedures of Tests 4.6.3.8 through 4.6.3.11 were used to verify the RSS. The RSS scheduler, filters and downlink functions were checked out. Results are recorded on Data Sheet 4.6. The RSS successfully passed all requirements.

9.2.6.6 MLA. The procedures of Tests 4.6.3.12 and 4.6.3.13 were used to verify the MLA. Results are recorded on Data Sheet 4.6. The MLA successfully passed all requirements.

9.2.6.7 Function Generator. The procedures of Tests 4.6.3.14 and 4.6.3.15 were used to verify operation of the function generator. Results are recorded on Data Sheet 4.6. The function generator successfully passed all requirements.

9.2.6.8 Value Drivers. The procedures of Test 4.6.3.16 were used to check out the left and right outboard value drivers. Data are recorded on Data Sheets 4.1.3.6.

The procedures of Test 4.6.3.17 were used to check out the left and right, inboard and outboard segments of the inboard value drivers. Results are recorded on Data Sheet 4.6.

All value drivers successfully passed all requirements.

9.2.6.9 Uplink Confirmation. The procedures of Test 4.6.3.18 were used to check out the uplink confirmation (downlink) signals. All signals were within the required tolerances and are recorded on Data Sheet 4.6.

9.2.6.10 AFCS, Right Wing, Downlink Connector Interface. The procedures of Tests 4.6.3.19 through 4.6.3.21 were used to check the signals on the AFCS, right wing and downlink connector. The signal interface data are recorded on Data Sheet 4.6. The signal interface successfully passed all requirements.

(This page intentionally left blank)

10. FLIGHT RESTRICTIONS

The wing structure is designed for positive 2.5g maneuver with the load alleviation system on at the maneuver design condition and the loads at the maneuver test condition will be slightly less than the design level. The test condition maneuvers should be restricted to a maximum of 2.1g without the load alleviation systems engaged.

The wing structure is sized for a design gust of 62 fps peak with the load alleviation system on. At the gust test condition, the critical load level will occur at a gust peak of 40 fps without the load alleviation system engaged.

Because of the limited phase margin of the primary AFCS and the RSS at the maximum dynamic pressure condition with the load alleviation systems off, the dynamic pressure of 412 psf occurring at the GLA test condition should not be exceeded significantly with the load alleviation systems disengaged.

PRECEDING PAGE BLANK NOT FILMED

(This page intentionally left blank)

11. CONCLUSIONS AND RECOMMENDATIONS

11.1 Conclusions. The third design cycle iteration analysis has been completed and results indicate that the ARW-2 wing structure and control systems meet the design objectives.

System hardware has been fabricated and functional, EMC and environmental tests have been successfully completed.

Boeing furnished hardware is ready for installation, checkout and flight test on the DAST ARW-2 vehicle.

11.2 Recommendations. The DAST ARW-2 wing with integrated active controls should be flight tested to verify the performance and benefits of active controls in the design of high aspect ratio wings.

It is recommended that the following testing sequence be established to proceed from the most stable flight conditions to most unstable conditions:

Recommended sequence of tests

a.   Primary AFCS and RSS system verification at launch and load alleviation test conditions

b.   Load alleviation systems evaluation tests

c.   RSS system verification at cruise and maximum altitude conditions

d.   Flutter system evaluation

It is also recommended that the backup AFCS be verified, perhaps at the end of a flight, before advancing to the more unstable flight conditions.

REFERENCES

1. Boeing Document D3-11535-1, Integrated Design of a High Aspect Ratio Research Wing with an Active Control system for Flight Tests on a BQM-34E/F Drone Vehicle, 25 June 1979. (Available as NASA CR-166108, Volume I; NASA CR-166109, Volume I, Appendices)

2. Olen E. Visor and Francis D. Severt, Preliminary Design Study of Flutter Suppression Control System for the BQM-34E/F Drone Aircraft with a Supercritical Wing, NASA CR-145208, 7 July 1976.

3. C. R. McGehee and G. E. Hodges, Final Design and Fabrication of an Active Control System for Flutter Suppression on a Supercritical Aeroelastic Research Wing, NASA CR-165714, June 1981.

4. Book, Herbert E. Merritt, Hydraulic Control System, John Wiley & Sons, 1967.

5. John W. Edwards, NASA TN D-6928, Analysis of an Electrohydraulic Aircraft Control-Service Servo and Comparison with Test Results, dated August 1972.

Standard Bibliographic Page

1. Report No. NASA CR-177959, Part 1	2. Government Accession No.	3. Recipient's Catalog No.
4. Title and Subtitle DESIGN VERIFICATION AND FABRICATION OF ACTIVE CONTROL SYSTEMS FOR THE DAST ARW-2 HIGH ASPECT RATIO WING, PART 1		5. Report Date January 1986
		6. Performing Organization Code
7. Author(s) C. R. McGehee		8. Performing Organization Report No. D500-10897-1
9. Performing Organization Name and Address Boeing Military Airplane Company P.O. Box 7730 Wichita, Kansas 67277-7730		10. Work Unit No.
		11. Contract or Grant No. NAS1-16010
12. Sponsoring Agency Name and Address National Aeronautics and Space Administration Washington, DC 20546		13. Type of Report and Period Covered Contractor Report
		14. Sponsoring Agency Code

15. Supplementary Notes

16. Abstract

A study was conducted under Drones for Aerodynamic and Structural Testing (DAST) program to accomplish the final design and hardware fabrication for four active control systems compatible with and ready for installation in the NASA Aeroelastic Research Wing No. 2 (ARW-2) and Firebee II drone flight test vehicle. The wing structure was designed so that Active Control Systems (ACS) are required in the normal flight envelope by integrating control system design with aerodynamics and structure technologies. The DAST ARW-2 configuration uses flutter suppression, relaxed static stability and gust and maneuver load alleviation ACS systems, and an automatic flight control system. Performance goals and criteria were applied to individual systems and the systems collectively to assure that vehicle stability margins, flutter margins, flying qualities and load reductions were achieved.
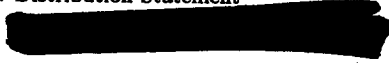
17. Key Words (Suggested by Authors(s)) Flutter Suppression Relaxed Static Stability Maneuver Load Alleviation Gust Load Alleviation	18. Distribution Statement Until January 1988
19. Security Classif.(of this report) Unclassified	20. Security Classif.(of this page) Unclassified	21. No. of Pages 332	22. Price